Chiral Symmetry in Hamiltonian Lattice Field Theory

A Tensor Network Perspective

Gertian Roose

Thesis submitted in fulfillment of the requirements for the degree of
Doctor (Ph.D.) in sciences: Physics

Academic year 2021-2022

Supervisor:

Prof. Dr. Jutho Haegeman
Ghent university

Co-supervisors:

Dr. Karel Van Acoleyen
Ghent university

Dr. Nick Bultinck
Ghent university

Members of the Examination Committee:

Prof. Dr. Jan Ryckebusch (chairman)
Ghent university

Prof. Dr. Erez Zohar
Hebrew University of Jeruzalem

Prof. Dr. Yannick Meurice
University of Iowa

Prof. Dr. Henri Verschelde
Ghent university

Prof. Dr. Michal Heller
Ghent university

ACKNOWLEDGEMENTS

It is often said that the journey and the people you meet throughout are more important than the destination. In fact, my arrival at this crazy destination would not have been possible without the many people that I met along the way.

As every traveler know, good adventures start with good guides and this journey was no different. With this in mind, I would like to thank my supervisors Jutho Haegeman, Nick Bultinck and Karel Van Acoleyen for their trust, never ending stream of knowledge and occasional much needed pep-talks when I was loosing the metaphorical trail. I would also like to thank my "non official guides" Frank Verstraete and Laurens Vanderstraeten for sharing their passion for physics and Inge Van der Vennet helping me with the administrative part of the journey.

Furthermore I would like to thank my fellow travelers (i.e. office mates) Benoit, Robijn, Quinten, Laurens (junior), Tom, Maarten and Daan for the many laughs, discussions and the occasional practical joke. In particular I would like to thank Bram Vanhecke for our many discussions about quantum field theory that helped shape the third chapter of this work.

I would also like to thank all "tjoempies" from the highline community for the somewhat precarious practical application of physics and for teaching me that every destination can be reached as long as you keep walking. In particular I would like to thank Korneel, Anji, Moran, Julie, Laura and Viktor for the moments shared amongst the (campfire) clouds.

From the Ghentisch homefront I would like to thank my buddies Mathias, Arno, Arthuur and Bastiaan for the many jams, climbing, pubcrawling, biking and munchkin sessions. You guys were wonderfull "hirelings" and provided a solid +10 bonus throughout my journey. Special thanks to Mathias for teaching me how to communicate science to a broader audience and to Bastiaan for his Latex wizardry.

Last, but not least, I thank my parents for their constant support and motivational calls even when I vanished from the world for prolonged periods of time.

SYNOPSIS

The central theme of this thesis are quantum field theories, a set of theories devised in 1920-1970 with the goal of describing the interactions between elementary particles such as electrons, quarks and photons. For weakly interacting particles, such as low energetic electrons, these field theories can be approximately solved through perturbation theory and this solution provides us with predictions for observable quantities such as the decay rates of these particles. Since about the 1970s, these predictions have been tested, and verified, with astounding accuracy in particle accelerators such as the ones at CERN. When these particles are strongly interacting, as is the case for low energetic quarks, this approximate solution no longer works and we must usually rely on computer simulations. Such simulations can evidently only consider information at a finite number of positions, which forces us to approximate them by quantum theories on a lattice. These lattice field theories can then be linked to the original field theory by taking the limit where the lattice points are infinitely close.

This discretization trick eliminates a lot of degrees of freedom, but nevertheless, dealing with the remaining degrees of freedom has a complexity that still scales exponentially with the system size. This is still unmanageable if we consider realistically sized systems. In fact, this exponential complexity is one of the main properties of any quantum theory of interacting particles and there exist many ways to deal with this. In this thesis we will use a relatively new method, which uses the fact that these degrees of freedom can be represented by so called tensor networks.

One of the quantum field theories that we will simulate with this approach is the (chiral) Gross-Neveu model, which was devised in 1974 to study the phenomenon of spontaneous mass generation in the proton and neutron in a simpler one-dimensional context. Here we will encounter an important shortcoming of lattice models, i.e. the fact that they cannot respect all symmetries of the continuous field theories. Indeed, it is obvious that a lattice theory can not have all translation and rotation symmetries that are possible in the continuum world, so that we can only hope that these symmetries reappear if we take the grid points sufficiently close. For some symmetries, such as translation symmetry, this is not very surprising, but the continuous formulation of the chiral Gross-Neveu model has a chiral symmetry which enforces a gapless excitation in the spectrum, and this symmetry is also broken by the discretization procedure. The simulated field theory will therefore not have this guarantee, and it is far from trivial that these massless particles would still appear if we take the grid sufficiently fine. Nevertheless, throughout our research we constructed a suitable lattice regularisation of the chiral Gross-Neveu model and, on top of this, we also identified a mechanism that motivates the emergence of the massless particle.

Broadly speaking this thesis consists of two parts. A first part where I explain the relevant literature in three chapters. In the second part, I will present my publications, each with a small introductory paragraph to connect the presented research to the relevant parts of the introduction.

In the first chapter of the first part I will present the postulates of quantum mechanics and motivate them through a simple experiment that will show that this, admittedly strange, set of rules is necessary to understand the interaction of electrons with a magnetic field. In the next step, I will define quantum lattice models by considering long chains of electrons i.e. spin chains, and here we will see why these systems have so many degrees of freedom.

In the last part of the first chapter, I introduce tensor networks and analyse their most important properties. Firstly, I will introduce “matrix product tensor network states” as an ansatz for ground-states of quantum systems. I will also look to correlations within these states and introduce the concept of quantum entanglement. Furthermore, I will present an algorithm to find the MPS with minimal energy gives some Hamiltonian. Secondly, I will introduce “quasi-particle tensor network

states" as an ansatz for excitations on top of the groundstate. Lastly, I will analyse which tensor networks are symmetric with respect to certain symmetry, an analysis that will later help us identify some interesting properties of spin chains.

In the second chapter, I will take a look at two spin chains that are particularly important in the lattice description of field theories, these are the Ising model and the Su-Schrieffer-Heeger model. During the analysis of the Ising model, I will learn about spontaneous symmetry breaking and the associated concept of phases and transitions between them. Note that everybody who ever made ice cubes is already familiar with the classical analogue of these concepts. Here the phases are the liquid and solid forms of water, and the associated symmetry is the translation symmetry of the liquid that is broken when the water crystallizes. These models are also the starting point of the physics that I investigated during my own research. I will then use the SSH model to introduce the concept of (symmetry-protected) topological order. For our purposes this is a symmetry that guarantees the presence of a massless excitation at the edge of our chain. To prove the existence of these excitations, I will use the MPS methods presented in the first chapter.

In the first part of the third chapter, I review the one-dimensional version of quantum field theory. Here, I will present the chiral Gross-Neveu model, which is a model for self-interacting fermions, and approximately solve the model so that I can compare these results to later simulations. During this analysis, I will also discuss the chiral symmetry and its impact on the spectrum. I will also discuss bosons, such as the famous Higgs boson, that are self interacting. The reoccurring theme in all these field theory calculation will be a divergent energy density, and to deal with it I will take a look at renormalisation. This will lead to the conclusion that field theories are only well defined as limits of underlying models with less degrees of freedom. The conclusion is that lattice models are more then a numerical tool, they offer a beautiful interpretation of the renormalisation theory that is a key ingredient of quantum field theory.

In the second part of the third chapter, I take a closer look at this lattice construction and explicitly show that the SSH model can be used to describe and simulate non-interacting fermions. I will also reconsider the chiral symmetry and discuss why it cannot survive on the lattice.

In the second half of the thesis, I take a closer look at my research. The reoccurring theme here is the before mentioned limit of lattice models. In the first paper, I studied a generalization of the Ising model that turns out to be a lattice regulator for some rather complex field theory that we will also study in the first half. The second and third papers discuss a novel lattice regularization of the (chiral) Gross-Neveu model. Throughout the process of finding this regularization we learn a lot about the field theory itself.

NEDERLANDSTALIGE SAMENVATTING

Het centrale thema van deze thesis is kwantumveldentheorie, een theorie die ontstaan is omstreeks 1920-1970, met als doel de interaties tussen elementaire deeltjes zoals elektronen, quarks en fotonen te beschrijven. Wanneer deze deeltjes zwak interageren, zoals het geval is voor laag-energetische elektronen, kan de veldentheorie benaderend opgelost worden en kunnen we voorspellingen maken aan de hand van storingsrekening. Deze voorspellingen worden sinds ongeveer 1970 met enorme nauwkeurigheid experimenteel bevestigd door deeltjesversnellers zoals deze in CERN. Wanneer deze deeltjes echter sterk interageren, zoals bijvoorbeeld het geval is voor laag-energetische quarks, kunnen we de theorie niet meer benaderend oplossen en moeten we vertrouwen op computersimulaties. Dergelijke computersimulaties kunnen echter slechts rekening houden met informatie op een eindig aantal locaties, wat aanleiding geeft tot kwantum theorieen die op een rooster leven. Om deze kwantummechanische roostersystemen dan te linken aan de oorspronkelijke kwantumveldentheorie, nemen we de roosterpunten dichter en dichter tot we opnieuw een continue wereld hebben.

Door de kwantumveldentheorieën op een rooster te benaderen, is het aantal vrijheidsgraden en dus de numerieke complexiteit wel afgenomen. Maar deze schaalt nog steeds exponentieel met het aantal roosterpunten en wordt dus veel te groot als realistische systeemgroottes beschouwen. Deze exponentiële schaling is één van de typerende kenmerken van elke kwantumtheorie van interagerende deeltjes, en door de jaren heen zijn er enorm veel manieren bedacht om hier mee om te gaan. In deze thesis gebruiken we een relatief nieuwe methode, waarbij gebruik gemaakt wordt van het feit dat de enorme hoeveelheid vrijheidsgraden kan voorgesteld worden door zogenaamde tensornetwerken.

Één van de kwantumveldentheorieen die we op deze manier zullen simuleren is het (chiraal) Gross-Neveu model, dat in 1974 werd opgeschreven om in een ééndimensionale context het fenomeen te bestuderen waar de protonen en neutronen hun massa aan te danken hebben. Hierbij komt er een andere beperking van de roostermodellen naar boven, met name het feit dat ze niet alle symmetrieën van de continue wereld kunnen respecteren. Zo kan een roostertheorie natuurlijk nooit symmetrisch zijn onder alle mogelijke verschuivingen en rotaties van een continue wereld. We kunnen dus alleen maar hopen dat dergelijke symmetrieën op een emergente manier naar boven komen wanneer we de afstand van tussen roosterpunten voldoende klein wordt. Voor sommige symmetrieën, zoals deze vershuivingssymmetrie is dit niet zo verbazingwekkend, maar de continue formulering van het chiraal Gross-Neveu model heeft een symmetrie die ervoor zorgt dat het spectrum altijd een massaloze excitatie bevat, en deze wordt ook noodzakelijk gebroken op het rooster. De simuleerbare roostertheorie zal deze garantie dus niet hebben, en het is dan ook helemaal niet evident dat deze massaloze deeltjes toch tevoorschijn zouden komen wanneer we het rooster voldoende fijn maken. Desondanks zijn we er tijdens ons onderzoek in geslaagd om een roosterformuling van het chiraal Gross-Neveu model te vinden waarbij deze emergente symmetrie en bijhorende massaloze excitatie op een robuste manier tevoorschijn als we het rooster voldoende fijn maken.

In grote lijnen bestaat de thesis uit twee delen. Het eerste deel is een literatuurstudie, waarin we in drie hoofstukken de relevante voorkennis uit de doeken doen. In het tweede deel presenteer ik mijn publicaties met steeds een kort woordje uitleg om de connectie te maken met de literatuurstudie uit eerste deel.

Concreet zal ik in het eerste hoofdstuk de postulaten van de kwantummechanica invoeren en kijken naar een simpel experiment om in te zien dat deze (toch wel vreemde) verzameling aan regels nodig zijn om de interactie van elektronen met magnetische velden te beschrijven. In de volgende stap

definieer ik de nodige roostersystemen door lange kettingen van dergelijke elektronen te beschouwen. We zien hier ook waarom deze systemen zoveel vrijheidsgraden hebben.

Ik rond het eeste hoofdstuk af door tensornetwerken en hun belangrijkste kenmerken te analyseren. Eerst zal ik "matrix product tensor network states" invoeren als beschrijving voor laag-energetische kwantumtoestanden. Ik zal ook kijken naar correlaties binnen dergelijke toestanden en het concept van kwantumentanglement introduceren. Ik beschrijf ook een algoritme om de toestand met minimale energie te vinden voor een bepaald model. Vervolgens voer ik "quasi-particle tensor network states" als beschrijving van excitaties bovenop de laagst energetische toestand. Tenslotte bestudeer ik welke tensornetwerken symmetrisch zijn onder bepaalde symmetrieën. Dit zal me later helpen om bepaalde interessante kenmerken van de elektronenkettingen te identificeren.

In het tweede hoofdstuk bekijken we twee spinketens die zeer belangrijk zijn voor de roosterbeschrijving van veldentheorieën, deze zijn het Ising model en het Su-Schrieffer-Heeger (SSH) model. Tijdens de analyse van het Ising model bespreek ik ook het concept van spontane symmetriebreking en het gerelateerde concept van fasen en fasetransities. Merk op dat iedereen die al eens een ijsblokje gemaakt heeft deze concepten eigenlijk al kent. In die context zijn de verschillende fasen de vloeibare en vaste vorm van water, en de relevante symmetrie is deze van verschuivingen die niet meer aanwezig is wanneer het water een ijskristal vormt. Via het SSH model introduceren we vervolgens het concept van topologische orde. Voor onze doeleinden is dit een exotische symmetrie die de aanwezigheid van een massaloze excitatie op de rand van onze ketting garanderen. Om het bestaan van deze excitaties aan te tonen steun ik op de MPS die we eerder invoerden.

Tenslotte kijken ik in het eerste deel van het derde hoofstuk naar de ééndimensionale versie van kwantumveldentheorie. Concreet beschouwen we een model voor fermionen, zoals bijvoorbeeld elektronen, die sterk met zichzelf interageren. Dit is het (chiraal) Gross-Neveu model en we zullen dit model benaderend oplossen, zodat we dit resultaat kunnen vergelijken met latere simulaties. Ik zal hier ook in meer detail uitwijden over de chirale symmetrie. Ik bestudeer bovendien bosonen, zoals bijvoorbeeld het gekende Higgs boson, die met zichzelf interageren. Tijdens deze analyses worden we steeds opnieuw geconfronteerd met het feit dat continue wereld aanleiding geeft tot een divergente energiedensiteit. We zullen dit probleem oplossen met behulp van renormalisatie en komen tot de conclusie dat veldentheorieën eigenlijk enkel te begrijpen zijn als limieten van onderliggende modellen met minder vrijheidsgraden, zoals bijvoorbeeld een roostermodel. De conclusie is dat roostersystemen veel meer zijn dan een numerieke methode; ze bieden ons een prachtige interpretatie van de renormalisatieprocedure die nodig is om veldentheorieën te bestuderen.

In het tweede deel van het derde hoofdstuk ga ik dieper in op deze roosterconstructie en toon ik concreet aan dat het SSH model gebruikt kan worden om niet-interagerende fermionen te beschrijven/simuleren. Ik ga hier ook in op de chirale symmetrie en waarom deze niet kan overleven op het rooster.

In het tweede helft van de thesis presenteer ik mijn eigen onderzoek. Het overkoepelende thema is hier dat ik de eerder genoemde roosterprocedure om veldentheorieën te definiëren. In de eerste paper kijk ik naar een veralgemening van het Ising model dat perfect kan dienen als definitie van de interagerende boson theorie. In de tweede en derde papers gebruik ik een veralgemening van het SSH model om een roosterregularisatie van het Gross-Neveu model op te schrijven.

LISTING OF PUBLICATIONS

Below is a list of all my publications, their authors and the journal in which they have been published. For all these works, I am the first author and consequently I was responsible for a majority of the work. In particular, I performed all numerical simulations and analyzed the resulting data thereof.

Anomalous domain wall condensation of a modified Ising chain
Authors : Gertian Roose, Laurens Vanderstraeten, Jutho Haegeman and Nick Bultinck
Journal : Physical Review B

Lattice regularisation and entanglement spectrum of the Gross-Neveu model
Authors : Gertian Roose, Nick Bultinck, Laurens Vanderstraeten, Frank Verstraete
Karel Van Acoleyen and Jutho Haegeman
Journal : Journal of High Energy Physics

The chiral Gross-Neveu model on the lattice via a Landau-forbidden phase transition
Authors : Gertian Roose, Laurens Vanderstraeten, Jutho Haegeman and Nick Bultinck
Journal : Journal of High Energy Physics

CONTENTS

Part I

COLLECTED RESULTS FROM THE LITERATURE

1

THE ESSENTIALS OF QUANTUM MECHANICS

> If you are not completely confused by quantum mechanics, you do not understand it.
>
> John Wheeler

Before we delve into quantum mechanics, let us first think about the ingredients that are essential for any theory of nature. Firstly, our description must contain a set of labels that characterizes the configuration of our system of interest; physicist call this set of labels the state. Additionally, if we want to connect the theory to reality, we must specify the outcome of measurements given the state. Finally, if we want our theory to make predictions about the future we must specify a set of rules that specify how the state changes as time moves forward. For example, to describe the state of your favorite coffee mug you must specify its location, speed, color, etc. and clearly the outcome of a measurement of any of these properties will simply tell you what that label is, furthermore the time evolution in this example is given by Newton's famous laws.

In essence, quantum mechanics is simply a different set of rules/postulates that seem to be very good at describing the behaviour of certain phenomena in nature. In what follows we will however see that these rules are very counter-intuitive hence Wheeler's famous quote.

1.1 The postulates

In quantum mechanics the state $|\psi\rangle$ of a system is described by a vector in some Hilbert space $\mathbf{H}$, the details of this Hilbert space depend on the degrees of freedom that are relevant for the physical system under investigation.

The observables (i.e. quantities that we can measure) of a quantum theory are represented by self-adjoint linear operators $\hat{O}$ acting on this Hilbert space. Such self-adjoint operators can always be decomposed in terms of their eigenvectors $\hat{O} = \sum_i \lambda_i |O_i\rangle \langle O_i|$ so that $\hat{O}|O_i\rangle = \lambda_i |O_i\rangle$. A measurement of this observable in the state $|\psi\rangle$ has outcome λ_i with probability $p_i = \langle\psi|O_i\rangle \langle O_i|\psi\rangle$. Contrary to classical physics, a measurement also influences the state of the system itself. Indeed, after a measurement with outcome λ_i, the state of the system has changed to $|O_i\rangle$. Schematically, we can represent a measurement as

$$|\psi\rangle \xrightarrow{p_i = \langle O_i|\psi\rangle^2} \begin{cases} \text{outcome of the measurement} & : \lambda_i \\ \text{state after the measurement} & : |O_i\rangle \end{cases} . \tag{1}$$

It is now easy to show that the average outcome of a measurement is $\sum_i p_i \lambda_i = \langle\psi|O|\psi\rangle$.

One particularly important observable is the Hamiltonian $\hat{H}$ that can be used to measure the energy of a state, but also generates its time evolution according to the Schrodinger equation

$$i\frac{\mathrm{d}}{\mathrm{d}t}|\psi(t)\rangle = \hat{H}|\psi(t)\rangle \leftrightarrow |\psi(t)\rangle = e^{-i\hat{H}t}|\psi(t=0)\rangle . \tag{2}$$

Note that this means that the expected value of any measurement remains constant under time evolution for states that satisfy $H|\psi(t)\rangle = E|\psi(t)\rangle$, we can therefore call such states stationary solutions of the schrodinger equation.

1.1.1 A spinning electron: the Stern Gerlach experiment

Before accepting these strange postulates, let us at try to come up with some experiment that motivates their validity. The setup of the experiment is shown in figure 1 and consists of some hot electrons that are sent through a magnetic field $\vec{B} = z\vec{e}_z$ and then hit a screen at the right.

If we interpret these electrons as tiny spinning charged balls they will have some magnetic dipole proportional to their angular momentum $\vec{L}$ so that they will feel a force $F_z \propto L_z \partial_z(B_z)$ that accelerates them up or downwards by an amount proportional to L_z, their rotation speed around the z-axis. The upshot is that we can measure the rotation speed of the electron along the z-axis by looking at its final position when it hits the screen. For hot electrons, we expect random spins and consequently random upward acceleration, so that they should be hitting the screen at all possible locations highlighted in red in the figure. However, if this experiment is performed we find that the electrons only end up in the two green spots which means that the measured electron spin can only take on two discrete values.

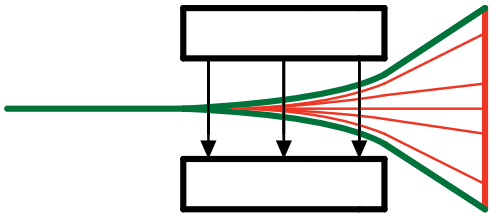

Figure 1: Hot electrons are shot through through a uniformly changing magnetic field before they hit a screen. The classical and quantum predictions for their paths are respectively shown in red and green. In reality we only observe the green result.

The solution to this discrepancy is to interpret the electron spin as a quantum degree of freedom. To do this let us consider the Hilbert space that is spanned by two mutually orthogonal vectors

$$|\uparrow\rangle = \begin{bmatrix} 1 \\ 0 \end{bmatrix} \quad \text{and} \quad |\downarrow\rangle = \begin{bmatrix} 0 \\ 1 \end{bmatrix} \tag{3}$$

so that we have the states

$$|\psi(\alpha,\beta)\rangle = \sum_{i\in\{\uparrow,\downarrow\}} \psi_i |i\rangle = \alpha|\uparrow\rangle + \beta|\downarrow\rangle = \begin{bmatrix} \alpha \\ \beta \end{bmatrix} \qquad \text{with} \qquad |\alpha|^2 + |\beta|^2 = 1\,. \tag{4}$$

Furthermore, we define operators

$$\begin{aligned} \sigma_x &= \begin{bmatrix} 0 & 1 \\ 1 & 0 \end{bmatrix} & \sigma_y &= \begin{bmatrix} 0 & -i \\ i & 0 \end{bmatrix} & \sigma_z &= \begin{bmatrix} 1 & 0 \\ 0 & -1 \end{bmatrix} \\ &= |\uparrow\rangle\langle\downarrow| + |\downarrow\rangle\langle\uparrow| & &= -i|\uparrow\rangle\langle\downarrow| + i|\downarrow\rangle\langle\uparrow| & &= |\uparrow\rangle\langle\uparrow| - |\downarrow\rangle\langle\downarrow| \end{aligned} \tag{5}$$

and postulate that these can be used to measure the spin of our electron, up to some constant, along the x,y and z axis respectively. The second postulate then learns us that the outcome of measurements of the z-component of the electron spin must be ± 1, up to that constant, as is observed in the experiment.

Finally, to fully appreciate the weirdness of quantum mechanics, let us consider the a setup where the electrons first move through a a magnetic field in the z-direction, then the upper beam moves through a magnetic field in the x-direction and finally the left beam goes through a magnetic field in the z-direction. By the time the electrons hit the third magnetic field we have already measured their z-spin in the first magnet, so we would expect to observe a single spot. However, once again we see two spots of equal brightness. To understand, or at least reproduce this result, let us carefully apply the measurement postulate. After the first magnet we know that the state must be $|\uparrow\rangle$. However, the second gate measured $\mu_x = +1$ so that the post measurement state is the eigenvector of σ_x with positive eigenvalue $+1$: $|\odot\rangle = \frac{1}{\sqrt{2}}\begin{bmatrix}1 & 1\end{bmatrix}^T = \frac{1}{\sqrt{2}}\left(|\uparrow\rangle + |\downarrow\rangle\right)$ and the outcomes of the last measurement of the z-component will be $+1$ / -1 with respective probabilities $\langle\uparrow|\odot\rangle^2$ and $\langle\downarrow|\odot\rangle^2$ that are both $1/2$ thus explaining the outcome of the experiment.

1.1.2 Many spinning electrons: spin chains

Now that we know how to apply these postulates to a single electron, let us take a look at the more interesting case where there are many electrons placed in long one dimensional chains. States in this system live in the tensor product space of all the individual local Hilbert spaces and for a chain of length L they can be written as

$$|\psi\rangle = \sum_{i_1,i_2,\cdots i_L \in \{\uparrow,\downarrow\}} \psi_{i_1,i_2,\cdots i_L} |i_1\rangle \otimes |i_2\rangle \otimes \cdots |i_L\rangle$$
$$\sum_{i_1,i_2,\cdots i_L \in \{\uparrow,\downarrow\}} |\psi_{i_1,i_2,\cdots i_L}|^2 = 1 \tag{6}$$

where the $\psi_{i_1,i_2,\cdots i_L}$ tensor has one index per electron in the chain. The reason that we are interested in such spin chains is because large systems are often much more interesting than their individual building blocks due to the phenomenon of emergence. For example, even though the behaviour of a single isolated human is quite boring, when many humans are together we get emergent phenomena such as cities, traffic, politics etc. which cannot be understood in terms of the individual humans.

1.2 Tensor networks

To situate this section let us first note that the total number of degrees of freedom in these spin chain wavefunctions is $\dim(\psi) = 2^L - 1$ and that this becomes extremely large as L grows. In fact, storing the wavefunction of a 37 site spin chain already requires 1 terabyte of storage and even more alarmingly simply increasing the length to 38 sites already doubles the required storage to 2 terabyte ! Furthermore, finding the wavefunction which has the lowest possible expectation value for the energy (i.e. find $|\psi\rangle$ so that $\langle\psi|\hat{H}|\psi\rangle$ is minimal) w.r.t. some Hamiltonian amounts to optimizing a function with 2^{L-1} parameters which, for $L > 40$ is sure to crash almost any computer! One possible solution, that is the topic of this section, is to constrain the optimization problem to a smaller class of wavefunctions that contain less parameters and are therefore more manageable.

1.2.1 Matrix product states

To find and motivate our ansatz, let us first remember that a general tensor T_{ij} can always be rewritten as its QR decomposition

$$T_{ij} = \sum_{\alpha \in 1:\min(\dim(i),\dim(j))} Q_{i\alpha} R_{\alpha j} \tag{7}$$

where Q is left orthogonal, i.e. $\sum Q^*_{kj} Q_{ki} = \delta_{ij}$. Furthermore, for later convenience, we rewrite the wavefunction $\psi_{i_1,i_2,\cdots i_L}$ as

$$\psi_{i_1,i_2\cdots i_N} = [B_l]_{\alpha_1} \psi_{\alpha_1,i_1,i_2\cdots i_N,\alpha_{N+1}} [B_r]_{\alpha_{N+1}} \tag{8}$$

where $B_l = B_r = [1]$ and $\psi_{1,i_1,i_2\cdots i_N,1} = \psi_{\alpha_1,i_1,i_2\cdots i_N,\alpha_N}$.

If we now perform a QR decomposition of $\psi_{\alpha_1,i_1,i_2\cdots i_N,\alpha_N}$ with $i = \{\alpha_1, i_1\}$ and $j = \{i_2, \cdots i_N, \alpha_{N+1}\}$ we get

$$\psi_{\alpha_1,i_1,i_2\cdots i_N,\alpha_N} = Al_{\alpha_1,i_1,\alpha_2}\psi_{\alpha_2,i_2,i_3,\cdots i_N,\alpha_{N+1}} \tag{9}$$

and this procedure can be iteratively repeated, always taking $i = \{\text{the first two indices}\}$ and $j = \{\text{all other indices}\}$, until we obtain

$$\begin{aligned}\psi_{\alpha_1,i_1,i_2\cdots i_N,\alpha_N} &= Al_{\alpha_1,i_1,\alpha_2}Al_{\alpha_2,i_2,\alpha_3}\psi_{\alpha_3,i_3,i_4,\cdots,i_N,\alpha_{N+1}} \\ &= \cdots \\ &= Al_{\alpha_1,i_1,\alpha_2}Al_{\alpha_2,i_2,\alpha_3}\cdots\psi_{\alpha_N,i_N,\alpha_{N+1}}\end{aligned} \tag{10}$$

which is now in terms of smaller 3-leg tensors that each have one "physical" leg and two "bond" legs that communicate with neighbouring tensors. Nevertheless, this trick did not reduce the complexity of the state because the dimension of the internal leg grows as $2^{(\text{distance to the edge of the chain})}$ so that these tensors are still impractically large if the length of the chain is long enough to be interesting. Therefore, to get a useful ansatz we enforce that the bond dimensions of the 3-leg tensors remains below some threshold which leads to the ansatz

$$\psi_{MPS;i_1,\cdots i_N}(\{A_n \hat{=} A_{\alpha_n,i_n,\alpha_{n+1}}\}) = [B_l]_{\alpha_1}A_{\alpha_1,i_1,\alpha_2}A_{\alpha_2,i_2,\alpha_3}\cdots A_{\alpha_N,i_N,\alpha_{N+1}}[B_r]_{N+1} \tag{11}$$

that depends on the set of N distinct A_n tensors with dimension strictly below $D \times 2 \times D$, the total number of parameters is now $L \times D \times 2 \times D$ which scales only linearly with the length of the chain. One big advantage of this ansatz is that we can use it to describe infinitely long spin chains with a finite number of parameters by imposing some repeating pattern onto the $\{A_n\}$, for example in the case of a one-site unit cell we get

$$\psi_{MPS}(A) = \cdots A_{\alpha_{n-1},i_{n-1},\alpha_n}A_{\alpha_n,i_n,\alpha_{n+1}}A_{\alpha_{n+1},i_{n+1},\alpha_{n+2}}\cdots \tag{12}$$

which now only depends on a single tensor A with dimension $D \times 2 \times D$. Note that this no longer contains the boundary tensors B_l and B_r because they are moved to infinity.

Finally, before we move on to analyse these matrix product states, let us first introduce some graphical notation that will greatly simplify everything that follows. In this notation, We represent N-index tensors as a box with N-legs sticking out, for example a 2-leg tensor A_{ij} is drawn as

$A_{ij} =$ 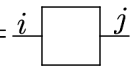

(13)

and its contraction with another 2-leg tensor is

$\sum_\alpha A_{i\alpha}B_{\alpha j} =$ 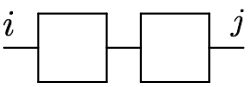

. (14)

With this notation our matrix product 12 state become :

$\psi_{MPS}(A) =$ 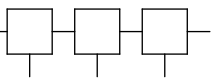
. (15)

Gauge fixing and expectation values

The first important property of the infinite matrix product states is that there is some freedom in the choice of the local tensor A. Indeed, for any invertable tensor T the matrix product states

$$\psi_{MPS}(A) \qquad \text{and} \qquad \psi_{MPS}(TAT^{-1}) \tag{16}$$

generate identical wavefunctions $\psi_{i_1,\cdots i_N}$. Such freedom is called a gauge freedom and we can use it to enforce some additional useful properties onto the local A tensors. In particular, we could try to find a gauge transformation L so that the new tensor

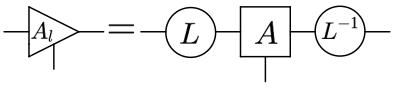

(17)

is left orthogonal, a property that we can graphically depict as

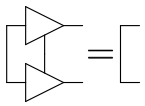

(18)

From a numerical perspective we can always find this Al by first constructing some initial guess L_{guess} (this could be any random tensor) and then performing a QR decomposition on the $L_{guess}A$ tensor i.e.

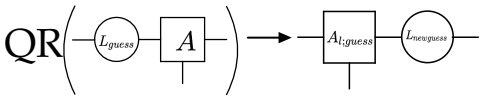

(19)

From this first step we get some guess for Al and a new, hopefully better, guess for the gauge transformation L. This new guess can then be used to re-iterate the algorithm and if it converges we have found our Al and L. Similarly, we can always find a gauge transformation R such that

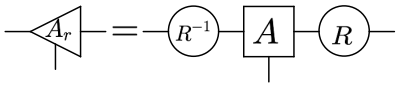

(20)

with

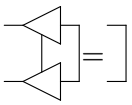

(21)

through a similar algorithm based on the RQ decomposition.

Finally, note that if such gauge fixings are found, we can additionally define $LAR = A_c$ and $C = LR$ and gauge fix the matrix product state in the so called mixed representation

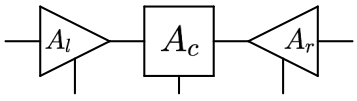

(22)

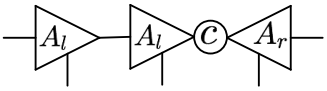

(23)

where the position of the A_c or C is arbitrary because the mixed gauge tensors satisfy

$$AlC = A_c = CAr\,. \tag{24}$$

A final gauge fixing is that C can always be made diagonal by absorbing the required unitaries (coming from the singular value decomposition of C) into the A_l and A_r.

Local observables and two point functions

The upshot of all this gauge fixing is that expectation values of local one site observables, computed in the center gauge, are

$\langle\psi|O|\psi\rangle =$ 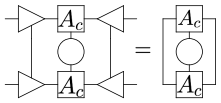 (25)

where we used the left and right orthogonality conditions of the gauge fixed tensors to "collapse" the part of the network that does not contain any operators. Note that this implies that the A_c tensor alone must contain all the local information about the state.

Furthermore, it is also often interesting to look at the two point function of some operator O :

$$\begin{aligned} C(O)_{n,m} &= \langle \quad (O_n - \langle O_n\rangle)(O_m - \langle O_m\rangle) \quad \rangle \\ &= \langle O_n O_m\rangle - \langle O_n\rangle \langle O_m\rangle \end{aligned} \tag{26}$$

where the subscripts n and m signify sites of the lattice. The physical motivation behind this object is that it tells us how much a measurement of O at site m will influence a later measurement of that operator at site n. In particular if $C_{n=m} = \langle (O - \langle O\rangle)^2\rangle = 0$ we have that the outcome of a measurement of O is predetermined so that, for this particular observable, these states behave like classical states would. In terms of our center gauged representation we get :

$C_{n,m} =$ 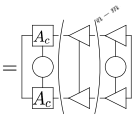 $- \langle O_n\rangle \langle O_n\rangle$. (27)

To proceed we expand the transfer matrix $T^{\alpha_1,\alpha_2}_{\beta_1,\beta_2} = \sum_i Ar_{\beta_1,i,\beta_2} Ar^*_{\alpha_1,i,\alpha_2}$ in terms of its left and right eigenvectors

$T^{\alpha_1,\alpha_2}_{\beta_1,\beta_2} =$ 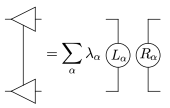 , (28)

which upon insertion into expression 27 gives

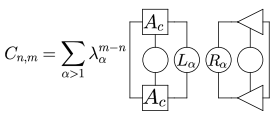 . (29)

Note that the term with $\alpha = 1$ does not appear due to the fact that $(\lambda_1, L_1, R_1) = (1, \mathbf{1}, C^2)$ so that it neatly cancels with $\langle O_n\rangle \langle O_m\rangle$. For large separations the term with the largest λ_α dominates and we get

$$\begin{aligned} C(O)_{n,m} &\propto \lambda_2^{m-n} \\ &\propto e^{-(m-n)\log(1/\lambda_2)} \end{aligned} \tag{30}$$

which shows us that correlations of measurements in quantum states represented by matrix product states decay on length scales of the order

$$\xi_{MPS} = \log(1/\lambda_2)\,. \tag{31}$$

We call this the correlation length, and note that we have found that its long distance behaviour does not depend on the operator of choice, but only on the state itself.

Entanglement entropy

Another important concept in quantum many body physics is the entanglement entropy of a state. To arrive at this concept and see why it can be helpful, let us consider an observer that can only perform measurements on a part of the chain. In particular, we will be interested in observers that can only look at the right half of a spin chain. For such observers all accessible information will be of the form

$$\langle O_{obs}\rangle = \sum_i c_i^2 \,\langle \psi_{R_i;MPS}(Ar)|O_{obs}|\psi_{R_i;MPS}(Ar)\rangle \tag{32}$$

where we have introduced the singular values c_i of the C tensor and a set of states

$$|\psi_{R_i;MPS}(Ar)\rangle =_i \; ArArArArAr \tag{33}$$

that satisfy $\langle \psi_{R_i;MPS}(Ar)|\psi_{R_j;MPS}(Ar)\rangle = \delta_{ij}$. The interpretation of this is that the expected outcome of a measurement for a local observer is according to the classical probability distribution

$$\text{probability}_i = c_i^2 \qquad \text{with} \qquad \text{outcome}_i = \langle \psi_{R_i;MPS}(Ar)|O_{obs}|\psi_{R_j;MPS}(Ar)\rangle \tag{34}$$

to which we can associate an entropy

$$S = -\sum_i p_i \log(p_i) = -\sum_i c_i^2 \log(c_i^2)\,. \tag{35}$$

In our context this entropy can be interpreted as a measure for the uncertainty in measurement outcomes on the right half of the chain due to its coupling with the left half.

Energy Optimization

Up to now we have been studying properties of fixed matrix product states. However, to really make this ansatz relevant we must find an algorithm that helps us find the MPS that minimizes the expectation value of a Hamiltonian

$$H = \sum_{n\in lattice} H_n \tag{36}$$

that is the sum of local interactions H_n. To proceed, it is worth noting that such operators can always be represented as a product of local 4-leg tensors

$H =$ 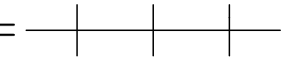 . (37)

Such operators are called matrix product operators and they form an active research topic by themselves. Here however, we will simply use them as a simple graphical trick to represent the infinite sum of local contributions. As an example, the MPO tensor

α 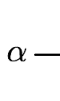 β $= \begin{bmatrix} 1 & -g\sigma_z & \sigma_x \\ 0 & 0 & \sigma_z \\ 0 & 0 & 1 \end{bmatrix}_{\alpha\beta}$ (38)

represents the sum of local terms $H = \sum_{n \in lattice} -g\sigma_{z,n}\sigma_{z,n+1} + \sigma_{x,n}$ which is a Hamiltonian that we will study in the next chapter. To see that this is true let us multiply two such matrices

$$\begin{bmatrix} 1 & -g\sigma_z & \sigma_x \\ 0 & 0 & \sigma_z \\ 0 & 0 & 1 \end{bmatrix}_n \begin{bmatrix} 1 & -g\sigma_z & \sigma_x \\ 0 & 0 & \sigma_z \\ 0 & 0 & 1 \end{bmatrix}_{n+1} = \begin{bmatrix} 1_n 1_{n+1} & -g 1_n \sigma_{z,n+1} & 1_n \sigma_{x,n+1} + \sigma_{x,n} 1_{n+1} - g\sigma_{z,n}\sigma_{z,n+1} \\ 0 & 0 & \sigma_{z,n+1} 1_n \\ 0 & 0 & 1_n 1_{n+1} \end{bmatrix} \tag{39}$$

and observe that the topright element of this tensor (that now acts on two physics sites) is exactly the two-site Ising Hamiltonian. Further multiplication with the MPO tensor then leads to the N-site Ising Hamiltonian appearing in the topright corner. With this matrix product representation the expectation value of the energy becomes

$\langle \psi_{MPS}|H|\psi_{MPS}\rangle = \cdots$ 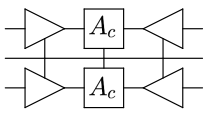 $\cdots = \cdots$ 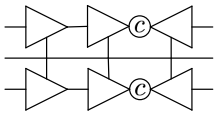 $\cdots .$ (40)

To proceed, let us assume that there exist H_l and e so that

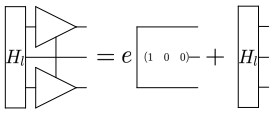 (41)

where the first tensor on the right-hand side is the left fix point of the state, MPO transfer matrix. Together with a similar expression for H_r in terms of the right fix point we then get

$\langle \psi_{MPS}|H|\psi_{MPS}\rangle =$ 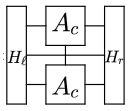 $+ (L-1)e =$ 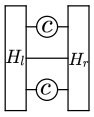 $+ Le\,.$ (42)

which, not surprisingly, diverges in the limit $L \leftrightarrow \infty$.

Nevertheless, we can still interpret the non divergent terms in this formula as a local energy density and try to optimize those. To do this we momentarily relax the gauge fixing conditions from equation 24 and reinterpret the A_C and c tensors as independent variables. With this assumption it is easy to find the $A_{c;opt}$ and c_{opt} that optimize the energy and from those we get two matrix product states

$$...AlAlAlA_{c;opt}ArArAr... \qquad \text{and} \qquad ...AlAlAlC_{opt}ArArAr... \tag{43}$$

that are no longer invariant under translations but nevertheless have lower energy then the initial state $\psi_{MPS}([A_l, A_r, A_c]_{\text{gauge fixed}})$. To proceed we try to find $A_{l;opt}$ that can be used to construct a new translation invariant state

$$A_{l;opt}Al_{l;opt}Al_{l;opt}Al_{l;opt}Al_{l;opt} \tag{44}$$

which could then be brought into the center gauged representation so that the first step could be repeated until convergence. Naively, we could simply take new $A_{l;opt} = A_{c;opt}C_{opt}^{-1}$ but this choice is not guaranteed to be left orthogonal. Instead we try to find left orthogonal $A_{l;opt}$ so that :

$$\epsilon_L \hat{=} ||A_{c;opt} - A_{l;opt}C_{opt}||^2 \tag{45}$$

is minimal. Luckily the solution to this kind of matrix optimization problem is well known to be $A_{l;opt} = U^l V^{l,\dagger}$ where U^l, $V^{l,\dagger}$ are the isometries in the singular value decomposition of $A_{c;opt}C_{opt}^{\dagger}$. As said, we can now reiterate this algorithm until converged in which case we have found a state for which the energy cannot be lowered by making local changes. One important subtlety is that this

algorithm is not guaranteed to converge towards the lowest energy eigenstate, in fact, it is not even guaranteed to converge at all. However, in practice the algorithm seems sufficiently robust to tackle the problems presented in this thesis.

Finally, to find this e and H_l let us first define the projector

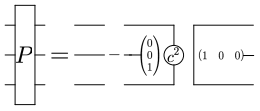

(46)

and instead find the solution to

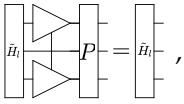

(47)

which no longer depends on e and is therefore a is simple linear problem that can be solved numerically with the generalized minimal residual method or similar. The solution of the original problem is then $H_l = \tilde{H}_l$ with

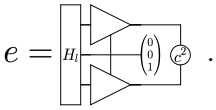

(48)

1.2.2 Quasi particle states

Let us now try to use the tensor network idea to create a suitable ansatz for excited states of a Hamiltonian. At first glance, we might want to re-use the matrix product states, but the optimization algorithm for these states is only suited to find the groundstate. We could circumvent this by adding a Lagrange multiplier, imposing orthogonality to the groundstate, to the cost-function but this becomes unpractical for higher excited states[1]. Instead we will use the intuition that excitations typically only differ from the groundstate on a small number of sites so that they may be well described by states of the form

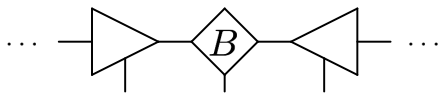

(49)

where the left and right isometries represent the groundstate. Furthermore, expressing this Ansatz in momentum space gives

$$|B_p\rangle = \sum_n e^{ipn}$$

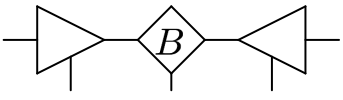

(50)

which, similarly to the matrix product states, have some gauge freedom that is given by

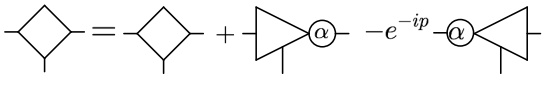

(51)

[1] In fact this would even be ill defined in the thermodynamic limit.

We can use this freedom to find impose orthogonality of B and A_l i.e.

$$0 =$$ 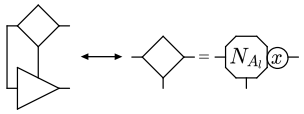 (52)

where N_{A_l}, x are respectively the nullspace of A_l and the remaining gauge invariant information that uniquely parameterizes the excitation. The final, gauge fixed ansatz for the excitations is therefore

$$|x_p\rangle = \sum_n e^{ipn}$$ 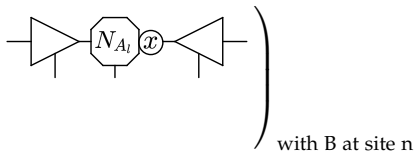 with B at site n (53)

and this state is by construction orthogonal to the groundstate. Furthermore, it is easy to check that, due to this gauge fixing

$$\langle x_p | y_k \rangle = 2\pi\delta(p-k)\ tr(x * y)\,. \tag{54}$$

Energy optimization

Now that we have a smart ansatz for excited states, let us consider its energy

$$\langle B_p|H|B_p\rangle = \sum_{n,\,m} e^{ip(n-m)}$$ 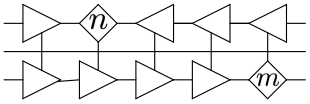 . (55)

To simplify, note that this contains three types of terms where the upper B is respectively left, right or on the same site as the lower B, grouping these terms gives us

$$\langle B_p|H|B_p\rangle = \underbrace{(\sum_n e^{ipn})}_{L_{chain}}$$ 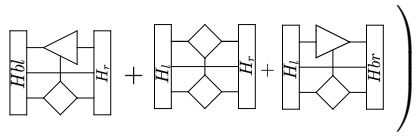 (56)

which is in terms of the H_l, H_r tensors from equation 41 and two new tensors Hl_l and Hb_r that are defined as :

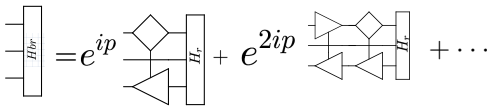 (57)

and similarly for Hbl. To extract the actual Hbr tensor from this we first rewrite this equation as

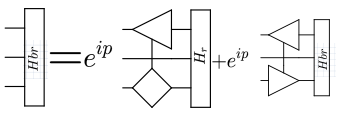 (58)

and note that is a simple linear problem of the form $Hbr = a + b\ Hbr$ with solutions that are easily obtained through numerical methods such as using the generalized minimal residual method (i.e. GMRES).

Finally, optimizing $\frac{1}{L_{chain}} \frac{\langle B_p|H|B_p\rangle}{\langle B_p|B_p\rangle}$ leads to the eigenvalue problem

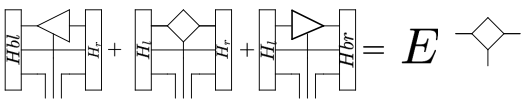 (59)

where in fact B should be interpreted as $N_{A_l} x$ with x the degrees of freedom that are to optimized.

Note that this algorithm must not be iterated so that it is in principle relatively cheap to find these excited states given the groundstate. Furthermore, higher excited states are easily found by probing different momenta which immediately results in orthogonal states.

1.2.3 Symmetries in quantum mechanics and tensor networks

In the remainder of this thesis we will often encounter scenarios where we want to consider wavefunctions that are symmetric under the action of elements g from a symmetry group G [2] i.e. $\forall g \in G : g \cdot |\psi\rangle = |\psi\rangle$. In particular, we will be interested in so called local symmetry groups of the form

$$\begin{aligned} \hat{g} &= \bigotimes_{n \in \text{lattice}} \hat{g}_{local} \\ &= \bigotimes_{n \in \text{lattice}} \left(\sum_{i,j \in \{\uparrow,\downarrow\}} U(g)_{i,j} \left|i_n\right\rangle \left\langle j_n\right| \right) \end{aligned} \tag{60}$$

where the set $\{U(g)_{i,j}\}$ satisfies the group properties under matrix multiplication. Furthermore, because of Maschke's theorem, we can always write g_{local} as a direct sum of irreducible group elements $D_{l,phys}$ with possible degeneracy d_l

$$g_{local} = \bigoplus_{l \in irreps} D_{l,phys}(g)^{d_l} \tag{61}$$

i.e. there exists a basis $\{|l, m, \alpha\rangle : l \in irreps, m = 1, \cdots, \dim(l_{th}\ irrep), \alpha = 1, \cdots, d_l\}$ where the representations of the group elements are all block diagonal. [3]

If we express the symmetry condition, $\otimes^{n \in \text{lattce}} \hat{g}_{local} \cdot |\psi\rangle = |\psi\rangle$ in terms of matrix product states we get

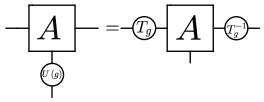

(62)

where, for the second equation, we used the fact that the states $\psi_{MPS}(A)$ and $\psi_{MPS}(AU(g))$ are equal if and only if their local tensors are related by a gauge transformation $T(g)$. Furthermore, because $U(g)U(h) = U(gh)$, we must also have that $T_g T_h = T_{gh}$ such that these gauge transformations must also be a representation of the group[4] so that they are also block diagonal in basis that we will label $\{|l_\alpha, m_\alpha, \alpha\rangle : l \in \text{virtual irreps}, m = 1, \cdots, dim(l_{alpha}), \alpha = 1, \cdots, d_{l_\alpha}\}$.

With this labeling for the physical and virtual levels we get

$$A = \sum_{\substack{l_\alpha, m_\alpha, \tilde{\alpha} \\ l_i, m_i, \tilde{i} \\ l_\beta, m_\beta, \tilde{m}}} \left|l_\alpha, m_\alpha, \tilde{\alpha}\right\rangle \left|l_i, m_i, \tilde{i}\right\rangle \left\langle l_\beta, m_\beta, \tilde{\beta}\right| A^{\substack{l_\alpha, m_\alpha, \tilde{\alpha} \\ l_i, m_i, \tilde{i} \\ l_\beta, m_\beta, \tilde{m}}} \tag{63}$$

and because of the Winger-Eckard theorem

$$A^{\substack{l_\alpha, m_\alpha, \tilde{\alpha} \\ l_i, m_i, \tilde{i} \\ l_\beta, m_\beta, \tilde{m}}} = \left\langle l_\beta, m_\beta, \tilde{\beta}\right| A \left|l_\alpha, m_\alpha, \tilde{\alpha}\right\rangle \left|l_i, m_i, \tilde{i}\right\rangle \tag{64}$$

[2] A group G is a set of elements $\{g\}$ and a rule $\cdot$ for combining them so that (1) $\forall g, h \in G : g \cdot h \in G$ (2) $\exists\, 1 \in G$ *s.t.* $\forall g \in G : 1 \cdot g = g \cdot 1 = g$ (3) $\forall g \in G\ \exists\, h \in G$ *s.t.* $g \cdot h = 1$. For example, the set $\{1_{2\times 2}, \sigma_x\}$ form a group under matrix multiplication. Another, more complicated, example is the set $\{e^{i\phi\sigma_x} : \forall \phi\}$ which again forms a group under matrix multiplication.

[3] For the examples in the previous footnote this is the basis where σ_x is diagonal i.e. $\{|+\rangle, |-\rangle\}$ and to make the connection with the main text we simply relabel these as $\{|l = +\rangle, |l = -\rangle\}$. Note that we do not need the m and α here.

[4] In fact it is sufficient that $T_g T_h = e^{i\omega(g,h)} T_{gh}$ for some collections of phases $\omega(g, h)$ so that T_g may be a projective representation of the group.

this can be written as

$$A^{\substack{l_\alpha,m_\alpha,\tilde{\alpha} \\ l_i,m_i,\tilde{i} \\ l_\beta,m_\beta,\tilde{m}}}_{\substack{l_\alpha,\tilde{\alpha} \\ l_i,\tilde{i} \\ l_\beta,\tilde{\beta}}} = A^{reduced}_{\substack{l_\alpha,\tilde{\alpha} \\ l_i,\tilde{i} \\ l_\beta,\tilde{\beta}}} \langle l_\beta, m_\beta | l_\alpha, m_\alpha; l_i, m_i \rangle \ . \tag{65}$$

Here $\langle l_\beta, m_\beta | l_\alpha, m_\alpha; l_i, m_i \rangle$ is a Clebsch-Gordan coefficient that encodes the structure of the group, the $A^{reduced}$ tensors, which no longer depends on the internal indices, contains all remaining free variational parameters.

Up to now this section was very theoretical because we kept the group G undefined, in the following sections we will study some examples to gain some intuition for the implications of our analysis.

Example : Z_2 symmetry

Let us start with the simplest symmetry group which contains only the identity and the spin flip (i.e. $G_{local} = \{1, \sigma_x\}$) which gives us two symmetry constraints

$$|\psi\rangle = |\psi\rangle \qquad \text{and} \qquad \otimes^{n \in \text{lattice}} \sigma_{x,n} |\psi\rangle = |\psi\rangle \ . \tag{66}$$

Note that the second condition clearly eliminates some degrees of freedom from the state because, for example, the coefficients $\psi_{\uparrow,\uparrow,\cdots,\uparrow}$ and $\psi_{\downarrow,\downarrow,\cdots,\downarrow}$ in Eq. 6 must be the same. To see how this observation follows from our more general framework, let us first note that the representation of our group in the $\{|+\rangle = |l=0\rangle, |-\rangle = |l=-1\rangle\}$ basis is

$$U_{g=1} = \begin{bmatrix} 1 & 0 \\ 0 & 1 \end{bmatrix} \qquad \text{and} \qquad U_{g=\sigma_x} = \begin{bmatrix} 1 & 0 \\ 0 & -1 \end{bmatrix} \ . \tag{67}$$

Similarly, on the virtual level our T_g must be built from the irreducible representations $[1] = D_{l=0}(g=1) = D_{l=0}(g=\sigma_x) = D_{l=-1}(g=1) = -D_{l=-1}(g=\sigma_x)$ which means that, in the right basis $|l, \alpha\rangle$, the T_g tensors will be of the form

$$T_{g=1} = \begin{bmatrix} 1_{d_0 \times d_0} & \\ & 1_{d_{-1} \times d_{-1}} \end{bmatrix} \qquad \text{and} \qquad T_{g=\sigma_x} = \begin{bmatrix} 1_{d_0 \times d_0} & \\ & -1_{d_{-1} \times d_{-1}} \end{bmatrix} \tag{68}$$

with d_0 and d_{-1} the multiplicity of the trivial (i.e. charge zero) and nontrivally (i.e. charge -1) transforming basis vectors.

With these representations, it is now clear that, Eq. 62 can only be satisfied if the A tensor is of the form

$$A_{\alpha,0,\beta} = \begin{bmatrix} A^{reduced}_{d_{triv} \times d_{triv}} & 0 \\ 0 & A^{reduced}_{d_{nontriv} \times d_{nontriv}} \end{bmatrix} \qquad \text{and} \qquad A_{\alpha,-1,\beta} = \begin{bmatrix} 0 & A^{reduced}_{d_{triv} \times d_{nontriv}} \\ A^{reduced}_{d_{nontriv} \times d_{riv}} & 0 \end{bmatrix} \tag{69}$$

which is consistent with Eq. 65 if $\langle l_\beta | l_\alpha; l_i \rangle = \delta_{l_\beta + l_i, l_\alpha}$. From a numerical point of view this is great because we can now represent these tensors as sparse matrices which requires less storage space and avoids needless multiplications of zero times something.

Example : $U(1)$ symmetry

For this example we will work with the slightly more complicated $U(1)$ group $G_{local} = \{e^{i\phi\sigma_x} : \forall \phi\}$. In the $\{|+\rangle = |l=1\rangle, |-\rangle = |-1\rangle\}$ basis, the local action of this group is represented by the matrices

$$U(\phi) = \begin{bmatrix} e^{i\phi} & 0 \\ 0 & e^{-i\phi} \end{bmatrix} \tag{70}$$

which is indeed in terms of the $U(1)$ irreps $\{D_l(\phi) = [e^{il\phi}] \ \forall \ l \in \mathbb{Z}\}$. Similarly any gauge transformation must be built from these irreps and in the $|l, \alpha\rangle$ basis they are of the form

$$T(\phi) = \begin{bmatrix} \ddots & & & & & & & & \\ & e^{-2i\phi}1_{d_{-2}\times d_{-2}} & & & & & & & \\ & & e^{-i\phi}1_{d_{-1}\times d_{-1}} & & & & & & \\ & & & 1_{d_0\times d_0} & & & & & \\ & & & & e^{i\phi}1_{d_1\times d_1} & & & & \\ & & & & & e^{2i\phi}1_{d_2\times d_2} & & & \\ & & & & & & \ddots & & \end{bmatrix} \tag{71}$$

with d_l the multiplicity of the charge l sector. The conclusion is that A can only satisfy the symmetry constraint if

$$A_{\alpha,1,\beta} = \begin{bmatrix} \ddots & A_{red} & & & & & & \\ & 0_{d_{-2}\times d_{-2}} & A_{red} & & & & & \\ & & 0_{d_{-1}\times d_{-1}} & A_{red} & & & & \\ & & & 0_{d_0\times d_0} & A_{red} & & & \\ & & & & 0_{d_1\times d_1} & A_{red} & & \\ & & & & & 0_{d_2\times d_2} & A_{red} & \\ & & & & & & \ddots & \end{bmatrix} \tag{72}$$

and

$$A_{\alpha,-1,\beta} = \begin{bmatrix} \ddots & & & & & & & \\ A_{red} & 0_{d_{-2}\times d_{-2}} & & & & & & \\ & A_{red} & 0_{d_{-1}\times d_{-1}} & & & & & \\ & & A_{red} & 0_{d_0\times d_0} & & & & \\ & & & A_{red} & 0_{d_1\times d_1} & & & \\ & & & & A_{red} & 0_{d_2\times d_2} & & \\ & & & & & A_{red} & \ddots & \end{bmatrix} \tag{73}$$

which is of the proposed form if $\langle l_\beta | l_\alpha l_i \rangle = \delta_{l_\beta + l_i, l_\alpha}$. Note that, these tensors only couple even virtual charges to odd virtual charges and vice versa, we can represent this graphically as:

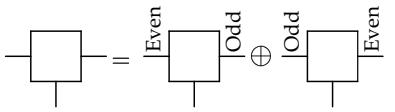

(74)

The contraction of these tensors into a state will lead to the equal weight superposition of two matrix product states with a larger unit cell

$$\psi(A) = $$

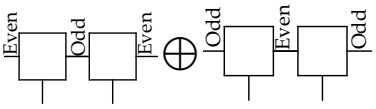

(75)

so that that injective $U(1)$ symmetric MPS cannot have a one site unit cell i.e. they must always break the translation symmetry.

2

SPIN CHAINS

The whole is greater than the sum of the parts.

Aristotle

In this chapter we will apply the postulates and MPS ansatz to study two spin chains : the Ising and Su-Schrieffer-Heeger model. We will see that these spin chains display complicated emergent behaviour, that leads to e.g. magnetisation, due to the entanglement between the different sites.

The first model is relatively simple, but nevertheless serves as a great example to apply the ideas of quantum mechanics to a concrete problem. Furthermore, in the first paper we studied a modification of the Ising model that introduces a new kind of symmetry with far reaching implications for the possible groundstates, hence the introduction of the model here.

The SSH is similarly simple but allows us to showcase some very nontrivial implications of certain symmetries. This is also the model that we built upon for the second and third papers contained in this work.

2.1 The transverse field Ising model

The Hamiltonian operator, for the quantum Ising model is given by

$$\hat{H} = \frac{1}{a} \sum_{n \in lattice} -g\hat{\sigma}_{z,n}\hat{\sigma}_{z,n+1} + \hat{\sigma}_{x,n} \tag{76}$$

where $\hat{\sigma}_{x,n}$, $\hat{\sigma}_{y,n}$ and $\hat{\sigma}_{z,n}$ are the Pauli matrices that measure the magnetic field for the individual spins and a is the distance between the points on the lattice. For positive g the interpretation of the first term is that neighbouring spins want to align their spins along the z direction. Similarly the second term makes it so that all spins want to align along the x direction[1]. The subtlety of the model is that $[\sigma_{z,n}\sigma_{z,n+1}, \sigma_{x,n}] \neq 0$ so that it is impossible to find states that simultaneously optimize both constraints. In general such inability to optimize different terms in a Hamiltonian is called frustration and we will see that it leads to interesting emergent behaviour when $g \approx \pm 1$.

2.1.1 Discrete symmetry and the breaking thereof

To start, let us note that both operators in the Z_2 group containing the identity and the spin flip along the x-direction

$$\hat{X} = \prod_{n \in \text{lattice}} \hat{\sigma}_{x,n} \tag{77}$$

commute with the Hamiltonian i.e. the group $G_{Z_2} = \{\hat{1}, \hat{X}\}$ is a symmetry of the Ising Hamiltonian. Consequently $\langle\psi|X|\psi\rangle = \langle\psi|e^{iHt}Xe^{-iHt}|\psi\rangle$ so that $\forall\,|\psi\rangle$ the expectation value of X is conserved throughout the time evolution generated by the Schrodinger equation. Furthermore, because $\langle\psi|H|\psi\rangle = \langle\psi|XHX|\psi\rangle$ we find that the states $|\psi\rangle$ and $X\,|\psi\rangle$ must have the same energy so that the

[1] More accurately, the expectation value of the first term will be low for states that have their spins aligned along the z direction. Similarly, the expectation value of th second term will be low for states with all spins pointing in the x-direction.

spectrum must either contain states that are symmetric under the spin flip operator or pairs of states that are mapped onto one another under the pin flip operator.

For example, when $g = 0$, the first term in the Hamiltonian vanishes and the Hamiltonian is no longer frustrated so that we can simply write down the state that optimizes all remaining terms in the Hamiltonian :

$$|\psi_{\odot}\rangle = \cdots |\odot\rangle\,|\odot\rangle\,|\odot\rangle\,|\odot\rangle\cdots \tag{78}$$

with $|\odot\rangle = \frac{1}{2}\left(|\uparrow\rangle + |\downarrow\rangle\right)$ the eigenvector of σ_x with negative eigenvalue (i.e the spin is "pointing" in the negative x-direction), the energy density of this state is $E(g=0)/L = e(g=0) = -1$. The low lying excitations, i.e. eigenstates of the Hamiltonian with energy just above that of the groundstate are obtained by flipping a single spin of the groundstate along the x-direction e.g.

$$|\psi_{\text{single flip}}\rangle = \hat{\sigma}_{z,2}\,|\psi_{\odot}\rangle = \cdots |\odot\rangle\,|\otimes\rangle\,|\odot\rangle\,|\odot\rangle\cdots \tag{79}$$

and such states carry some localized energy $E_{\text{single flip}} - E_{GS} = 2$ at the site where the spin was flipped. Note that all these state are mapped onto themselves by the action of the spin flip operator i.e. $\hat{X}\,|\psi\rangle = \lambda\,|\psi\rangle \;\; \forall\,|\psi\rangle \in$ (the spectrum of H) so that this spectrum is an example of a symmetric phase.

Similarly for $g \gg 1$ the first term in the Hamiltonian vanishes so that we can again simultaneously optimize all terms in the Hamiltonian. However, in this case we find that there exist two states

$$|\psi_{\uparrow}\rangle = \cdots |\uparrow\rangle\,|\uparrow\rangle\,|\uparrow\rangle\,|\uparrow\rangle\cdots \qquad \text{and} \qquad |\psi_{\downarrow}\rangle = \cdots |\downarrow\rangle\,|\downarrow\rangle\,|\downarrow\rangle\,|\downarrow\rangle\cdots$$

with lowest energy density $e(g \gg 1) = -g$ that are mapped onto each other by the action of the spin flip operator. Similarly, the low lying excitations come in pairs

$$|\psi_{\text{single kink}}\rangle = \left(\cdots \hat{\sigma}_{x,1}\hat{\sigma}_{x,2}\right)|\psi_{\uparrow}\rangle = \cdots |\downarrow\rangle\,|\downarrow\rangle\,|\uparrow\rangle\,|\uparrow\rangle\cdots \tag{80}$$

or

$$|\psi_{\text{single anti-kink}}\rangle = \cdots |\downarrow\rangle\,|\downarrow\rangle\,|\uparrow\rangle\,|\uparrow\rangle\cdots \tag{81}$$

with local energy cost $E_{\text{single kink or antikink}} - E_{GS} = 2g$. These states are also mapped onto one another by the action of the symmetry group. This phenomenon where the symmetry of the Hamiltonian is no longer present in its individual eigenstates is named spontaneous symmetry breaking and it plays a crucial role in the description of many physical processes throughout many fields.

To differentiate between these two types of behaviour it is useful to consider the so called ferromagnetic order parameter

$$O_{\text{ferromagnet}} = \langle\omega(g)|\sigma_{z,n}|\omega(g)\rangle \tag{82}$$

where $|\omega(g)\rangle$ is the groundstate at that coupling. This order parameter is zero (nonzero) in the symmetric (symmetry broken) regime respectively. Physically, a nonzero expectation value for this quantity implies that measurements of σ_z at different sites will tend to give a coordinated result, which means that our spin chin will have a macroscopic magnetic field that is pointing in the z-direction. In fact, Ising model was first introduced to explain the spontaneous magnetization of naturally occurring materials such as magnetite $(Fe^{2+}Fe_2^{3+}O_4)$.

2.1.2 Kink condensation and the restoration of symmetry

Let us now move away from these extremal points and look at large but finite couplings g. Here $|\psi_{\uparrow}\rangle$ is no longer an eigenstate of the Hamiltonian but it is fair to assume that we can Taylor expand the actual lowest energy eigenstate $|\omega\rangle$ and eigenvalue E_{ω} in terms of the small parameter $1/g$ i.e.

$$\begin{cases} |\omega\rangle & =^{up\ to}_{normalization} |\psi_{\uparrow}\rangle + \frac{1}{g}|\psi^{(1)}\rangle + \frac{1}{g^2}|\psi^{(2)}\rangle + \cdots \\ E_{\omega} & = -gL + E^{(1)} + \frac{1}{g}E^{(2)} + \cdots \end{cases}. \tag{83}$$

With these assumptions, and after neglecting small terms containing $1/g$, the eigenvalue problem $H|\omega\rangle = E_\omega|\omega\rangle$ becomes

$$\underbrace{\left(\sum_{n\in\text{lattice}} \sigma_{z,n}\sigma_{z,n+1}\right)|\psi^{(1)}\rangle}_{\substack{\text{large term in Hamiltonian}\\ \text{acts on}\\ \text{sought after correction of wavefunction}}} + \underbrace{\left(\sum_{n\in\text{lattice}} \sigma_{x,n}\right)|\psi_\uparrow\rangle}_{\substack{\text{small term in Hamiltonian}\\ \text{acts on}\\ \text{original wavefunction}}} = -L|\psi^{(1)}\rangle + E^{(1)}|\psi^{(\uparrow)}\rangle\,. \tag{84}$$

To proceed we project this equation onto the original groundstate $\langle\psi_\uparrow|$ and exited states

$$\langle k| \in \{\langle\psi_{\text{single kink or antikink}}|\,, \langle\psi_{\text{pairs of kinks and anti-kinks}}|\,, \cdots\}$$

which leads to

$$E^{(1)} = \langle\psi_\uparrow|\left(\sum_{n\in\text{lattice}} \sigma_{x,n}\right)|\psi_\uparrow\rangle \tag{85}$$

$$(E_k - L)\langle k|\psi^{(1)}\rangle = \langle k|\left(\sum_{n\in\text{lattice}} \sigma_{x,n}\right)|\psi_\uparrow\rangle\,. \tag{86}$$

so that

$$|\psi^{(1)}\rangle = \sum_{k\in\text{excited states of } H_0} |k\rangle\langle k|\psi^{(1)}\rangle = \sum_k \sum_{n\in\text{lattice}} \left(\frac{\langle k|\sigma_{x,n}|\psi_\uparrow\rangle}{\Delta E_k}\right)|k\rangle \tag{87}$$

where E_k is the original local energy of the $|k\rangle$ excitation compared to that of the groundstate.

The upshot is that, for small nonzero $1/g$, the groundstate becomes a quantum superposition containing all states $|k\rangle$ that can be reached by acting on the original groundstate $|\psi_\uparrow\rangle$ with a single σ_x operator; physically these are kink-antikink pairs with separation 1. As $1/g$ grows $|\psi^{(2)}\rangle$ will also become relevant and one can easily check that this correction contains all states that can be reached by acting on $|\psi_\uparrow\rangle$ with two σ_x operators i.e. the kink-antikink states with separation 2 and the states containing two kink-antikink pairs with separation 1. In general acting with subsequent σ_x, to generate the higher order terms that become relevant as $1/g$ grows, can either increase the distance of the already existing kink-antikinks or introduce a new separation one kink-antikink. The emerging picture is that the groundstate is no longer a simple product state and that measurements of $\sigma_{z,n}$ may also result in projection of the state onto one of these bubbles. This leads to a decrease in the order parameter.

Furthermore, because the correct groundstate is now a superposition of different product states, we get that knowledge of some part of the chain results affects later measurements of the remaining part. For example, if we measure a kink between sites n and $n+1$ we know that the remaining part of the chain must contain an antikink somewhere[2]. Consequently the entropy of these states will increase as $1/g$ grows larger.

2.1.3 Analytical solution

Finally, for completeness let us try to find the spectrum of H at general couplings. To do this, we first redefine our coordinate system so that

$$\sigma_{x,n} \to \sigma_{z,n} \qquad \text{and} \qquad \sigma_{z,n} \to -\sigma_{x,n}$$

and the Hamiltonian becomes

$$H = \sum_{n\in\text{lattice}} -\sigma_{x,n}\sigma_{x,n+1} - g\sigma_{z,n}\,. \tag{88}$$

[2] This is true because every $|k\rangle$ in 87 contains an even number of kink-antikink pairs.

Further re-expressing this in terms of the raising operator $\sigma_n^\dagger = \frac{1}{\sqrt{2}}\left(\sigma_{x,n} + i\sigma_{y,n}\right)$ and its Hermitian conjugate $\sigma_n^- \frac{1}{\sqrt{2}}\left(\sigma_{x,n} - i\sigma_{y,n}\right)$ gives

$$H = \sum_{n\in\text{lattice}} \left(\sigma_n^\dagger + \sigma_n^-\right)\left(\sigma_{n+1}^\dagger + \sigma_{n+1}^-\right) - g\left(2\sigma_n^\dagger\sigma_n^- - 1\right) \tag{89}$$

which is quadratic in the operators so that the different length scales will decouple after a Fourier transform. However, a naive Fourier transform $\sigma_k^\dagger = \sum_{n\in lattice} e^{-ikn}\sigma_n^\dagger$ of these raising and lowering operators is not favourable because these σ_k would not satisfy the usual fermionic $\{c_k^\dagger, c_l\} = 2\pi\ \delta_{k,l}$ or bosonic $[c_k^\dagger, c_l] = 2\pi\delta_{k,l}$ commutation relations that, as we will see, are crucial for the construction of eigenstates of H. The origin of this problem sits in the fact that the original spin degrees of freedom satisfy the fermionic commutation relations $\{c_m^\dagger, c_n\} = 1$ when $m = n$ but behave as bosons $[c_m^\dagger, c_n] = 0$ when $m \neq n$. To fix this problem, we add strings of σ_z tensors to the creation operators i.e.

$$c_n^\dagger = \left(\prod_{m<n} \sigma_{z,m}\right)\sigma_m^\dagger \tag{90}$$

so that the $c_n^\dagger$ now satisfy the fermionic commutation relations $\{c_n^\dagger, c_m\} = \delta_{n,m}$ for all n and m. In terms of these operators the Hamiltonian becomes

$$H = \sum_{n\in\text{lattice}} -\left(c_n^\dagger - c_n^-\right)\left(c_{n+1}^\dagger + c_{n+1}^-\right) - 2gc_n^\dagger c_n^- \tag{91}$$

and a Fourier transform in terms of $c_k^\dagger = \sum_{n\in\text{lattice}} e^{-ikn}c_n^\dagger$ leads to

$$H = \int_{-\pi}^{\pi} \frac{dk}{2\pi}\ \left(-2\left(g + \cos(k)\right)c_k^\dagger c_k + e^{ik}c_k c_{-k} + e^{-ik}c_{-k}^\dagger c_k^\dagger\right) \tag{92}$$

$$= \int_0^{\pi} \frac{dk}{2\pi}\begin{bmatrix} c_k^\dagger & c_{-k}\end{bmatrix}\underbrace{\begin{bmatrix} -2g(1+\cos(k)) & 2i\sin(k) \\ -2i\sin(k) & 2g(1+\cos(k))\end{bmatrix}}_{H_k(g)}\begin{bmatrix} c_k \\ c_{-k}^\dagger\end{bmatrix}. \tag{93}$$

Finally, we diagonalize $H_k(g) = U^\dagger(g)\begin{bmatrix} E_k(g) & 0 \\ 0 & -E_k(g)\end{bmatrix}U(g)$ with $E_k = 2\sqrt{1+g^2-2g\cos(k)}$ so that

$$H = \int_0^{\pi} \frac{dk}{2\pi}\ E_k(p_k^\dagger p_k - p_{-k}p_{-k}^\dagger) \tag{94}$$

where we have defined new creation and annihilation operators $\begin{bmatrix} p_k \\ p_{-k}^\dagger\end{bmatrix} = U_k(g)\begin{bmatrix} c_k \\ c_{-k}^\dagger\end{bmatrix}$ that still satisfy $\{p_k^\dagger, p_l\} = 2\pi\ \delta_{k,l}$. The final form of the Hamiltonian is then

$$H = \int_{-\pi}^{\pi} \frac{dk}{2\pi}\ E_k\ p_k^\dagger p_k - \int_0^{\pi} dk\ E_k \tag{95}$$

$$= \int_{-\pi}^{\pi} \frac{dk}{2\pi}\ E_k p_k^\dagger p_k - E_0\,. \tag{96}$$

To find the spectrum we define the so called number operators $n_k = p_k^\dagger p_k$ and note that $[n_k, n_l] = 0$ so that we can simultaneously diagonalize all these operators. In particular, the groundstate will be the "empty" state $|\omega(g)\rangle$ for which

$$\langle\omega(g)|n_k|\omega(g)\rangle = 0\ \forall\ k\,, \tag{97}$$

higher excited states can be built by "filling" some of the available energy levels by acting on $|\omega(g)\rangle$ with some particle creation operators $p_k^\dagger$ and this introduces an additional energy E_k. The energy of the available levels, labeled by their momentum, is shown in figure 2 below. Note that the energy cost associated to the first few excited states becomes lower as g approaches one. In particular, at $g = 1$ the elementary excitation becomes gapless which causes them to condense.

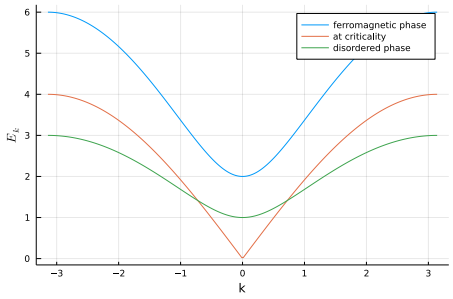

Figure 2: The available energy levels for the transverse field Ising model. The vacuum is the state where all these levels are empty and excited states are constructed by filling one (or more) of these levels which creates an energy $E_k(g)$ on top of the energy density of the vacuum.

2.2 The SSH model

For this model, we immediately work in terms of the fermionic c_n operators that satisfy $\{c_n^\dagger, c_m\} = \delta_{n,m}$ because these turned out to be more suitable for Fourier transforms. The Hamiltonian is

$$H = \frac{1}{a}\sum_{n\in\mathcal{Z}} -i\left(1+\frac{m}{2}\right)c_{2n}^\dagger c_{2n+1} - i\left(1-\frac{m}{2}\right)c_{2n+1}^\dagger c_{2n+2} + \text{h.c.} \tag{98}$$

and the interpretation of this Hamiltonian is that the fermions may hop to neighbouring sites due to the time evolution. Furthermore, for $m > 0$ they would rather hop across even bonds then odd bonds. Note that $[c_{2n}^\dagger c_{2n+1} + h.c., c_{2n+1}^\dagger c_{2n+2} + h.c.] \neq 0$ so that the groundstates for $m \neq \pm 2$ cannot optimize all terms that appear in the Hamiltonian.

2.2.1 Continuous symmetry and the lack of breaking thereof

The Hamiltonian of the SSH model commutes with all operators in the $U(1)$ group :

$$g(\phi) = \prod_{n\in\text{lattice}} e^{i\phi}c_n^\dagger c_n + e^{-i\phi}(1-c_n^\dagger c_n) = \prod_{n\in\text{lattice}} e^{2i\phi\left(c^\dagger c - 1/2\right)}, \tag{99}$$

the local action of this group is simply to give a phase $e^{i\phi}$ to the occupied part of the wavefunction and a phase $e^{-i\phi}$ to the empty part of the wavefunction. Similarly to what we discussed for the Ising model this symmetry implies that the states $\hat{g}(\phi)|\psi\rangle$ and $|\psi\rangle$ must have the same energy $\forall\ \phi$ and at first sight this seems to imply that there might be two regimes with broken/unbroken $U(1)$ symmetry respectively. However, it turns out that continuous symmetries of one dimensional quantum systems are always respected in the spectrum. To intuitively understand this let us first look at the $m = 2$ case where the fermions can only hop over even bonds (i.e. between sites $2n$ and $2n+1$). Here the Hamiltonian describes an infinite set of uncoupled 2-spin systems and the groundstate becomes

$$|\psi_{\text{even dimer}}\rangle = \cdots |D\rangle_{2n-2,2n-1}|D\rangle_{2n,2n+1}|D\rangle_{2n+2,2n+3}\cdots \tag{100}$$

where $|D\rangle_{2n,2n+1} = \frac{1}{\sqrt{2}}\left(|01\rangle - i|10\rangle\right)$ satisfies

$$i\left(c_{2n}^\dagger c_{2n+1} - c_{2n+1}^\dagger c_{2n}\right)|D_{2n,2n+1}\rangle = -|D_{2n,2n+1}\rangle \tag{101}$$

i.e. $D_{2n,2n+1}$ locally minimizes the energy of the hopping term. Note that $g(\phi)D_{2n,2n+1} = D_{2n,2n+1}$ so that the state 100 is symmetric with respect to the action of the $U(1)$ symmetry. Furthermore, as we move away from this $m = 2$ point the perturbative corrections to the groundstate will come from

states $|k\rangle$ that can be reached by acting on the original groundstate with the perturbation. These corrections are therefore of the form

$$|\text{corrections to dimer state at } m=2\rangle = i\left(c_\alpha^\dagger c_{\alpha+1} - h.c.\right)|\psi_{\text{even dimer}}\rangle \qquad \forall \alpha \in \mathbb{Z} \tag{102}$$

and these are all $U(1)$ symmetric so that the corrected vacuum will remain $U(1)$ symmetric, even after these corrections.

Although enticing, the previous argument is not necessarily true because the perturbative expansion for the groundstate may fail when the couplings are sufficiently far from $m = 2$. Nevertheless, there exists a more general argument, that proves that states in the spectrum of Hamiltonians with continuous symmetries will always be invariant under the action of the symmetry group.

2.2.2 Analytic solution

For general m we can easily find a solution to the Schrodinger equation if we separate the length scales by going to momentum space. Before doing so it is important to note that the Hamiltonian 113 and state 100 break translation symmetry. With this in mind we propose independent Fourier expansions for the even/odd sites

$$\begin{cases} c_{2n}^\dagger &= \int_{-\pi}^{\pi} \frac{dk}{2\pi} \exp(ikn)\phi_k^\dagger \\ c_{2n+1}^\dagger &= \int_{-\pi}^{\pi} \frac{dk}{2\pi} \exp(ikn)\psi_k^\dagger \end{cases} \tag{103}$$

and after this transformation the Hamiltonian becomes

$$H = \frac{1}{a}\int_{-\pi}^{\pi}\frac{dk}{2\pi}\begin{bmatrix}\phi_k^\dagger & \psi_k^\dagger\end{bmatrix}\begin{bmatrix} 0 & e^{\frac{ik}{2}}\left(2\sin(\frac{k}{2}) + im\cos(\frac{k}{2})\right) \\ e^{\frac{-ik}{2}}\left(2\sin(\frac{k}{2}) - im\cos(\frac{k}{2})\right) & 0\end{bmatrix}\begin{bmatrix}\phi_k \\ \psi_k\end{bmatrix}. \tag{104}$$

Similar to what we did for the Ising model, it is now straightforward to find $U_k(m)$ so that :

$$H = \frac{1}{a}\int_{-\pi}^{\pi}\frac{dk}{2\pi}\begin{bmatrix}\phi_k^\dagger & \psi_k^\dagger\end{bmatrix} U_k^\dagger \begin{bmatrix}E_k & 0 \\ 0 & -E_k\end{bmatrix} U_k \begin{bmatrix}\phi_k \\ \psi_k\end{bmatrix} \tag{105}$$

$$= \frac{1}{a}\int_{-\pi}^{\pi}\frac{dk}{2\pi}\left(p_k^\dagger p_k E_k - h_k^\dagger h_k E_k\right) \tag{106}$$

where $E_k = \sqrt{4\sin^2 k/2 + m^2\cos^2(k/2)}$. Note that there are now two available energy levels E_k and $-E_k$ per momentum that respectively correspond to the modes $p_k^\dagger$ and $h_k^\dagger$. Consequently, the lowest energy eigenstate $|\omega(m)\rangle$ will now be the state where all negative/positive energy levels are respectively filled/empty i.e.

$$\begin{cases} \langle\omega(g)|h_k^\dagger h_k|\omega(g)\rangle = 2\pi \\ \langle\omega(g)|p_k^\dagger p_k|\omega(g)\rangle = 0 \end{cases} \quad \forall\, k\,. \tag{107}$$

Excited states can be constructed by removing/adding particles with respectively negative/positive energy. The available energy levels are shown in figure 3 below.

2.2.3 Winding numbers and the symmetries protecting them

From the analytical solution we see that, at $m = 0$, the mass of the elementary excitation vanishes so that we could also interpret this point as a phase transition where some excitation condenses. At first sight it seems as if this transition cannot be associated to an order parameter because states on both

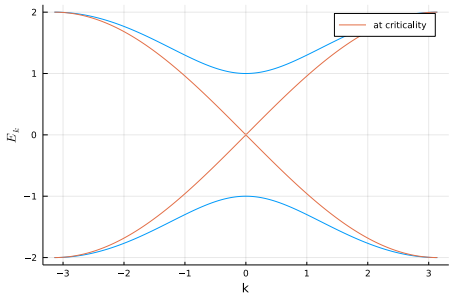

Figure 3: The available energy levels for the SSH model. The vacuum is the state where levels with positive/negative energy are respectively empty/full. Note that there are two types of excitation per momentum created by emptying the lower branch with h_k or filling the upper branch with $p_k^\dagger$.

sides of the transition are $U(1)$ symmetric states with a two site unit cell, in fact the groundstate at $-m$ is simply the one at m translated over a single site.

Nevertheless, we are still able to define some notion of order parameter if we first realize that the model has two Z_2 symmetries, particle hole $\mathcal{P}$ and time reversal $\mathcal{T}$, that act as

$$\begin{cases} \mathcal{P}^\dagger\, c_{2n}\quad \mathcal{P} &= c_{2n}^\dagger \\ \mathcal{P}^\dagger\, c_{2n+1}\mathcal{P} &= c_{2n+1}^\dagger \end{cases} \qquad \text{and} \qquad \begin{cases} \mathcal{T}^\dagger\, c_{2n}\quad \mathcal{T} &= c_{2n} \\ \mathcal{T}^\dagger\, c_{2n+1}\quad \mathcal{T} &= -c_{2n+1} \\ \mathcal{T}^\dagger\, c_{\text{number}}\mathcal{T} &= c_{\text{number}}^* \end{cases} . \tag{108}$$

To proceed, let us note that their action on the momentum dependent creation and annihilation operators must be

$$\begin{cases} \mathcal{P}^\dagger\, \phi_k\, \mathcal{P} &= \phi_{-k}^\dagger \\ \mathcal{P}^\dagger\, \psi_k\, \mathcal{P} &= \psi_{-k}^\dagger \end{cases} \qquad \text{and} \qquad \begin{cases} \mathcal{T}^\dagger\, \phi_k\quad \mathcal{T} &= \phi_{-k} \\ \mathcal{T}^\dagger\, \psi_k\quad \mathcal{T} &= -\psi_{-k} \\ \mathcal{T}^\dagger\, c_{\text{number}}\mathcal{T} &= c_{\text{number}}^* \end{cases} . \tag{109}$$

so that invariance of a generic quadratic Hamiltonian

$$H = \frac{1}{a}\int_{-\pi}^{\pi}\frac{\mathrm{d}k}{2\pi}\begin{bmatrix}\phi_k^\dagger & \psi_k^\dagger\end{bmatrix}\underbrace{\vec{d}(k)\vec{\sigma}}_{H_k}\begin{bmatrix}\phi_k \\ \psi_k\end{bmatrix} \tag{110}$$

under their combined actions requires

$$\mathcal{P}^\dagger\mathcal{T}^\dagger\, H\, \mathcal{T}\mathcal{P} = H \;\rightarrow\; H(k) = -\sigma_z H(k)\sigma_z\,. \tag{111}$$

The upshot is that any such Hamiltonian will be for the form $H(k) = d_x(k)\sigma_x + d_y(k)\sigma_y$ with $\vec{d}(0) = \vec{d}(2\pi)$ so that the $\vec{d}(k)$ traces closed loops through the $\{d_x, d_y\}$ plane with which we can associate a winding number ν, that is $+1$ when the loop encircles the $d_x = d_y = 0$ point and 0 if it does not. This winding number can then be interpreted as an order parameter because we can not tune a Hamiltonian with $\nu = 1$ to another with $\nu = 0$ without closing the gap or breaking the $\mathcal{TP}$ symmetry.

For our Hamiltonian in particular we find that

$$H_k = \left(1 - \frac{m}{2}\right)\sin k \cdot \sigma_x + \left(\left(1 - \frac{m}{2}\right)\cos k - 1 - \frac{m}{2}\right)\cdot\sigma_y$$

and the corresponding loops are depicted in figure 4 above. Here the winding number is $\nu = 1$ form $m > 0$ and 0 when $m < 0$.

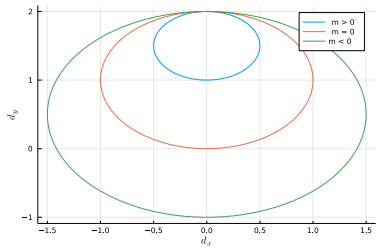

Figure 4: The loops traced by $\vec{d}(k)$ as k goes from $-\pi$ to π. Note that we can associate a winding number that is respectively +1, 0 for the green, blue loops and that a transition from one phase to the other must either cross the $d_x = d_y = 0$ point or include $d_z(k) \neq 0$.

2.2.4 Interfaces between topologically distinct chains

One particularly interesting property of this winding number can be observed if we note that any matrix product state, that is symmetric under the combined actions of the $g(\phi)$ and $\mathcal{TP}$ symmetries, must necessarily break translation symmetry and be associated with a set of virtual unitaries $T(\phi)$ and T_{TP} that can counteract the action of the symmetry on the virtual level. Furthermore, these virtual unitaries must satisfy $T_{TP}^{\dagger} U(\phi) T_{TP} = U(-\phi)$ which forces the degeneracies of positive and negative $U(1)$ charges to be equal i.e. $dl_{U(1)} = -l_{U(1)}$. The conclusion is that any gapped state with these symmetries must be represented as

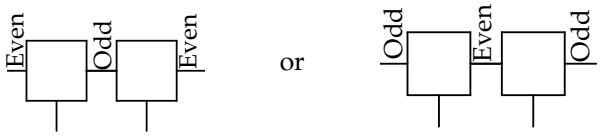

(112)

where the smallest allowed representations on the odd leg are of the form $q_{U(1)} \bigoplus -q_{U(1)}$. Furthermore, we know that translations map $H(m) \to H(m)$ and $|\psi_{even/odd/even}\rangle \to |\psi_{odd/even/odd}\rangle$ so these different types of matrix product states must correspond to groundstates of Hamiltonians with different winding numbers.

Consequently, the groundstate for a Hamiltonian

$$H = \frac{1}{a} \sum_{n \in \text{lattice}} -i \left(1 + \frac{m_n}{2}\right) c_{2n}^{\dagger} c_{2n+1} - i \left(1 - \frac{m_n}{2}\right) c_{2n+1}^{\dagger} c_{2n+2} + \text{h.c.} \tag{113}$$

with site dependent mass m_n chosen so that it extrapolates from the $\nu = +1$ to the $\nu = 0$ phase, must be of the form

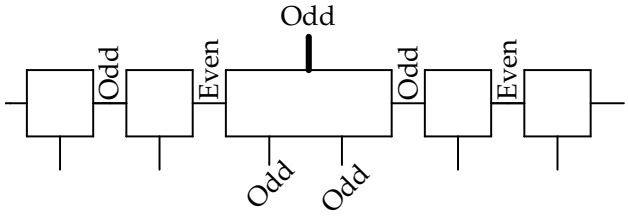

, (114)

where the central tensor that represents the interpolation region must carry an extra "odd" leg if we want to avoid it being identically zero due to the symmetry constraints. The upshot is that the groundstate of this model is at least twofold degenerate because the smallest odd representation of $U(1)$ is two dimensional. Furthermore, the difference between these two degenerate groundstates must be localized at the interface because we know that, far away from the interface nothing special is going on. Therefore we arise at the conclusion that the spectrum of any Hamiltonian that describes an interface between topologically distinct phases must necessarily contain a localized massless excitation.

3

QUANTUM FIELD THEORIES

> It doesn't matter how beautiful your theory is, it doesn't matter how smart you are. If it doesn't agree with experiment, it's wrong.
>
> Richard Feynman

Up to now we have been studying models where the degrees of freedom lived on a discrete grid (i.e. lattice) which is a natural construction when describing the behavior of electrons (and other particles) in crystalline materials. We will now try to define a different type of theory, where the degrees of freedom are defined everywhere in space (i.e a continuous space), and which are more natural to describe situations where particles move around in an empty background such as space.

To start this endeavour, we will try to construct the Hilbert space for such continuous theories. As a reminder, for lattice models we characterized states $|\psi\rangle$ in the Hilbert space by a set of numbers $\psi_{i_1,i_2,\cdots i_N}$ with $i_\alpha \in \{\uparrow,\downarrow\}$ that tell us how much the basis vector $|i_1\rangle\,|i_2\rangle\cdots|i_N\rangle$ contributes to the superposition in $|\psi\rangle$. Similarly, a state for a continuous theory would have to be characterized by a set of numbers $\psi_{\text{some indices}}$ which has one index for every position in the uncountable many points in our continuous space. The implication of this is that every set of basis vectors for a possible Hilbert space would fail to contain some vectors, i.e. we cannot really define this Hilbert space. In fact, we already encountered this problem when we were studying infinitely long spin chains in the previous section and the solution was to simply interpret the infinitely long chains as a limit of chains with ever increasing lengths. Here, however, this limit is not well defined because any infinitesimally small part of our continuous world must already contain infinitely many degrees of freedom and is therefore already ill defined.

In the first half of this chapter we will mostly ignore this problem and act as if such a Hilbert space exists. The idea is that we define a set of operators that represent creation and annihilation operator and then interpret the Hilbert space as the collection of vectors that can be reached by acting with these operators onto a reference state $|0\rangle$. For example, we could have created all possible basis vectors for our spin chain Hilbert space from the reference state $|0\rangle = |\cdots\downarrow\downarrow\downarrow\cdots\rangle$ and the action of all spin flip operators $\{\sigma_{x,n}, \sigma_{y,n}\forall n\}$. The downside of this construction is that we are still dealing with states in an uncountably large Hilbert space and that it is therefore impossible to perform numerical simulations even when the system is small. In the second half of this chapter we will therefore explore an alternative formulation where the continuous world is interpreted as the limit $a \to 0$ of a sequence of lattice worlds. In fact, we will see that this interpretation of a field theory as a limit of underlying theories is also forced onto us if we use the construction.

From a philosophical perspective, these theories are very strange as they are only defined as the limit of a series of underlying models. Nevertheless, these theories have been proven to be incredibly accurate descriptions of the sub-atomic world so that they, according to the inverse of Feynman's quote, must be correct at the length scales that are currently available through these experiments.

3.1 Fermionic field theories

The first type of field theory that we will be interested in is built by the action of the operators $\psi_\alpha^\dagger(x)$ and $\psi_\beta(x)$ that are defined through the fermionic commutation relations

$$\begin{cases} \{\psi_\alpha^\dagger(x), \psi_\beta(y)\} = \delta_{\alpha\beta}\delta(x-y) \\ \{\psi_\alpha(x), \psi_\beta(y)\} = 0 \\ \{\psi_\alpha^\dagger(x), \psi_\beta^\dagger(y)\} = 0 \end{cases}, \tag{115}$$

where the subscript index signifies that there may exist several of these operators at every position. Note that these commutation relations are simply a continuous generalization of $\{c_n^\dagger, c_m\} = \delta_{n,m}$.

From these operators we can define the density operators $\rho_\alpha(x) = \psi_\alpha^\dagger(x)\psi_\alpha(x)$ that satisfy $\rho_\alpha(x)\psi_\alpha^\dagger(y)\,|\psi\rangle = \psi_\alpha^\dagger(y)(\rho_\alpha(x) + \delta(x-y))\,|\psi\rangle$ so that the $\psi_\alpha^\dagger(x)$ create particles that are being counted by this density operator. Furthermore, these density operators all commute so that we can define the reference state by the condition

$$\langle 0_F|N_\alpha(x)|0_F\rangle = 0 \;\forall\; x, \alpha \tag{116}$$

i.e. the reference state is the state that contains zero particles everywhere. Finally, note that the commutation relations guarantee that

$$\psi_\alpha^\dagger(x)\psi_\alpha^\dagger(x)\,|0_F\rangle = 0 \tag{117}$$

so that the local fermionic Hilbert space cannot contain states with two of these fermionic degrees of freedom at the same position.

3.1.1 Free fermions

Let us now consider the (1+1)-dimensional Dirac Hamiltonian

$$H = \int \mathrm{d}x \left(\psi_\alpha^\dagger(x) i\gamma^0_{\alpha\beta}\gamma^x_{\beta\gamma}\partial_x\psi_\gamma(x) + m\psi_\alpha^\dagger(x)\gamma^0_{\alpha\beta}\psi_\beta(x)\right) \tag{118}$$

that contains two fermionic flavours (i.e. $\alpha \in 1,2$). The matrices γ^0 and γ^x satisfy $\{\gamma^\mu, \gamma^\nu\} = 2\eta^{\mu\nu}$. One important detail is that different solutions for the γ^μ matrices are related by local unitary transformations of the fields $\psi_\alpha \to U_{\alpha\beta}\psi_\beta$ that leave the spectrum of the Hamiltonian unchanged i.e. different choices such as ($\gamma^0 = \sigma_y$, $\gamma^x = i\sigma_x$) or ($\gamma^0 = \sigma_z$, $\gamma^x = i\sigma_y$) generate identical physics. In what follows we will use the first of these choices.

Before we analyse the spectrum let's note that the Hamiltonian commutes with

$$\begin{aligned} g_V(\theta_V) = e^{i\theta_V Q_{vector}} \text{ with } Q_{vector} &= \int dx \left(\psi^\dagger(x)\psi(x)\right) \\ &= \int dx \left(\psi_1^\dagger(x)\psi_1(x) + \psi_2^\dagger(x)\psi_2(x)\right) \end{aligned} \tag{119}$$

$\forall\theta_V$ so that $\langle Q_{vector}\rangle$ is a conserved quantity. Furthermore if $m = 0$ we find an additional symmetry :

$$\begin{aligned} g_A(\theta_A) = e^{i\theta_A Q_{axial}} \text{ with } Q_{axial} &= \int dx \left(\psi^\dagger(x)\gamma^5\psi(x)\right) \\ &= \int dx \left(\psi_1^\dagger(x)\psi_1(x) - \psi_2^\dagger(x)\psi_2(x)\right) \end{aligned} \tag{120}$$

$\forall\theta_A$ with $\gamma^5 = \gamma^0\gamma^x$, that guarantees the conservation of $\langle Q_{axial}\rangle$.

To diagonalize this Hamiltonian we simply re-express it in terms of the usual momentum modes $\psi_\gamma(x) = \int \frac{dk}{2\pi}\, e^{ikx}\psi_\gamma(k)$ that satisfy $\{\psi^\dagger_\alpha(k), \psi_\beta(l)\} = 2\pi\delta_{\alpha\beta}\delta(k-l)$ to get

$$H = \int \frac{dk}{2\pi} \begin{bmatrix} \psi_1^\dagger(k) & \psi_2^\dagger(k) \end{bmatrix} \begin{bmatrix} k & -im \\ im & -k \end{bmatrix} \begin{bmatrix} \psi_1(k) \\ \psi_2(k) \end{bmatrix}, \tag{121}$$

which can be further diagonalized with some $U(k)$

$$H = \int \frac{dk}{2\pi} \begin{bmatrix} \psi_1^\dagger(k) & \psi_2^\dagger(k) \end{bmatrix} U^\dagger(k) \begin{bmatrix} E(k) & 0 \\ 0 & -E(k) \end{bmatrix} U(k) \begin{bmatrix} \psi_1(k) \\ \psi_2(k) \end{bmatrix} \tag{122}$$

$$= \int \frac{dk}{2\pi} E(k) \Big(\rho_p(k) - \rho_h(k) \Big) \tag{123}$$

where $E(k) = \sqrt{k^2 + m^2}$ and $\rho_{p,h}(k)$ the number operators corresponding to the positive/negative energy branches that are displayed in figure 5 below.

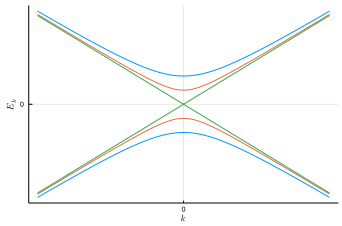

Figure 5: The available energy levels for the free fermion.

As per usual, the groundstate is the state where all negative/positive energy levels are filled/empty so that we can no longer add/remove particles from them. Consequently $p\,|GS\rangle = h^\dagger\,|GS\rangle = 0$ so that

$$\langle GS|n_h|GS\rangle = 2\pi\delta(0) \qquad \text{and} \qquad \langle GS|n_p|GS\rangle = 0 \qquad \forall\, k\,. \tag{124}$$

Excited states are build by adding/removing particles with positive/negative energy, their energy compared to that of the groundstate is simply $E(k)$.

Finally, we note that the energy of the groundstate itself is

$$E_{GS} = \langle GS|\, H\,|GS\rangle = -2\pi\delta(0) \int \frac{dk}{2\pi} \sqrt{k^2 + m^2} \tag{125}$$

which has a divergence due to the $\delta(0)$ and an additional divergence that is coming from the integral over the infinitely many momenta. The first integral can be understood if we realize that

$$2\pi\delta(0) = \lim_{p\to 0} \lim_{L\to\infty} \int_{-L/2}^{L/2} dx\, e^{ipx} = \lim_{L\to\infty} L \tag{126}$$

where L is the length of our continuous universe that was assumed to be infinite. Consequently, this first divergence is simply due to the fact that we are calculating the total energy rather then the energy density. The second integral diverges because we keep integrating up to $k \to \infty$ which corresponds to fluctuations of the field at arbitrarily small length scales. Nevertheless this term is not really a problem because it is a simple constant term that does not influence the energy of the excited states.

3.1.2 Self-interacting fermions : the generalized Gross-Neveu model

Let us now try to find the spectrum of the following Hamiltonian

$$H_{GN} = \int dx \sum_c \psi_c \gamma^0\gamma^x i\partial_x \psi_c - \frac{g_x^2}{2N}(\sum_c \psi^\dagger\gamma^0\psi)^2 - \frac{g_y^2}{2N}(\sum_c \psi^\dagger\gamma^0\gamma^5\psi)^2 \tag{127}$$

where c runs over N different fermions flavours. These different flavours are indistinguishable and therefore this model has a $SU(N)$ symmetry that mixes up those flavours. Additionally, whenever $g_x^2 = g_y^2$ we find that the Hamiltonian commutes with the vector and axial $U(1)$ symmetries, here the model is named the chiral Gross-Neveu model. If we however pick $g_x^2 \neq g_y^2$ we find that only a Z_2 subgroup $\{1, g_{axial}(\theta_V = \pi)\}$ of the axial $U(1)$ still commutes with the Hamiltonian. Finally for $g_x^2 = 0$ or $g_y^2 = 0$ we get that the $SU(N)$ flavour symmetry and $U(1)$ vector symmetry mix up with charge conjugation symmetry which gives rise to an enlarged $O(2N)$ symmetry group. Furthermore, we note that g_x^2 and g_y^2 are dimensionless parameters so that there is no mass scale present in this theory, consequently we do not expect to find massive particles in this theory.

To reveal the physics contained in this model let us try to find an eigendecomposition for the Hamiltonian. To do this we can no longer rely on a Fourier transform since it is not quadratic in the fermions. There are however many approximate methods that do the trick quite well. For example, if we focus on states $|\Phi\rangle$ that can be written as direct product $|\Phi\rangle = |\phi\rangle^{\otimes N}$ of single flavour wavefunctions $|\phi\rangle$ we find that the energy per flavour is

$$\frac{\langle H\rangle_\Phi}{N} = \int dx\, \langle\phi|\psi^\dagger\gamma^0 i\partial_x\psi|\phi\rangle - \frac{g_x^2}{2N^2}\langle\Phi|\left(\sum_c \psi^\dagger\gamma^0\psi\right)^2|\Phi\rangle - \frac{g_y^2}{2N^2}\langle\Phi|\left(\sum_c \psi^\dagger\gamma^0 i\gamma^5\psi\right)^2|\Phi\rangle \quad (128)$$

where we have used the fact that the first term does not couple the different flavours. To proceed we expand the square of the sum that appears in the second term

$$\langle\Phi|\left(\sum_c \psi_c^\dagger\gamma^0\psi_c\right)^2|\Phi\rangle = \sum_c \langle\Phi|\left(\psi_c^\dagger\gamma^0\psi_c\right)^2|\Phi\rangle + \sum_c\sum_{c'\neq c}\langle\Phi|\left(\psi_c^\dagger\gamma^0\psi_c\right)\left(\psi_{c'}^\dagger\gamma^0\psi_{c'}\right)|\Phi\rangle \quad (129)$$

$$= N\langle\phi|\left(\psi^\dagger\gamma^0\psi\right)^2|\phi\rangle + N(N-1)\langle\phi|\psi^\dagger\gamma^0\psi|\phi\rangle^2, \quad (130)$$

and similar for the third term. If we are then only interested in the spectrum when N is large we can neglect the first type of contribution and the energy per flavour becomes

$$\frac{\langle H\rangle_\Phi}{N} = \int dx\, \langle\phi|\psi^\dagger\gamma^0 i\partial_x\psi|\phi\rangle - \frac{g_x^2}{2}\langle\phi|\psi^\dagger\gamma^0\psi|\phi\rangle^2 - \frac{g_y^2}{2}\langle\phi|\psi^\dagger\gamma^0 i\gamma^5\psi|\phi\rangle^2 \quad (131)$$

which must now be optimized w.r.t. the wavefunction $\langle\phi|$. However, a much simpler task is to optimize

$$V_{eff}(\sigma,\pi,\phi) = \int dx\, \langle\psi^\dagger\gamma^0\gamma^x i\partial_x\psi\rangle_\phi + g_x^2\sigma\left(\frac{\sigma}{2} - \langle\psi^\dagger\gamma^0\psi\rangle_\phi\right) + g_y^2\pi\left(\frac{\pi}{2} - \langle\psi^\dagger\gamma^0 i\gamma^5\psi\rangle_\phi\right) \quad (132)$$

which is equivalent because the variational optima for σ and π satisfy

$$\sigma = \langle\phi|\psi^\dagger\gamma^0\psi|\phi\rangle \qquad \text{and} \qquad \pi = \langle\phi|\psi^\dagger\gamma^0 i\gamma^5\psi|\phi\rangle \quad (133)$$

and can be re-inserted into $V_{eff}(\sigma,\pi,\phi)$ to get back the original expression 131. Alternatively, optimization of V_{eff} w.r.t $\langle\phi|$ gives

$$\int dx\left(\psi^\dagger\gamma^0\gamma^x i\partial_x\psi - g_x^2\sigma\psi^\dagger\gamma^0\psi - g_y^2\pi\psi^\dagger\gamma^0 i\gamma^5\psi\right)|\phi\rangle = E_{eff}|\phi\rangle \quad (134)$$

which after a Fourier transform of the ψ field becomes

$$\int\frac{\mathrm{d}k}{2\pi}\begin{bmatrix}\psi_1^\dagger(k) & \psi_2^\dagger(k)\end{bmatrix}\begin{bmatrix}k & -ig_x^2\sigma + g_y^2\pi \\ ig_x^2\sigma + g_y^2\pi & -k\end{bmatrix}\begin{bmatrix}\psi_1(k)\\ \psi_2(k)\end{bmatrix}|\phi\rangle = E_{eff}|\phi\rangle\,. \quad (135)$$

After a final diagonalization we find

$$\int\frac{dk}{2\pi}\sqrt{k^2 + (g_x^2\sigma)^2 + (g_y^2\pi)^2}\left(n_p(k) - n_h(k)\right)|\phi\rangle = E_{eff}|\phi\rangle \quad (136)$$

so that the sought after state with minimal E_{eff} will have all hole/particle states occupied/empty. Its effective energy density is : $\mathcal{E}_{eff} = \frac{E_{eff}}{2\pi\delta(0)} = -\int \frac{\mathrm{d}k}{2\pi}\sqrt{k^2 + (g_x^2\sigma)^2 + (g_y^2\pi)^2}$ and with this the density of the effective potential becomes

$$\mathcal{V}_{eff} = \frac{V_{eff}}{2\pi\delta(0)} = \frac{\langle H\rangle_\Phi}{2\pi N\delta(0)} = \frac{1}{2}g_x^2\sigma^2 + \frac{1}{2}g_y^2\pi^2 - \int\frac{\mathrm{d}k}{2\pi}\sqrt{k^2 + (g_x^2\sigma)^2 + (g_y^2\pi)^2} \tag{137}$$

which can be optimized w.r.t. the auxiliary fields σ and π.

However, similarly to the groundstate energies of the free theories above we find that this quantity is divergent due to the infinitely many momenta i.e. $\mathcal{V}_{eff}(\sigma,\pi) = -\infty$ so that it makes no sense to optimize it. To solve this we must cut off the momentum integral at some large but finite value Λ which essentially means that we neglect fluctuations at the smallest scales. We then get the following, regularized effective potential

$$\mathcal{V}_{eff} = \frac{g_x^2\sigma^2}{2} + \frac{g_y^2\pi^2}{2} - \frac{1}{2}(g_x^4\sigma^2 + g_y^4\pi^2)\log\left(\frac{2\Lambda}{\sqrt{g_x^4\sigma^2 + g_y^4\pi^2}}\right) + \cdots \tag{138}$$

where the $\cdots$ indicate that we have neglected terms that are suppressed as the cutoff Λ grows to infinity. In what follows we will analyse the optima of this effective potential in the $O(2N)$ and chiral cases separately.

O(2N) Gross-Neveu model

For the $g_y^2 = 0$ case we get that the variational minimum of the effective potential lies at

$$g_y^2 = 0 \to \begin{cases}\sigma^2 = \frac{4\Lambda^2}{g_x^4 e}e^{-2/g_x^2}\\ \pi^2 = 0\end{cases} \tag{139}$$

and according to 134 this means that the elementary excitations have gained a mass

$$m_f = g_x^2\sigma = 2\Lambda e^{-1/g_x^2} \tag{140}$$

despite the dimensionless couplings. There is however one big problem remaining, namely the fact that this fermion mass diverges in the limit $\Lambda \to \infty$. To remedy this we must further modify the theory and state that the coupling g_x depends on the cutoff in a way defined by the condition

$$\frac{\partial m_f(\Lambda, g_x(\Lambda))}{\partial\Lambda} = 0 \to \Lambda\frac{\partial g_x(\Lambda)}{\partial\Lambda} = -\frac{g_x^3}{2} \tag{141}$$

the final renormalized theory should then be interpreted as the limit of a series of field theories

$$H_{GN,true} = \lim_{\Lambda\to\infty} H_{GN}(g(\Lambda),\Lambda) \tag{142}$$

and this limit will have a well defined fermion mass m_f that no longer depends the cutoff. Note that we define such a limit procedure for any desired m_f mass by simply fixing the initial conditions for the differential equation 141.

Finally we note that this model actually has two groundstates corresponding to $\sigma = \pm\sigma_0$. Consequently the elementary excitations will be kinks propagating from one vacuum to the other rather than local fermionic excitations one one vacuum. The mass ratios of these kinks compared to that of the fermions can be extracted from the $O(2N)$ symmetry, most importantly the elementary excitation is always $2N$-fold degenerate due to this symmetry.

Chiral Gross-Neveu model

Let us now focus on couplings $g_x^2 = g_y^2 = g^2$, here we get that the optimum of the effective potential sits at

$$g_x^2 = g_y^2 = g^2 \to \sigma^2 + \pi^2 = \frac{4\Lambda^2}{g^4 e} e^{-2/g^2} \tag{143}$$

and the corresponding fermion mass

$$m_f = g^2 \sqrt{\sigma^2 + \pi^2} = 2\Lambda e^{-1/g^2} \tag{144}$$

remains identical to what we found before. In particular this still depends on the cutoff Λ so that it must be renormalized by defining a suitable limit of models.

One important detail is that 143 implies that there are infinitely many groundstates lying on the circle with $\sigma^2 + \pi^2$ constant. However, this is a result of our mean field calculation, had we taken quantum fluctuations into consideration we would have found a single groundstate with infinite correlation length that is the superposition of all these infinite solutions. A stricter motivation for this is that our model started with a $U(1)$ axial symmetry which cannot be broken due to a continuum version of the arguments discussed in section 2.2.1, in particular there exists a continuum version of the Mermin Wagner theorem the proof that is named after Coleman.

3.2 Bosonic field theories

The second type of field theory arises from the action of operators $c(x)$ and $c^\dagger(x)$ with bosonic commutation relations

$$\begin{cases} [c(x), c^\dagger(y)] = \delta(x-y) \\ [c(x), c(y)] = 0 \\ [c^\dagger(x), c^\dagger(y)] = 0 \end{cases} \tag{145}$$

that also lead to a set of density operators $\rho(x) = c^\dagger(x)c(x)$ that mutually commute and therefore allow us to define the empty reference state

$$\langle 0_B | \rho_\alpha(x) | 0_B \rangle = 0 \; \forall \; x \, . \tag{146}$$

The crucial distinction with our fermionic degrees of freedom is that

$$\left(c^\dagger(x)\right)^n |0_B\rangle \neq 0 \; \forall n \tag{147}$$

so that the local Hilbert space at position x_0 spanned by $c(x_0)$ and $c^\dagger(x_0)$ contains countable infinite many states that correspond to the eigenvalues $0, 1, 2, \cdots$ of the bosonic number operator.

From these creation and annihilation operators we can also define the operators

$$\begin{cases} \phi(x) &= \int \frac{dk}{2\pi} \sqrt{\frac{1}{2|k|}} \left(e^{ikx} c(k) + e^{-ikx} c^\dagger(k) \right) \\ \Pi(x) &= -i \int \frac{dk}{2\pi} \sqrt{\frac{|k|}{2}} \left(e^{ikx} c(k) - e^{-ikx} c^\dagger(k) \right) \end{cases} \tag{148}$$

where the $c(k)$ are the Fourier exponents of $c(x)$. Note that we have introduced factors $\sqrt{k}$ and $\sqrt{k}^{-1}$ so that the ϕ, Π operators are respectively dimensionless and of mass dimension one. One can easily check that these new operators satisfy

$$\begin{cases} [\phi(x), \Pi(y)] = i\delta(x-y) \\ [\phi(x), \phi(y)] = 0 \\ [\Pi(x), \Pi(y)] = 0 \end{cases} \tag{149}$$

which is the position dependent generalization of the commutation relation $[q, p] = i$ that has been experimentally shown to hold for the operators that measure te position and momentum of sub-atomic particles.

3.2.1 The free boson

The Hamiltonian that we want to study is

$$H_{fb} = \int \mathrm{d}x \frac{1}{2}\Pi^2 + \frac{1}{2}\partial_x\phi\partial_x\phi \tag{150}$$

and to find its spectrum we simply re-express it in of the original creation and annihilation operators by inserting the definitions 148

$$H_{fb} = \int \frac{\mathrm{d}k}{2\pi}|k|\, c^\dagger(k)c(k) \tag{151}$$

which reveals that the groundstate is simply the empty reference state $|0_B\rangle$ and the first excited state is gapless.

To nevertheless reveal some interesting physics let us look at the two point function of the fields

$$\begin{aligned}\langle\phi(x)\phi(y)\rangle - \langle\phi(x)\rangle\langle\phi(y)\rangle &= \int \frac{dk_1 dk_2}{(2\pi)^2}\frac{1}{2\sqrt{|k_1k_2|}}e^{ik_1x-ik_2y}\underbrace{\langle 0_B|c(k_1)c^\dagger(k_2)|0_B\rangle}_{\delta(k_1-k_2)} \\ &= \int \frac{dk}{4\pi}\frac{1}{k}e^{ik(x-y)}\end{aligned} \tag{152}$$

which diverges due to contributions from both small and large momenta. The latter divergence is similar to what we encountered before, and can be dealt with by the introduction of a momentum cutoff and a suitable limit procedure. To deal with the first divergence we subtract the similarly divergent term $\langle\phi^2(0)\rangle$. The regularized two point function is then

$$\begin{aligned}\langle\phi(x)\phi(y)\rangle - \langle\phi^2(0)\rangle &= \int \frac{dk}{4\pi}\frac{1}{|k|}\left(e^{ik(x-y)}-1\right)e^{-\frac{|k|}{\Lambda}} \\ &= -\int_{-\infty}^{\infty}\frac{dk}{4\pi}\int_{1/\Lambda}^{\infty}d\alpha\left(e^{ik(x-y)}-1\right)e^{-\alpha|k|}\end{aligned} \tag{153}$$

where on the second line we eliminated the $|k|^{-1}$ by expressing it as an integral. Furthermore, if we split the positive and negative k contributions we get

$$\begin{aligned}\langle\phi(x)\phi(y)\rangle - \langle\phi^2(0)\rangle &= -\int_0^{\infty}\frac{dk}{4\pi}\int_{1/\Lambda}^{\infty}d\alpha\, e^{-\alpha k}\left(e^{ik(x-y)}+e^{-ik(x-y)}-2\right) \\ &= \frac{1}{4\pi}\int_{1/\Lambda}^{\infty}d\alpha\left(\frac{1}{\alpha-i(x-y)}+\frac{1}{\alpha+i(x-y)}-\frac{2}{\alpha}\right) \\ &= \frac{1}{4\pi}\left(\log(\frac{1}{\Lambda}-i(x-y))+\log(\frac{1}{\Lambda}+i(x-y))-2\log(\frac{1}{\Lambda})\right) \\ &= \frac{1}{2\pi}\log(\Lambda(x-y))\,.\end{aligned} \tag{154}$$

Note that this result seems to implies that, at fixed and finite cutoff, the correlations between measurements of the ϕ field grow with the spatial distance between these measurements. This is, however, unphysical and to find bounded two point correlations we must instead interpret $e^{i\sqrt{K\pi}\phi}$,

with K a dimensionless parameter, as the elementary operator. Indeed the two point correlation function of these operators is

$$\langle e^{i\sqrt{K\pi}\phi(x)}e^{-i\sqrt{K\pi}\phi(y)}\rangle - \langle e^{i\sqrt{K\pi}\phi(x)}\rangle\langle e^{-i\sqrt{K\pi}\phi(y)}\rangle = e^{-\pi K\left(\langle\phi(x)\phi(y)\rangle - \langle\phi^2(0)\rangle\right)} \tag{155}$$

$$= \left(\frac{1}{\Lambda(x-y)}\right)^{K/2} \tag{156}$$

which has a well defined limit $x - y \to \infty$ but still diverges in the limit $\Lambda \to \infty$. To avoid this last divergence we could again try to make K cutoff dependant in a way that makes the limit $\Lambda \to \infty$ well defined. However, if we try this we find that $K(\Lambda)$ must satisfy $(x-y)\log(\frac{1}{\Lambda(x-y)})\frac{dK}{d\Lambda} = K$ which depends on $(x-y)$ so that this method cannot make the two point function well defined for all $(x-y)$. Instead we will choose to make our elementary operator cutoff dependant, i.e. $\phi_R = \Lambda^{K/4}e^{i\sqrt{K\pi}\phi}$ so that that the cutoff dependency naturally drops out at all separations $(x-y)$. This process is named field renormalisation.

3.2.2 The self interacting boson

In the previous section we found that the physically meaningful bosonic operators are complex exponentials $\phi_R = \Lambda^{K/4}e^{i\sqrt{K\pi}\phi}$ and $\phi_R^\dagger = \Lambda^{K/4}e^{-i\sqrt{K\pi}\phi}$ of the field rather then the field itself. With this in mind we propose the interacting Hamiltonian

$$H_{fb} = \int \mathrm{d}x \frac{1}{2}\Pi^2 + \frac{1}{2}\partial_x\phi\partial_x\phi - 2y\cos(2\sqrt{\pi K}\phi)\,, \tag{157}$$

note that the cosine term can be interpreted as $\phi_R\phi_R + \phi_R^\dagger\phi_R^\dagger$ i.e. a simple two point term for our renormalized fields. To find the spectrum of this Hamiltonian we can not rely on Fourier transforms because the interaction term is not quadratic or perturbation theory because the interaction term contains all powers of the θ field. In fact, to deal with this theory we will first need to introduce some additional machinery that will be the topic of the next two subsections.

Local bosonic Hilbert space

The first thing we will need are two bases of eigenvectors for the local field $\hat{q} = \phi(x_0)$ and momentum operators $\hat{p} = \Pi(x_0)$. To achieve this we will start from the orthonormal set $\{|q\rangle\,,\ \forall q\}$ of $\hat{q}$ eigenvectors i.e. $\hat{q}\,|q\rangle = q\,|q\rangle$. From these we can then build the resolution of the identity $1 = \int dq\,|q\rangle\langle q|$ which allows us to write a general vector $|\phi\rangle$ in terms of this first basis

$$|\phi\rangle = \int dq\ |q\rangle\langle q|\phi\rangle = \int dq\phi(q)\,|q\rangle\ . \tag{158}$$

Note that this is just the infinite dimensional generalisation of equation 4. If we now define the action of the momentum operator in this basis as

$$\hat{p}\,|\phi\rangle = \int dq\ i\partial_q\phi(q)\,|q\rangle \tag{159}$$

we get

$$(\hat{q}\hat{p} - \hat{p}\hat{q})\,|\phi\rangle = \int dq\ \left(iq\partial_q\phi(q) - i\partial_q(q\phi(q))\right)|q\rangle \tag{160}$$

$$= \int dq(-i)\phi(q)\,|q\rangle \tag{161}$$

$$= -i\,|\phi\rangle \tag{162}$$

so that our q and p operators satisfy the desired commutation relations.

Now that we have defined the action of the momentum operator in the position basis we can search its eigenvectors

$$\hat{p}\,|p\rangle = p\,|p\rangle = \int dq i\partial_q p(q)\,|q\rangle \tag{163}$$

so that $p(q) = e^{-ikq}$ and $|p\rangle = \int dq e^{-ikq}\,|q\rangle$. This provides us with an alternative expression for the identity $1 = \int dp\,|p\rangle\,\langle p|$.

Finally, the overlap between these vectors is given by :

$$\langle p|q\rangle = \int dx e^{ipx}\,\langle x|q\rangle = e^{ipq} \tag{164}$$

where we have used the fact that the $|x\rangle$ vectors are orthonormal i.e. $\langle x|q\rangle = \delta_{x,q}$.

As a sidenote we remark that these operators can also be represented as infinitely large matrices

$$\hat{q} = \frac{1}{\sqrt{2}}\begin{bmatrix} 0 & \sqrt{1} & 0 & 0 & \\ \sqrt{1} & 0 & \sqrt{2} & 0 & \\ 0 & \sqrt{2} & 0 & \sqrt{3} & \\ 0 & 0 & \sqrt{3} & 0 & \\ & & & & \ddots \end{bmatrix} \qquad \text{and} \qquad \hat{p} = \frac{i}{\sqrt{2}}\begin{bmatrix} 0 & -\sqrt{1} & 0 & 0 & \\ \sqrt{1} & 0 & -\sqrt{2} & 0 & \\ 0 & \sqrt{2} & 0 & -\sqrt{3} & \\ 0 & 0 & \sqrt{3} & 0 & \\ & & & & \ddots \end{bmatrix} \tag{165}$$

which can be shown to also satisfy the desired commutation relation. One could then, in principle, also find the eigenvectors of these matrices establish equation 164 and the different resolutions of the identity.

Path integrals

The second thing we need is the transition probability from an initial state $|q_0\rangle$ at time o to a finial state $|q_N\rangle$ at time T through the time evolution generated by some Hamiltonian

$$Z = \langle q_N|e^{-i\hat{H}T}|q_0\rangle = \langle q_N|e^{-i\hat{H}\Delta T}e^{-i\hat{H}\Delta T}\cdots e^{-i\hat{H}\Delta T}|q_0\rangle \tag{166}$$

or, using the resolution of the identity $1 = \int dq\,|q\rangle\,\langle q|$

$$Z = \int dq_{N-1}dq_{N-2}\cdots dq_1 \underbrace{\langle q_N|e^{iH\Delta T}|q_{N-1}\rangle}_{Z_{N,N-1}}\underbrace{\langle q_{N-1}|e^{iH\Delta T}|q_{N-2}\rangle}_{Z_{N-1,N-2}}\cdots\underbrace{\langle q_1|e^{iH\Delta T}|q_0\rangle}_{Z_{1,0}}. \tag{167}$$

If we now focus on a single term, and assume that our Hamiltonian is of the form $\hat{H} = p^2/2 + V(\hat{q})$ we find that

$$\begin{aligned} Z_{N,N-1} &= e^{-iV(q_N)\Delta T}\,\langle q_N|e^{-i\frac{1}{2}\hat{p}^2\Delta T}|q_{N-1}\rangle && (168)\\ &= e^{-iV(q_N)\Delta T}\,\langle q_N|\,e^{-i\frac{1}{2}\hat{p}^2\Delta T}\left(\int dp_N\,|p_N\rangle\,\langle p_N|\right)|q_{N-1}\rangle && (169)\\ &= \int dp_N e^{-i(\frac{1}{2}p_N^2+V(q_N))\Delta T}\,\langle q_N|p_N\rangle\,\langle p_N|q_{N-1}\rangle && (170)\end{aligned}$$

which, due to $\langle p|q\rangle = e^{ipq}$, can be rewritten as

$$Z_{N,N-1} = \int dp_N e^{i\Delta T\left(p_N\frac{q_N-q_{N-1}}{\Delta T}-\frac{p_N^2}{2}-V(q)\right)}. \tag{171}$$

The remaining integral over the momenta is now Gaussian and its solution is well known to be

$$Z_{N,N-1} = e^{i\Delta T\left(\frac{1}{2}\left(\frac{q_N - q_{N-1}}{\Delta T}\right)^2 - iV(q)\right)} \tag{172}$$

so that Z becomes

$$Z = \underbrace{\int \left(\prod_{\alpha \in N-1,\cdots 1} dq_\alpha\right)}_{\text{integration over paths}} \underbrace{e^{i\Delta T \sum_{\beta \in N,\cdots 0}\left(\frac{1}{2}\left(\frac{q_\beta - q_{\beta-1}}{\Delta T}\right)^2 - V(q)\right)}}_{\text{contribution per path}} . \tag{173}$$

To gain some intuition on why this is a useful result let us look at figure 6. First, for one particular

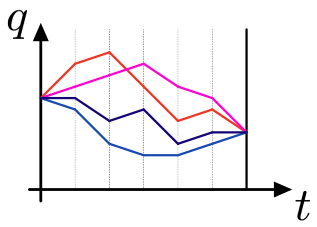

Figure 6: graphical representation of the sum over histories interpretation of quantum mechanics that is obtained from the path integral formulation.

set of values for the integration variables $\{q_\alpha\}$ we can draw the resulting path through space and time. The exponential in equation 173 can then be interpreted as the contribution of that path towards the total transition probability. The integration over the different sets of $\{q_\alpha\}$ then simply adds up all these individual contributions. Note that these individual contributions are phases so that they may interfere with each other. This picture is easily generalized to the limit $\Delta T \to 0$; here we get

$$Z = \int [dq(t)] e^{i\int dt\left(\frac{1}{2}\left(\frac{\partial q(t)}{\partial t}\right)^2 - V(q(t))\right)} \tag{174}$$

where $\int [dq(t)]$ is compact notation for the integration over all possible histories of the field configuration. Finally, a "straightforward" generalization to include the position dependent fields leads to

$$Z = \int [d\phi(x,t)] e^{i\int dtdx\left(\frac{1}{2}(\partial_t\phi(x,t))^2 - \frac{1}{2}(\partial_x\phi(x,t))^2 - V(\phi(x,t))\right)} \tag{175}$$

which will turn out to be a formidable tool in the next section.

Note that the fields $\phi(x,t)$ are now no longer non commuting operators but simple scalar fields. The "quantumness" of this formulation sits in the fact that the probability to end up at the final state is a sum over all possible histories that this field could have taken to end up there.

Effective infrared theories from path integrals

If we apply the path integral formulation to our self interacting bosonic theory we find

$$Z = \int [d\phi(x,t)] e^{i\int dtdx\left(\frac{1}{2}\left(\partial_t\phi\partial_t\phi - \partial_x\phi\partial_x\phi\right) + 2y\cos 2\sqrt{\pi K}\phi\right)} \tag{176}$$

and this is often expressed in terms rescaled fields $\phi_{res} = \sqrt{\pi K}\phi$ and a complex time coordinate $\tau = it$

$$Z = \int [d\phi(x,\tau)] e^{\int d\tau dx\left(-\frac{1}{2\pi K}\left(\partial_t\phi\partial_t\phi + \partial_x\phi\partial_x\phi\right) + 2y\cos 2\phi\right)} . \tag{177}$$

Note that we are again implicitly assuming the existence of momentum cutoff Λ and corresponding minimal length scale $\Delta x_{cut} = 1/\Lambda$ so that integrals converge. Let us now define

$$\phi(x,\tau) = \phi_{IR}(x,\tau) + \phi_{UV}(x,\tau) \tag{178}$$

where $\phi_{IR}(x)$ and $\phi_{UV}(x)$ respectively correspond to the long and short wavelength fluctuations of the field; in terms of Fourier components they respectively have momenta $|k_{IR}| \in [0, \Lambda/b]$ and $|k_{UV}| \in [\Lambda/b, \Lambda]$. Consequently the path integral can be rewritten as

$$Z = \int [d\phi_{IR}][d\phi_{UV}] e^{\int d^2x \left(-\frac{1}{2\pi K}\left((\partial\phi_{IR})^2 + (\partial\phi_{UV})^2 \right) + 2y\cos 2(\phi_{IR}+\phi_{UV}) \right)} \tag{179}$$

where we have used the shorthand notation $(\partial\phi)^2 = (\partial_t\phi)^2 + (\partial_x\phi)^2$ and $d^2x = dxd\tau$.

The big idea of the following section consists of two steps. First we will (approximately) solve the integral over the UV degrees of freedom which results in an effective path integral that has a new (slightly larger) minimal length scale $\Delta x_{cut}(b) = b\Delta x_{cut}$. In the second step we define a new "Laboratory" coordinate frame $x_{lab} = bx$ so that, in terms of these coordinates, the minimal length scale and cutoff remain constant. The net effect of this procedure is that we will have obtained a new path integral that describes only the low energy degrees of freedom of the original compact boson Hamiltonian.[1]

To begin this endeavour, let us first assume that y is small and Taylor expand the exponential

$$Z = Z_{IR} \int [d\phi_{UV}] e^{-\frac{1}{2\pi K}\int d^2x \left(\partial\phi_{UV}\right)^2} \left\{ \begin{array}{l} 1 \\ +2y \int d^2\tilde{x} \cos 2(\tilde{\phi}_{IR} + \tilde{\phi}_{UV}) \\ +2y^2 \left(\int d^2\tilde{x} \cos 2(\tilde{\phi}_{IR} + \tilde{\phi}_{UV}) \right)^2 \end{array} \right\} \tag{180}$$

where we have denoted $Z_{IR} = \int [d\phi_{IR}] e^{-\frac{1}{2\pi K}\int d^2x \left(\partial\phi_{IR}\right)^2}$ and $\tilde{\phi} = \phi(\tilde{x}, \tilde{\tau})$ for co

In what follows we will repeatedly use the identity

$$\int [d\phi] e^{\int d^2p \, \left(-\frac{1}{2}\phi(p)A(p)\phi(p) + J(p)\phi(p) \right)} = \alpha(\Lambda) e^{\int d^2p \, \frac{1}{2} J(p)^\dagger A^{-1}(p) J(p)} \tag{181}$$

with $\alpha(\Lambda)$ some cutoff dependant factor. This identity is simply the multidimensional generalization of the Gaussian integral $\int dx e^{-\frac{1}{2}ax^2 + bx} = \sqrt{2\pi/a} e^{b^2/2a}$.

(1) If we express the first term in momentum space we get the Gaussian integral with $J(p) = 0$ and $A(p) = p^2/\pi K$ so that :

$$Z_1 = Z_{IR} \int [d\phi_{UV}] e^{-\frac{1}{2\pi K}\int d^2x \left(\partial\phi_{UV}\right)^2} \tag{182}$$

$$= \alpha(\Lambda) Z_{IR} = \alpha(\Lambda) Z_{IR;lab} \tag{183}$$

where $Z_{IR;lab}$ is the infrared path integral in the laboratory coordinates.

(2) For the second term we must do some more work: first we expand the cosine into

$$\cos 2(\tilde{\phi}_{IR} + \tilde{\phi}_{UV}) = \cos(2\tilde{\phi}_{IR}) \cos(2\tilde{\phi}_{UV}) - \sin(2\tilde{\phi}_{IR}) \sin(2\tilde{\phi}_{UV}) \tag{184}$$

to get

$$Z_2 = 2y Z_{IR} \int d^2\tilde{x} \cos(2\tilde{\phi}_{IR}) \underbrace{\int [d\phi_{UV}] e^{-\frac{1}{2\pi K}\int d^2x (\partial\phi_{UV})^2} \frac{1}{2} \left(e^{2i\tilde{\phi}_{UV}} + h.c. \right)}_{\text{independent of } \phi_{IR}} \tag{185}$$

[1] To my best knowledge a similar procedure is not known in the Hamiltonian, formalism hence the effort to explain path integrals.

where we have dropped the terms proportional to $\sin(2\tilde{\phi}_{UV})$ because those are integrals of asymmetric functions. The remaining ϕ_{IR} independent part can be again be solved by re-expressing $\phi(x,\tau)$ field as Fourier series so that

$$Z_2 = yZ_{IR}\int d^2\tilde{x}\cos(2\tilde{\phi}_{IR})\int [d\phi_{UV}]e^{\int \frac{d^2p}{4\pi^2}\left(\frac{1}{2\pi K}\phi_{UV}(p)p^2\phi_{UV}(p)+2ie^{ip\tilde{x}}\phi_{UV}(p)\right)} + h.c. \tag{186}$$

which through application of the Gaussian integral becomes

$$Z_2 = y\ \alpha(\Lambda)Z_{IR}\int d^2\tilde{x}cos(2\tilde{\phi}_{IR})\underbrace{e^{-\frac{1}{2}\int_{p\in UV}d^2p\frac{K}{2\pi p^2}} + h.c.}_{2e^{-K\ln(b)}} \tag{187}$$

$$\tag{188}$$

which only depends on the width of the integrated momenta so that we can easily take the limit Λ to infinity. Finally, in the laboratory coordinates $x_{lab} = bx$ we get

$$Z_2 = 2\ b^2y\ e^{-K\ln(b)}\ \alpha(\Lambda)Z_{IR;lab}\int d^2\tilde{x}_{lab}cos(2\tilde{\phi}_{IR;x_{lab}}) \tag{189}$$

(3) If we consider the square in the first term

$$Z = 2y^2\ Z_{IR}\int [d\phi_{UV}]e^{-\frac{1}{2\pi K}\int d^2x(\partial\phi_{UV})^2}\left(\int d^2\tilde{x}\cos 2(\tilde{\phi}_{IR}+\tilde{\phi}_{UV})\right)\left(\int d^2\tilde{\tilde{x}}\cos 2(\tilde{\tilde{\phi}}_{IR}+\tilde{\tilde{\phi}}_{UV})\right) \tag{190}$$

and expand $cos(\cdots)^2$ as

$$\begin{aligned} cos2(\tilde{\phi}_{IR}+\tilde{\phi}_{UV})cos2(\tilde{\tilde{\phi}}_{IR}+\tilde{\tilde{\phi}}_{UV}) &= cos2(\tilde{\phi}_{IR}-\tilde{\tilde{\phi}}_{IR})cos2(\tilde{\tilde{\phi}}_{UV}-\tilde{\phi}_{UV}) \\ &\quad + \text{terms proportional to } \sin(\tilde{\phi}_{UV}) \text{ and } \sin(\tilde{\tilde{\phi}}_{UV}) \end{aligned} \tag{191}$$

we get

$$Z_3 = 2y^2Z_{IR}\int d^2\tilde{x}d^2\tilde{\tilde{x}}\cos 2(\tilde{\phi}_{IR}-\tilde{\tilde{\phi}}_{IR})\underbrace{\int [d\phi_{UV}]e^{-\frac{1}{2\pi K}\int d^2x(\partial\phi_{UV})^2}\frac{1}{2}\left(e^{2i(\tilde{\phi}_{UV}-\tilde{\tilde{\phi}}_{UV})}+h.c.\right)}_{\text{independent of }\phi_{IR}} \tag{192}$$

$$= y^2Z_{IR}\int d^2\tilde{x}d^2\tilde{\tilde{x}}\cos 2(\tilde{\phi}_{IR}-\tilde{\tilde{\phi}}_{IR})\int [d\phi_{UV}]e^{\int \frac{d^2p}{4\pi^2}\left(\frac{1}{2\pi K}\phi_{UV}(p)p^2\phi_{UV}(p)+2i(e^{ip\tilde{x}}-e^{ip\tilde{\tilde{x}}})\phi_{UV}(p)\right)} + h.c. \tag{193}$$

$$= y^2\alpha(\Lambda)Z_{IR}\int d^2\tilde{x}d^2\tilde{\tilde{x}}\cos 2(\tilde{\phi}_{IR}-\tilde{\tilde{\phi}}_{IR})\left(\underbrace{e^{-\frac{1}{2}\int \frac{d^2p}{4\pi^2}(e^{ip\tilde{x}}-e^{ip\tilde{\tilde{x}}})\frac{\pi K}{p^2}(e^{-ip\tilde{x}}-e^{-ip\tilde{\tilde{x}}})}+h.c.}_{f(\tilde{x}-\tilde{\tilde{x}})}\right). \tag{194}$$

To proceed we note that the $x\to 0$ and $x > b/\Lambda$ limits of $f(x)$ are respectively $f(x\to 0) = 1$ and $f(x > b/\Lambda) = \frac{1}{b}$. The second, not so obvious, limit can be derived from the realization that, for these separations, the phases in the complex exponential will be rapidly oscillating functions so that they will cancel under the integral. The upshot of all this is that the $\int d^2\tilde{x}d^2\tilde{\tilde{x}}$ integral will only pick up contributions if $\tilde{x}-\tilde{\tilde{x}}$ is sufficiently small. With this, and the further approximation $\tilde{\phi}_{IR}-\tilde{\tilde{\phi}}_{IR}\approx\partial\phi_{IR}$ we get :

$$Z_3 \approx y^2\alpha(\Lambda)Z_{IR}\int d^2\tilde{x}(\partial\phi_{IR})^2 \tag{195}$$

which remains unchanged in the laboratory coordinates.

(1+2+3) Finally, bringing everything together we get :

$$Z \approx \alpha(\Lambda)\int [d\phi_{IR}]e^{-\frac{1}{2\pi K}\int d^2x_{lab}(\partial\phi_{IR;lab})^2}\left(1+2yb^2e^{-K\ln(b)}\int d^2\tilde{x}_{lab}\cos(2\tilde{\phi}_{IR;lab})+y^2\int d^2\tilde{x}_{lab}(\partial\tilde{\phi}_{IR;lab})^2\right) \tag{196}$$

which can be interpreted as the first order Taylor expansion of

$$Z(b) = \alpha(\Lambda) \int [d\phi] e^{\int d^2 x_{lab} \left(-\left(\frac{1}{2\pi K} + y^2\right) \left(\partial \phi_{IR;lab}\right)^2 + 2\left(e^{-K \ln b} b^2 y\right) \cos 2\phi_{IR;lab} \right)} . \tag{197}$$

Therefore, the low energy degrees of freedom (i.e. those with momentum $p < \Lambda/b$) are described by an effective action with new couplings

$$\begin{cases} y \to y(b) = y e^{-K \ln b} b^2 \\ \frac{1}{2\pi K} \to \frac{1}{2\pi K(b)} = \frac{1}{2\pi K} + y^2 \end{cases} . \tag{198}$$

To simplify these expressions we choose $b = 1 + db$ i.e. we only trace away a very thin momentum shell. With this we get

$$\begin{cases} \frac{dy}{db} = \lim_{db \to 0} \frac{y(1+db) - y(1)}{db} = (2 - K) y \\ \frac{dK}{db} = \lim_{db \to 0} \frac{K(1+db) - K(1)}{db} = -y^2 \end{cases} \tag{199}$$

so that $\frac{d}{db}\left((2-K)^2 - y^2\right) = 0$ i.e. $\delta = (2 - K(b))^2 - y^2(b)$ remains constant throughout the flow towards the effective IR. In figure 7 we show the lines of constant δ as blue lines and with arrows pointing towards the low energy effective theories.

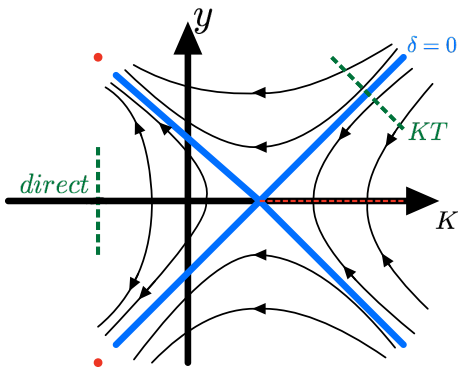

Figure 7: The renormalization group flow of the self interacting boson. The black lines have constant δ and the arrows point towards increasing b i.e. lower energies. The red dots in the top/bottom left show the zero correlation length fix points and the dotted red line at the $K > 2$ axis shows the free boson model with infinite correlation length. The leftmost dashed green line indicates a direct transition from the $\langle \phi \rangle = n\pi$ to the $\langle \phi \rangle = \pm \pi/2$ phase, along this line the correlation length diverges as a power-law as approach the K-axis. The second dashed green line indicates a KT transition where the correlation length diverges exponentially fast near $\delta \to 0_+$.

From this figure see that every compact boson theory with initial couplings in the right wedge will eventually flow towards the $y = 0$ axis. This means that, in this wedge, the $\cos(2\phi)$ term has no influence on the infrared physics i.e. this term is irrelevant. For all other initial $y \neq 0$ points the flow is to the fix points in the upper or lower left corners that correspond to some gapped phase where the $\cos(2\phi)$ term is the most relevant contribution to the Hamiltonian. The effect is that ϕ will develop long range order along the minima/maxima of $\cos(2\phi)$. Finally we note that the initial cutoff Λ no longer appears in these flow equations so that the flow diagram of the $\Lambda \to \infty$ model will still be the one displayed in figure 7.

Kosterlitz Thoules transition

In this section we will study the behaviour of the correlation length as we tune the couplings of our model from the the top wedge to the right wedge as indicated by the rightmost green line in figure 7.

Before we start, note that we already know that the correlation length must diverge as we approach the edge of the right wedge, so that the only remaining question is the nature of the divergence. To find this, let us first rewrite dK/db in terms of δ

$$\frac{dK}{db} = -y^2 = \delta - (2-K)^2 \tag{200}$$

and then use δ as a measure of distance to the critical point. Additionally, we know that the correlation length, in terms of the laboratory coordinates behaves as $\xi_{lab} \to \xi_{lab}(b+db)$ so that : $d\xi_{lab} = \xi_{lab} db$.

If we now integrate these equations along a path of constant δ that starts at our point of interest (where $\xi_{lab} = \xi$ and $K = K_{UV} \gg 2$) and ends at the fixed point (where $K_{IR} = -\infty$) we get

$$\begin{cases} b = \frac{1}{\sqrt{\delta}} \left(\arctan(\frac{K_{UV}-2}{\sqrt{\delta}}) - \arctan(\frac{K_{IR}-2}{\sqrt{\delta}}) \right) = \frac{\pi}{\sqrt{\delta}} \\ \frac{\xi}{\xi_{fixpoint}} = e^b \end{cases} . \tag{201}$$

The first equation tells us that we must trace over more momenta to reach the trivial IR theory if we start from a UV theory closer to the critical line and together with the second equation, which relates the original correlation length with that of the IR theory, we get :

$$\xi = \xi_{fixpoint} e^{\frac{\pi}{\sqrt{\delta}}} \tag{202}$$

which is the desired behaviour of the correlation length as we approach the critical point.

Furthermore, it is worth noting that the Taylor expansion of $1/\xi$ in terms of δ is identically zero which means that a perturbative treatment of the y term in the original Hamiltonian would have never revealed this kind of phase transition.

Direct phase transistion

In this section, we want to know the scaling of the correlation length as we cross the $y = 0$ line for $K < 2$. Looking back at figure 7 we see that, close to the $y = 0$ line the value of K remains unchanged under our RG flow. Consequently we can just integrate

$$\frac{dy}{db} = (2-K)y \tag{203}$$

along a path of constant K that starts at our point of interest (where $\xi_{lab} = \xi$) and ends at some reference point (where $\xi = \xi_{ref}$ an $y = y_{ref}$), this gives us

$$\begin{cases} \ln(y_{ref}/y) = (2-K)b \\ \xi/\xi_{ref} = e^b \end{cases} \tag{204}$$

which leads to

$$\xi = \xi_{ref} \left(\frac{1}{y} \right)^{\frac{1}{2-K}} \tag{205}$$

a power law divergence of the correlation length as the $y = 0$ axis is approached.

Higher cosine terms in the compact boson

The y term in the Hamiltonian 177 has a Z_2 symmetry :

$$\phi \to \phi + \pi \tag{206}$$

and we saw that the phase diagram contained two symmetry broken phases, one where y becomes infinitely positive and ϕ condenses around $0 = 2\pi$ and π and another where y becomes infinitely negative and ϕ condensed around $\pm\pi/2$).

Similarly, we can define the model

$$H_{LL} = \int dx \frac{\pi K}{2}\Pi^2 + \frac{1}{2\pi K}(\partial_x\phi)^2 + 2y_N\cos(N\phi) \tag{207}$$

that contains the $N-$th power of the physical fields that we defined in section 3.2.1. This model now has a Z_N symmetry

$$\phi \to \phi + 2\pi/N \tag{208}$$

and a similar analysis reveals a phase diagram where the symmetry broken phases now have N distinct groundstates with $\phi = 0, 2\pi/N, 3\pi/N, \cdots$ and $\phi = \pi/2 + 2\pi/N, \pi/2 + 3\pi/N \cdots$.

One very important property of these higher order terms is that the lowest N perturbation will always be the most relevant. To clarify, consider a UV theory with $y_N\cos(N\phi)$ and $y_{M>N}\cos(M\phi)$. In the large K regime both terms will be irrelevant and effective theory for the infrared degrees of freedom has $y_N = y_M = 0$. As we move K to smaller values we will eventually pass through a KT transition and enter a phase where Z_N symmetry is broken because the y_N coupling starts to grow towards the IR. Eventually, for even smaller values the y_M coupling will also become relevant and break the remaining Z_M symmetry.

3.3 Fermionic lattice field theories

In the previous sections we have introduced quantum field theory in its usual formulation. This approach turned out to be very effective for free models but we saw that interactions lead to divergent corrections that had to be regularized, i.e. ,we had to introduce a cutoff Λ for the allowed momenta in the Fourier transforms of the fields. Furthermore, we found that observables such as the IR mass scale depends on this cutoff, which lead to the idea that a continuous model had to be interpreted as a limit of a series of models. The idea of this section is that we can similarly take the limit of a series of lattice models with ever decreasing intersite distance a.

In what follows we will demonstrate this by first demonstrating one particular approximation of the free fermion field theory on a lattice and then define the limit procedure that reproduces the spectrum of the original continuum construction. In the final part we will highlight a limitation of this method and discuss the profound physical consequences of this limitation.

3.3.1 There: From free fermions to the SSH model

As a reminder the Hamiltonian for the free fermion was

$$H = \int \mathrm{d}x \left(\psi^\dagger_\alpha(x) i\gamma^0_{\alpha\beta}\gamma^x_{\beta\gamma}\partial_x\psi_\gamma(x) + m\psi^\dagger(x)\gamma^0\psi(x)\right) \tag{209}$$

and the particular choice of gamma matrix did not influence the spectrum. For this discussion it will be useful to make a choice where $\gamma^0\gamma^x = \sigma_x$ and $\gamma^0 = \sigma_y$ so that

$$H = \int \mathrm{d}x\; i\left(\psi^\dagger_1(x)\partial_x\psi_2(x) + \psi^\dagger_1(x)\partial_x\psi_2(x)\right) + im\left(\psi^\dagger_1(x)\psi_2(x) - \psi^\dagger(2)\psi_1(x)\right). \tag{210}$$

By now we already know that such Hamiltonians are only well defined when supplemented with some momentum cutoff Λ so that it only describes physics at lengths scales smaller then $a = \frac{1}{\Lambda}$. Consequently, it is fair to assume that we must only look at the following subset of field operators

$$\begin{cases} \psi^\dagger_1(x = na) = \frac{c^\dagger_{2n}}{\sqrt{a}} \\ \psi^\dagger_2(x = na) = \frac{c^\dagger_{2n+1}}{\sqrt{a}} \end{cases} \tag{211}$$

where we divide by $\sqrt{a}$ to get dimensionless lattice operators. Note that we have placed the first/second component of the fermion field at even/odd lattice sites respectively and that this step makes it so that the $U(1)_{axial}$ symmetry of the $m = 0$ field theory does not survive on the lattice. We will motivate this peculiar staggered pattern in section 3.3.3 below, for now let us just move on and also approximate derivatives as

$$\begin{cases} \partial_x \psi_1^\dagger(x = na) = \frac{c_{2n+2}^\dagger - c_{2n}^\dagger}{a\sqrt{a}} \\ \partial_x \psi_2^\dagger(x = na) = \frac{c_{2n+1}^\dagger - c_{2n-1}^\dagger}{\sqrt{a}} \end{cases} \tag{212}$$

and define a dimensionless lattice mass $m_{latt} = ma$ so that

$$H \approx \frac{1}{a} \sum_n i c_{2n}^\dagger \left(c_{2n+1} - c_{2n-1}\right) + i c_{2n+1}^\dagger \left(c_{2n+2} - c_{2n}\right) + i m_{latt} \left(c_{2n}^\dagger c_{2n+1} - c_{2n+1}^\dagger c_{2n}\right) . \tag{213}$$

For $m_{latt} = 0$ this model has a symmetry $c_{2n} \to c_{2n+1}$ and $c_{2n+1} \to c_{2n+2}$ which in terms of the original fermionic fields

$$\begin{cases} \psi_1^\dagger(x) \to \psi_2^\dagger(x) \\ \psi_2^\dagger(x) \to \psi_1^\dagger(x = x + a) \end{cases} \tag{214}$$

represents the Z_2 subgroup of the axial $U(1)$ symmetry up to corrections of $\mathcal{O}(a)$. Furthermore, if want the field theory property $\gamma^5 H(m) \gamma^5 = H(-m)$ to hold on the lattice, i.e. $H(m) \xrightarrow[\text{shift}]{\text{single}} H(-m)$ we must modify Equation 213 to

$$\begin{aligned} H \approx \frac{1}{a} \sum_n & i c_{2n}^\dagger \left(c_{2n+1} - c_{2n-1}\right) + i c_{2n+1}^\dagger \left(c_{2n+2} - c_{2n}\right) \\ & + i \frac{m_{latt}}{2} \left(c_{2n}^\dagger c_{2n+1} - c_{2n+1}^\dagger c_{2n}\right) \\ & - i \frac{m_{latt}}{2} \left(c_{2n+1}^\dagger c_{2n+2} - c_{2n+2}^\dagger c_{2n+1}\right) \end{aligned} \tag{215}$$

which is exactly the SSH Hamiltonian that we studied before!

One crucial remark is that we could have made a different initial choice for the γ matrices and that the resulting lattice model would not necessarily describe the same physics. In fact the unitary equivalence of fermion models with different γ matrices was lost together with the chiral $U(1)_{axial}$ when we staggered the fermions. For example, the original formulation of this discretization procedure by Kogut and Susskind chose $\gamma^0 \gamma^5 = \sigma^x$ and $\gamma^0 = \sigma_z$, which leads to

$$\begin{aligned} H \approx \frac{1}{a} \sum_n & c_{2n}^\dagger \left(c_{2n+1} + c_{2n-1}\right) + c_{2n+1}^\dagger \left(c_{2n+2} + c_{2n}\right) \\ & + m_{latt} \left(c_{2n} c_{2n}^\dagger - c_{2n+1} c_{2n+1}^\dagger\right) \end{aligned} \tag{216}$$

$$\tag{217}$$

which now has a mass term that prefers anti-ferromagnetic order instead of dimer order. The upshot is that, dependant on the choice of γ matrices, we will find a different type of mass term on the lattice. In the second chapter we will discuss an example where the Kogut Susskind discretization is unfavourable compared to the one presented here. For now, let us just accept that the one presented here is a more logical choice.

3.3.2 And back again: From SSH to free fermions

From the previous section we suspect that

$$\lim_{a \to 0} H_{SSH}(a, m_{latt}(a)) = \lim_{\Lambda \to \infty} H_{free fermion}(\Lambda, m(\Lambda)) , \tag{218}$$

to verify this let us remind ourselves of the dispersion relation of the SSH model

$$E_{k_{latt}} = \pm\frac{1}{a}\sqrt{4\sin^2(k_{latt}/2) + m_{latt}^2\cos^2(k_{latt}/2)} \tag{219}$$

where we have written k_{latt}, m_{latt} to stress that these are dimensionless quantities on the lattice. For the momentum specifically this means that k_{latt} describes physics on the length scale of $1/k_{latt}$ lattice sites, the inverse physical distance associated with these phenomena is therefore $k_{phys}^{-1} = ak_{latt}^{-1}$.

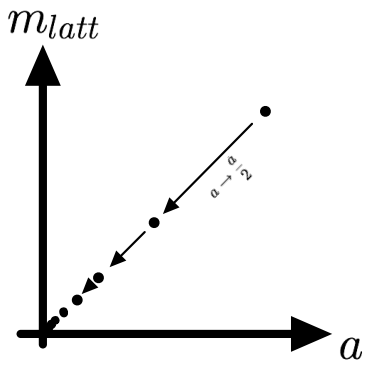

Figure 8: Starting at some initial lattice model with $a = a_0$ and $m_{latt} = m_0$ we reach the continuumlimit $a \to 0$ by simultaneously and iteratively halving both m_{latt} and a so that $m_{latt}(a)/a = m_{phys}$ remains constant. This procedure defines a continuous model where the mass of the elementary excitation is well defined.

Sadly, simply taking the limit $a \to 0$ is not a valid procedure as this pushes the energy of all excitations to infinity. The correct procedure is shown in figure 8 above, we start with some lattice model with $a = a_0$ and $m_{latt} = m_0$ so that the energy gap in terms of dimensionfull variables is $E_{phys} = m_0/a_0$. From this initial model we can reach $a = 0$ by iteratively and simultaneously halving a and m_{latt} so that the gap expressed in physical units $E_{phys} = \frac{m_{latt,new}}{a_{new}}$ remains constant.

Furthermore, we can also re-express the dispersion relation in terms of a dimensionfull momentum $k = \frac{k_{latt}}{a}$

$$\omega_k = \pm\sqrt{\frac{4}{a^2}\sin^2(\frac{ka}{2}) + m^2\cos^2(\frac{ka}{2})} \tag{220}$$

and for sufficiently small momenta $ka \ll 1$ (i.e. momenta that correspond to length scales much larger then the lattice spacing) this can be expanded as

$$\omega_k = \pm\sqrt{k^2 + m^2}\,. \tag{221}$$

Therefore, as $a \to 0$ we recover the original dispersion relation.

3.3.3 Fermion doubling

Let us now reconsider the ad-hoc step where we staggered the fermions and broke the $U(1)$ symmetry. The natural choice, which respects the symmetry, would have been

$$\psi_\alpha^\dagger(x = na) = \frac{c_{n,\alpha}^\dagger}{\sqrt{a}} \tag{222}$$

and

$$\partial_x\psi_\alpha^\dagger(x = na) = \frac{c_{n+1,\alpha}^\dagger - c_{n-1,\alpha}^\dagger}{2a\sqrt{a}}\,. \tag{223}$$

If we still work with the previous convention for the γ matrices, the $m = 0$ lattice Hamiltonian becomes

$$H \approx \frac{1}{a}\sum_n \frac{i}{2} c^\dagger_{n,1}\left(c_{n+1,2} - c_{n-1,2}\right) + \frac{i}{2} c^\dagger_{n,2}\left(c_{n+1,1} - c_{n-1,1}\right) + h.c. \tag{224}$$

and at first sight we can now simply perform the continuum procedure and identify the field theoretic dispersion with that of lattice around $k_{latt} = 0$. However upon closer inspection equation 224 only couples $c_{even,1}$ to $c_{odd,2}$ and $c_{even,2}$ to $c_{odd,1}$ so that we can write

$$H \approx H_{even,1;odd,2} \bigoplus H_{odd,1;even2} \tag{225}$$

where, up to relabeling of the indices

$$H_{1,2} = H_{2,1} = \frac{1}{a}\sum_n \frac{i}{2} c^\dagger_{n,1}\left(c_{n+1,2} - c_{n-1,2}\right) + h.c. \tag{226}$$

is the critical SSH model ! Consequently, the number of infrared degrees of freedom of this lattice model is double that of the original field theory. More general, one can show that it is impossible to discretize the Dirac Hamiltonian so that the resulting lattice Hamiltionian has continuous chiral symmetry, locality and the correct particle content in the limit $a \to 0$. Therefore, if we want the correct number of degrees of freedom in the continuum we have to break the continuous chiral symmetry, the best we can do is to still retain its (approximate) Z_2 subgroup, which is exactly what we did in the previous section.

3.4 Bosonic lattice field theories

For bosonic theories the approach is very similar to what we did before. For example the operators in the interacting boson from equation can be represented by

$$\begin{cases} \phi(x = na) = q_n \\ \Pi(x = na) = \frac{1}{a} p_n \end{cases} \tag{227}$$

where the q_n and p_n matrices are the infinite dimensional matrices from equation 165. If we also define the dimensionless lattice coupling $y_{latt} = a^2 y$ we find

$$H_{LL} \approx \sum_a \frac{1}{a}\left(\frac{\pi K}{2} p_n^2 + \frac{1}{2\pi K}\left(\phi_{n+1} - \phi_n\right)^2 + 2y_{latt}\cos(2q_n)\right) \tag{228}$$

and one could then also define a suitable limit of such lattice models.

Part II

COLLECTED PUBLICATIONS WITH INTRODUCTIONS

4

A MODIFIED ISING CHAIN

The motivation for this project was a tweaked version of the Ising Hamiltonian

$$H_{mod} = \sum_i -g\sigma_i^z\sigma_{i+1}^z + CZ_{i-1,i+1}\sigma_i^x \tag{229}$$

where $CZ_{i-1,i+1}$ is the controlled Z-operator $|\downarrow\downarrow\rangle\langle\downarrow\downarrow| + |\downarrow\uparrow\rangle\langle\downarrow\uparrow| + |\uparrow\downarrow\rangle\langle\uparrow\downarrow| - |\uparrow\uparrow\rangle\langle\uparrow\uparrow|$ that acts as the identity except when it acts on two spin up spins, in which case it generates a minus sign. Similarly to the original Ising model, there is a Z_2 symmetry which now contains contains the identity and a nonlocal generalization of the spin flip operator

$$\hat{X}_{mod} = \bigotimes \sigma_i^x \bigotimes CZ_{i-1,i+1} \tag{230}$$

which can be represented by a matrix product operator, similar to how we represented the Ising Hamiltonian in equation 37.

To intuitively appreciate the impact of this modification, let us consider the third order corrections to one of the large g groundstates e.g. $|\uparrow\rangle^{\otimes N}$. According to section 2.1.2 this contribution will contain (among others) states that contain three consecutive down spins. In this case these spins are flipped through the action of the modified spinflips $CZ_{i-i,i+1}\sigma_i^x$ and the addition CZ generates a phase that depends on the order of operations as is depicted in figure 9 below.

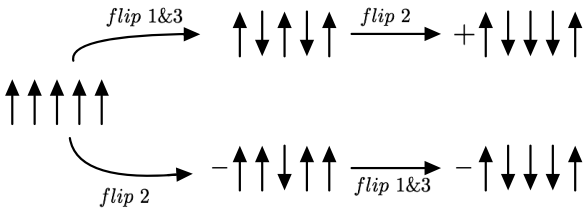

Figure 9: Two different orders of operations that can be used to construct the third order correction containing Kink-Antikink pairs with separation 3. Due to the presence of the additional CZ these two orders will generate the same same state up to a minus sign so that it is conceivable that their contributions will cancel in the perturbative series.

The upshot is that the contribution of these three spin bubbles to the corrected vacuum will be suppressed (compared to the usual Ising model), because the contributions from the different diagrams will tend to cancel out. Consequently we do not expect the mechanism by which the order is restored to be the simple kink condensation of the Ising model. In fact, this simple intuitive perturbative argument can be made rigorous by a modification of the arguments in section 1.2.3. This type of generalization is a whole field in itself, so we will not discuss the details of the procedure. All we need to know is that Hamiltonians with nonlocal Z_2 symmetries can never have a symmetric phase where the elementary excitation is massive; we are therefore guaranteed that the phase diagram of this model will be drastically different from that of the usual Ising model.

To find this, a priori unknown, phase diagram we approximated the grounstate and excited states of this model with MPS en quasiparticle states respectively. The phase diagram we found contained an extended critical phase for $g \in [-0.9, 0]$ where the infrared degrees of freedom are well described by

the Luttinger Liquid field theory we discussed in section 3.2.1. Furthermore, the transition at $g = 0$ turns out to be a KT transition driven by a $\cos(2\phi)$ term [1].

[1] In the paper the compactification ratio of the compact scalar is $\pi/2$ so we have that $\phi_{maintext} = 2\phi_{paper}$. Therefore the $cos(4\phi)$ perturbation that is mentioned in the paper corresponds to a $\cos(2\phi)$ perturbation in terms of the convention handled in the previous chapter.

Anomalous domain wall condensation in a modified Ising chain

Gertian Roose,[1] Laurens Vanderstraeten,[1] Jutho Haegeman,[1] and Nick Bultinck[2]
[1]*Department of Physics and Astronomy, University of Ghent, Krijgslaan 281, 9000 Gent, Belgium*
[2]*Department of Physics, University of California, Berkeley, California 94720, USA*

(Received 7 January 2019; revised manuscript received 23 April 2019; published 20 May 2019)

We construct a one-dimensional local spin Hamiltonian with an intrinsically nonlocal, and therefore anomalous, global $\mathbb{Z}_2$ symmetry. The model is closely related to the quantum Ising model in a transverse magnetic field, and contains a parameter that can be tuned to spontaneously break the nonlocal $\mathbb{Z}_2$ symmetry. The Hamiltonian is constructed to capture the unconventional properties of the domain walls in the symmetry-broken phase. Using uniform matrix product states, we obtain the phase diagram that results from condensing the domain walls. We find that the complete phase diagram includes a gapless phase that is separated from the ordered ferromagnetic phase by a Berezinskii-Kosterlitz-Thouless transition, and from the ordered antiferromagnetic phase by a first-order phase transition.

DOI: 10.1103/PhysRevB.99.195132

I. INTRODUCTION

Spontaneous symmetry breaking in quantum many-body systems can be characterized by the nonzero expectation value of an order parameter. In symmetry-broken systems, there exists a basis such that each ground state is uniquely characterized by its uniform and nonzero value for the order parameter. For certain symmetry-breaking patterns and in certain spatial dimensions, it is possible to consider states where the order parameter is nonuniform and contains a topological defect [1,2], such as, for example, a domain wall in one dimension or a vortex in two dimensions. Because such topological defects are stable and cannot be created by local operators, it is possible that they bind fractional quantum numbers associated with unbroken global symmetries. In fact, many examples of systems where this occurs are known. Among the earliest examples are the Jackiw-Rebbi [3] or the Su-Schrieffer-Heeger model [4], where domain walls bind half-integer U(1) charge, and the spin-1/2 soliton in quantum spin chains [5].

The binding of fractional quantum numbers to topological defects is closely related to Lieb-Schultz-Mattis-Oshikawa-Hastings (LSMOH) theorems [6–8], which forbid the existence of short-range entangled phases that do not break any microscopic on-site and spatial symmetries. In the original LSMOH theorems, the relevant on-site symmetry was U(1) or SU(2), and the spatial symmetry was simply lattice translation symmetry. However, by now, LSMOH theorems exist for many other on-site and spatial symmetries [9–13]. An intuitive way to understand the connection between LSMOH theorems and fractionalization of topological defects is to imagine a system in a symmetry-broken phase, such that condensation of topological defects drives it to a disordered phase. If the defects carry fractional quantum numbers, this condensation transition cannot result in a short-range entangled, featureless state. An interesting example is the spin-1/2 Heisenberg antiferromagnet on the square lattice. Because this model has half-odd integer spin per unit cell, the LSMOH theorem forbids a short-range entangled symmetric ground state. If we assume the ground state is a valence-bond solid (VBS), topological defects in the $\mathbb{Z}_4$ valued order parameter carry spin-1/2 [14]. In the Néel phase, spin-wave excitations in topological sectors with an odd skyrmion number carry momenta around $(0, \pi)$ or $(\pi, 0)$ [15]. Condensing the skyrmions therefore leads to the fourfold ground-state degeneracy of the VBS phase [16,17]. These observations also lie at the basis for the original theory of deconfined quantum criticality [18], which was proposed to describe a Landau-forbidden continuous phase transition between the Néel and VBS orders. Recently, a 1D Hamiltonian with a LSMOH constraint was constructed such that in the VBS phase the domain walls bind a nontrivial projective representation of $\mathbb{Z}_2 \times \mathbb{Z}_2$ [19]. The authors of Ref. [19] argued that condensing these domain walls results in a deconfined quantum critical point in the phase diagram, separating two different symmetry-broken phases.

Another context in which fractionalized quantum numbers and/or unconventional zero modes bind to topological defects, is at the boundary of symmetry-protected topological (SPT) phases [20–24]. One of the most notable examples is the time-reversal symmetric superconducting boundary state of the 3D topological insulator, where a vortex traps a Majorana mode [25]. In the nontrivial 3D bosonic SPT phase with $\mathrm{U}(1) \times \mathbb{Z}_2^T$ symmetry, where $\mathbb{Z}_2^T$ is time-reversal symmetry, boundary vortices bind a Kramers pair in their core [26]. In Ref. [27], the authors showed that for certain 2D SPT phases with $\mathbb{Z}_n \times \mathbb{Z}_m$ symmetry, boundary domain walls associated with broken $\mathbb{Z}_n$ symmetry carry fractional charge under $\mathbb{Z}_m$, and vice versa. When the symmetry group is $\mathbb{Z}_n \times \mathbb{Z}_m \times \mathbb{Z}_p$, there exist 2D bosonic SPT phases such that a boundary domain wall of $\mathbb{Z}_n$ binds a nontrivial projective representation of $\mathbb{Z}_m \times \mathbb{Z}_p$ [27].

It was recognized early on that the physics of deconfined quantum critical points and the boundaries of SPT phases are closely related [26]. More recently, systems where a LSMOH theorem applies were interpreted as the boundary of a SPT phase with both on-site and spatial symmetries [28,29]. All these systems also share the property that a topological

theta term or Wess-Zumino-Witten term is essential to obtain the correct nonlinear sigma model effective-field theory [15,29–32]. The physical meaning of such terms is exactly that they provide the topological defects with the correct properties such as fractional quantum numbers. By now, a deeper unified language for the physics of LSMOH theorems, SPT surface states, and deconfined quantum critical points has emerged in terms of 't Hooft anomalies [33–39]. For UV lattice models, a 't Hooft anomaly simply means that a global symmetry is realized in an intrinsically nonlocal way [23,34]. In the context of LSMOH theorems, 't Hooft anomalies can occur because of the non-on-site nature of the spatial symmetries. In the context of SPT phases, a local symmetry in the bulk can effectively act as a nonlocal symmetry on the low-energy boundary or surface modes. The common wisdom is that when a nonlocal symmetry with nontrivial 't Hooft anomaly gets spontaneously broken, topological defects in the corresponding order parameter will acquire unconventional properties such as fractional quantum numbers. However, it is important to note that fractionalization is not the only unconventional property of defects that can occur when a nonlocal symmetry gets broken. Another possibility is that the defects have nontrivial statistics [40]. For example, on the boundary of a 3D bosonic topological insulator with $\mathrm{U}(1) \rtimes \mathbb{Z}_2^T$ symmetry, the vortices become fermions [26,41].

In this paper, we consider a 1D model with a $\mathbb{Z}_2$'t Hooft anomaly where similar phenomena occur. In particular, we construct a spin Hamiltonian for which, in the symmetry-broken phase, the domain walls between the two vacua behave as semions in a sense that we specify below. It can be interpreted as the edge Hamiltonian of a 2D bosonic SPT phase corresponding to the nontrivial element of $H^3(\mathbb{Z}_2, U(1)) = \mathbb{Z}_2$ [23,24,42]. The Hamiltonian is closely related to the 1D quantum Ising model in transverse magnetic field, and contains a parameter that we can tune to condense the domain walls. We show that this model indeed has a nonlocal $\mathbb{Z}_2$ symmetry that can be written in matrix product operator (MPO) form. We find that the Hamiltonian we construct has close connections to anyon chains [43,44] and that—-not surprisingly—its symmetry is of the CZX type [23]. Upon condensing the "semionic" domain walls, there occurs a Berezinskii-Kosterlitz-Thouless (BKT) transition [45,46] to a Luttinger liquid phase [47] with an emergent $\mathrm{U}(1) \times \mathrm{U}(1)$ symmetry. The Luttinger liquid description of the gapless regime agrees with the Chern-Simons description of 2D SPT phases [48]. We numerically study the entire phase diagram with uniform matrix product states and also find a first-order transition, making the phase diagram very similar to that of the XXZ model. We expect our model to capture the generic boundary phase diagram of the nontrivial 2D bosonic $\mathbb{Z}_2$ SPT phase. In Ref. [49], the authors constructed gapped boundaries of SPT phases using symmetry extensions. However, we did not find a natural way to incorporate these symmetry extensions in our minimal effective model for the domain walls.

II. "SEMIONIC" DOMAIN WALLS

We imagine a situation where the $\mathbb{Z}_2$ symmetry of a 2D nontrivial bosonic SPT is spontaneously broken on the boundary. We also assume that the symmetry-breaking-induced gap is much smaller than the bulk gap. In this case, the low-energy degrees of freedom will be the domain walls on the boundary and the dynamics will be effectively 1D. In this section, we discuss the imprint of the $\mathbb{Z}_2$'t Hooft anomaly on the boundary symmetry-breaking phase.

Based on the group cohomology classification of bosonic SPT phases [24], a natural guess for the property of the boundary domain walls that distinguishes them from conventional Ising domain walls is that they have unusual fusion rules. In particular, if we consider three domain walls localized in some region, pairwise annihilating the first two or pairwise annihilating the last two gives a relative minus sign. Schematically,

$$(1,2)3 = -1(2,3)\,, \tag{1}$$

where we numbered the domain walls and the brackets denote a pairwise annihilation process. That this is indeed the correct property of the anomalous domain walls can be verified by the tensor network constructions of 2D SPT phases [23,50]. The intuition behind these unusual fusion rules is now, analogous to Haldane's argument for the gaplessness of the spin-1/2 chain [15,51,52], that in a path integral representation these minus signs will lead to destructive interference which prevents the disordered phase from having short-range correlations.

Let us elaborate on why Eq. (1) implies that the domain walls can be interpreted as semionic quasiparticles. For this, we consider a state with $2N$ domain walls. We order the domain walls and pair them up in neighboring pairs, i.e., we represent the state as

$$(1,2)(3,4)\ldots(2N-1,2N)\,, \tag{2}$$

where now we interpret the brackets as indicating that these domain wall pairs were created together from the vacuum. This choice of pairing is arbitrary and merely serves as a reference configuration. Let us now create an additional domain wall pair. There are two possibilities to do this. The first is that we create the pair between two other pairs, such that the state, e.g., becomes

$$(1,2)(3,4)(1',2')(5,6)\ldots(2N-1,\ 2N)\,, \tag{3}$$

where we denote the newly created pair with primes. This state can simply be relabeled to obtain the reference state with $2N+2$ domain walls:

$$\begin{aligned}&(1,2)(3,4)(1',2')(5,6)\ldots(N-1,\ N)\\ &\quad\to (1,2)(3,4)(5,6)(7,8)\ldots(2N+1,\ 2N+2)\,.\end{aligned} \tag{4}$$

The second possibility is that we create the pair in between two domain walls that were paired up in the reference state. In that case, we obtain, for example,

$$(1,2)(3,4)(5(1',2')6)\ldots(2N-1,\ 2N)\,. \tag{5}$$

Now applying rule Eq. (1) implies that this state is equal to

$$\begin{aligned}&(1,2)(3,4)(5(1',2')6)\ldots(2N-1\,,2N)\\ &\quad\to -(1,2)(3,4)(5,6)(7,8)\ldots(2N+1,\ 2N+2)\,.\end{aligned} \tag{6}$$

So, we see that the creation of a pair of domain walls at position x gives a minus sign if the number of domain walls to the left of x is odd, while we get no minus sign if the number of domain walls to the left of x is even. This implies that the creation operator for a *single* domain wall at site x would produce a factor of $\pm i$ if the number of domain walls to the left is odd, which agrees with the findings of Ref. [53]. This justifies the term semionic, which refers to "half-fermion" statistics.

III. EFFECTIVE MODEL

A. The Hamiltonian

In this section, we construct a 1D effective Hamiltonian that captures the semionic nature of the domain walls described above. As a first step, we recall the Kramers-Wannier self-duality mapping of the 1D quantum Ising model in a transverse magnetic field. If we call the original Ising spins the σ spins, then we can introduce τ spins living in between the Ising spins, which represent domain walls. We use the convention that a τ spin is zero if its two neighboring σ spins are equal and is one when its neighboring spins are different. The Ising Hamiltonian can be written either in terms of the original σ spins, or in terms of the domain walls represented by τ spins:

$$H = \sum_i -J\sigma_i^z\sigma_{i+1}^z + B\sigma_i^x,$$
$$\leftrightarrow H' = \sum_i -J\tau_{i+1/2}^z + B\tau_{i-1/2}^x\tau_{i+1/2}^x\,. \tag{7}$$

Here τ^i represent the Pauli matrices, but acting on the domain-wall states. The σ spins are taken to live on the integer-valued lattice sites, while the τ spins live on the half-integer lattice sites. Under this duality, the ferromagnetic interaction of the σ spins maps to a chemical potential for the τ domain walls, while the magnetic field maps to a hopping and pair creation term for the domain walls. This is easily understood, since increasing the ferromagnetic interacting suppresses the existence of domain walls while the magnetic field will flip σ spins and cause domain walls to be created and move around. So, H' represents the dynamics of domain walls, which can condense (by lowering their chemical potential) and give rise to a disordered phase.

To construct a Hamiltonian that has semionic domain walls, we first keep both the σ and τ spins. Since now our Hilbert space consists of both the σ and τ spins simultaneously, we need a term that enforces the τ spins to represent domain walls of the σ spins. This is easily done with a $\mathbb{Z}_2$ Gauss-law term:

$$H_{\text{Gauss}} = -g\sum_i \sigma_i^z\tau_{i+1/2}^z\sigma_{i+1}^z\,. \tag{8}$$

The Gauss constraint term commutes with all terms that we will add to the Hamiltonian later on; so, by taking $g > 0$ large enough, the low-energy states will live in the subspace where the τ spins represent domain walls of the σ spins. This subspace characterized by $\sigma_i^z\tau_{i+1/2}^z\sigma_{i+1}^z = 1$ has a nice graphical representation. If we represent the σ spins as horizontal links and the τ spins as vertical links, such that we obtain a 1D lattice that is a sequence of coordination number three vertices, then the low-energy subspace is in one-to-one correspondence with all coverings of this lattice with strings that end on the vertical links. The precise correspondence is that a zero state represents the absence of a string, and the one state represents the presence of a string. We illustrate this graphical representation in Fig. 1(a).

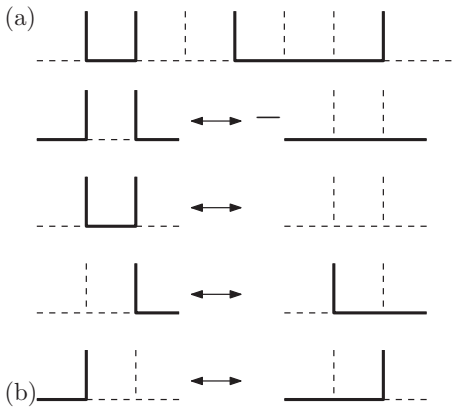

FIG. 1. (a) Graphical representation of the state $|0\tilde{1}1\tilde{1}0\tilde{0}0\tilde{1}1\tilde{0}1\tilde{0}1\tilde{1}0\rangle$, where $\tilde{j}$ denote the τ spins and j denote the σ spins. (b) Action of the Hamiltonian term H_{Dyn} on states in the subspace satisfying $\sigma_i^z\tau_{i+1/2}^z\sigma_{i+1}^z = 1$.

The chemical potential term for the domain walls is the same as in the Ising model:

$$H_\mu = -\mu\sum_i \tau_{i+1/2}^z\,. \tag{9}$$

As a final term, we need an analog of the domain-wall hopping/pair creation term $\tau_{i-1/2}^x\tau_{i+1/2}^x$ of the transverse field Ising model. Denoting the domain-wall states with $\{|\tilde{0}\rangle, |\tilde{1}\rangle\}$ and the σ-spin states with $\{|0\rangle, |1\rangle\}$, we define the term H_{Dyn} by its action on any subsequent τ-σ-τ triplet as

$$|\tilde{1}0\tilde{1}\rangle \leftrightarrow -|\tilde{0}1\tilde{0}\rangle, \tag{10}$$
$$|\tilde{1}1\tilde{1}\rangle \leftrightarrow |\tilde{0}0\tilde{0}\rangle, \tag{11}$$
$$|\tilde{0}0\tilde{1}\rangle \leftrightarrow |\tilde{1}1\tilde{0}\rangle, \tag{12}$$
$$|\tilde{1}0\tilde{0}\rangle \leftrightarrow |\tilde{0}1\tilde{1}\rangle\,, \tag{13}$$

and H_{Dyn} is zero on any state that violates the Gauss term. We give a graphical representation of the action of H_{Dyn} in Fig. 1(b). The only difference between H_{Dyn} and the conventional Ising model term $\tau_{i-1/2}^x\tau_{i+1/2}^x$ is the minus sign in Eq. (10). This term represents the creation of a domain-wall pair when there are an odd number of domain walls to the left of it. Equation (11) also represents a pair creation/annihilation process, but with an even number of domain walls to the left. The easiest way to see this is to look at Fig. 1(b), and to realize that the σ spins encode the parity of the number of τ spins to the left of it. Equations (12) and (13) represent domain-wall hopping.

We now take the Hamiltonian H to be the sum of all preceding terms:

$$H = H_{\text{Gauss}} + H_{\mu} + H_{\text{Dyn}} . \tag{14}$$

We claim that this Hamiltonian captures the universal low-energy physics at the boundary of the nontrivial 2D bosonic $\mathbb{Z}_2$ SPT phase. In the next section, we first discuss the global $\mathbb{Z}_2$ symmetry of this Hamiltonian. In Sec. V, we numerically study the phase diagram of H as a function of μ and show that this model indeed does not have a gapped, disordered phase, which is the hallmark of the edge physics of a nontrivial 2D SPT phase. At this point, we also want to mention that for $\mu = 0$, our Hamiltonian H is very closely related to the anyonic chains that have previously been constructed in the literature [43,44]. Specifically, our model at $\mu = 0$ can be obtained by constructing an anyon chain with the F symbols of the $\text{SU}(2)_1$ modular category. However, there is one important difference compared to the usual anyonic-chain construction. In Refs. [43,44], the vertical links, corresponding to our domain wall or τ degrees of freedom, are fixed while here they are allowed to fluctuate. We will see below that the connection with the $\text{SU}(2)_1$ anyon chain at $\mu = 0$ fits nicely with the phase diagram we obtain numerically.

B. $\mathbb{Z}_2$ symmetry

Although the Hamiltonian in Eq. (14) is very closely related to the transverse Ising model, it does not have the same $\mathbb{Z}_2$ symmetry $\bigotimes_i \sigma_i^x$. However, H does have a *low-energy* $\mathbb{Z}_2$ symmetry. To expose it, we focus on states in the Hilbert space that do not violate the Gauss term, i.e., we only consider states that satisfy $\sigma_i^z \tau_{i+1/2}^z \sigma_{i+1}^z = 1$. We now claim that the relevant $\mathbb{Z}_2$ symmetry is given by

$$(-1)^{\#\text{strings}} \bigotimes_i \sigma_i^x , \tag{15}$$

i.e., it flips all the σ spins and adds a minus sign when the number of strings is odd. Note that we can add the minus sign before or after flipping all the σ spins, since this does not change the number of strings. Because the minus sign commutes with the product of σ^x, it is clear that this symmetry squares to the identity.

The sign $(-1)^{\#\text{strings}}$ appears to be a very nonlocal operator. However, we can encode it via local operators by noting that counting the number of strings is equivalent to counting the number of right-hand endpoints of strings. A right-hand endpoint of a string can be detected locally, and we can assign a minus sign to it using a diagonal matrix for every τ spin and the σ spin to the left of it. We then let the operator add a minus sign when both these spins are one, which indeed corresponds to the situation where a string comes from the left and ends on that τ spin. Concretely, if we define

$$CZ_i = |0\tilde{0}\rangle\langle 0\tilde{0}| + |1\tilde{0}\rangle\langle 1\tilde{0}| + |0\tilde{1}\rangle\langle 0\tilde{1}| - |1\tilde{1}\rangle\langle 1\tilde{1}| \tag{16}$$

to act on σ-spin i and τ-spin $i + 1/2$, then the symmetry can be written as a product of local matrices as

$$\bigotimes_i CZ_i \bigotimes_i \sigma_i^x . \tag{17}$$

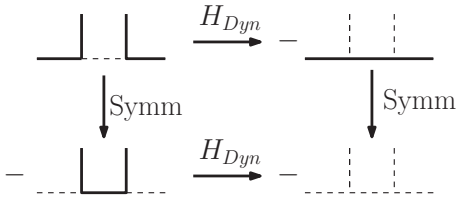

FIG. 2. Graphical illustration of the commutation relation between the $\mathbb{Z}_2$ symmetry in Eq. (17) and H_{Dyn}. Both paths in the diagram (first H_{Dyn}, then the symmetry, and vice versa) commute.

Using the graphical representation one can easily check that this operator commutes with H_{Dyn}, as we illustrate in Fig. 2. The operator Eq. (17) also trivially commutes with H_{μ}.

There are a few important points we need to clarify about the $\mathbb{Z}_2$ symmetry. The operators $\bigotimes_i CZ_i$ and $\bigotimes_i \sigma_i^x$ do not commute. As a result, the operator in Eq. (17) does not square to the identity and does not truly represent a $\mathbb{Z}_2$ symmetry. It is only when we project into the low-energy subspace satisfying the Gauss constraint $\sigma_i^z \tau_{i+1/2}^z \sigma_{i+1}^z = 1$ that it acts as in Eq. (15), and is a true $\mathbb{Z}_2$ symmetry. If we take the tensor product of local matrices in Eq. (17) and project it into the subspace satisfying the Gauss term, then we end up with a nonlocal MPO representation of the $\mathbb{Z}_2$ symmetry. So, the correct statement is that the Hamiltonian we are considering has a $\mathbb{Z}_2$ MPO symmetry in its low-energy subspace satisfying the Gauss term.

C. Simplified Hamiltonian

The Hamiltonian in Eq. (14) has the clearest physical interpretation in terms of the dual domain-wall variables we used in the previous sections. However, we can also reformulate it using only the original σ spins. In these variables, the Hamiltonian Eq. (14) becomes

$$H = \sum_i CZ_{i-1,i+1} \sigma_i^x - \mu \sigma_i^z \sigma_{i+1}^z , \tag{18}$$

where we introduced the notation CZ_{ij}, which is the same matrix as defined in Eq. (16), but now acting on the σ spins labeled by i and j. Since we have omitted the domain walls, we no longer need the Gauss term in the Hamiltonian. In terms of the σ spins, the $\mathbb{Z}_2$ symmetry becomes

$$\bigotimes_i \sigma_i^x \bigotimes_i CZ_{i,i+1} \sigma_i^z . \tag{19}$$

One can check that this operator, which is now manifestly a MPO, indeed squares to the identity and commutes with the Hamiltonian Eq. (18). Because this MPO corresponds to the nontrivial element in $H^3(\mathbb{Z}, \text{U}(1))$, the Hamiltonian in Eq. (18) cannot have a unique, short-range entangled ground state [23].

IV. CONDENSATION OF DOMAIN WALLS: FIELD THEORY ANALYSIS

Before discussing our numerical results in the next section, we first turn to a low-energy field theory analysis. Given that gapless boundary modes of 2D bosonic symmetry-protected

phases are known to have a Luttinger liquid description [48], we expect that if our model has a gapless regime it will flow to this effective field theory in the IR. Here we follow the conventional notation (with units such that $u = 1$) [54], and write the Luttinger liquid or compact free-boson action as

$$\mathcal{L}_0 = \frac{1}{2\pi K}(\partial_\mu \phi)^2 . \tag{20}$$

The compactification radius of ϕ is taken to be π. We define the dual field $\theta(x)$ via the relation $\partial_x \theta = \partial_t \phi / K$. Canonical quantization implies that the boson fields ϕ and θ satisfy the commutation relation

$$[\phi(x), \partial_y \theta(y)] = i\pi \delta(x - y) . \tag{21}$$

From the canonical commutation relation, it follows that the operator which shifts ϕ by a constant α is given by $\exp[-i\frac{\alpha}{\pi}\int dx\, \partial_x \theta(x)]$. The compactification condition on ϕ implies that this operator should be the identity operator when $\alpha = \pi$, which implies that θ is also compact with compactification radius 2π. We can write the Luttinger liquid Hamiltonian as

$$H = \frac{1}{2\pi}\int dx \left(K(\partial_x \theta)^2 + \frac{1}{K}(\partial_x \phi)^2 \right) . \tag{22}$$

From this Hamiltonian, we recognize the R-duality $2\phi \leftrightarrow \theta$, $K \leftrightarrow 1/4K$ of the free-boson Conformal Field Theory (CFT).

As was shown in previous works [42,48,55], in the nontrivial SPT phase the global $\mathbb{Z}_2$ symmetry acts on the fields as

$$\phi \to \phi + \frac{\pi}{2} , \qquad \theta \to \theta + \pi . \tag{23}$$

From this symmetry action, we see that there exist no $\mathbb{Z}_2$ symmetric terms of the form $\cos(2m\phi)$ or $\cos(m\theta)$ with $m \in \mathbb{Z}$ that we can add to the Luttinger liquid Lagrangian to create a gap, and at the same time obtain a unique, symmetric ground state. This is the fingerprint of the 't Hooft anomaly, which excludes the existence of a gapped, disordered phase.

The global symmetry operator which implements the shifts in Eqs. (23) is given by $\exp(-i\int dx[\frac{1}{2}\partial_x \theta(x) + \partial_x \phi(x)])$. It follows that the operator which creates a domain wall at position x is given by [53]

$$\hat{D}^\dagger(x) = e^{-i\left(\frac{1}{2}\theta(x) + \phi(x)\right)} . \tag{24}$$

At this point, we import a result from our numerical simulations presented in the next section. As detailed below, we find that the translation symmetry of the lattice Hamiltonian acts an internal $\mathbb{Z}_3$ symmetry in the low-energy Luttinger liquid description. Specifically, our numerics show that under a translation by one lattice site, the domain-wall creation operator $\hat{D}^\dagger$ picks up a phase $e^{i2\pi/3}$. This is to be compared with the Luttinger liquid description of the XXZ spin chain, where translation symmetry acts as an internal $\mathbb{Z}_2$ symmetry in the effective field theory. The $\mathbb{Z}_3$ symmetry action on the domain-wall creation operator does not allow us to unambiguously determine its action on the boson fields ϕ and θ. However, we do not expect the $\mathbb{Z}_3$ symmetry to be anomalous because the gapped ferromagnetic phase of our lattice Hamiltonian is translationally invariant. So, we can without loss of generality take the internal $\mathbb{Z}_3$ symmetry to act as [48]

$$\phi \to \phi , \qquad \theta \to \theta - \frac{4\pi}{3} . \tag{25}$$

The scaling dimension of $\cos(m\phi)$ is $\frac{m^2 K}{4}$, while the scaling dimension of $\cos(m\theta)$ is given by $\frac{m^2}{4K}$. The most RG-relevant perturbations of the Luttinger liquid respecting all symmetries are therefore given by $\cos(4\phi)$ and $\cos(6\theta)$. So in the parameter range $1/2 < K < 9/2$, the Luttinger liquid has no symmetry respecting relevant perturbations. The $\cos(4\phi)$ term is irrelevant for $K > 1/2$, while it is relevant for $K < 1/2$. So, at $K = 1/2$, which is the self-dual point of the free-boson CFT, there is a BKT transition to a gapped phase where the ϕ field gets pinned to one of the minima of the $\cos(4\phi)$ term. This gapped phase spontaneously breaks the global $\mathbb{Z}_2$ symmetry, but preserves translation symmetry. We therefore identify it with the ferromagnetic phase of our microscopic Hamiltonian [Eq. (18)] obtained for large $\mu > 0$. From the perspective of the ferromagnetic phase, the BKT transition into the Luttinger liquid phase results from the condensation of $\mathbb{Z}_2$ domain walls. As noted above, the Hamiltonian in Eq. (18) constructed to describe this domain-wall condensation takes the form of an $SU(2)_1$ anyon chain when $\mu = 0$. Therefore, it is natural to expect that the BKT transition in this model will occur at $\mu = 0$, since the self-dual point of the free-boson CFT is equivalent to the $SU(2)_1$ Wess-Zumino-Witten CFT. We will confirm this in the next section containing our numerical results.

The sine-Gordon Lagrangian $\mathcal{L}_0 + g\cos(4\phi)$ of course also describes the original BKT transition in the 2D classical XY model [56] or 1D quantum XXZ Hamiltonian. However, there is one important distinction compared to the present discussion. In the XY model, there is a microscopic U(1) symmetry on both sides of the BKT transition, which in the field theory language is associated with the charge $Q = \int dx\, \partial_x \phi$, i.e., the winding of the boson field. In the Luttinger liquid phase, there is an additional emergent U(1) symmetry, with charge $\tilde{Q} = \int dx\, \partial_t \phi$. In the semionic domain-wall Hamiltonian, both U(1) symmetries are emergent and only present in the Luttinger liquid phase. This distinction does not appear in the field theory description, however, which captures the behavior around the Luttinger liquid fixed point. Once the cosine term becomes relevant, the theory will flow to a gapped fixed point, where the U(1) symmetry ceases to have any physical meaning.

V. NUMERICAL RESULTS

In this section, we explore the phase diagram of our effective model numerically, and confirm the theoretical considerations above. Our simulations were performed using tangent-space methods for uniform matrix product states (MPS) [57]; in particular, we use the VUMPS algorithm [58] for finding variational MPS approximations for the ground state of the Hamiltonian, and apply the quasiparticle excitation ansatz [59] for computing the low-lying excited states. Because the framework of uniform MPS works directly in the thermodynamic limit, we do not experience any finite-size errors, and the only refinement parameter is the MPS bond dimension. For simplicity, we simulate the model using the reduced form

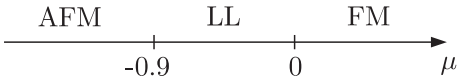

FIG. 3. The phase diagram of the Hamiltonian [Eq. (14)] as obtained by uniform MPS simulations. Both the ferromagnetic (FM) and antiferromagnetic (AFM) phases can be understood in the limit of large $|\mu|$ by the relation to the standard transverse-field Ising model. The semionic nature of the domain-wall hopping and creation introduces a gapless Luttinger liquid (LL) phase in between; the transitions are of the BKT type (LL $\rightarrow$ FM) and first-order (LL $\rightarrow$ AFM).

of the Hamiltonian in Eq. (18). In Fig. 3, we summarize the phase diagram that we have obtained by our simulations.

We start in the ferromagnetic phase ($\mu > 0$). In the limit of large μ, we recover the standard ferromagnetic transverse-field Ising model, for which the order parameter $\langle \sigma_i^z \rangle$ signals the $\mathbb{Z}_2$ symmetry breaking. For the Ising model, a variational MPS simulation generically yields one of the two states with maximal symmetry breaking; moreover, since these two ground states are connected by the symmetry operation $\bigotimes_i \sigma_i^x$, these two ground states have exactly the same entanglement structure. For the nonlocal MPO symmetry [Eq. (19)] in our model, this is no longer the case as we always find the same MPS $|\psi_{\mathrm{MPS}}\rangle$ as a variational optimum at a given bond dimension. The second ground state is found by acting with the MPO on the first, which increases the bond dimension. Correspondingly, the entanglement spectra of the two ground states are different and, in particular, the bipartite entanglement entropy of $|\psi_{\mathrm{MPS}}\rangle$ is smaller. As MPS ground-state approximations induce a bias towards low-entanglement states, this explains why we find only one variationally optimal ground state at a given bond dimension. To characterize the $\mathbb{Z}_2$ symmetry breaking in our simulations, we compute the quantity $\lambda = \langle \psi_{\mathrm{MPS}} | O | \psi_{\mathrm{MPS}} \rangle^{1/N}$, where O is the MPO operator in Eq. (19) and N is the diverging system size; in uniform MPS simulations this "overlap per site" is easily computed directly in the thermodynamic limit. From the inset of Fig. 4, we clearly see that the $\mathbb{Z}_2$ symmetry is spontaneously broken in the ferromagnetic phase, but that the symmetry breaking vanishes as $\mu = 0$ is approached.

In a system where different ground states are related through an MPO symmetry, the elementary excitations have a topological nature, in the sense that they are created by a local operator with an MPO string attached [60]. Here, the MPO string serves as the generalization of the Jordan-Wigner string in the Ising model. The MPS quasiparticle ansatz is straightforwardly generalized to the case of MPO strings [60], and we can compute the excitation energy within the nontrivial topological sector for every value of the momentum. In Fig. 4, we plot the spectrum for different values of μ. Interestingly, the absolute minimum of the dispersion relation continuously shifts from momentum $p = \pi$ in the Ising limit to $p = \frac{2\pi}{3}$ at the critical point where the gap closes. This tells us that the domain-wall creation operator in a long-wavelength continuum theory for the gapless phase picks up a phase $e^{i2\pi/3}$ under translation. So, in an effective field theory description, translation symmetry will act as an internal $\mathbb{Z}_3$ symmetry. In the previous section, we used this result in our

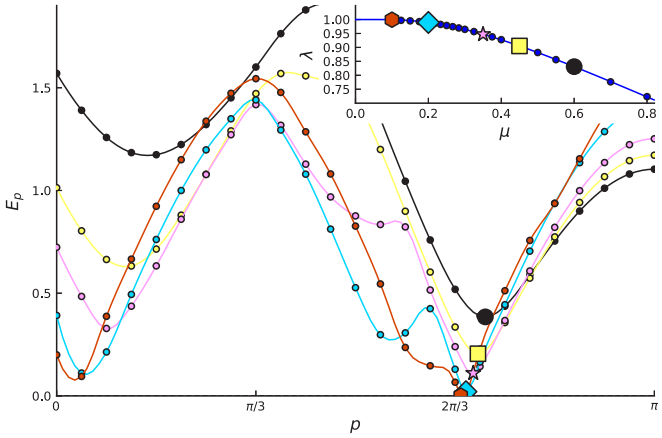

FIG. 4. The excitation energy as a function of momentum in the topological (domain wall) sector for five values of μ (the spectrum is reflection symmetric for $p \rightarrow -p$). Energies were obtained with the MPS quasiparticle ansatz with an MPO string and bond dimensions up to $D = 100$. We observe that the minimum of the dispersion relation (indicated with the larger symbol) shifts as μ varies, where the gap closes at momentum $\pm 2\pi/3$ as $\mu = 0$ is approached. In the inset, we provide the value of $\lambda = \langle \psi_{\mathrm{MPS}} | O | \psi_{\mathrm{MPS}} \rangle^{1/N}$ as a function of μ (for system size $N \rightarrow \infty$), and we indicate the five points for which we have computed the spectrum.

Luttinger liquid analysis. Next to the gap closing at $p = \frac{2\pi}{3}$, we also find additional local minima close to momentum zero and $\frac{2\pi}{3}$ that correspond to the lower edges of the three- and five-particle continuum, respectively (note that two-kink and four-kink states do not show up in the topological sector).

From the excitation spectra in the topological sector (kink sector), we learn that the kink gap closes around $\mu = 0$, resulting in the condensation of kink-antikink pairs. Because of the nontrivial fusion properties of these kinks, the result cannot be an isolated critical point. Rather, the model enters a gapless phase for $\mu \leqslant 0$. The central charge in this phase can be determined from MPS simulations through the scaling of the entanglement entropy as a function of the effective correlation length in the MPS ground-state approximations (a technique known as finite-entanglement scaling [61,62]). In Fig. 5, we clearly show that the central charge is $c = 1$ throughout the gapless phase. The phase transition from this U(1) phase into the gapped phase for $\mu > 0$ is expected to be of the BKT type, which we can confirm from the behavior of the correlation length as the critical point is approached in the gapped phase. The correlation length is a quantity that converges slowly with the bond dimension, so we apply extrapolation techniques [63] for finding the correct value of the correlation length at each value of $\mu > 0$. In Fig. 6, we observe that the correlation length diverges exponentially as $\log \xi \propto (\mu - \mu_c)^{-1/2}$ and find a value for the critical point that is close to $\mu_c = 0$.

For large negative μ, we expect to recover the properties of the antiferromagnetic Ising model, for which the order parameter is the staggered magnetization $\langle (-1)^i \sigma_i^z \rangle$. In Fig. 7 one can see that the staggered magnetization clearly signals the phase transition into the gapless phase around $\mu = -0.9$, where it drops discontinuously to zero. This suggests that

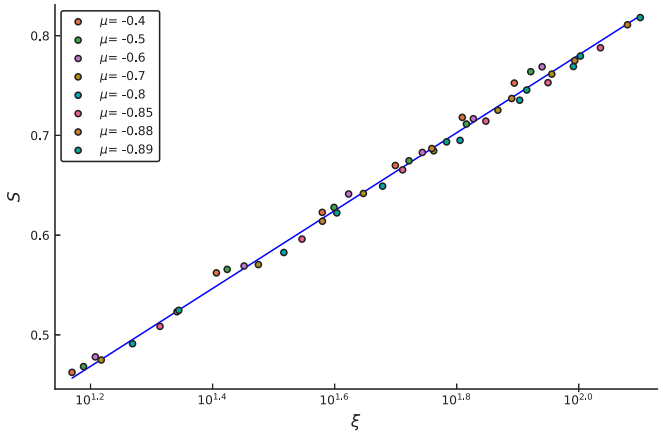

FIG. 5. The bipartite entanglement entropy S as a function of the correlation length ξ for variational MPS ground states at different values of μ in the critical region and varying bond dimensions. In the gapless phase, we consistently find a scaling $S = \frac{c}{6}\log\xi + S_0$ with values of c around 1, where S_0 is a nonuniversal (i.e., μ-dependent) constant related to the UV scale of the problem. To collapse the data for different values of μ, we have subtracted S_0. Fitting a single line through all data points, we find $c \approx 1.02$ (blue line), in very good agreement with the effective Luttinger-liquid theory.

the transition is first order, which is confirmed by plotting the behavior of the correlation length as a function of the bond dimension in our MPS simulations (inset of Fig. 7). We observe that the correlation length remains finite upon approaching the transition from the antiferromagnetic side. In fact, even arbitrarily close to the first-order transition, the correlation length in the antiferromagnetic phase remains of order one.

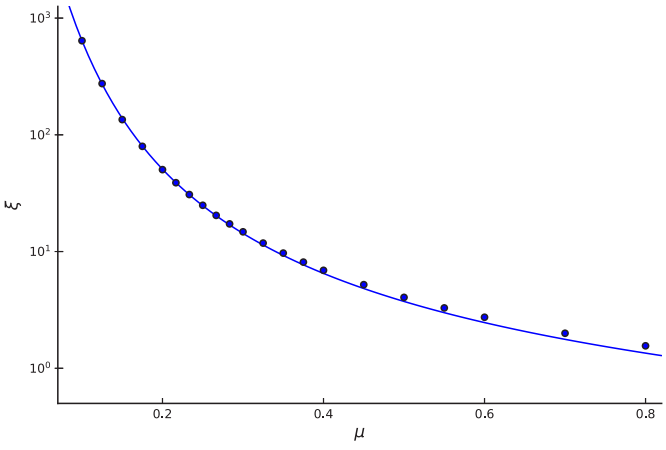

FIG. 6. The correlation length ξ as a function of μ as the BKT transition is approached; the values for the correlation length were extrapolated from MPS simulations up to bond dimension $D = 70$. We have fitted (blue line) these values to the form $\log\xi \propto (\mu - \mu_c)^{-1/2}$; we find a value of about $\mu_c \approx -0.05$, which is consistent with the expected value of $\mu_c = 0$ given the relatively small bond dimensions used in our simulations.

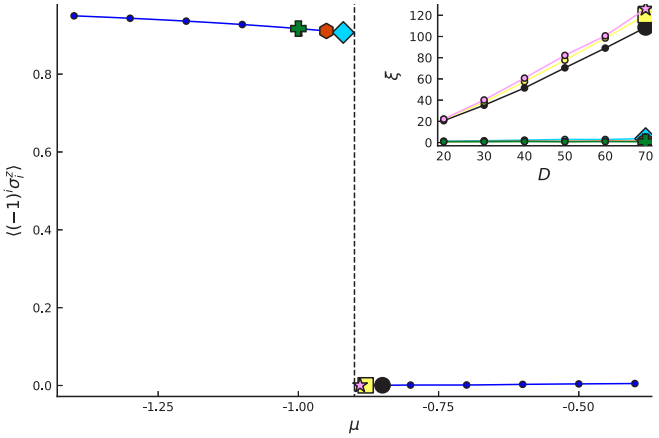

FIG. 7. The staggered magnetization $m_s = \langle(-1)^i\sigma_i^z\rangle$ as a function of μ; the discontinuous jump clearly signals a first-order transition. As a further confirmation, in the inset we plot the effective correlation lengths as a function of the MPS bond dimension D for different values of μ around the transition (the markers indicate the chosen values); in the critical region the correlation length grows indefinitely, whereas in the gapped region it remains clearly finite.

VI. DISCUSSION

1D Hamiltonians with an anomalous $\mathbb{Z}_2$ MPO symmetry have previously been studied in the literature [23,64–66], but to the best of our knowledge these models do not contain a parameter that enables a spontaneous breaking of the anomalous symmetry, and are therefore not based on a physical picture of the unconventional domain-wall fusion properties. Reference [27] did construct microscopic models to study domain walls on the boundaries of SPT states, but only those with fractional quantum numbers or nontrivial projective representations. The modified Ising chain is expected to be closely related to strange correlator partition functions obtained from the nontrivial bosonic $\mathbb{Z}_2$ SPT phase, as studied previously in Refs. [67–70]. These strange correlator partition functions have a natural interpretation as loop models [67,68], which makes them tractable for certain analytical calculations. However, there is no unique strange correlator partition function, and different partition functions can give rise to very different critical behavior. Given the simplicity and associated physical picture of the modified Ising chain, we expect it to be a faithful effective model for the boundary of the nontrivial $\mathbb{Z}_2$ SPT. It would therefore be interesting to understand whether the modified Ising chain can be mapped to other (integrable) models known in the literature. Because of its simplicity, it might also be worth it to see if it can be realized in cold atom experiments.

The phase diagram we obtain for the modified Ising chain is very similar to that of the spin-1/2 XXZ model. Upon varying the chemical potential for the domain walls, we find three phases: a ferromagnetic phase, a Luttinger liquid regime, and an antiferromagnetic phase. The ferromagnetic phase is separated from the Luttinger liquid by a BKT transition and the antiferromagnetic phase is separated from the Luttinger liquid by a first-order transition. In the antiferromagnetic regime, the correlation length in our model stays order of order one, even close to the first-order transition into the Luttinger liquid.

This behavior is again very similar to the XXZ spin chain, where the correlation length is exactly zero in this regime. Interestingly, the XXZ Hamiltonian also has a "perturbative" anomaly that is closely related to the 't Hooft anomaly of our model [33,37,38]. The perturbative anomaly in the XXZ model is associated to translation symmetry, which acts on the low-energy modes as an effective $\mathbb{Z}_2$ symmetry. This anomaly is the same as the chiral anomaly of the 1D Dirac fermion [36], and the $g \leftrightarrow -g$ anomaly of the $SU(2)_1$ Wess-Zumino-Witten CFT [38,71]. It is also the same anomaly as the one associated with the nonlocal MPO symmetry of our model [37,38,69].

Condensation of defects in the order parameter of spontaneously broken anomalous symmetries often leads to emergent symmetries. In fact, such emergent symmetries are one of the hallmarks of deconfined quantum critical points [18,39,72]. For example, at the proposed deconfined quantum critical point describing the 2D Néel-VBS transition, there is an emergent SO(5) symmetry which allows to rotate between the Néel and VBS order parameters, which should be treated on equal footing at the transition point [72]. In the 1D model studied here, there is a $U(1) \times U(1)$ symmetry that emerges after condensing the anomalous domain walls, although there is no deconfined quantum critical point or a physical interpretation for the emergent symmetry in terms of rotating between different order parameters. One point to make in this context is that the emergent $U(1) \times U(1)$ symmetry of the Luttinger liquid, acting as $(\phi, \theta) \to (\phi + \alpha_1, \theta + \alpha_2)$, is closely related to the self-duality of the free-boson CFT, which interchanges ϕ and θ. From the symmetry action Eqs. (23), we see that both ϕ and θ can serve as order parameters for the $\mathbb{Z}_2$ symmetry, so it is the self-duality which states the equivalence of these two order parameters (which signal the breaking of the *same* symmetry) at the BKT transition. In the context of deconfined quantum critical points, recent progress has shown that also in two spatial dimensions emergent symmetries are often closely related to dualities, in the sense that knowing dual formulations of a particular theory can help in understanding its emergent symmetries [39].

Our construction of the microscopic model can be generalized to arbitrary discrete groups, by doing a similar "anyonic-chain" construction with the group cohomology data instead of the F symbols of a modular category. As was shown in Ref. [53] using a field theory analysis, in the case of $\mathbb{Z}_N$ symmetry, the domain walls are expected to have parafermionic statistics [73]. It would be interesting to understand the connection between these symmetry-broken phases and the recently studied parafermionic chains [74,75], which were argued to also realize BKT transitions [76]. The anyonic-chain construction, however, is not restricted to Abelian symmetries and realizes domain walls which cannot be captured by the parafermion formalism. In particular, we can even go back to the original anyonic-chain construction based on F symbols and ask what is the precise nature of the defects in the corresponding "symmetry-broken" phases of the nonlocal MPO "symmetries" [43,44]. These symmetry-broken phases are closely related to gapped boundaries of 2D topologically ordered phases. This connection is manifested clearly in tensor-network representations of the relevant topological phases, and has been exploited to study anyon condensation numerically [60,77,78].

VII. CONCLUSION

In this paper, we have constructed a simple spin-chain Hamiltonian that exhibits an anomalous $\mathbb{Z}_2$ symmetry by explicitly modeling the semion statistics of the associated $\mathbb{Z}_2$ domain wall configurations. The resulting Hamiltonian is analogous to the Ising model, and shares with it an ordered ferromagnetic phase and antiferromagnetic phase. However, due to the anomalous realization of the symmetry, a gapped disordered phase is ruled out [23]. Instead, we find a gapless Luttinger liquid phase that is separated from the ordered ferromagnetic phase by a phase transition of the BKT type, and from the ordered antiferromagnetic phase by a first-order phase transition. This model is believed to capture the universal physics of the boundary of 2D SPT phases.

The reasoning on which this paper is based can also be applied to the boundaries of 3D SPT phases with discrete symmetries. In the symmetry-broken phase, the 't Hooft anomaly will manifest itself via unconventional properties of the junctions of domain walls, which again have a natural interpretation in terms of the group cohomology data specifying the SPT phase. If one could construct an effective model that captures the anomalous properties of the domain-wall junctions, then one could perhaps gain some insight into the boundary phase diagram of 3D SPT phases.

ACKNOWLEDGMENTS

We thank Frank Verstraete for helpful and stimulating discussions, and an anonymous referee for helping us clarify our arguments in Sec. IV. N.B. acknowledges an inspiring discussion with Ruben Verresen. G.R. and J.H. are supported by the European Research Counsil (ERQUAF 715861), L.V. by the Research foundation Flanders (Fonds Wetenschappelijk Onderzoek), and N.B. by a BAEF Francqui Fellowship.

[1] N. D. Mermin, The topological theory of defects in ordered media, Rev. Mod. Phys. **51**, 591 (1979).

[2] S. Coleman, *Aspects of Symmetry: Selected Erice Lectures* (Cambridge University Press, Cambridge, England, 1988).

[3] R. Jackiw and C. Rebbi, Solitons with fermion number $\frac{1}{2}$, Phys. Rev. D **13**, 3398 (1976).

[4] W. P. Su, J. R. Schrieffer, and A. J. Heeger, Solitons in Polyacetylene, Phys. Rev. Lett. **42**, 1698 (1979).

[5] L. D. Faddeev and L. A. Takhtajan, What is the spin of a spin wave? Phys. Lett. A **85**, 375 (1981).

[6] E. Lieb, T. Schultz, and D. Mattis, Two soluble models of an antiferromagnetic chain, Ann. Phys. **16**, 407 (1961).

[7] M. Oshikawa, Commensurability, Excitation Gap, and Topology in Quantum Many-Particle Systems on a Periodic Lattice, Phys. Rev. Lett. **84**, 1535 (2000).

[8] M. B. Hastings, Lieb-Schultz-Mattis in higher dimensions, Phys. Rev. B **69**, 104431 (2004).

[9] S. A. Parameswaran, A. M. Turner, D. P. Arovas, and A. Vishwanath, Topological order and absence of band insulators at integer filling in non-symmorphic crystals, Nat. Phys. **9** (2013).

[10] M. P. Zaletel and A. Vishwanath, Constraints on Topological Order in Mott Insulators, Phys. Rev. Lett. **114**, 077201 (2015).

[11] H. Watanabe, H. C. Po, A. Vishwanath, and M. Zaletel, Filling constraints for spin-orbit coupled insulators in symmorphic and nonsymmorphic crystals, Proc. Natl. Acad. Sci. **112**, 14551 (2015).

[12] H. C. Po, H. Watanabe, C.-M. Jian, and M. P. Zaletel, Lattice Homotopy Constraints on Phases of Quantum Magnets, Phys. Rev. Lett. **119**, 127202 (2017).

[13] Y.-M. Lu, Y. Ran, and M. Oshikawa, Filling-enforced constraint on the quantized Hall conductivity on a periodic lattice, arXiv:1705.09298.

[14] M. Levin and T. Senthil, Deconfined quantum criticality and Néel order via dimer disorder, Phys. Rev. B **70**, 220403(R) (2004).

[15] F. D. M. Haldane, O(3) Nonlinear σ Model and The Topological Distinction between Integer- and Half-Integer-Spin Antiferromagnets in Two Dimensions, Phys. Rev. Lett. **61**, 1029 (1988).

[16] N. Read and S. Sachdev, Valence-Bond and Spin-Peierls Ground States of Low-Dimensional Quantum Antiferromagnets, Phys. Rev. Lett. **62**, 1694 (1989).

[17] N. Read and S. Sachdev, Spin-Peierls, valence-bond solid, and Néel ground states of low-dimensional quantum antiferromagnets, Phys. Rev. B **42**, 4568 (1990).

[18] T. Senthil, A. Vishwanath, L. Balents, S. Sachdev, and M. P. A. Fisher, Deconfined quantum critical points, Science **303**, 1490 (2004).

[19] S. Jiang and O. Motrunich, Ising ferromagnet to valence bond solid transition in a one-dimensional spin chain—analogies to deconfined quantum critical points, Phys. Rev. B **99**, 075103 (2019).

[20] L. Fidkowski and A. Kitaev, Topological phases of fermions in one dimension, Phys. Rev. B **83**, 075103 (2011).

[21] F. Pollmann, E. Berg, A. M. Turner, and M. Oshikawa, Symmetry protection of topological phases in one-dimensional quantum spin systems, Phys. Rev. B **85**, 075125 (2012).

[22] X. Chen, Z.-C. Gu, and X.-G. Wen, Classification of gapped symmetric phases in one-dimensional spin systems, Phys. Rev. B **83**, 035107 (2011).

[23] X. Chen, Z.-X. Liu, and X.-G. Wen, Two-dimensional symmetry-protected topological orders and their protected gapless edge excitations, Phys. Rev. B **84**, 235141 (2011).

[24] X. Chen, Z.-C. Gu, Z.-X. Liu, and X.-G. Wen, Symmetry protected topological orders and the group cohomology of their symmetry group, Phys. Rev. B **87**, 155114 (2013).

[25] L. Fu and C. L. Kane, Superconducting Proximity Effect and Majorana Fermions at the Surface of a Topological Insulator, Phys. Rev. Lett. **100**, 096407 (2008).

[26] A. Vishwanath and T. Senthil, Physics of Three-Dimensional Bosonic Topological Insulators: Surface-Deconfined Criticality and Quantized Magnetoelectric Effect, Phys. Rev. X **3**, 011016 (2013).

[27] J. C. Wang, L. H. Santos, and X.-G. Wen, Bosonic anomalies, induced fractional quantum numbers, and degenerate zero modes: The anomalous edge physics of symmetry-protected topological states, Phys. Rev. B **91**, 195134 (2015).

[28] M. Cheng, M. Zaletel, M. Barkeshli, A. Vishwanath, and P. Bonderson, Translational Symmetry and Microscopic Constraints on Symmetry-Enriched Topological Phases: A View from the Surface, Phys. Rev. X **6**, 041068 (2016).

[29] C.-M. Jian, Z. Bi, and C. Xu, Lieb-Schultz-Mattis theorem and its generalizations from the perspective of the symmetry-protected topological phase, Phys. Rev. B **97**, 054412 (2018).

[30] A. Tanaka and X. Hu, Many-Body Spin Berry Phases Emerging from the π-Flux State: Competition between Antiferromagnetism and The Valence-Bond-Solid State, Phys. Rev. Lett. **95**, 036402 (2005).

[31] T. Senthil and M. P. A. Fisher, Competing orders, nonlinear sigma models, and topological terms in quantum magnets, Phys. Rev. B **74**, 064405 (2006).

[32] Z. Bi, A. Rasmussen, K. Slagle, and C. Xu, Classification and description of bosonic symmetry protected topological phases with semiclassical nonlinear sigma models, Phys. Rev. B **91**, 134404 (2015).

[33] S. Ryu, J. E. Moore, and A. W. W. Ludwig, Electromagnetic and gravitational responses and anomalies in topological insulators and superconductors, Phys. Rev. B **85**, 045104 (2012).

[34] X.-G. Wen, Classifying gauge anomalies through symmetry-protected trivial orders and classifying gravitational anomalies through topological orders, Phys. Rev. D **88**, 045013 (2013).

[35] A. Kapustin and R. Thorngren, Anomalous Discrete Symmetries in Three Dimensions and Group Cohomology, Phys. Rev. Lett. **112**, 231602 (2014).

[36] G. Y. Cho, C.-T. Hsieh, and S. Ryu, Anomaly manifestation of Lieb-Schultz-Mattis theorem and topological phases, Phys. Rev. B **96**, 195105 (2017).

[37] M. A. Metlitski and R. Thorngren, Intrinsic and emergent anomalies at deconfined critical points, Phys. Rev. B **98**, 085140 (2018).

[38] S. C. Furuya and M. Oshikawa, Symmetry Protection of Critical Phases and a Global Anomaly in 1 + 1 Dimensions, Phys. Rev. Lett. **118**, 021601 (2017).

[39] C. Wang, A. Nahum, M. A. Metlitski, C. Xu, and T. Senthil, Deconfined Quantum Critical Points: Symmetries and Dualities, Phys. Rev. X **7**, 031051 (2017).

[40] F. Wilczek and A. Zee, Linking Numbers, Spin, and Statistics of Solitons, Phys. Rev. Lett. **51**, 2250 (1983).

[41] M. A. Metlitski, C. L. Kane, and M. P. A. Fisher, Bosonic topological insulator in three dimensions and the statistical Witten effect, Phys. Rev. B **88**, 035131 (2013).

[42] M. Levin and Z.-C. Gu, Braiding statistics approach to symmetry-protected topological phases, Phys. Rev. B **86**, 115109 (2012).

[43] A. Feiguin, S. Trebst, A. W. W. Ludwig, M. Troyer, A. Kitaev, Z. Wang, and M. H. Freedman, Interacting Anyons in Topological Quantum Liquids: The Golden Chain, Phys. Rev. Lett. **98**, 160409 (2007).

[44] C. Gils, E. Ardonne, S. Trebst, D. A. Huse, A. W. W. Ludwig, M. Troyer, and Z. Wang, Anyonic quantum spin chains: Spin-1 generalizations and topological stability, Phys. Rev. B **87**, 235120 (2013).

[45] V. L. Berezinskii, Destruction of Long-range order in one-dimensional and two-dimensional systems having a continuous symmetry group I. Classical systems, Zh. Eksp. Teor. Fiz. **59**, 907 (1970) [Sov. J. Exp. Theor. Phys. **32**, 493 (1971)].

[46] J. M. Kosterlitz and D. J. Thouless, Ordering, metastability and phase transitions in two-dimensional systems, J. Phys. C **6**, 1181 (1973).

[47] F. D. M. Haldane, 'Luttinger liquid theory' of one-dimensional quantum fluids. I. Properties of the luttinger model and their extension to the general 1D interacting spinless fermi gas, J. Phys. C **14**, 2585 (1981).

[48] Y.-M. Lu and A. Vishwanath, Theory and classification of interacting integer topological phases in two dimensions: A Chern-Simons approach, Phys. Rev. B **86**, 125119 (2012).

[49] J. Wang, X.-G. Wen, and E. Witten, Symmetric Gapped Interfaces of Spt and Set States: Systematic Constructions, Phys. Rev. X **8**, 031048 (2018).

[50] D. J. Williamson, N. Bultinck, M. Mariën, M. B. Şahinoğlu, J. Haegeman, and F. Verstraete, Matrix product operators for symmetry-protected topological phases: Gauging and edge theories, Phys. Rev. B **94**, 205150 (2016).

[51] F. D. M. Haldane, Continuum dynamics of the 1-D Heisenberg antiferromagnet: Identification with the O(3) nonlinear sigma model, Phys. Lett. A **93**, 464 (1983).

[52] F. D. M. Haldane, Nonlinear Field Theory of Large-Spin Heisenberg Antiferromagnets: Semiclassically Quantized Solitons of the One-Dimensional Easy-Axis Neel State, Phys. Rev. Lett. **50**, 1153 (1983).

[53] Y.-M. Lu and D.-H. Lee, Gapped symmetric edges of symmetry protected topological phases, Phys. Rev. B **89**, 205117 (2014).

[54] T. Giamarchi, *Quantum Physics in One Dimension*, International Series of Monographs on Physics (Clarendon Press, Oxford, 2004).

[55] X. Chen and X.-G. Wen, Chiral symmetry on the edge of two-dimensional symmetry protected topological phases, Phys. Rev. B **86**, 235135 (2012).

[56] J. V. José, L. P. Kadanoff, S. Kirkpatrick, and D. R. Nelson, Renormalization, vortices, and symmetry-breaking perturbations in the two-dimensional planar model, Phys. Rev. B **16**, 1217 (1977).

[57] L. Vanderstraeten, J. Haegeman, and F. Verstraete, Tangent-space methods for uniform matrix product states, arXiv:1810.07006.

[58] V. Zauner-Stauber, L. Vanderstraeten, M. T. Fishman, F. Verstraete, and J. Haegeman, Variational optimization algorithms for uniform matrix product states, Phys. Rev. B **97**, 045145 (2018).

[59] J. Haegeman, B. Pirvu, D. J. Weir, J. I. Cirac, T. J. Osborne, H. Verschelde, and F. Verstraete, Variational matrix product ansatz for dispersion relations, Phys. Rev. B **85**, 100408(R) (2012).

[60] M. Mariën, J. Haegeman, P. Fendley, and F. Verstraete, Condensation-driven phase transitions in perturbed string nets, Phys. Rev. B **96**, 155127 (2017).

[61] L. Tagliacozzo, T. R. de Oliveira, S. Iblisdir, and J. I. Latorre, Scaling of entanglement support for matrix product states, Phys. Rev. B **78**, 024410 (2008).

[62] F. Pollmann, S. Mukerjee, A. M. Turner, and J. E. Moore, Theory of Finite-Entanglement Scaling at One-Dimensional Quantum Critical Points, Phys. Rev. Lett. **102**, 255701 (2009).

[63] M. M. Rams, P. Czarnik, and L. Cincio, Precise Extrapolation of the Correlation Function Asymptotics in Uniform Tensor Network States with Application to the Bose-Hubbard and XXZ Models, Phys. Rev. X **8**, 041033 (2018).

[64] L. H. Santos and J. Wang, Symmetry-protected many-body Aharonov-Bohm effect, Phys. Rev. B **89**, 195122 (2014).

[65] J. C. Bridgeman, Effective edge states of symmetry protected topological systems, Master's thesis, Perimeter Institute, 2014.

[66] J. C. Bridgeman and D. J. Williamson, Anomalies and entanglement renormalization, Phys. Rev. B **96**, 125104 (2017).

[67] Y.-Z. You, Z. Bi, A. Rasmussen, K. Slagle, and C. Xu, Wave Function and Strange Correlator of Short-Range Entangled States, Phys. Rev. Lett. **112**, 247202 (2014).

[68] T. Scaffidi and Z. Ringel, Wave functions of symmetry-protected topological phases from conformal field theories, Phys. Rev. B **93**, 115105 (2016).

[69] N. Bultinck, R. Vanhove, J. Haegeman, and F. Verstraete, Global Anomaly Detection in Two-Dimensional Symmetry-Protected Topological Phases, Phys. Rev. Lett. **120**, 156601 (2018).

[70] W.-T. Xu and G.-M. Zhang, Tensor network state approach to quantum topological phase transitions and their criticalities of $\mathbb{z}_2$ topologically ordered states, Phys. Rev. B **98**, 165115 (2018).

[71] D. Gepner and E. Witten, String theory on group manifolds, Nucl. Phys. B **278**, 493 (1986).

[72] A. Nahum, P. Serna, J. T. Chalker, M. Ortuño, and A. M. Somoza, Emergent SO(5) Symmetry at the Néel to Valence-Bond-Solid Transition, Phys. Rev. Lett. **115**, 267203 (2015).

[73] E. Fradkin and L. P. Kadanoff, Disorder variables and parafermions in two dimensional statistical mechanics, Nucl. Phys. B **170**, 1 (1980).

[74] P. Fendley, Parafermionic edge zero modes in zn invariant spin chains, J. Stat. Mech.: Theory Exp. (2012) P11020.

[75] J. Alicea and P. Fendley, Topological phases with parafermions: Theory and blueprints, Annu. Rev. Condens. Matter Phys. **7**, 119 (2016).

[76] W. Li, S. Yang, H.-H. Tu, and M. Cheng, Criticality in translation-invariant parafermion chains, Phys. Rev. B **91**, 115133 (2015).

[77] J. Haegeman, V. Zauner, N. Schuch, and F. Verstraete, Shadows of anyons and the entanglement structure of topological phases, Nat. Commun. **6**, 8284 (2015).

[78] M. Iqbal, K. Duivenvoorden, and N. Schuch, Study of anyon condensation and topological phase transitions from a $\mathbb{Z}_4$ topological phase using the projected entangled pair states approach, Phys. Rev. B **97**, 195124 (2018).

5

A LATTICE REGULARIZATION OF THE GROSS NEVEU MODEL

In this work we construct a lattice regularization of the Gross Neveu model

$$H = \int dx \sum_c \psi_c^\dagger \gamma^0 \gamma^x \partial_x \psi_c - \frac{g_x^2}{2} \left(\sum_c \psi_c^\dagger \gamma^0 \psi_c \right) \tag{231}$$

which, as mentioned before has a chiral Z_2 and a continuous $O(2N)$ symmetry.

The first step towards this lattice regularisation was already made during Jutho his PhD where he used the recipe of Kogut and Susskind, where $\gamma^0\gamma^5 = \sigma_x$ and $\gamma^0 = \sigma_z$ to find the Hamiltonians

$$H = \frac{1}{a} \sum_n \sum_c c_{n,c} c_{n+1,c}^\dagger + c_{n+1,c}^\dagger c_{n,c} + \frac{g_x^2}{2} \left(\sum_c c_{n,c} c_{n,c}^\dagger - c_{n+1,c} c_{n+1,c}^\dagger \right)^2 \tag{232}$$

$$= \frac{1}{a} \sum_n \sum_c \sigma_{n,c} \sigma_{n+1,c}^\dagger + \sigma_{n+1,c}^\dagger \sigma_{n,c} - g_x^2 \sigma_{z,n,c} \sigma_{z,n+1,c} \tag{233}$$

that are respectively in terms of the N fermionic degrees of freedom that satisfy $\{c_{n,c}, c_{m,\tilde{c}}^\dagger\} = \delta_{c,\tilde{c}} \delta_{n,m}$ and their hard boson equivalents that satisfy $\{\sigma_{n,c}, \sigma_{n,c}^\dagger\} = \delta_{c,\tilde{c}}$ and $[\sigma_{n,c}, \sigma_{m\neq n,\tilde{c}}^\dagger] = \delta_{c,\tilde{c}}$. With this choice the lattice regularized self interaction term is simply that of the Ising model so that the elementary excitations are kinks as is to expected from a good lattice regularization of the Gross Neveu. However, it turns out that this choice breaks the $O(2N)$ so that the kinks are no longer guaranteed to have the correct degeneracy. The hope was that this degeneracy and the corresponding symmetry would be restored in the limit $g, a \to 0$ but this did not happen.

After a lot of frustration we later realized that the $O(4)$ symmetry only remains local if we choose $\gamma^0\gamma^5 = \sigma_y$ and $\gamma^0 = \sigma_x$ before discretizing the continuum Hamiltonian. This insight lead us to

$$H = \frac{1}{a} \sum_n \sum_c i \left(c_{n,c} c_{n+1,c}^\dagger - c_{n+1,c}^\dagger c_{n,c}^\dagger \right) + \frac{g_x^2}{2} \left(\sum_c i \left(c_{n,c} c_{n+1,c}^\dagger - c_{n+1,c}^\dagger c_{n,c}^\dagger \right) - i \left(c_{n+1,c} c_{n+2,c}^\dagger - c_{n+2,c}^\dagger c_{n+1,c}^\dagger \right) \right)^2 \tag{234}$$

which has the correct $O(4)$ symmetry so that it is guaranteed to have the correct kink degeneracies. An in depth derivation of this Hamiltonian and its relation with topological phases such as those in the SSH model are described in the 2nd and 3th part of the paper. In the 4th part we identify the spectrum of the lattice model at large N and find that this reproduces all field theory results. The 5th part discusses some tensor network tools and in the 6th part these are applied to find the $N = 2$ spectrum and discuss the corresponding continuum limit. In the final section we discuss the entanglement of the groundstate for different couplings, in particular show that the entanglement spectrum of the interacting theory is simply that of the free Hamiltonian at a finite interval.

Published for SISSA by Springer

Received: *April 21, 2021*
Accepted: *July 9, 2021*
Published: *July 27, 2021*

Lattice regularisation and entanglement structure of the Gross-Neveu model

Gertian Roose,[a] **Nick Bultinck,**[a,b] **Laurens Vanderstraeten,**[a] **Frank Verstraete,**[a] **Karel Van Acoleyen**[a] **and Jutho Haegeman**[a]

[a] *Department of Physics and Astronomy, University of Ghent, Krijgslaan 281, 9000 Gent, Belgium*
[b] *Department of Physics, University of California, Berkeley, CA 94720, U.S.A.*

E-mail: gertian.roose@ugent.be, nibultinck@gmail.com, laurens.vanderstraeten@ugent.be, frank.verstraete@ugent.be, karel.vanacoleyen@ugent.be, jutho.haegeman@ugent.be

Abstract: We construct a Hamiltonian lattice regularisation of the N-flavour Gross-Neveu model that manifestly respects the full $\mathsf{O}(2N)$ symmetry, preventing the appearance of any unwanted marginal perturbations to the quantum field theory. In the context of this lattice model, the dynamical mass generation is intimately related to the Coleman-Mermin-Wagner and Lieb-Schultz-Mattis theorems. In particular, the model can be interpreted as lying at the first order phase transition line between a trivial and symmetry-protected topological (SPT) phase, which explains the degeneracy of the elementary kink excitations. We show that our Hamiltonian model can be solved analytically in the large N limit, producing the correct expression for the mass gap. Furthermore, we perform extensive numerical matrix product state simulations for $N = 2$, thereby recovering the emergent Lorentz symmetry and the proper non-perturbative mass gap scaling in the continuum limit. Finally, our simulations also reveal how the continuum limit manifests itself in the entanglement spectrum. As expected from conformal field theory we find two conformal towers, one tower spanned by the linear representations of $\mathsf{O}(4)$, corresponding to the trivial phase, and the other by the projective (i.e. spinor) representations, corresponding to the SPT phase.

Keywords: Lattice Quantum Field Theory, Nonperturbative Effects, Spontaneous Symmetry Breaking, Topological States of Matter

ArXiv ePrint: 2010.03441

https://doi.org/10.1007/JHEP07(2021)207

Contents

JHEP07(2021)207

1 Introduction

Lattice field theory, and in particular, lattice gauge theory, has been among the most successful techniques to probe the non-perturbative behaviour of quantum field theories (QFTs), such as those appearing in the standard model. The accurate determination of the proton and neutron masses has been one of the most noteworthy triumphs resulting from this effort. The default approach is to apply Monte Carlo sampling to the path integral in discretised Euclidean spacetime [1–5].

In recent years, the use of tensor network methods has been proposed as an alternative [6], with the promise that these are able to access dynamical information and do not suffer from sign problems in the case of fermionic densities or far-from-equilibrium situations [7]. One can apply tensor renormalisation group techniques as an alternative to Monte Carlo sampling to the path integral in discretised spacetime [8–18]. Alternatively, one can target the wave functional using a tensor network ansatz and apply variational techniques using the field theory hamiltonian (where only the spatial dimensions are discretised) [19–44]. This approach is also closely related to the various experiments and proposals for the analog or digital quantum simulation of lattice field theory using various platforms such as trapped ions, superconducting circuits or cold atoms in optical lattices (see ref. [6] and references therein). Aside from preliminary explorations of $\mathbb{Z}_2$ and $\mathsf{U}(1)$ gauge theories in (2+1)

dimensions [21, 26, 28, 34, 43], most of the tensor network effort has so far been invested in QFTs in (1+1) dimensions, and in particular the $\lambda\phi^4$ model [8, 9, 17, 18, 20, 22, 24] and the Schwinger model, i.e. (1+1)-dimensional quantum electrodynamics, (as well as non-abelian generalizations thereof) [19, 23, 25, 27, 29–31, 33, 35–39, 41, 44]. These models are superrenormalizable, meaning that the coupling constant has a positive mass dimension and sets the energy scale. The relation between the lattice and continuum parameters is governed by a limited number of divergent diagrams, and observables converge like power laws in the lattice spacing a as the continuum limit is approached.

In this manuscript, we use lattice field theory and tensor network tools (numerical and analytical) to probe the non-perturbative properties of the Gross-Neveu (GN) model [45], a (1+1)-dimensional model of N massless but interacting fermion flavours, which shares several non-perturbative features with (3+1)-dimensional quantum chromodynamics (see refs. [13, 42] for tensor network studies of the closely related Thirring model, an integrable model for a single massive interacting fermion flavour). The GN interaction has a discrete chiral symmetry and is marginally relevant, (i.e. renormalisable and asymptotically free). The interaction term leads to spontaneous breaking of this chiral symmetry and, associated with this, dynamical mass generation. Here observables converge logarithmically slow as the continuum limit is reached. This increases the importance of symmetries prohibiting the presence of other marginally relevant perturbations that could spoil the already slow convergence. Indeed, it turns out to be crucial to meticulously construct the lattice Hamiltonian so as to maximally preserve the symmetries of the field theory, in order to reliably obtain the continuum limit.

Being a paradigmatic model, the GN model has been the subject of several numerical and theoretical studies. Theoretical studies have focused on determining the scattering matrix and full excitation spectrum [46–48], as well as a precise determination of the mass gap [49–54] using a variety of techniques, including thermodynamic Bethe ansatz, large N expansions and the variationally optimised renormalisation group. Most numerical lattice studies use Monte Carlo techniques on the Euclidean lattice, where the fermions are dealt with by replacing the four point interaction by a coupling to an auxiliary bosonic field (using a Hubbard-Stratonovich transformation) and integrating out the resulting quadratic fermion terms, leaving the calculation of the fermion determinant as a computational problem [55–57]. In particular, there has been interest in the phase diagram at finite temperature and chemical potential, and the possible existence of an inhomogeneous phase [58, 59].

A lattice prescription of the kinetic term of the fermion model can be obtained using the Wilson prescription [60] or using the staggered formulation of Kogut and Susskind [61, 62]. The former explicitly breaks the chiral symmetry, resulting in additive mass corrections that need to be compensated by a properly tuned bare mass term, in order to reach the continuum limit. Furthermore, the Wilson prescription also leads to Aoki phases [63, 64], where reflection (parity) symmetry is broken and a pseudoscalar condensate is formed. Triggered by interest from the optical lattice community, the phase diagrams of this 'Gross-Neveu-Wilson' lattice model and its chiral extension in the limits $N \to \infty$ and $N = 1$ were studied in recent publications [65, 66], and feature both trivial, topological and symmetry broken Aoki phases.

JHEP07(2021)207

The staggered formulation, on the other hand, exhibits remnant lattice symmetries which prohibit perturbative mass corrections. For the particular case of a lattice Hamiltonian (i.e. continuous time) in (1+1) dimension, this remnant symmetry corresponds to full translation invariance of the staggered model [62]. Spontaneous breaking of discrete chiral symmetry can then be related to Peierls dimerisation, so that the GN model with $N = 2$ also arises as a continuum description of polyacetylene. In particular, the GN model provides a good description of the resulting topological soliton (kink) that interpolates between the two ground states [67, 68] and which is traditionally described as an explicit domain wall in the Su-Schrieffer-Heeger (SSH) model [69]. While the GN model as low-energy field theory in the context of the SSH model is well documented [70], the reverse direction where the SSH model is used as inspiration to construct a precise lattice regularisation of the GN model was, to the best of our knowledge, not considered.

The outline of this paper is as follows. Section 2 summarises the field theoretic description of the model. In section 3 we construct the lattice model and discuss the dynamical mass generation and kink degeneracy from a condensed matter perspective. In section 4, a large-N mean-field solution is given and found to be consistent with the large N field theory. Section 5 introduces the symmetric uniform matrix product state (MPS) ansatz, which is then used in section 6 to numerically probe the low-energy behaviour of the model for $N = 2$. In section 7, we discuss the continuum limit from the point of view of entanglement. Finally, section 8 provides a concluding discussion and outlook.

2 Gross-Neveu model in a nutshell

We first provide a short introduction to the GN model and its symmetries before porting it to the lattice. The Lagrangian density for the GN field theory reads

$$\mathcal{L} = \sum_{c=1}^{N} \bar{\psi}_c \mathrm{i}\partial\!\!\!/ \psi_c + \frac{g^2}{2} \left(\sum_{c=1}^{N} \bar{\psi}_c \psi_c \right)^2 \tag{2.1}$$

where c labels the N different flavours or colours of fermions, ψ_c is the two-component Dirac spinor for flavour c, $\partial\!\!\!/ = \gamma^0\partial_0 + \gamma^1\partial_1$ and $\bar{\psi}_c = \psi_c^\dagger\gamma^0$, where $\{\gamma^\mu, \gamma^\nu\} = 2g^{\mu\nu}$ and $g^{\mu\nu}$ is the inverse metric tensor.

The model has an obvious $\mathsf{SU}(N)$ flavour mixing symmetry that can be extended to an $\mathsf{O}(2N)$ symmetry, which also includes the total $\mathsf{U}(1)$ particle number symmetry and the charge conjugation symmetry (which relates the two disconnected components of $\mathsf{O}(2N)$). This $\mathsf{O}(2N)$ symmetry is made explicit by rewriting the Dirac spinor in terms of its Majorana components. By choosing a specific set of gamma matrices where both γ^0 and γ^1 are strictly imaginary (so that $\beta = \gamma^0$ is imaginary and thus antisymmetric, whereas $\alpha = \gamma^0\gamma^1$ is real symmetric), the Majorana components correspond to the real and imaginary components of the Dirac spinor, i.e. $\psi_c = (\lambda_{2c-1} + \mathrm{i}\lambda_{2c})/\sqrt{2}$ and thus $\lambda_{2c-1} = (\psi_c + \psi_c^*)/\sqrt{2}$ and $\lambda_{2c} = -\mathrm{i}\,(\psi_c - \psi_c^*)/\sqrt{2}$, which then yields

$$\mathcal{L} = \sum_{m=1}^{2N} \bar{\lambda}_m \mathrm{i}\partial\!\!\!/ \lambda_m + \frac{g^2}{2} \left(\sum_{m=1}^{2N} \bar{\lambda}_m \lambda_m \right)^2 \tag{2.2}$$

JHEP07(2021)207

with $\bar{\lambda}_m = \lambda_m^{\mathrm{T}}\gamma^0$. This formulation shows the explicit invariance under $\lambda_m \to O_{mn}\lambda_n$ for $O \in \mathsf{O}(2N)$. Coleman's theorem for relativistic theories [71], related to the Mermin-Wagner theorem in condensed matter or statistical physics [72], guarantees that this continuous symmetry cannot be broken and is thus present in the spectrum of the theory.

The GN model has an additional $\mathbb{Z}_2$ chiral symmetry that acts as $\psi \to \gamma_5\psi$ and prohibits perturbative contributions to the condensate $\sigma = \sum_{c\in N}\langle\bar{\psi}_c\psi_c\rangle$, or thus, a perturbative mass term. Nonetheless, this $\mathbb{Z}_2$ symmetry is spontaneously broken and gives rise to a non-perturbative mass scale. The effect that the ground state exhibits a dimensionful condensate, despite the absence of dimensionful parameters, other than the ultraviolet (UV) regulator scale, is known as dimensional transmutation. The required renormalization group (RG) invariant mass scale can be obtained from the β function

$$\beta(g) = \frac{\mathrm{d}g}{\mathrm{d}\log\mu} = \beta_0 g^3 + \beta_1 g^5 + \mathcal{O}(g^7) \tag{2.3}$$

as

$$\Lambda = \mu \mathrm{e}^{-\int^{g(\mu)}\beta(g)^{-1}\mathrm{d}g} = \mu\left(-\beta_0 g^2\right)^{\frac{\beta_1}{2\beta_0^2}} e^{\frac{1}{2\beta_0 g^2}}\left[1+\mathcal{O}(g^2)\right] \tag{2.4}$$

where μ is the regulator scale. This mass scale Λ is only an infrared (IR) scale for asymptotically free theories ($\beta_0 < 0$). Furthermore, the mechanism by which it enters the IR theory (if any) must necessarily be non-perturbative. For the $\mathsf{O}(2N)$-symmetric GN model, the first terms in the β function were calculated to be $\beta_0 = -\frac{N-1}{2\pi}$ and $\beta_1 = \frac{N-1}{4\pi^2}$ [73, 74].

The condensation of σ gives rise to a rich spectrum of massive particles [46, 48, 75, 76]. Given the $\mathsf{O}(2N)$ symmetry, some understanding of the representation theory of the corresponding Lie-algebra $\mathfrak{so}(2N)$ is useful to label this spectrum. There are two distinct fundamental (half) spin representations of dimension 2^{N-1}, which are transformed into each other by conjugation or by application of a reflection element from $\mathsf{O}(2N)$ (determinant -1). The other fundamental representations $r = 1, \ldots, N-2$ are tensor representations, with $r = 1$ the defining (vector) representation. We also refer to the spinor representations as projective representations, which generalise the concept of 'representations up to a phase' — as opposed to linear representations such as the tensor representations — to arbitrary groups.

The spectrum of the GN model contains both trivial and topological excitations, i.e. kinks that interpolate between the two vacuum states. Unlike in conventional (i.e. Ising-type) $\mathbb{Z}_2$ symmetry breaking, where the kink from one vacuum to the other is unique, in the case of GN the kinks are of the Callen-Coleman-Gross-Zee type [77] and bind massless fermions. They transform according to the fundamental spinor representations [47]. This is similar to Jackiw-Rebbi kinks [78] and we will interpret this from a condensed matter perspective as the protected gapless edge modes on the interface between a trivial and SPT phase, when constructing the lattice model. Trivial elementary excitations are labelled by a principal quantum number $n = 1, \ldots, N-2$ and have a mass m_n relative to the kink mass m_K given by [48, 75]

$$m_n = 2m_K \sin\frac{\pi n}{2N-2} \tag{2.5}$$

JHEP07(2021)207

For every n, there are multiplets of these excitations labeled by $r = n, n-2, \ldots, \geq 0$, the linear fundamental representations of $\mathfrak{so}(2N)$. These multiplets are fermionic (bosonic) for r (and thus also n) odd (even). The elementary fermion corresponds to $n = 1$ and thus transforms according to the defining vector representation of $\mathsf{O}(2N)$. An exact result for the mass of this elementary fermion was derived in ref. [49], namely

$$m_1 = \frac{(4e)^{\frac{1}{2N-2}}}{\Gamma\left(1-\frac{1}{2N-2}\right)}\Lambda_{\overline{\text{MS}}} \tag{2.6}$$

in terms of a specific choice for the RG-invariant scale $\Lambda_{\overline{\text{MS}}}$, known as the modified minimal subtraction scheme when using dimensional regularisation. Note that for $N = 2$, the elementary fermion is not stable and decays into two kinks, i.e. $m_1 = 2m_K$. In that case, eq. (2.6) is providing a definition for (twice) the kink mass m_K.

When using a different regularisation scheme, such as the lattice Hamiltonian introduced next, the coupling and its UV dependence differ. As a result, the RG independent scales Λ defined from eq. (2.4) need to be matched between different regularisation schemes. In what follows, we obtain $\Lambda_{\overline{\text{MS}}} = \frac{8}{e}\Lambda_{\text{lat}}$ using an exact solution of the lattice model in the limit $N \to \infty$. A more standard yet involved Feynman diagram calculation of the scattering matrix in appendix A proves that this relation is valid for all values of N.

3 Lattice Hamiltonian

To construct a lattice regulated version of the GN Hamiltonian, we follow the staggered fermion formulation from ref. [62]. While this procedure is well known, we review it with some detail, in order to properly motivate our lattice proposal for the GN interaction.

One interpretation of the staggering procedure, which is useful for what follows, is to discretise the two components of the Dirac spinor at positions differing by half a lattice spacing, i.e. $\psi_{c,1}(na) \to \phi_{c,2n}/\sqrt{a}$ and $\psi_{c,2}((n+\frac{1}{2})a) \to \phi_{c,2n+1}/\sqrt{a}$, with a the lattice spacing. Furthermore, we choose the matrix $\alpha = \gamma^0\gamma^1$ appearing in the kinetic term of the Dirac Hamiltonian off-diagonal. With this choice the free massless Dirac Hamiltonian only couples derivatives of the first component to the second component of the Dirac spinor, and vice versa. For such terms a symmetric finite difference approximation of the derivative[1] leads to e.g.

$$\begin{aligned}\int \psi^\dagger_{c,2}(x)\partial_x\psi_{c,1}(x)dx &\to \sum_n a\ \ \psi^\dagger_{c,2}\left(\left(n+\frac{1}{2}\right)a\right)\partial_x\psi_{c,1}\left(\left(n+\frac{1}{2}\right)a\right)\\ &\to \sum_n a\ \ \psi^\dagger_{c,2}\left(\left(n+\frac{1}{2}\right)a\right)\frac{\psi_{c,1}((n+1)a)-\psi_{c,1}(na)}{a}\\ &\to \sum_n \frac{1}{a}\ \ \phi^\dagger_{c,2n+1}\left(\phi_{c,2n+2}-\phi_{c,2n}\right)\end{aligned} \tag{3.1}$$

[1] The staggered fermion formulation is often introduced with the two spinor components discretized at the same positions and an asymmetric finite difference scheme, e.g. forward for $\partial\psi_1$ and backward for $\partial\psi_2$. Explicitly shifting the discretisation positions of the two components leads to the same end result, but is somewhat more aesthetically pleasing, and also clarifies how to deal with terms where both components (not their derivates) appear on the same position, e.g. $\psi_1^\dagger\psi_2$.

JHEP07(2021)207

Combined with the requirement that α is real to make the $\mathsf{O}(2N)$ symmetry explicit (and thus easier to preserve in the lattice model) leads to $\alpha = \sigma^x$, and the resulting lattice Hamiltonian is given by

$$aH = \sum_n K_{n,n+1} \tag{3.2}$$

with K the (N-flavor) tight-binding or hopping operator

$$K_{n,n+1} = \sum_{c=1}^{N} (-\mathrm{i})(\phi^\dagger_{c,n}\phi_{c,n+1} - \phi^\dagger_{c,n+1}\phi_{c,n}) = \sum_{m=1}^{2N} (-\mathrm{i})\chi_{m,n}\chi_{m,n+1} \tag{3.3}$$

where we have introduced Majorana modes $\chi_{m,n}$ as $\phi_{c,n} = (\chi_{2c-1,n} + \mathrm{i}\chi_{2c,n})/\sqrt{2}$ to make the $\mathsf{O}(2N)$ symmetry of this lattice operator explicit.

Before adding the GN four point interaction, let us first discuss how to add an explicit mass term. Having fixed $\alpha = \gamma^0\gamma^1 = \sigma^x$, the field theory allows for any choice $\beta = \gamma^0 = \cos(\theta)\sigma^y + \sin(\theta)\sigma^z$. The original proposal of Susskind in ref. [62] was $\beta = \gamma^0 = \sigma_z$, which is then trivially discretised into a lattice mass term on the doubled lattice as

$$\Delta \sum_n (-1)^n \sum_{c=1}^{N} \phi^\dagger_{c,n}\phi_{c,n} \tag{3.4}$$

with $\Delta = ma$ the mass in dimensionless lattice units. This clearly indicates how one-site translations on the staggered lattice flip the sign of the mass term, and can thus be related to a lattice remnant of the discrete chiral transformation $\psi \to \gamma^5\psi$. However, this lattice term breaks the $\mathsf{O}(2N)$ symmetry, as can be made explicit by rewriting it in terms of the Majorana components.

The alternative choice $\beta = \sigma^y$ yields terms involving both components of the Dirac spinor on the same position, which can be discretised on our staggered lattice by averaging one of the two components over the two nearby positions. This gives rise to an alternative lattice mass term, which takes the form of a staggered hopping

$$\frac{\Delta}{2} \sum_n (-1)^n K_{n,n+1} \tag{3.5}$$

and thus respects the $\mathsf{O}(2N)$ symmetry. This term is well known from the SSH model, where the alternating hopping strengths result from dimerisation.

On the lattice, these two mass terms, resulting from two different choices for β (and thus, ultimately, a different choice of basis for the Dirac spinor in the continuum) are not equivalent. From the periodic table of topological insulators and superconductors [79, 80], it is well known that the SSH mass term preserves sublattice symmetry (class AIII or BDI), which gives rise to a protected topological invariant labeled by $\mathbb{Z}$. Sublattice symmetry is also known as chiral symmetry in that context, but we refrain from using this terminology, as it is clearly different from the chiral symmetry of the field theory relevant to our study, and which is broken by either mass term.

Writing the Hamiltonian terms in momentum space after blocking two sites, they take the form

$$\sum_{c=1}^{N} \int_{-\pi}^{\pi} \Psi_c(p)^\dagger \left(\vec{d}(p)\cdot\vec{\sigma}\right) \Psi_c(p)\, \mathrm{d}p \tag{3.6}$$

JHEP07(2021)207

similar to the field theory Hamiltonian but with $\vec{d}(p)$ a periodic function of the lattice momentum $p \in [-\pi, +\pi)$ on the blocked lattice. A gapped model has nonzero $\vec{d}(p)$ for all p. Sublattice symmetry imposes that $\vec{d}(k)$ is confined to a two-dimensional space, and the topological invariant corresponds to the winding number of $\vec{d}(p)$ around the origin. Both the kinetic term in eq. (3.2) and the SSH mass term in eq. (3.5) only have non-zero d_x and d_y components, in particular $d_x(p) = \sin(p)(1 + \frac{\Delta}{2})$ and $d_y(p) = (1 + \frac{\Delta}{2}) + \cos(p)(1 - \frac{\Delta}{2})$. They lead to a well-defined winding number, which is non-zero for $\Delta < 0$ (shifting the unit cell definition is equivalent to $\Delta \to -\Delta$), thus indicating a symmetry-protected topological (SPT) phase protected by either sublattice symmetry or bond-centred inversion, where the latter is also defined for interacting systems. Susskind's mass term [eq. (3.4)] corresponds to $d_z(p) = \Delta$ and breaks the topological invariant. In the field theory, the kinetic term has a single component (i.e. $d_x(p) = p$ if $\alpha = \sigma^x$), and so either choice of β is equivalent. While the winding number is undefined as momentum space is unbounded, topological features still manifest themselves when considering a domain between positive and negative mass, which gives rise to gapless edge modes, as described by Jackiw and Rebbi [78]. Hence, the SSH mass term provides a more faithful lattice description of the massive Dirac field.

We can rewrite the mass term from eq. (3.5) as

$$\frac{\Delta}{2}\sum_n (-1)^n K_{n,n+1} = \frac{\Delta}{2}\sum_n (-1)^n \Sigma_{n,n+1,n+2} \tag{3.7}$$

with the three-site operator

$$\Sigma_{n,n+1,n+2} = \frac{K_{2n,2n+1} - K_{2n+1,2n+2}}{2}, \tag{3.8}$$

which plays the role of a local order parameter, i.e. the lattice equivalent of $\bar{\psi}\psi$. Whereas $K_{n,n+1}$ has non-zero expectation value even with respect to the $\Delta = 0$ ground state, $\Sigma_{n,n+1,n+2}$ is an absolute measure for the mass condensate. With this, it has now become straightforward to formulate a lattice Hamiltonian for the GN model,

$$aH = \sum_n \left(K_{n,n+1} - \frac{g^2}{4}\Sigma^2_{n,n+1,n+2} \right), \tag{3.9}$$

where the interaction coefficient was changed from $g^2/2$ to $g^2/4$ as we associated one interaction term with every site of the doubled lattice. Doing so, this model has single-site translation invariance, which corresponds to the lattice remnant of discrete chiral symmetry, as well as $\mathsf{O}(2N)$ symmetry. The projective nature of the $\mathsf{O}(2N)$ action on the single-site Hilbert space, which is discussed in section 5, in combination with translation invariance enables the application of the Lieb-Schultz-Mattis theorem [81]: this model cannot have a unique, gapped ground state. It is critical for $g = 0$, but we expect the interaction to be marginally relevant and lead to a symmetry broken state for $g \neq 0$. The Mermin-Wagner theorem excludes the $\mathsf{O}(2N)$ symmetry to be broken, thus leading to dimerisation, the lattice manifestation of a mass condensate, as the most likely scenario. By adding an explicit SSH mass term, a two-dimensional phase diagram is obtained, depicted in figure 1, where the Hamiltonian in eq. (3.9) (i.e. the $\Delta = 0$ line) can be identified as a

JHEP07(2021)207

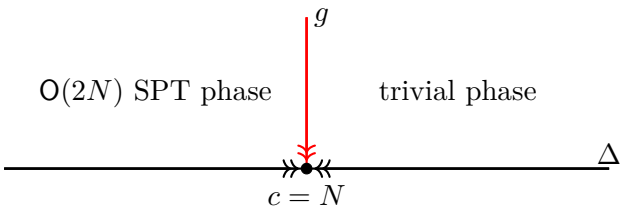

Figure 1. Phase diagram of the lattice GN Hamiltonian from eq. (3.9) with additional SSH mass term from eq. (3.5). The point $g = \Delta = 0$ is the lattice realisation of the N-flavour free fermion conformal field theory, which plays the role of a UV fixed point. For negative/positive mass perturbations the ground state is in a symmetry protected/trivial gapped phase respectively. The GN model has no explicit mass term and corresponds to a first order phase transition between those phases, i.e. it has two gapped ground states with zero and non-zero topological invariant respectively. The continuum limit of the Gross Neveu model approaches the $c = N$ point via the red arrows, while the black arrows denote the continuum limit of N massive fermions.

first order phase transition between the trivial and non-trivial SPT phase. While this is somewhat similar to the $\mathbb{Z}_2$-symmetry breaking phase of the Ising model being a first order line between the explicit symmetry-broken regimes with positive and negative longitudinal field, the topologically distinct nature of the phases at both sides of the transition results in symmetry fractionalisation in the kink excitations that interpolate between the two ground states at the first order line.

We confirm that the low-energy behaviour of this lattice model does indeed replicate all features of the Gross-Neveu field theory in the next sections using a large N calculation (section 4) and by constructing an MPS ansatz (sections 5 and 6). The MPS ansatz is not only used for numerical simulations for $N = 2$, but also provides further insight into the symmetry structure of the excitation spectrum for general N.

4 Large-N solution

Similar to the original paper of Gross and Neveu [45], we first study our lattice model in the limit of $N \to \infty$, but within the Hamiltonian formalism. In the limit $N \to \infty$, the permutation symmetry corresponding to exchanging the different flavours in combination with monogamy of entanglement [82, 83] can be used to argue that the ground state $|\Psi\rangle$ will be a product state over the different flavours, where each flavour is described by the same state: $|\Psi\rangle = |\phi\rangle^{\otimes N}$. The energy of this state is given by

$$E_\Psi = \sum_n \left(N \langle\phi| k_{n,n+1} - \frac{g^2}{4} \sigma^2_{n,n+1,n+2} |\phi\rangle - \frac{g^2}{4} N(N-1) \langle\phi|\sigma_{n,n+1,n+2}|\phi\rangle^2 \right) \tag{4.1}$$

with $k_{n,n+1}$ and $\sigma_{n,n+1,n+2}$ the single-flavour versions of $K_{n,n+1}$ and $\Sigma_{n,n+1,n+2}$ respectively. The GN interaction splits into N terms which act on a single flavour, and $N(N-1)$ terms which act across different flavours, and are transformed into a product of expectation values due to our product state ansatz: correlations between flavours vanish for $N \to \infty$. In order to obtain finite results, we take the limit $N \to \infty$ while keeping $\lambda = g^2(N-1)$ fixed. As g^2 itself goes to zero, the self-interaction of the flavours vanishes.

JHEP07(2021)207

Minimising the energy with respect to ϕ yields, after adding a Langrange constraint for the normalisation, a self-consistent eigenvalue problem for the state $|\phi\rangle$:

$$\sum_n \left(k_{n,n+1} - \frac{\lambda \langle \sigma_{n,n+1,n+2} \rangle}{2} \sigma_{n,n+1,n+2} \right) |\phi\rangle = E_\phi |\phi\rangle \tag{4.2}$$

where the Lagrange parameter E_ϕ can be interpreted as the energy of a single flavor, and

$$E_\Psi = N(E_\phi + \frac{\lambda}{4} \sum_n \langle \phi | \sigma_{n,n+1,n+2} | \phi \rangle^2) \tag{4.3}$$

Assuming a dimerised solution, we set $\langle \phi | \sigma_{n,n+1,n+2} | \phi \rangle = (-1)^n \sigma_0$. The state $|\phi\rangle$ of a single flavor is now determined as the ground state of the quadratic mean-field (i.e. Hartree-Fock) Hamiltonian

$$H_{\mathrm{MF}} = \sum_n k_{n,n+1} + \frac{\lambda \sigma_0}{2} (-1)^n \sigma_{n,n+1,n+2} \tag{4.4}$$

in which $\lambda\sigma_0$ plays the role of an SSH mass. The mean-field Hamiltonian is diagonalised by blocking the lattice and going to momentum space, which gives rise to single particle energies

$$\varepsilon(p) = \pm \sqrt{4 \sin^2(p/2) + \lambda^2 \sigma_0^2 \cos^2(p/2)}. \tag{4.5}$$

with, as before, $p \in [-\pi, +\pi)$ the lattice momentum on the blocked lattice. One can verify that the self-consistency condition for σ_0 is equivalent to minimising $E_\Psi / N = \langle \phi | H_{\mathrm{MF}} | \phi \rangle + \sum_n \frac{\lambda}{4} \sigma_0^2$, or thus

$$\frac{e_\Psi}{N} = \frac{\lambda}{2} \sigma_0^2 - \int_{-\pi}^{\pi} \frac{\mathrm{d}p}{2\pi} \sqrt{4 \sin^2(p/2) + \lambda^2 \sigma_0^2 \cos^2(p/2)} \tag{4.6}$$

with e_Ψ the energy density associated with the sites of the blocked lattice. The value of σ_0 is thus determined by the condition

$$\frac{1}{\lambda} = \int_{-\pi}^{\pi} \frac{\mathrm{d}p}{2\pi} \frac{\cos^2(p/2)}{\sqrt{4 \sin^2(p/2) + \lambda^2 \sigma_0^2 \cos^2(p/2)}}. \tag{4.7}$$

This can be further expanded as

$$\frac{1}{\lambda} = \frac{1}{\pi} \frac{K\left(1 - \frac{\lambda^2 \sigma_0^2}{4}\right) - E\left(1 - \frac{\lambda^2 \sigma_0^2}{4}\right)}{1 - \frac{\lambda^2 \sigma_0^2}{4}} \tag{4.8}$$

with K and E the complete elliptic integral of the first and second kind, respectively. An asymptotic expansion for small $\lambda\sigma_0$, which is the dimensionless mass and should go to zero to recover the continuum limit, yields

$$\frac{1}{\lambda} = -\frac{1}{2\pi} \left[\log\left(\frac{\lambda^2 \sigma_0^2}{64} \right) + 2 \right] + O\left(\lambda^2 \sigma_0^2 \log\left(\lambda^2 \sigma_0^2 \right) \right) \tag{4.9}$$

JHEP07(2021)207

As a result, the effective fermion mass is in the large-N limit given by

$$am_1 = \lambda\sigma_0 = \frac{8}{\mathrm{e}}\exp\left[-\frac{\pi}{(N-1)g^2}\right]\left(1+\mathcal{O}(g^2)\right) \tag{4.10}$$

such that m_1 is indeed proportional to the RG-invariant mass scale Λ that was introduced in section 2, with $\mu = a^{-1}$. In particular, by comparing to the $N \to \infty$ limit of the exact result in eq. (2.6), i.e. $m_1 = \Lambda_{\overline{\mathrm{MS}}}$, we are lead to conclude that if we define

$$\Lambda_{\mathrm{lat}} = \frac{1}{a}\left(\frac{(N-1)g^2}{2\pi}\right)^{\frac{1}{2N-2}}\exp\left[-\frac{\pi}{(N-1)g^2}\right] \tag{4.11}$$

then $\Lambda_{\mathrm{lat}} = \frac{8}{e}\Lambda_{\overline{\mathrm{MS}}}$ and thus we should recover

$$m_1/\Lambda_{\mathrm{lat}} = \frac{8}{e}\frac{(4e)^{\frac{1}{2N-2}}}{\Gamma(1-\frac{1}{2N-2})}(1+O(g^2)) \tag{4.12}$$

in the continuum limit $g \to 0$. However, the $N \to \infty$ solution is in itself not sufficient to support this conclusion, as other N dependent scale factors might appear. A careful comparison between Λ_{lat} and $\Lambda_{\overline{\mathrm{MS}}}$ using the fermion-fermion scattering amplitude at finite N leads to the same result, as explained in appendix A.

Henceforth, we omit the lattice spacing a, as it appears trivially in length or mass scale quantities and does not directly affect the distance to the continuum limit. So we stop differentiating between dimensionless lattice and field theory quantities.

5 Matrix product states

For finite N, correlations between the different flavours cannot be ignored, and the ground state of our lattice model is a fully correlated quantum state, both in the spatial and in the flavour direction. We now try to approximate this ground state using a MPS ansatz, which is known to capture the quantum correlations in low-energy states of gapped local Hamiltonians for quantum spin chains [84]. The MPS ansatz associates with every site n of such a spin chain a 3-leg tensor $A(n)$ of size $D_{n-1} \times d \times D_n$, with d the local Hilbert space dimension of the physical index. The left (respectively right) virtual index of size D_{n-1} (D_n) is then contracted with the right virtual index of the previous (left virtual index of the next) tensor, resulting in a correlated state whose bipartite entanglement for a cut between site n and site $n+1$ is upper bounded by $\log(D_n)$, independent of the system size (in accordance with the area law for entanglement entropy in one-dimensional systems [85]). By defining a unit cell, i.e. a periodic n dependence in the tensors $A(n)$, we can describe quantum states directly in the thermodynamic limit.

Our lattice model is easily translated into a spin chain using a Jordan-Wigner transformation

$$\phi_{c,n} = \left(\prod_{n'<n}\prod_{c'}\sigma^z_{c',n'}\right)\left(\prod_{c'<c}\sigma^z_{c',n}\right)\sigma^-_{c,n} \tag{5.1}$$

JHEP07(2021)207

where we introduce a linear ordering in the flavour direction $c = 1, \ldots, N$, and thus associate N qubits or spins with each site, so that the local Hilbert space dimension is 2^N. We keep these N qubits together (as opposed to treating them as N individual sites) in order to preserve the $\mathsf{O}(2N)$ symmetry and to be able to capture it in the MPS ansatz. Using this particular ordering in the Jordan-Wigner transformation, the generators of the associated Lie algebra $\mathfrak{so}(2N)$ transform into a sum of one-site operators so that the resulting symmetry transformations act on-site. The local Hilbert space of a site can be identified with the direct sum of the two fundamental $\mathfrak{so}(2N)$ spinor representations (each of which has dimension 2^{N-1}) with opposite total fermion parity.

In order to construct $\mathsf{SO}(2N)$ symmetric MPS,[2] the virtual indices of the tensors should also carry representations of the group [86, 87] and the local tensors $A(n)$ should intertwine the representation on the right virtual index with the tensor product of the representations on left virtual and physical index. The representation on the physical index, i.e. the direct sum of the two fundamental spinor representations, is projective.[3] Therefore, if the right virtual index is associated with a linear representation (i.e. a direct sum of tensor representations of $\mathsf{SO}(2N)$), then the left virtual index should also be projective (and thus be composed of spinor irreducible representations), and vice versa. We are thus naturally led to a two-site unit cell. This is the MPS manifestation of the Lieb-Schultz-Mattis theorem [88]: MPS represent finitely correlated (and thus gapped) states, and cannot be simultaneously invariant under translation symmetry and an on-site symmetry whose physical action is projective. As the on-site symmetry is continuous and cannot be broken, we thus propose an ansatz for the ground state with a two-site unit cell, in line with the expected dimerisation:

$$|\psi[A_1, A_2]\rangle = \sum_{\vec{s}} \left(\prod_{n \in \mathcal{Z}} A_{1,s_{2n}} A_{2,s_{2n+1}} |s_{2n} s_{2n+1}\rangle \right) = \cdots - A_1 - A_2 - A_1 - A_2 - \cdots \tag{5.2}$$

We can also formulate MPS-based ansätze for elementary excitations on top of the ground state [89–91], as well as kink excitations that interpolate between the two ground states. Both topologically trivial excitations and kinks can be created by modifying a single tensor (which has an effect on an extended region) and building a proper momentum superposition (unlike in semiclassical studies where the kinks or solitons are localised in real-space). The ansatz for kinks, where the two different ground states (corresponding to a one-site shift of the unit cell) surround the new tensor, is diagrammatically represented as

$$|K_p\rangle = \sum_n \left(e^{ipn} \cdots - A_1 - A_2 - \left(A_1 - B_2 \;+\; B_1 - A_1 \right) - A_2 - A_1 - \cdots \right) \tag{5.3}$$

[2] By working with the representations of the Lie-algebra $\mathfrak{so}(2N)$, we effectively only impose $\mathsf{SO}(2N)$ symmetry. However, we discuss the role of the additional mirror symmetry that extends $\mathsf{SO}(2N)$ to $\mathsf{O}(2N)$ for the particular case $N = 2$ which was used in our simulations, and find that it is unbroken.

[3] The spinor representations of $\mathsf{(S)O(N)}$ are linear representations of the universal covering group, known as $\mathsf{(S)Pin}(N)$.

JHEP07(2021)207

with once again $p \in [-\pi, +\pi)$ the momentum on the blocked lattice. The new tensors (labelled B_i) carry an additional leg corresponding to the Hilbert space of the irreducible representation of the excitation that is being targeted. In the case of kinks, as depicted here, the two virtual legs of B tensors need to be identical and thus carry the same representations, and it follows automatically that physical symmetry sector of the kink states needs to be a spinor representation. These constructions are well-known in the case of half-integer spin chains [92], where they also correspond to the renowned result that the elementary excitations in e.g. the half-integer spin Heisenberg chain are spinors [93, 94]. The analogous construction for topologically trivial excitations on top of a single ground state illustrates that these are labelled by linear irreducible representations of $\mathsf{SO}(2N)$. For an in-depth review on these excited states and their implementation we refer to ref. [91].

The variational ansatz for excitations gives rise to an energy-momentum dispersion relation, e.g. $E_K(p)$ for the kink state $|K_p\rangle$, from which we can extract a range of mass scales related to its value, inverse curvature and higher derivatives at $p = 0$, where the dispersion relation has its minimum. Indeed, by fitting

$$E_K(p) = m_{K,1}\left(1 + \frac{p^2}{2m_{K,2}^2} + \cdots\right) \tag{5.4}$$

to the dispersion relation for small values of the lattice momentum p, we obtain two different mass scales.[4] Alternatively, expecting relativistic invariance, we can rewrite this expansion for the square of the energy as

$$E_K(p)^2 = m_{K,1}^2 + \frac{m_{K,1}^2}{m_{K,2}^2}p^2 + \cdots \tag{5.5}$$

and thus interpret the ratio $m_{K,1}/m_{K,2}$ as an effective speed of light, which should go to one if Lorentz invariance is obtained in the continuum limit.

In a theory near a relativistic continuum limit, information about the particle masses is also encoded in the ground state, more particularly in the spectrum of inverse correlation lengths. This is true for trivial excitations, by writing two-point correlation functions using the Källén-Lehmann representation [95]. To extract the kink mass from a correlation function, one needs to study the correlation of string operators. In the MPS language, the corresponding inverse correlation length can easily be extracted by studying the *mixed* transfer matrix, made from two different ground states. In this particular case, these two ground states are related by a one-site shift, and we define

$$m_{K,3} = -\log\left(\rho\left(\right.\right. \tag{5.6}$$

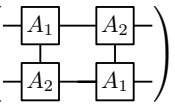

$$\left.\left.\right)\right) ,$$

with ρ the spectral radius (largest magnitude eigenvalue). The right hand side of this equation gives an inverse length scale, and requires a (dimensionless) velocity to give an energy scale. Again we assume this velocity to be one as we approach the continuum

[4] One could expand further and introduce an arbitrary amount of mass scales.

JHEP07(2021)207

limit, and we will directly compare $m_{K,3}$ as another estimate of the kink mass. Note that the eigenvectors of the mixed transfer matrix, due to the different nature of the two legs on which they act, also transform according to spinor representations, reflecting the spinorial nature of the kinks to which the mixed transfer matrix is related. One could also calculate the leading eigenvalue in the trivial transfer matrix as an estimate for the fermionic correlation length an hence inverse fermion mass.

While (inverse) correlation lengths converge slowly as a function of the MPS bond dimension, a scaling theory for their behaviour was recently developed based on a parameter δ that quantifies the level spacing in the logarithmic eigenvalue spectrum of the transfer matrix (which should become continuous in the infinite bond dimension limit). We refer to refs. [17, 96] and use these techniques to extrapolate reported mass values to the infinite bond dimension limit.

6 Simulation of the $N = 2$ mass gap

As a first application of our MPS simulations, we compute the different estimations of the mass gap m_K of the kink that interpolates between the two vacua for $N = 2$. Hereto, we first find the optimal MPS representation of the ground state using the "variational algorithm for uniform matrix product states" (VUMPS) [97], which directly minimises the energy (density) (i.e. variationally) in the thermodynamic limit.

Our implementation of this algorithm, as well as the algorithm for computing the dispersion relation using the excitation ansatz, can be found in "MPSKit.jl" [98], an open source package for MPS algorithms using the scientific programming language Julia. This package builds upon "TensorKit.jl" [99], a lower level open source package for representing and manipulating tensors with arbitrary (abelian and non-abelian) symmetries.

Specifically for $N = 2$, we enforced the tensors to be representations of $\mathsf{SO}(4)$, or rather its universal cover $\mathsf{Spin}(4)$. This group is equivalent to $\mathsf{SU}(2) \times \mathsf{SU}(2)$ and irreducible representations are labeled by a tuple of two $\mathsf{SU}(2)$ quantum numbers, i.e. half integers or integers. The resulting representation is a projective (i.e. spinor) representation of $\mathsf{SO}(4)$ if only one of both quantum numbers is a half-integer. With both quantum numbers integer or half-integer, a linear (i.e. tensor) representation of $\mathsf{SO}(4)$ is obtained. This symmetry can easily be understood by considering the two sets of generators,

$$S^+ = (S^-)^\dagger = \sum_n \phi^\dagger_{1,n}\phi_{2,n} \tag{6.1}$$

$$S^z = \sum_n \frac{\phi^\dagger_{1,n}\phi_{1,n} - \phi^\dagger_{2,n}\phi_{2,n}}{2} \tag{6.2}$$

$$T^+ = (T^-)^\dagger = \mathrm{i}\sum_n \phi^\dagger_{1,n}\phi^\dagger_{2,n} \tag{6.3}$$

$$T^z = \sum_n \frac{\phi^\dagger_{1,n}\phi_{1,n} + \phi^\dagger_{2,n}\phi_{2,n} - 1}{2} \tag{6.4}$$

corresponding to rotations in flavour space (odd fermion subspace of single occupancy) and in some pseudospin space (even fermion subspace of zero or double occupancy), exactly

JHEP07(2021)207

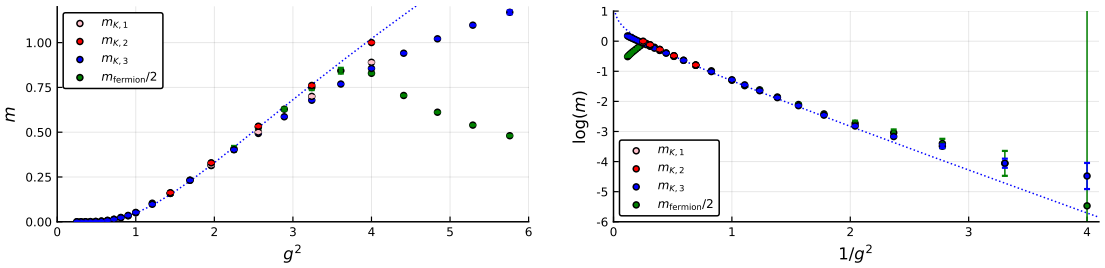

Figure 2. Extrapolated mass scales and a fit to small couplings, presented in two different ways. The linear behaviour in the second panel follows from the leading order contribution in $\log(m_K)$. The error bars correspond to the uncertainty in the $\delta \to 0$ extrapolations. Fits are made against the inverse correlation length ($m_{K,3}$) data and take the form $\log(m_{K,3}) = \log(C\Lambda_{\text{lat}})$ and C is consistent with the value predicted by the field theory results up to 4%.

as in the Hubbard model at half filling [100]. The disconnected part of $\mathsf{O}(4)$ (or its double cover, $\mathsf{Pin}(4)$) is generated by a fermionic particle-hole transformation on one of the fermion flavours, and has the effect of interchanging the two $\mathsf{SU}(2)$ factors. It thus results in degeneracies between sectors (j_1, j_2) and (j_2, j_1), i.e. whenever $j_1 \neq j_2$, these two representations will always come together as $(j_1, j_2) \oplus (j_2, j_1)$, where the direct sum constitutes a proper (linear or projective) representation of $\mathsf{O}(4)$. While this extra symmetry is not enforced on our MPS representation, it does seem to be perfectly preserved in the ground states we find numerically. Exploiting the $\mathsf{Spin}(4) \cong \mathsf{SU}(2) \times \mathsf{SU}(2)$ symmetry has enabled us to push the bond dimension to $D \approx 4000$.

Using the exact equation for the mass gap [eq. (2.6)], the relation between $\Lambda_{\overline{\text{MS}}}$ and Λ_{lat} proven in appendix A, and the fact that the kink mass is half the fermion mass for $N = 2$, we obtain that the dimensionless mass of the elementary kinks for $N = 2$ should approach the value

$$m_K = \frac{8}{e}\sqrt{\frac{e}{\pi}}\frac{1}{\sqrt{2\pi}} g e^{-\pi/g^2} \tag{6.5}$$

in the continuum limit.

Figure 2 depicts four extrapolated mass scales as a function of the coupling. The blue dots, referred to as $m_{K,3}$, i.e. the inverse correlation length extracted from the mixed transfer matrix, are relatively cheap to compute but require careful extrapolation towards $\delta = 0$. This extrapolation is illustrated in figure 3. Here, we present a handful of linear extrapolations for each coupling. One fit considers only the 5 highest bond dimension simulations, other extrapolations discard the highest bond dimensions and use the 5 next best bond dimensions. The resulting variation in the extrapolated mass gap gives rise the error bars depicted in figure 2. In a similar manner, the largest correlation length extracted from the normal transfer matrix (topologically trivial sector) should be determined by the fermion mass, and half of this value should also provide an estimate of the kink mass in the continuum limit. It is depicted by the green dots in figure 2. Note that for large values $g \gtrsim 4$ (which are not relevant for the continuum limit), the fermion mass (as extracted from the inverse correlation length), is less than twice the kink mass. Hence, at those

JHEP07(2021)207

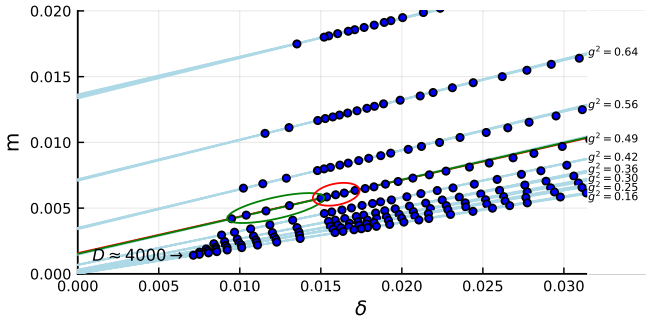

Figure 3. Extrapolation of the inverse correlation length of the mixed transfer matrix (topological sector), corresponding to the mass estimator $m_{K,3}$, as a function of δ, the spacing in the logarithmic spectrum of the transfer matrix [96]. For every value of the coupling g^2 we show a handful of linear extrapolations towards $\delta = 0$ each taking different points into consideration. For example at $g^2 = 0.56$ we have highlighted the 5 points with highest bond dimension and the corresponding extrapolation in green. Another extrapolation where we discarded the 4 points with highest bond dimension is highlighted in red. These extrapolate to slightly different masses which allows us to estimate the error on the extrapolation that is shown in figure 2.

values of the coupling constant, the lattice model is likely to exhibit a stable particle in the topologically trivial sector.

The pink and red dots in figure 2 correspond to the gap and inverse curvature obtained from the excitation ansatz, referred to as $m_{K,1}$ and $m_{K,2}$ before. These points converge more quickly with bond dimensions and require little extrapolation, yet are more costly to obtain. We have only calculated these points for a selection of couplings. The observation that the value of the gap, its curvature and the inverse correlation length coincide clearly shows an emergent Lorentz symmetry with speed of light equal to one, as intended. To further illustrate this, we plot the kink dispersion relation at $g = 1.4$ in figure 4 and compare the dispersion to the relativistic prediction $E_p^2 = m^2 + p^2$. Even for relatively large lattice momenta up to $p \approx \pi/2$ the correspondence is good. Note that the mass here is already of the order of 0.4 in lattice units, and we are thus already quite far from the proper continuum limit. For even larger values of g^2, where the mass becomes of the order of one in lattice units, deviations between the different mass scales can be observed, as expected.

To compare our mass data to the proposed continuum limit of eq. (6.5), it is useful to consider the right panel of figure 2 where $\log(m_K)$ is displayed as a function of $1/g^2$. For sufficiently small couplings the logarithm is dominated by $-\pi/g^2$ resulting in a linear relation that is ideal for fitting. A fit of the form $\log(m_K) = -\frac{\pi}{g^2} + \log(g) + \log(C)$ is shown in both panels and we find $C \approx 1.121$ for the inverse correlation length data $m_{K,3}$. This value compares well with the expected result $C = \frac{8}{e}\sqrt{\frac{e}{\pi}}\frac{1}{\sqrt{2\pi}} = 1.092$, but shows a small overshoot of about 3%. Note that the logarithmic contribution to the fit complicates the fitting process and makes the fit parameter very sensitive to data in the small g regime, where the masses become extremely small and thus hard to pinpoint exactly. Nonetheless, we do conclude that this data provides ample evidence for the continuum limit of our lattice model being well described by the GN field theory, as intended.

JHEP07(2021)207

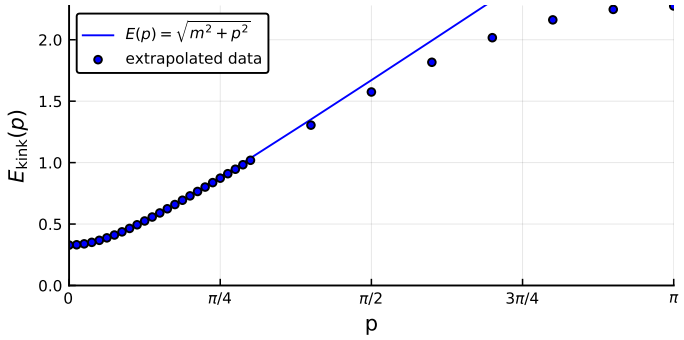

Figure 4. The kink energy as a function of the momentum on the blocked lattice for $g = 1.4$, as compared to the corresponding Einstein energy-momentum relation, indicating Lorentz invariance over a relatively large range of momenta.

7 Entanglement structure of the groundstate

Another advantage of tensor network representations of quantum states is that they give full access to the entanglement structure of the state, which is an interesting concept in its own right as it provides an fresh perspective into the quantum correlations of the state and has thus received a lot of attention lately. In particular, the half-space reduced density matrix defines the entanglement Hamiltonian H_E via

$$\text{Tr}_{\text{half space}} \left(|\Psi\rangle \langle \Psi| \right) = \hat{\rho} = e^{-2\pi H_E} \tag{7.1}$$

which for a relativistic field theory is also known as the modular or Rindler Hamiltonian (corresponding to an accelerating observer). For a conformal field theory (CFT), the modular Hamiltonian can be mapped back to the original Hamiltonian using a conformal (logarithmic) transformation. In a gapped theory close to a CFT in the ultraviolet (UV), we expect the entanglement structure, which is anyway determined by UV modes of the theory,[5] to follow the CFT prediction closely up to length scales of the correlation length. The logarithmic mapping should thus transform the modular Hamiltonian onto the CFT Hamiltonian on a finite system with length approximately given by the logarithm of the correlation length in the system. This argument was recently formalised for CFTs perturbed by a relevant interaction by Cho, Ludwig and Ryu [101]. In what follows we will first calculate the prediction for the entanglement spectrum for general N. We will then check that the prediction matches our simulations for $N = 2$ despite the marginal nature of our interaction term.

7.1 General result

Anticipating that the entanglement spectrum corresponds to the CFT spectrum on a finite system with open boundary conditions, we thus compute the spectrum for N free fermions (the UV fixed point of our model) on a finite interval of length L. As before, we denote

[5] This is an example of a ultraviolet-inrared duality; the lowest entanglement modes (dominant singular values) are related to short-range degrees of the freedom, the infinite abundance of which causes the divergence of the entanglement entropy in the continuum limit.

JHEP07(2021)207

with λ_m ($m = 1, \ldots, 2N$) the $2N$ Majorana fields, and with $\lambda_{m,1}$ and $\lambda_{m,2}$ their two spinor components. After partial integration, the CFT Hamiltonian is given by

$$H_E = \int_0^L \sum_{m \in 2N} 2i\lambda_{m,1}\partial_x \lambda_{m,2} \tag{7.2}$$

Conformal boundary conditions can be of the type

$$\lambda_{m,1}|_0 = \lambda_{m,2}|_L = 0 \qquad \text{and} \qquad \partial_x\lambda_{m,2}|_0 = \partial_x\lambda_{m,1}|_L = 0 \tag{7.3}$$

which results in a standing wave expansion with half-integer momenta

$$\begin{cases} \lambda_{m,1}(x) = \sqrt{\dfrac{2}{L}} \displaystyle\sum_{k>0} \hat{\lambda}_{m,1}(k) \sin\left(\frac{\pi\,(k-1/2)\,x}{L}\right) \\ \lambda_{m,2}(x) = \sqrt{\dfrac{2}{L}} \displaystyle\sum_{k>0} \hat{\lambda}_{m,2}(k) \cos\left(\frac{\pi\,(k-1/2)\,x}{L}\right) \end{cases}, \tag{7.4}$$

and which we, in analogy to the boundary conditions on the circle, refer to as the Neveu-Schwarz type. Other possible boundary conditions are

$$\lambda_{m,1}|_0 = \lambda_{m,1}|_L = 0 \qquad \text{and} \qquad \partial_x\lambda_{m,2}|_0 = \partial_x\lambda_{m,2}|_L = 0 \tag{7.5}$$

with resulting standing-wave expansion

$$\begin{cases} \lambda_{m,1}(x) = \sqrt{\dfrac{2}{L}} \displaystyle\sum_{k>0} \hat{\lambda}_{m,1}(k) \sin\left(\frac{\pi k x}{L}\right) \\ \lambda_{m,2}(x) = \sqrt{\dfrac{2}{L}} \displaystyle\sum_{k>0} \hat{\lambda}_{m,2}(k) \cos\left(\frac{\pi k x}{L}\right) + \sqrt{\dfrac{1}{L}}\hat{\lambda}_{m,2}(0) \end{cases} \tag{7.6}$$

to which we refer as the Ramon type. In both cases, the prefactors where chosen such that the Majorana modes obey their usual anti-commutation relations

$$\{\hat{\lambda}(k)_{m,i}, \hat{\lambda}(l)_{n,i}\} = \delta_{m,n}\delta_{k,l}\delta_{i,j}. \tag{7.7}$$

To construct a Fock space we need to define normal fermionic modes. For $k \neq 0$ we can define $\hat{\phi}_m(k) = \hat{\lambda}_{m,1}(k) + \mathrm{i}\hat{\lambda}_{m,2}(k)$, which again transform under the fundamental (i.e. vector) representation of $\mathsf{SO}(2N)$. The $2N$ zero modes $\hat{\lambda}_{m,2}(0)$ are grouped into N additional fermions α_c with $c \in 1, \ldots, N$. In terms of these operators and after proper normalisation so that $\mathrm{Tr}(e^{-2\pi H_E}) = 1$, the resulting entanglement Hamiltonian is given by

$$H^{(\mathrm{NS})} = \sum_{k=1}^{+\infty}\sum_{m=1}^{2N} \frac{\pi(k-1/2)}{L}\phi_m^\dagger(k)\phi_m(k) + \frac{N}{\pi}\sum_{k=1}^{+\infty} \log\left(1 + e^{-2\pi\frac{\pi(k-1/2)}{L}}\right) \tag{7.8}$$

for the Neveu-Schwarz boundary conditions and

$$H^{(\mathrm{R})} = \sum_{k=1}^{+\infty}\sum_{m=1}^{2N} \frac{\pi k}{L}\phi_m^\dagger(k)\phi_m(k) + 0\sum_{c=1}^{N}\alpha_c^\dagger\alpha_c + \frac{N}{\pi}\sum_{k=1}^{+\infty} \log\left(1 + e^{-2\pi\frac{\pi k}{L}}\right) + \frac{N}{2\pi}\log(2) \tag{7.9}$$

JHEP07(2021)207

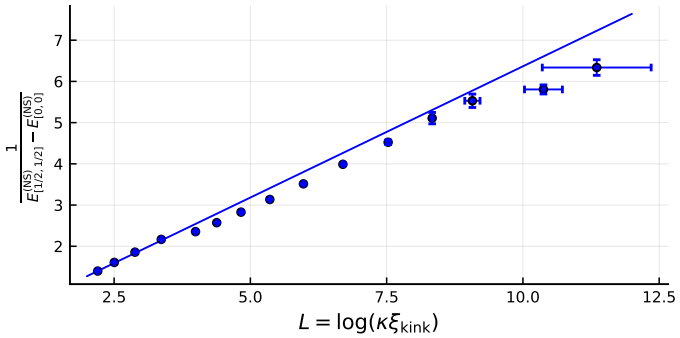

Figure 5. The inverse gap between the first two eigenvalues of the entanglement Hamiltonian in the trivial sector as a function of $L = \log(\kappa\xi_{\text{kink}})$. The error bars on the singular values are obtained in a similar fashion to those of the inverse correlation length (see figure 3). The blue line is the CFT prediction $\frac{2}{\pi}L$ and describes the extrapolated data well for $\kappa \approx 2.83$.

for Ramon boundary conditions. Due to the zero modes, all eigenvalues of $H^{(R)}$ will be at least 2^N fold degenerate. In particular, the ground state will be an $\mathsf{SO}(2N)$ scalar in the Neveu-Schwarz case and a direct sum of the two fundamental spinor representations in the Ramon case. More generally, as higher excited states are obtained by acting with the vector operators $\phi_m^\dagger$ on those ground states, all eigenspaces of $H_E^{(\text{NS})}$ will transform as tensor representations, whereas all eigenspaces of $H_E^{(\text{R})}$ will transform according to spinor representations. It is thus straightforward to relate these two towers of eigenvalues to the entanglement spectrum obtained across cuts corresponding to virtual bonds with linear representations (for NS) and with projective representations (for R).

7.2 Numerics for $N = 2$

For $N = 2$, the lowest excited state of the entanglement Hamiltonian with NS boundary conditions, i.e. $k = 1$ in eq. (7.8) is a $(1/2, 1/2)$ quartet (the $\mathsf{SO}(4)$ vector representation) with gap:

$$E_1^{(\text{NS})} - E_0^{(\text{NS})} = \frac{\pi}{2L} \tag{7.10}$$

Where $L = \log(\kappa\xi_{\text{kink}})$ is the typical length scale of the system after the comformal mapping. The free fit parameter κ takes care of setting the UV scale. In figure 5 we show the inverse gap $\frac{1}{E_1^{(\text{NS})} - E_0^{(\text{NS})}} = 2\pi \left(\log(\lambda_1^{(\text{NS})} - \lambda_0^{(\text{NS})})\right)^{-1}$ as a function of L, with $\lambda_i^{(\text{NS})}$ the i-th largest eigenvalue of $\hat{\rho}^{(\text{NS})}$, the reduced density matrix for a cut across the MPS bond with linear representations. The line corresponds to the prediction $\frac{2}{\pi}L$, and for $\kappa = \kappa_{\text{fit}} \approx 2.83$ the data coincides with this prediction.

Filling the $k = 1$ mode twice results in an energy $\frac{\pi}{L}$ sextet (the antisymmetric rank-2 tensor representation of $\mathsf{SO}(4)$). There are two possibilities to obtain energy $\frac{3}{2}\frac{\pi}{L}$, namely by filling the mode $k = 2$ (a vector representation), or filling the $k = 1$ mode with 3 particles (an antisymmetric rank-3 tensor representation, which is equivalent to the vector representation for $\mathsf{SO}(4)$). For the difference between the ground state energy in the two

JHEP07(2021)207

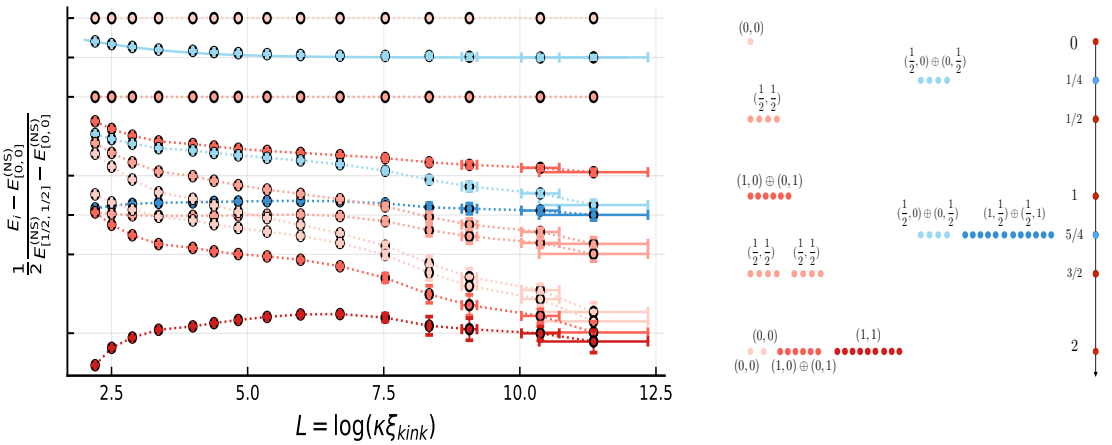

Figure 6. On the right we show the CFT prediction for the gaps in the entanglement spectrum, for $N = 2$ and in the limit of large L. The vertical axis is rescaled by π/L. The left and right towers corresponds to NS and R boundary conditions, respectively. The plot in the left shows gaps in the entanglement spectrum, relative to the first gap in the NS sector, as extracted from the MPS representation of the ground state of our lattice model. Error bars are obtained in a similar fashion to those of the inverse correlation length (see figure 3). For sufficiently small couplings the ratios converge to those predicted in the right panel. The dotted lines are a guides for the eye. The full blue line is the prediction for the first gap in the Raymond sector from 7.11.

sectors we find

$$E_0^{(\mathrm{R})} - E_0^{(\mathrm{NS})} = \frac{\log(2)}{\pi} + \frac{2}{\pi}\sum_{k=1}^{+\infty} \log\left(\frac{1+e^{-2\pi\frac{\pi k}{L}}}{1+e^{-2\pi\frac{\pi(k-1/2)}{L}}}\right) \tag{7.11}$$

which can be shown to converge to $\frac{\pi}{4L}$ for sufficiently large L (or thus, exponentially large correlation lengths). Here, we have assumed that the same length parameter L can be used for the two types of boundary conditions (NS or R). These eigenvalues, and a few more, for both $H^{(\mathrm{NS})}$ and $H^{(\mathrm{R})}$, relative to π/L, are depicted in the right panel of figure 6. In the left panel we show the corresponding ratios obtained trough extracted MPS data. The gaps $-\frac{1}{2\pi}\log\left(\lambda_i/\lambda_0^{(NS)}\right)$ are rescaled by twice the gap in the NS sector which according to figure 5 is approximatly π/L. As anticipated, towards the continuum limit (i.e. large L) all ratios converge to the predicted value. Note, however, that significant lattice effects for smaller L are present, as the logarithmic mapping in the definition of the modular Hamiltonian makes it exponentially harder for the entanglement spectrum (as compared to e.g. the excitation spectrum) to correspond with the continuum limit. In particular, additional degeneracies between different $\mathsf{SO}(N)$ representations which are predicted by the CFT result are not exactly reproduced away from the continuum limit. Finally, the predicted value for the gap between the groundstate energies in the Raymond and Neveu Schwarz sector (cfr. eqs. (7.11) and (7.10)) is also shown; it matches well with the data even for smaller L where this is not expected.

To further highlight this last peculiar observation, we use the gap between the dominating entanglement eigenvalues in the trivial sector to predict the gap for the topological

JHEP07(2021)207

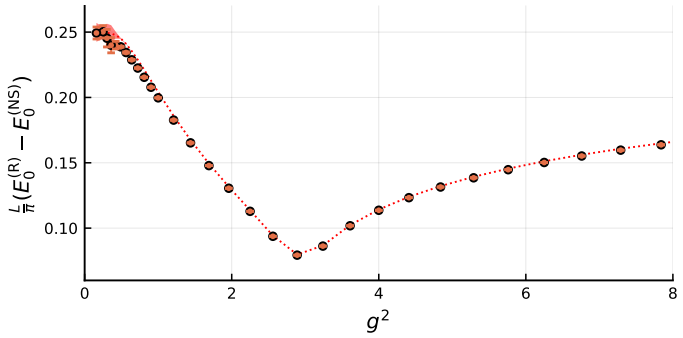

Figure 7. The gap between the two ground states of the modular Hamiltonian as a function of the squared coupling. The dotted line represents the CFT prediction from eq. (7.11), where L was eliminated using eq. (7.10), so that no free parameters remain. The error bars and shaded area correspond to uncertainties in the extrapolated entanglement eigenvalues.

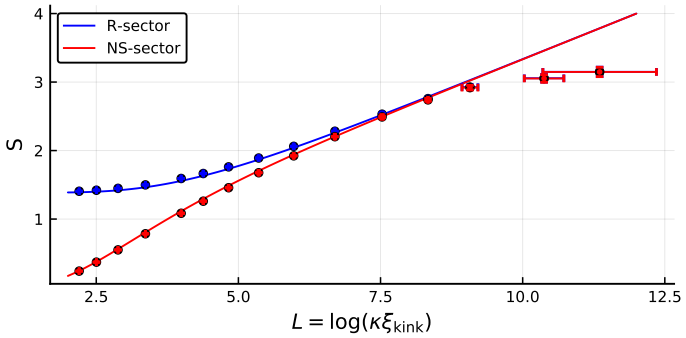

Figure 8. The bipartite entanglement entropy along the different cuts as a function of the logarithmic length scale L. The error bars are calculated in a similar fashion to those in figure 3. The curves represent the entropies corresponding to the entanglement spectra predicted from entanglement hamiltonians eqs. (7.8) and (7.9). We find good agreement except for very large L; this is due to ill converged MPS results, as was also the case in figure 2.

sector, by eliminating L between eq. (7.11) and eq. (7.10). Figure 7 compares this prediction to the actual values of $E_0^{(\mathrm{R})} - E_0^{(\mathrm{NS})} = -\frac{1}{2\pi}\log\left(\lambda_0^{(R)}/\lambda_0^{(NS)}\right)$. We obtain excellent agreement, even for large couplings far away from the continuum limit, where the CFT prediction is no longer expected to hold. Indeed, beyond $g^2 \gtrsim 4$, the correlation length ξ is less than a lattice site.

Finally, figure 8 shows the scaling of the total bipartite entanglement entropy along trivial and topological cuts of the MPS as a function of the logarithmic length scale $L = \log(\kappa_{\text{fit}}\xi_{\text{kink}})$. The curves are the predicted entropies calculated from reduced density matrices corresponding to eqs. (7.8) and (7.9). Again there is good agreement apart from large L where the MPS results are not sufficiently converged.

8 Discussion and outlook

We have constructed a lattice regulated version of the GN model that preserves the full $\mathsf{O}(2N)$ symmetry, and has a lattice remnant of the discrete chiral invariance. This pre-

JHEP07(2021)207

scription differs from the typical regularisation using Wilson fermions (i.e. the Gross-Neveu-Wilson model, which has recently received attention from the cold atoms community), and also takes a different prescription for the mass term as proposed in the original staggered formulation by Susskind. This prescription is well known in the context of the SSH model, but a Gross-Neveu type interaction resulting from it had, to the best of our knowledge, not been considered.

By studying this lattice model in the limit of large N — where mean field theory becomes exact — as well as at $N = 2$ using MPS simulations, we have established that its low energy behaviour replicates all the features (and in particular degeneracies) expected from the field theory. At the same time, we argued how the resulting lattice model lies at the first order phase transition between a trivial and topological insulator (according to symmetry class BDI in the ten-fold way), and much of the degeneracies in both the excitation and entanglement spectrum can be reinterpreted from that perspective. At the quantitative level, we observed that the non-perturbative behaviour of this marginally relevant interaction makes it especially challenging to accurately probe the continuum limit. The mass remains very small for a significant range of the coupling constant, and then shoots up quickly, so that the regime where MPS can probe the behaviour of the continuum limit is rather small.

As the spectrum of massive particles becomes more interesting for larger values of N, it would be interesting to also study the model in this regime. However, our results on the entanglement structure indicate why using MPS simulations for larger values of N is non-trivial. The entanglement structure, and in particular the entanglement entropy, is dominated by the UV CFT of the model, which is that of N massless free fermions. We thus anticipate a linear scaling of the entanglement entropy in the number of fermion flavours, which translates to an exponential scaling in N of the required MPS bond dimension, in order to obtain similarly accurate results. It is an interesting question whether exploiting the full $(\mathsf{S})\mathsf{O}(2N)$ symmetry of the model could help to overcome this exponential scaling. However, this first requires that the necessary representation data (Clebsch-Gordan coefficients and/or 6j-symbols) of $(\mathsf{S})\mathsf{O}(2N)$ are computed, as these are less readily available for general N.

Other potentially interesting directions of further research concern the phase diagram for finite values of the temperature and chemical potential, which are also within the scope of MPS simulations [13, 22, 30, 36, 38]. There is active interest in the possible existence of an inhomogeneous phase at sufficiently large values of the chemical potential [58, 59]. This interest is again spurred by the similarity of the GN model with QCD. Due to the sign problem, probing the QCD phase diagram with lattice Monte Carlo at moderate densities and with realistic values of the quark masses (the regime interesting for heavy ion experiments) is near impossible. While an inhomogeneous phase in the GN phase diagram would result in breaking of translation invariance, a continuous symmetry of the field theory, there might be arguments to believe that the Coleman-Mermin-Wagner theorem does not apply and the GN model could indeed exhibit such a phase. Coleman explicitly assumed relativistic invariance in his version of the theorem, which is broken by the chemical potential, whereas more general arguments against continuous symmetry breaking rely on

JHEP07(2021)207

the specific dispersion relation and the counting of the would-be Goldstone bosons that restore the symmetry, which is non-trivial when breaking spacetime symmetries. It would be interesting to study if MPS techniques can shed a new perspective on this question, though infinite MPS simulations would also need to choose a particular unit cell and would also struggle with incommensurate filling fractions.

A final extension, which we explore in a future publication,[6] is to apply the discretisation scheme presented in this paper to the chiral extension (with full continuous chiral symmetry) of the Gross-Neveu model. Preliminary results indicate that the resulting lattice model has emerging continuous chiral symmetry along a critical line in the phase diagram that corresponds to a deconfined quantum phase transition.

Acknowledgments

We acknowledge valuable discussions with Henri Verschelde, Erez Zohar , Bram Vanhecke, Maarten Van Damme and Daan Maertens. This work has received funding from the European Research Council (ERC) under the European Unions Horizon 2020 research and innovation programme (grant agreements No 715861 (ERQUAF) and 647905 (QUTE)), and from Research Foundation Flanders (FWO) via grant GOE1520N.

A Matching the lattice regularisation with $\overline{\text{MS}}$ dimensional regularisation

The beautiful result eq. (2.6) of Forgacs et al. [49] gives the exact mass gap for the $\mathsf{O}(2N)$ Gross-Neveu model in terms of $\Lambda_{\overline{\text{MS}}}$, where the latter is given by eq. (2.4), but with coupling $g^2_{\overline{\text{MS}}}(\mu = 1/a)$ of the $\overline{\text{MS}}$-scheme instead of our lattice coupling g^2. To relate $\Lambda_{\overline{\text{MS}}}$ to our Λ_{lat}, one needs to match the dimensional regularisation scheme to our lattice regularisation scheme. In particular, we require the first coefficient c_1 in the expansion

$$\frac{1}{g^2_{\overline{\text{MS}}}} = \frac{1}{g^2} + c_1 + c_2 g^2 + \dots \,. \tag{A.1}$$

The standard strategy to obtain such a matching is to compare results for a physical quantity, which by definition should be independent of the particular renormalisation scheme. We consider the two-fermion scattering S-matrix in the large energy/momentum regime, where perturbation theory is reliable, and the physics is well described by weakly interacting massless Dirac fermions. Notice that for the lattice regularised version 'large energy/momentum' E means $\Lambda_{\text{lat}} \ll E \ll 1/a$, with the first inequality assuring the weakly interacting regime and the latter inequality assuring the QFT continuum regime. In figure 9 we display the different Feynman diagrams that contribute up to one loop to this scattering process. Notice that, as in the original Gross-Neveu paper [45], it is convenient to decompose the quartic term $\frac{g^2}{2}\left(\bar{\psi}_a\psi_a\right)^2$ in the QFT (2.1) (or $-\frac{g^2}{4}\Sigma^2_{n,n+1,n+2}$ in the lattice

[6] G. Roose et al., *in preparation*.

JHEP07(2021)207

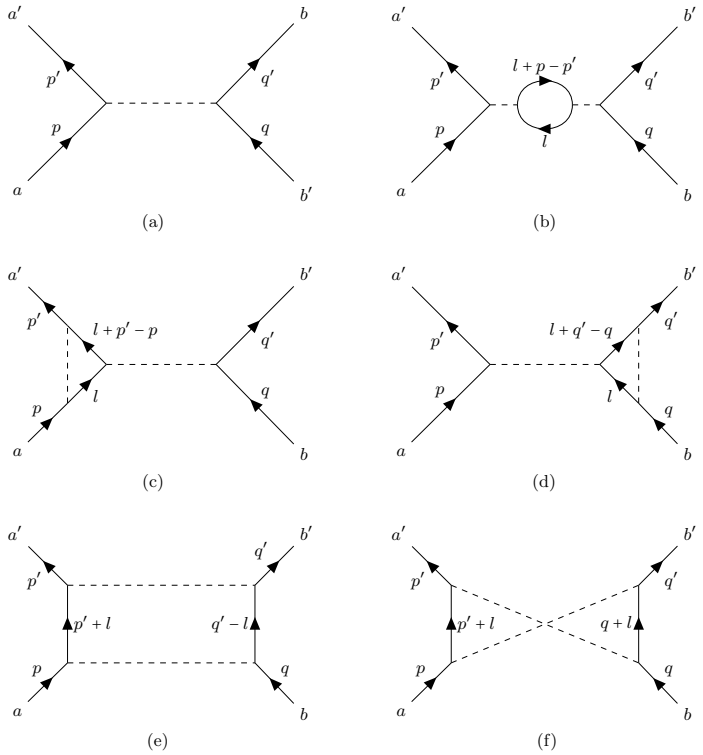

Figure 9. The Feynman diagrams contributing to the two fermion scattering S-matrix up to second order.

Hamiltonian (3.9)) by introducing a Hubbard-Stratanovich field σ with trivial propagator $-i$ and interactions:

$$-g\sigma\bar{\psi}_a\psi_a \qquad \text{in the QFT and} \qquad \frac{g}{\sqrt{2}}\sigma\Sigma_{n,n+1,n+2} \qquad \text{on the lattice} \tag{A.2}$$

For reference, we first briefly discuss the computation in the $\overline{\text{MS}}$ scheme. To get the Feynman rules one first needs the free-field propagator (see e.g. [102])

$$\langle 0|\, T(\psi_a(x^0,x^1)\overline{\psi}_b(y^0,y^1))\,|0\rangle = \int \frac{d^2p}{2\pi^2}\frac{i\not{p}}{p^2+i\epsilon}e^{-ip(x-y)} \tag{A.3}$$

using relativistic notation (with e.g. $p^2 = p_0^2 - p_1^2$, $x = (x^0, x^1)$).

The Feynman rules then read:

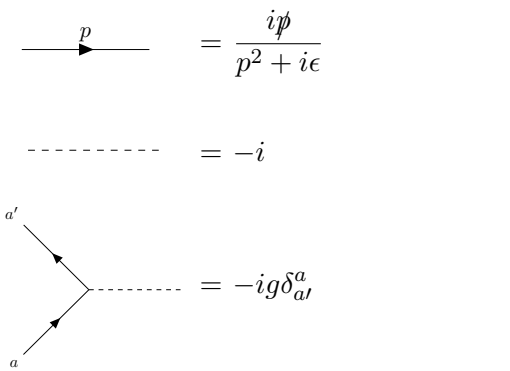

(A.4)

JHEP07(2021)207

With the conventions of [102], writing $S = 1 + iT$, the tree-level diagram (a) then gives for iT:

$$(a) \;=\; ig^2 \times \underbrace{(\overline{u}(p')u(p))(\overline{u}(q')u(p))}_{K_1} \times \underbrace{\delta^a_{a'}\delta^b_{b'}(2\pi)^2\delta^2(p+q-p'-q')}_{K_2} \tag{A.5}$$

with the second factor K_1 on the first line arising from the projection on the particular fermion polarisations of the in- and out-modes that we consider, while the third factor K_2 (second line) arises from the colour conservation and momentum conservation. Notice that we do not consider the crossing diagrams for the outgoing legs, which gives terms in iT proportional to a different colour pre-factor $\delta^a_{b'}\delta^b_{a'}$.

Using the standard machinery of dimensional regularisation and 'Diracology', we then obtain for the second diagram (b) in the $\overline{\text{MS}}$ scheme:

$$(b) = -i\frac{Ng^4}{2\pi}\log\frac{-(p-p')^2}{\mu^2} \times K \tag{A.6}$$

with $K = K_1 \times K_2$ the same polarisation factor and colour/momentum conservation factor as for (a). Furthermore for the diagrams (c) and (d) we find:

$$(c) + (d) = +i\frac{g^4}{2\pi}\log\frac{-(p-p')^2}{\mu^2} \times K \tag{A.7}$$

Finally one can verify that the individual (logarithmic) UV divergencies in diagrams (e) and (f) cancel out when summed together. (e)+(f) is therefore scheme independent and plays no role in the matching. Notice that these separate UV divergencies in (e) and (f) would require a marginal counter term $\propto (\overline{\psi}_a\gamma_\mu\psi_a)(\overline{\psi}_b\gamma^\mu\psi_b)$ which is prohibited by the full $\mathsf{O}(2N)$ symmetry.

Collecting the different terms together we finally find up to order g^4 (neglecting scheme independent terms and terms $\propto \delta^a_{b'}\delta^b_{a'}$):

$$iT = ig^2(1 - \frac{(N-1)g^2}{2\pi}\log\frac{-(p-p')^2}{\mu^2}) \times K \tag{A.8}$$

for the S-matrix in the $\overline{\text{MS}}$ scheme.

Let us now turn to the computation of the same diagrams, but now with our lattice Hamiltonian (3.9). As a first ingredient we consider the free-field propagator. From the free Hamiltonian (3.2) one easily shows:

$$\begin{aligned}\langle 0|\, T(\phi_m(t)^\dagger\phi_n(u))\,|0\rangle \;=\; &\theta(t-u)\int_0^\pi \frac{dk^1}{2\pi}e^{ik^1(m-n)-i\omega(k^1)(t-u)} \\ &-\theta(u-t)\int_0^\pi \frac{dk^1}{2\pi}e^{ik^1(n-m)-i\omega(k^1)(u-t)}\end{aligned} \tag{A.9}$$

with $\omega(k^1) = 2\sin|k^1|$, the particle energies (in lattice units) corresponding to the momenta k^1 (and we have omitted the colour indices). Using the Fourier representation of the step-function $\theta(t)$ we can rewrite the expression for the propagator above as:

$$\int_{-\infty}^{+\infty}\frac{dk^0}{2\pi}\int_{-\pi}^{\pi}\frac{dk^1}{2\pi}\left(\frac{\theta(k^1)\,i}{k^0-\omega(k^1)+i\epsilon}+\frac{\theta(-k^1)\,i}{k^0+\omega(k^1)-i\epsilon}\right)e^{ik^1(m-n)-ik^0(t-u)} \tag{A.10}$$

JHEP07(2021)207

Notice that here we are not blocking the staggered sites, and the two Dirac spinor components now transpire in the two different branches $-\pi/2 \leq k^1 < \pi/2$ and $\pi/2 \leq k^1 < 3\pi/2$ of the (angular) spatial momentum k^1 of our single component fermions. In particular, with the identification of the *physical* (lattice-independent) momentum

$$p^1 = \frac{2k^1}{a} \tag{A.11}$$

we have $\phi_{2n+1} \approx \phi_{2n}$ for small momenta $|p^1| \ll 1/a$, corresponding to the Fourier transformed right-handed Dirac component ψ_R in the Weyl representation, while the identification

$$p^1 = \frac{2k - 2\pi}{a} \tag{A.12}$$

gives $\phi_{2n+1} \approx -\phi_{2n}$ for $|p^1| \ll 1/a$, corresponding to the Fourier transformed left-handed Dirac component ψ_L. One can easily verify that these identifications give the correct positive energy $k^0 > 0$ poles (in lattice units) in the first term of our propagator (A.10) $k^0 \approx a|p^1|$, both for the right-moving fermions ($p^1 > 0$) and left-moving fermions ($p^1 < 0$), while the second term of our propagator gives the proper poles for the anti-fermions.

We are now ready to write down the Feyman rules for our Hamiltonian (3.9) with decomposed interaction term (A.2):

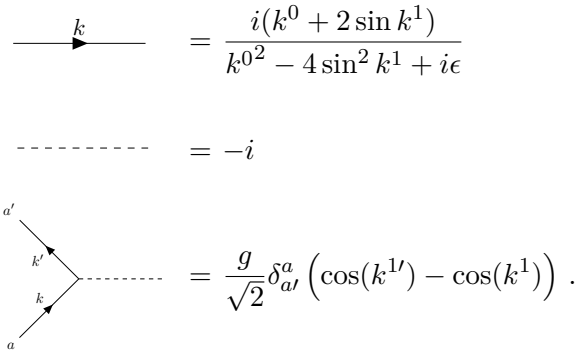

$$\begin{aligned} &= \frac{i(k^0 + 2\sin k^1)}{k^{0\,2} - 4\sin^2 k^1 + i\epsilon} \\ &= -i \\ &= \frac{g}{\sqrt{2}}\delta^a_{a\prime}\left(\cos(k^{1\prime}) - \cos(k^1)\right) . \end{aligned} \tag{A.13}$$

Here for the expression of the fermion-propagator we summed the two terms in (A.10). Also notice the extra momentum structure in the vertex vis-á-vis the vertex rule (A.4) in the $\overline{\text{MS}}$-scheme. For small physical momenta p^1 (see (A.11) and (A.12)) this structure simply expresses the fact that the $\bar{\psi}\psi$ term couples the right-handed Dirac components ($k^1 \approx 0$) to the left-handed components ($k^1 \approx \pi$).

For the tree-level diagram (a) in figure 9 we then find (replacing $p \to k$ and $q \to h$):

$$\begin{aligned} (a) = ig^2 \times &\underbrace{\left(\cos(k^{1\prime}) - \cos(k^1)\right)\left(\cos(h^1) - \cos(h^{1\prime})\right)}_{K_1} \\ &\times \underbrace{\delta^a_{a\prime}\delta^b_{b\prime}(2\pi)^2\delta^2(k + h - k' - h')/2}_{K_2} \end{aligned} \tag{A.14}$$

Taking into account the different normalisations (e.g. $\langle k|k'\rangle = 2\pi\delta(k-k')$ here, and $\langle p|p'\rangle = 4\pi E_p\delta(p-p')$ in the QFT computation) one can show that this reduces to the tree-level

$\overline{\text{MS}}$ result (as it should) for small momenta $|p^1 a| \ll 1$, either on the right branch from eq. (A.11) or on the left branch of eq. (A.12). Notice that for a non-vanishing scattering in this continuum limit, we either need $k^1, h^{1\prime} \approx 0$ (right-movers) and $k^{1\prime}, h^1 \approx \pi$ (left-movers) or the other way around. Since for the remainder we are only interested in the continuum QFT limit, we can effectively set $K_1 = 4$ and anticipate that $k^1 - k^{1\prime} = \pi + \Delta^1$, with $\Delta^1 \ll 1$.

For the loop diagram (b) we then find (with again $K = K_1 \times K_2$):

$$(b) = -\frac{Ng^4}{2} \times I_1 \times K \tag{A.15}$$

where I_1 is the loop-integral:

$$I_1 = \int \frac{d^2 l}{(2\pi)^2} \Bigg\{ \left(\frac{(l^0 + \Delta^0) - 2\sin(l^1 + \Delta^1)}{(l^0 + \Delta^0)^2 - 4\sin^2(l^1 + \Delta^1) + i\epsilon} \right) \times \left(\frac{l^0 + 2\sin l^1}{l^{0\,2} - 4\sin^2 l^1 + i\epsilon} \right) (\cos(l^1 + \Delta^1) + \cos l^1)^2 \Bigg\}$$

here $\Delta^0 = k^0 - k^{0\prime}$ and as we already mentioned $\Delta^1 = k^1 - k^{1\prime} - \pi$. By closing the contour for the l^0 integration either in the upper or lower complex plane, and with a proper change of variables, we then arrive at the following expression for I_1:

$$I_1 = i \int_{-\pi}^{0} \frac{dl^1}{2\pi} \Bigg\{ \left(\frac{-\Delta^0 + 2\sin l^1 - 2\sin(l^1 - \Delta^1)}{(\Delta^0 - 2\sin l^1)^2 - 4\sin^2(l^1 - \Delta^1)} \right) \times \Big(\cos l^1 + \cos(l^1 - \Delta^1)\Big)^2 + \left(\frac{\Delta^0 + 2\sin l^1 - 2\sin(l^1 + \Delta^1)}{(\Delta^0 + 2\sin l^1)^2 - 4\sin^2(l^1 + \Delta^1)} \right) \times \Big(\cos l^1 + \cos(l^1 + \Delta^1)\Big)^2 \Bigg\}$$

With some effort one can then finally extract the continuum limit $|\Delta^\mu| \ll 1$ of this integral, by isolating the logarithmic divergencies $\Delta^\mu \to 0$ around $l^1 = 0$ and $l^1 = -\pi$, arriving at the leading behaviour:

$$I_1 = \frac{i}{2\pi} \Big(4 - 12\log 2 + 2\log\Big(-(\Delta^{0\,2} - 4\Delta^{1\,2})\Big) + \mathcal{O}(\Delta^{\mu 2})\Big)$$

Notice that only this leading behaviour corresponds to the Gross-Neveu QFT continuum limit, the higher order power corrections are specific to the lattice regularisation, in QFT speak they correspond to irrelevant perturbations of the Gross-Neveu QFT.

Moving over to the loop diagram (c), we obtain:

$$(c) = -\frac{g^4}{4} \times I_2 \times K \tag{A.16}$$

with now the loop-integral I_2 reading (for the case $k^{1\prime}, h^1 \approx 0$):

$$I_2 = -\int \frac{d^2 l}{(2\pi)^2} \Bigg\{ \left(\frac{(l^0 - \Delta^0) - 2\sin(l^1 - \Delta^1)}{(l^0 - \Delta^0)^2 - 4\sin^2(l^1 - \Delta^1) + i\epsilon} \right) \times \left(\frac{l^0 + 2\sin l^1}{l^{0\,2} - 4\sin^2 l^1 + i\epsilon} \right) \times (\cos(k^{1\prime} + \cos(l^1 - \Delta^1)) \times (\cos l^1 + \cos(\Delta^1 + k')) \times (\cos l^1 + \cos(l^1 - \Delta^1)) \Bigg\}$$

JHEP07(2021)207

Proceeding in a completely similar fashion as for the computation of I_1, we eventually find the leading continuum behaviour:

$$I_2 = \frac{i}{2\pi}\left(12\log 2 - 4 - 2\log\left(-(\Delta^{0^2} - 4\Delta^{1^2})\right)\right) \tag{A.17}$$

It is easy to show that we get the same term from the diagram (d), while as we explained above we can forget about the (e) and (f) diagrams for the matching as these diagrams will be finite and universal for a manifest $\mathsf{O}(2N)$ symmetric regularisation scheme like ours. Collecting all the relevant diagrams we then find for the QFT S-matrix in our lattice regularisation:

$$iT = ig^2\left(1 - \frac{(N-1)g^2}{2\pi}\left(\log\left(\frac{-(p-p')^2}{\mu^2}\right) + 2 - 6\log 2\right)\right) \times K \tag{A.18}$$

where $\mu = 1/a$ and we have identified (see (A.11) and (A.12)) the physical momenta and energies:

$$\Delta^{0^2} - 4\Delta^{1^2} = \left((p^0 - p^{0'})^2 - (p^1 - p^{1'})^2\right) \times a^2 \tag{A.19}$$

Finally, we are ready to match the two schemes. By comparing the lattice result in eq. (A.18) with the $\overline{\text{MS}}$ result in eq. (A.8), and demanding $iT = iT$ we immediately find:

$$\frac{1}{g^2_{\overline{\text{MS}}}} = \frac{1}{g^2} - \frac{N-1}{2\pi}(6\log 2 - 2) + \dots \tag{A.20}$$

and if we plug this result in the definition (2.4) for Λ, we obtain:

$$\Lambda_{\overline{\text{MS}}} = \frac{8}{e}\Lambda_{\text{lat}} \tag{A.21}$$

by which we have shown explicitly that the matching result based on the large N mean-field computation of section 4, generalises to any finite N, in particular to $N = 2$.

References

[1] MILC collaboration, *Light pseudoscalar decay constants, quark masses, and low energy constants from three-flavor lattice QCD*, *Phys. Rev. D* **70** (2004) 114501 [hep-lat/0407028] [INSPIRE].

[2] HPQCD, UKQCD, MILC, FERMILAB LATTICE collaboration, *High precision lattice QCD confronts experiment*, *Phys. Rev. Lett.* **92** (2004) 022001 [hep-lat/0304004] [INSPIRE].

[3] A.S. Kronfeld, *Twenty-first century lattice gauge theory: Results from the quantum chromodynamics lagrangian*, *Annu. Rev. Nucl. Part. Sci.* **62** (2012) 265.

[4] S. Aoki et al., *Review of lattice results concerning low-energy particle physics*, *Eur. Phys. J. C* **74** (2014) 2890 [arXiv:1310.8555] [INSPIRE].

JHEP07(2021)207

[5] J. Aebischer, C. Bobeth and A.J. Buras, *On the importance of NNLO QCD and isospin-breaking corrections in ε'/ε*, *Eur. Phys. J. C* **80** (2020) 1 [arXiv:1909.05610] [INSPIRE].

[6] M.C. Bañuls et al., *Simulating lattice gauge theories within quantum technologies*, *Eur. Phys. J. D* **74** (2020) 1.

[7] Z. Fodor and S.D. Katz, *A New method to study lattice QCD at finite temperature and chemical potential*, *Phys. Lett. B* **534** (2002) 87 [hep-lat/0104001] [INSPIRE].

[8] Y. Shimizu, *Tensor renormalization group approach to a lattice boson model*, *Mod. Phys. Lett. A* **27** (2012) 1250035 [INSPIRE].

[9] Y. Shimizu, *Analysis of the $(1+1)$-dimensional lattice ϕ^4 model using the tensor renormalization group*, *Chin. J. Phys.* **50** (2012) 749.

[10] Y. Liu, Y. Meurice, M.P. Qin, J. Unmuth-Yockey, T. Xiang, Z.Y. Xie et al., *Exact Blocking Formulas for Spin and Gauge Models*, *Phys. Rev. D* **88** (2013) 056005 [arXiv:1307.6543] [INSPIRE].

[11] Y. Shimizu and Y. Kuramashi, *Grassmann tensor renormalization group approach to one-flavor lattice Schwinger model*, *Phys. Rev. D* **90** (2014) 014508 [arXiv:1403.0642] [INSPIRE].

[12] Y. Shimizu and Y. Kuramashi, *Critical behavior of the lattice Schwinger model with a topological term at $\theta = \pi$ using the Grassmann tensor renormalization group*, *Phys. Rev. D* **90** (2014) 074503 [arXiv:1408.0897] [INSPIRE].

[13] S. Takeda and Y. Yoshimura, *Grassmann tensor renormalization group for the one-flavor lattice Gross–Neveu model with finite chemical potential*, *PTEP* **2015** (2015) 043B01.

[14] Y. Shimizu and Y. Kuramashi, *Berezinskii-Kosterlitz-Thouless transition in lattice Schwinger model with one flavor of Wilson fermion*, *Phys. Rev. D* **97** (2018) 034502 [arXiv:1712.07808] [INSPIRE].

[15] M. Campos, G. Sierra and E. Lopez, *Tensor renormalization group in bosonic field theory*, *Phys. Rev. B* **100** (2019) 195106 [arXiv:1902.02362] [INSPIRE].

[16] N. Butt, S. Catterall, Y. Meurice, R. Sakai and J. Unmuth-Yockey, *Tensor network formulation of the massless Schwinger model with staggered fermions*, *Phys. Rev. D* **101** (2020) 094509 [arXiv:1911.01285] [INSPIRE].

[17] B. Vanhecke, J. Haegeman, K. Van Acoleyen, L. Vanderstraeten and F. Verstraete, *Scaling Hypothesis for Matrix Product States*, *Phys. Rev. Lett.* **123** (2019) 250604 [arXiv:1907.08603] [INSPIRE].

[18] C. Delcamp and A. Tilloy, *Computing the renormalization group flow of two-dimensional ϕ^4 theory with tensor networks*, *Phys. Rev. Res.* **2** (2020) 033278.

[19] T. Byrnes, P. Sriganesh, R.J. Bursill and C.J. Hamer, *Density matrix renormalization group approach to the massive Schwinger model*, *Phys. Rev. D* **66** (2002) 013002 [hep-lat/0202014] [INSPIRE].

[20] T. Sugihara, *Density matrix renormalization group in a two-dimensional $\lambda\phi^4$ hamiltonian lattice model*, *JHEP* **05** (2004) 007.

[21] T. Sugihara, *Matrix product representation of gauge invariant states in a Z_2 lattice gauge theory*, *JHEP* **07** (2005) 022.

JHEP07(2021)207

[22] D.J. Weir, *Studying a relativistic field theory at finite chemical potential with the density matrix renormalization group*, *Phys. Rev. D* **82** (2010) 025003 [arXiv:1003.0698] [INSPIRE].

[23] M.C. Bañuls, K. Cichy, K. Jansen and J.I. Cirac, *The mass spectrum of the Schwinger model with matrix product states*, *JHEP* **11** (2013) 158 [arXiv:1305.3765] [INSPIRE].

[24] A. Milsted, J. Haegeman and T.J. Osborne, *Matrix product states and variational methods applied to critical quantum field theory*, *Phys. Rev. D* **88** (2013) 085030 [arXiv:1302.5582] [INSPIRE].

[25] B. Buyens, J. Haegeman, K. Van Acoleyen, H. Verschelde and F. Verstraete, *Matrix product states for gauge field theories*, *Phys. Rev. Lett.* **113** (2014) 091601 [arXiv:1312.6654] [INSPIRE].

[26] L. Tagliacozzo, A. Celi and M. Lewenstein, *Tensor networks for lattice gauge theories with continuous groups*, *Phys. Rev. X* **4** (2014) 041024 [arXiv:1405.4811] [INSPIRE].

[27] P. Silvi, E. Rico, T. Calarco and S. Montangero, *Lattice gauge tensor networks*, *New J. Phys.* **16** (2014) 103015 [arXiv:1404.7439] [INSPIRE].

[28] J. Haegeman, K. Van Acoleyen, N. Schuch, J.I. Cirac and F. Verstraete, *Gauging quantum states: from global to local symmetries in many-body systems*, *Phys. Rev. X* **5** (2015) 011024 [arXiv:1407.1025] [INSPIRE].

[29] S. Kühn, J.I. Cirac and M.C. Bañuls, *Non-Abelian string breaking phenomena with matrix product states*, *JHEP* **07** (2015) 130 [arXiv:1505.04441] [INSPIRE].

[30] M.C. Bañuls, K. Cichy, J.I. Cirac, K. Jansen and H. Saito, *Thermal evolution of the schwinger model with matrix product operators*, *Phys. Rev. D* **92** (2015) 034519 [arXiv:1505.00279] [INSPIRE].

[31] T. Pichler, M. Dalmonte, E. Rico, P. Zoller and S. Montangero, *Real-time dynamics in* U(1) *lattice gauge theories with tensor networks*, *Phys. Rev. X* **6** (2016) 011023 [arXiv:1505.04440] [INSPIRE].

[32] A. Milsted, *Matrix product states and the non-Abelian rotor model*, *Phys. Rev. D* **93** (2016) 085012 [arXiv:1507.06624] [INSPIRE].

[33] B. Buyens, J. Haegeman, H. Verschelde, F. Verstraete and K. Van Acoleyen, *Confinement and string breaking for QED_2 in the Hamiltonian picture*, *Phys. Rev. X* **6** (2016) 041040 [arXiv:1509.00246] [INSPIRE].

[34] E. Zohar and M. Burrello, *Building projected entangled pair states with a local gauge symmetry*, *New J. Phys.* **18** (2016) 043008 [arXiv:1511.08426] [INSPIRE].

[35] M.C. Bañuls, K. Cichy, K. Jansen and H. Saito, *Chiral condensate in the Schwinger model with Matrix Product Operators*, *Phys. Rev. D* **93** (2016) 094512 [arXiv:1603.05002] [INSPIRE].

[36] B. Buyens, F. Verstraete and K. Van Acoleyen, *Hamiltonian simulation of the Schwinger model at finite temperature*, *Phys. Rev. D* **94** (2016) 085018 [arXiv:1606.03385] [INSPIRE].

[37] B. Buyens, J. Haegeman, F. Hebenstreit, F. Verstraete and K. Van Acoleyen, *Real-time simulation of the schwinger effect with matrix product states*, *Phys. Rev. D* **96** (2017) 114501.

JHEP07(2021)207

[38] P. Silvi, E. Rico, M. Dalmonte, F. Tschirsich and S. Montangero, *Finite-density phase diagram of a $(1+1)-d$ non-abelian lattice gauge theory with tensor networks*, *Quantum* **1** (2017) 9.

[39] B. Buyens, S. Montangero, J. Haegeman, F. Verstraete and K. Van Acoleyen, *Finite-representation approximation of lattice gauge theories at the continuum limit with tensor networks*, *Phys. Rev. D* **95** (2017) 094509 [arXiv:1702.08838] [INSPIRE].

[40] F. Bruckmann, K. Jansen and S. Kühn, *$O(3)$ nonlinear sigma model in $1+1$ dimensions with matrix product states*, *Phys. Rev. D* **99** (2019) 074501 [arXiv:1812.00944] [INSPIRE].

[41] P. Silvi, Y. Sauer, F. Tschirsich and S. Montangero, *Tensor network simulation of an* SU(3) *lattice gauge theory in* $1D$, *Phys. Rev. D* **100** (2019) 074512 [arXiv:1901.04403] [INSPIRE].

[42] M.C. Bañuls, K. Cichy, Y.-J. Kao, C.J.D. Lin, Y.-P. Lin and D.T.L. Tan, *Phase structure of the $(1+1)$-dimensional massive Thirring model from matrix product states*, *Phys. Rev. D* **100** (2019) 094504 [arXiv:1908.04536] [INSPIRE].

[43] P. Emonts and E. Zohar, *Gauss law, minimal coupling and fermionic PEPS for lattice gauge theories*, *SciPost Phys. Lect. Notes* (2020) 12.

[44] L. Funcke, K. Jansen and S. Kühn, *Topological vacuum structure of the Schwinger model with matrix product states*, *Phys. Rev. D* **101** (2020) 054507 [arXiv:1908.00551] [INSPIRE].

[45] D.J. Gross and A. Neveu, *Dynamical symmetry breaking in asymptotically free field theories*, *Phys. Rev. D* **10** (1974) 3235 [INSPIRE].

[46] A.B. Zamolodchikov and A.B. Zamolodchikov, *Exact S matrix of Gross-Neveu "elementary" fermions*, *Phys. Lett. B* **72** (1978) 481.

[47] E. Witten, *Some properties of the $(\bar{\psi}\psi)^2$ model in two-dimensions*, *Nucl. Phys. B* **142** (1978) 285 [INSPIRE].

[48] M. Karowski and H. Thun, *Complete s-matrix of the* O($2n$) *Gross-Neveu model*, *Nucl. Phys. B* **190** (1981) 61.

[49] P. Forgacs, F. Niedermayer and P. Weisz, *The exact mass gap of the Gross-Neveu model. 1. The thermodynamic Bethe ansatz*, *Nucl. Phys. B* **367** (1991) 123 [INSPIRE].

[50] P. Forgacs, F. Niedermayer and P. Weisz, *The exact mass gap of the Gross-Neveu model. 2. The $1/N$ expansion*, *Nucl. Phys. B* **367** (1991) 144 [INSPIRE].

[51] H. Verschelde, S. Schelstraete and M. Vanderkelen, *Nonperturbative calculation of the mass-gap in the Gross-Neveu model*, *Z. Phys. C* **76** (1997) 161 [INSPIRE].

[52] K. Van Acoleyen and H. Verschelde, *Dynamical mass generation by source inversion: calculating the mass gap of the Gross-Neveu model*, *Phys. Rev. D* **65** (2002) 085006 [hep-th/0111171] [INSPIRE].

[53] J.L. Kneur and D. Reynaud, *(Borel) convergence of the variationally improved mass expansion and the $O(N)$ Gross-Neveu model mass gap*, *Phys. Rev. D* **66** (2002) 085020 [hep-th/0205133] [INSPIRE].

[54] J.L. Kneur and A. Neveu, *Renormalization group improved optimized perturbation theory: revisiting the mass gap of the $O(2N)$ Gross-Neveu model*, *Phys. Rev. D* **81** (2010) 125012 [arXiv:1004.4834] [INSPIRE].

[55] Y. Cohen, S. Elitzur and E. Rabinovici, *A Monte Carlo study of the Gross-Neveu model*, *Nucl. Phys. B* **220** (1983) 102.

JHEP07(2021)207

[56] M. Campostrini, G. Curci and P. Rossi, *The Gross-Neveu model and the pseudofermion algorithm*, *Nucl. Phys. B Proc. Suppl.* **4** (1988) 557.

[57] W. Bietenholz, E. Focht and U.J. Wiese, *Perfect lattice actions for the Gross-Neveu model at large N*, *Nucl. Phys. B* **436** (1995) 385 [hep-lat/9409018] [INSPIRE].

[58] F. Karsch, J.B. Kogut and H.W. Wyld, *The Gross-Neveu model at finite temperature and density*, *Nucl. Phys. B* **280** (1987) 289 [INSPIRE].

[59] J. Lenz, L. Pannullo, M. Wagner, B. Wellegehausen and A. Wipf, *Inhomogeneous phases in the gross-neveu model in* $1+1$ *dimensions at finite number of flavors*, *Phys. Rev. D* **101** (2020) 094512.

[60] K.G. Wilson, *Quarks and strings on a lattice*, in *New phenomena in subnuclear physics*, A. Zichichi ed., Springer, Germany (1977), p. 69.

[61] J.B. Kogut and L. Susskind, *Hamiltonian formulation of Wilson's lattice gauge theories*, *Phys. Rev. D* **11** (1975) 395 [INSPIRE].

[62] L. Susskind, *Lattice fermions*, *Phys. Rev. D* **16** (1977) 3031 [INSPIRE].

[63] S. Aoki, *New phase structure for lattice QCD with Wilson fermions*, *Phys. Rev. D* **30** (1984) 2653 [INSPIRE].

[64] S. Aoki and K. Higashijima, *The recovery of the chiral symmetry in lattice Gross-Neveu model*, *Prog. Theor. Phys.* **76** (1986) 521 [INSPIRE].

[65] A. Bermudez, E. Tirrito, M. Rizzi, M. Lewenstein and S. Hands, *Gross-Neveu-Wilson model and correlated symmetry-protected topological phases*, *Ann. Phys.* **399** (2018) 149.

[66] Y. Kuno, *Phase structure of the interacting Su-Schrieffer-Heeger model and the relationship with the Gross-Neveu model on lattice*, *Phys. Rev. B* **99** (2019) 064105 [arXiv:1811.01487] [INSPIRE].

[67] D.K. Campbell and A.R. Bishop, *Soliton excitations in polyacetylene and relativistic field theory models*, *Nucl. Phys. B* **200** (1982) 297 [INSPIRE].

[68] A. Chodos and H. Minakata, *The Gross-Neveu model as an effective theory for polyacetylene*, *Phys. Lett. A* **191** (1994) 39 [INSPIRE].

[69] W.P. Su, J.R. Schrieffer and A.J. Heeger, *Soliton excitations in polyacetylene*, *Phys. Rev. B* **22** (1980) 2099 [INSPIRE].

[70] E. Fradkin and J.E. Hirsch, *Phase diagram of one-dimensional electron-phonon systems. i. the Su-Schrieffer-Heeger model*, *Phys. Rev. B* **27** (1983) 1680.

[71] S.R. Coleman, *There are no Goldstone bosons in two-dimensions*, *Commun. Math. Phys.* **31** (1973) 259 [INSPIRE].

[72] N.D. Mermin and H. Wagner, *Absence of ferromagnetism or antiferromagnetism in one-dimensional or two-dimensional isotropic Heisenberg models*, *Phys. Rev. Lett.* **17** (1966) 1133 [INSPIRE].

[73] W. Wetzel, *Two loop* β*-function for the Gross-Neveu model*, *Phys. Lett. B* **153** (1985) 297 [INSPIRE].

[74] J.A. Gracey, *Computation of the three loop* β*-function of the* $O(N)$ *Gross-Neveu model in minimal subtraction*, *Nucl. Phys. B* **367** (1991) 657 [INSPIRE].

JHEP07(2021)207

[75] R.F. Dashen, B. Hasslacher and A. Neveu, *Semiclassical bound states in an asymptotically free theory*, *Phys. Rev. D* **12** (1975) 2443 [INSPIRE].

[76] P. Fendley and H. Saleur, *BPS kinks in the Gross-Neveu model*, *Phys. Rev. D* **65** (2002) 025001 [hep-th/0105148] [INSPIRE].

[77] J. Feinberg, *On kinks in the Gross-Neveu model*, *Phys. Rev. D* **51** (1995) 4503 [hep-th/9408120] [INSPIRE].

[78] R. Jackiw and C. Rebbi, *Solitons with fermion number* 1/2, *Phys. Rev. D* **13** (1976) 3398 [INSPIRE].

[79] A. Schnyder, S. Ryu, A. Furusaki and A. Ludwig, *Classification of topological insulators and superconductors in three spatial dimensions*, *Phys. Rev. B* **78** (2008) 195125 [arXiv:0803.2786] [INSPIRE].

[80] A. Kitaev, *Periodic table for topological insulators and superconductors*, *AIP Conf. Proc.* **1134** (2009) 22 [arXiv:0901.2686] [INSPIRE].

[81] E. Lieb, T. Schultz and D. Mattis, *Two soluble models of an antiferromagnetic chain*, *Ann. Phys.* **16** (1961) 407.

[82] M. Fannes, J.T. Lewis and A. Verbeure, *Symmetric states of composite systems*, *Lett. Math. Phys.* **15** (1988) 255.

[83] B.M. Terhal, *Is entanglement monogamous?*, *IBM J. Res. Devel.* **48** (2004) 71.

[84] M.B. Hastings, *Solving gapped hamiltonians locally*, *Phys. Rev. B* **73** (2006) 085115.

[85] J. Eisert, M. Cramer and M.B. Plenio, *Area laws for the entanglement entropy — A review*, *Rev. Mod. Phys.* **82** (2010) 277 [arXiv:0808.3773] [INSPIRE].

[86] I.P. McCulloch and M. Gulácsi, *The non-Abelian density matrix renormalization group algorithm*, *Europhys. Lett.* **57** (2002) 852.

[87] A. Weichselbaum, *Non-abelian symmetries in tensor networks: a quantum symmetry space approach*, *Ann. Phys.* **327** (2012) 2972.

[88] M. Sanz, M.M. Wolf, D. Pérez-García and J.I. Cirac, *Matrix product states: Symmetries and two-body Hamiltonians*, *Phys. Rev. A* **79** (2009) 042308.

[89] J. Haegeman et al., *Variational matrix product ansatz for dispersion relations*, *Phys. Rev. B* **85** (2012) 100408 [arXiv:1103.2286] [INSPIRE].

[90] V. Zauner-Stauber, L. Vanderstraeten, J. Haegeman, I.P. McCulloch and F. Verstraete, *Topological nature of spinons and holons: elementary excitations from matrix product states with conserved symmetries*, *Phys. Rev. B* **97** (2018) 235155.

[91] L. Vanderstraeten, J. Haegeman and F. Verstraete, *Tangent-space methods for uniform matrix product states*, *SciPost Phys. Lect. Notes* (2019) 7.

[92] L. Vanderstraeten, E. Wybo, N. Chepiga, F. Verstraete and F. Mila, *Spinon confinement and deconfinement in spin-1 chains*, *Phys. Rev. B* **101** (2020) 115138.

[93] L. Faddeev and L. Takhtajan, *What is the spin of a spin wave?*, *Phys. Lett. A* **85** (1981) 375.

[94] B.S. Shastry and B. Sutherland, *Excitation spectrum of a dimerized next-neighbor antiferromagnetic chain*, *Phys. Rev. Lett.* **47** (1981) 964.

JHEP07(2021)207

[95] V. Zauner et al., *Transfer matrices and excitations with matrix product states*, *New J. Phys.* **17** (2015) 053002.

[96] M.M. Rams, P. Czarnik and L. Cincio, *Precise extrapolation of the correlation function asymptotics in uniform tensor network states with application to the bose-hubbard and xxz models*, *Phys. Rev. X* **8** (2018) 041033.

[97] V. Zauner-Stauber, L. Vanderstraeten, M.T. Fishman, F. Verstraete and J. Haegeman, *Variational optimization algorithms for uniform matrix product states*, *Phys. Rev. B* **97** (2018) 045145 [arXiv:1701.07035] [INSPIRE].

[98] M. Van Damme, G. Roose, M. Hauru and J. Haegeman, *MPSKit.jl*, https://github.com/maartenvd/MPSKit.jl.

[99] J. Haegeman, *TensorKit.jl*, https://github.com/Jutho/TensorKit.jl.

[100] F.H. Essler, H. Frahm, F. Göhmann, A. Klümper and V.E. Korepin, *The one-dimensional Hubbard model*, Cambridge University Press, Cambridge U.K. (2005).

[101] G.Y. Cho, A.W.W. Ludwig and S. Ryu, *Universal entanglement spectra of gapped one-dimensional field theories*, *Phys. Rev. B* **95** (2017) 115122 [arXiv:1603.04016] [INSPIRE].

[102] M.E. Peskin and D.V. Schroeder, *An introduction to quantum field theory*, Addison-Wesley, Reading, U.S.A. (1995),

JHEP07(2021)207

6

EMERGENT U(1) SYMMETRY IN THE CHIRAL GROSS-NEVEU MODEL

The next obvious step was to find a lattice regularization of the Chiral Gross Neveu model. Here, the impact of the Nielsen Ninoyima theorem is very prominent, because avoiding doublers forces us to replace the chiral Z_2 with translation symmetry which can not be expanded to a continous $U(1)$ group on the lattice. Consequently we lose the guarantee that there is a gapless mode in the spectrum of the lattice model. The upshot is that we must either fail to find the correct continuum limit or that there must exist some other mechanism that provides us with the gapless mode.

The first thing we did was to simply apply our discretisation procedure to the chiral Gross Neveu field theory. With this we found a Hamiltonian

$$\begin{aligned} H = \frac{1}{a}\sum_n\sum_c i\left(c_{n,c}c^\dagger_{n+1,c} - c^\dagger_{n+1,c}c^\dagger_{n,c}\right) \\ + \frac{g_x^2}{2}\left(\sum_c i\left(c_{n,c}c^\dagger_{n+1,c} - c^\dagger_{n+1,c}c^\dagger_{n,c}\right) - i\left(c_{n+1,c}c^\dagger_{n+2,c} - c^\dagger_{n+2,c}c^\dagger_{n+1,c}\right)\right)^2 \\ + \frac{g_y^2}{2}\left(c_{n,c}c^\dagger_{n,c} - c_{n+1,c}c^\dagger_{n+1,c}\right)^2 \end{aligned} \tag{235}$$

that has a ferromagnetic phase for $g_y^2 \gg g_x^2$ and a dimerized phase for $g_x^2 \gg g_y^2$. The continuum limit of this lattice model can only be the chiral Gross Neveu model if there is a direct transition from the ferromagnetic to the dimerized phase which is usually a fine tuned occurance. Indeed, a generic transition between these two regimes is either first order or via a intermediate phase where both symmetries are broken or both unbroken.

In the first part of the paper we obtain the phase diagram for large-N via a Slater determinant Ansatz and find that there is an intermediate phase where both symmetries are spontaneously broken. However, we also find that the width of this intermediate region is extremely small, so that it is not inconceivable that it may vanish due to quantum correction which usually destroy order. To verify this intuition, we performed a careful MPS analysis of the $N = 2$, case where we obtained the desired direct transition along which one can take the continuum limit.

In the remainder of the paperv we motivate that this phase diagram is in fact not fine tuned because, the symmetries of the model exclude a phase where both order parameters are unbroken. Furthermore we find that the kinks in the dimer order parameter carry some localized antiferromagnetic charge so that restoration of the dimer order due to kink condensation inevitably also leads to condensation of the ferromagnetic order parameter.

Published for SISSA by Springer

Received: January 28, 2022
Revised: April 22, 2022
Accepted: May 4, 2022
Published: June 6, 2022

The chiral Gross-Neveu model on the lattice via a Landau-forbidden phase transition

Gertian Roose,[a] **Jutho Haegeman,**[a] **Karel Van Acoleyen,**[a] **Laurens Vanderstraeten**[a] **and Nick Bultinck**[a,b]

[a] *Department of Physics and Astronomy, University of Ghent, Krijgslaan 281, 9000 Gent, Belgium*
[b] *Rudolf Peierls Centre for Theoretical Physics, Parks Road, Oxford, OX1 3PU, U.K.*

E-mail: gertian.roose@ugent.be, jutho.haegeman@ugent.be, karel.vanacoleyen@ugent.be, laurens.vanderstraeten@ugent.be, nibultinck@gmail.com

Abstract: We study the phase diagram of the $(1+1)$-dimensional Gross-Neveu model with both $g_x^2(\bar{\psi}\psi)^2$ and $g_y^2(\bar{\psi}i\gamma_5\psi)^2$ interaction terms on a spatial lattice. The continuous chiral symmetry, which is present in the continuum model when $g_x^2 = g_y^2$, has a mixed 't Hooft anomaly with the charge conservation symmetry, which guarantees the existence of a massless mode. However, the same 't Hooft anomaly also implies that the continuous chiral symmetry is broken explicitly in our lattice model. Nevertheless, from numerical matrix product state simulations we find that for certain parameters of the lattice model, the continuous chiral symmetry reemerges in the infrared fixed point theory, even at strong coupling. We argue that, in order to understand this phenomenon, it is crucial to go beyond mean-field theory (or, equivalently, beyond the leading order term in a $1/N$ expansion). Interestingly, on the lattice, the chiral Gross-Neveu model appears at a Landau-forbidden second order phase transition separating two distinct and unrelated symmetry-breaking orders. We point out the crucial role of two different 't Hooft anomalies or Lieb-Schultz-Mattis obstructions for this Landau-forbidden phase transition to occur.

Keywords: Chiral Symmetry, Effective Field Theories, Phase Transitions

ArXiv ePrint: 2111.14652

https://doi.org/10.1007/JHEP06(2022)019

JHEP06(2022)019

Contents

1 Introduction

Discretizing quantum field theory (QFT) on a lattice in space or spacetime has been a very successful strategy to study interacting quantum fields using computational methods. The prevalent approach for the last decades has been to study the partition function of a quantum field theory, often including interacting gauge fields, on a spacetime lattice using some kind of Monte Carlo sampling. Indeed, the research field of lattice gauge theory has been tremendously successful in explaining the hadron masses and various other equilibrium properties of the standard model [1–3]. More recently, there has been a renewed interest in quantum fields on a spatial lattice, either for classical simulation using the formalism of tensor networks, but also for quantum simulation using cold atoms or other discrete or analogue quantum simulators [4, 5].

While the lattice (both in space and in spacetime) has the advantage of regularizing the divergences that typically occur as a result of the infinitely many degrees of freedom in a QFT, it is well known that certain symmetries of the field theory cannot be realized exactly in the lattice description. The most notorious example is that of chiral symmetry, which is a continuous U(1) symmetry of the massless Dirac operator in even spacetime dimensions. Even the discrete $\mathbb{Z}_2$ subgroup of the chiral symmetry cannot be implemented as an on-site symmetry in a local lattice model without causing a doubling of the number

JHEP06(2022)019

of Dirac fermions, a result known as (or resulting from) the Nielsen-Ninomiya theorem [6]. By staggering the components of the Dirac spinor, it is possible to remove some of the doublers (and in particular all of them when only discretizing space in a (1+1)-dimensional theory) [7]. The staggered model still breaks the full continuous chiral symmetry, but a single-site shift in the direction of staggering behaves as a discrete chiral transformation in the low-energy limit. The difficulty of realizing the chiral symmetry on the lattice is a consequence of the mixed 't Hooft anomaly [8] between the chiral and charge U(1) symmetries [9]. Upon gauging the U(1) charge symmetry this 't Hooft anomaly gives rise to the Adler-Bell-Jackiw anomaly [10, 11], i.e. after gauging the current associated with the continuous chiral symmetry is no longer preserved.

In this work, we study the generalized Gross-Neveu (GGN) model in 1+1 dimensions [12]. The GGN model consists of N massless Dirac fermions interacting via two different interaction terms $g_x^2(\bar{\psi}\psi)^2$ and $g_y^2(\bar{\psi}i\gamma_5\psi)^2$. When $g_x^2 = g_y^2$, the interaction terms preserve the continuous chiral symmetry of the massless Dirac operator. Along this line with equal couplings, Coleman's theorem rules out the possibility that the chiral symmetry is broken spontaneously in $(1+1)$-dimensions. But even despite the absence of Goldstone modes, the mixed anomaly between the chiral symmetry and the charge conservation symmetry implies that the theory cannot be trivial in the infrared and must host a massless mode [8]. Everywhere away from the special line $g_x^2 = g_y^2$ with continuous chiral symmetry, the remaining discrete chiral symmetry in the GGN Lagrangian is broken spontaneously, just as in the conventional GN model. The main question we address here is how much of these features of the continuum GGN model survive after discretizing the theory on a spatial lattice. Given that many properties of the continuum GGN phase diagram crucially hinge on the chiral symmetry and its 't Hooft anomaly, it is a priori not clear that a lattice discretized model — which breaks the chiral symmetry explicitly due to that same 't Hooft anomaly — will reproduce the continuum phase diagram (both at small and large coupling).

Our analysis starts with a mean-field or large-N calculation, which produces two different phase diagrams for the continuum and the lattice model, but suggests that fluctuations beyond mean-field theory (or subleading terms in the $1/N$ expansion) could be able to remove the apparent discrepancy. A fully unbiased matrix product state simulation for the $N = 2$ lattice GGN model confirms this expectation, and produces a phase diagram which contains a critical line that has the same infrared behaviour as the chiral GN model. This critical line appears as a Landau-forbidden second order phase transition of the lattice model which separates two gapped phases with unrelated spontaneously broken discrete symmetries. We argue that this Landau-forbidden phase transition can occur as a critical *line* in the lattice model due to the presence of *two* different Lieb-Schultz-Mattis (LSM) obstructions [13–15], which are lattice versions of the continuum 't Hooft anomalies. One of these LSM obstructions is related to a lattice version of the mixed 't Hooft anomaly between the remaining discrete chiral symmetry and the charge conservation symmetry. The other LSM obstruction is less well-known, and it relies on a combination of several different symmetries including charge conjugation and spatial reflection symmetry.

The paper is structured as follows. In the following section, we start by providing a short review of the (chiral) GN model. More specifically, we highlight some often overlooked

JHEP06(2022)019

symmetries of the model and use bosonization to provide a nonperturbative argument for the existence of a critical line in the phase diagram. In the same section we introduce the lattice model based on the symmetries that are present in the continuum. Section 3 presents the mean field solution, which coincides with the large-N limit, for both the continuum and the lattice model, and discusses its shortcomings. In section 4 we use tensor network methods to determine the phase diagram of the $N = 2$ lattice model. The phase diagram exhibits a critical line between two symmetry broken phases, which we can identify with the chiral GN QFT in the continuum limit. In section 5, we reinterpret our lattice model from a condensed matter perspective to further discuss the nature of our critical line in the context of the LSM theorem. Section 6 summarises our main conclusions.

2 Generalized Gross-Neveu model

We study the generalized Gross-Neveu model [12] with N flavors, which in the continuum is described by the following action:

$$S = \int \mathrm{d}x\mathrm{d}t \left(\sum_c \bar{\psi}_c i\partial\!\!\!/ \psi_c + \frac{g_x^2}{2N} \left(\sum_c \bar{\psi}_c \psi_c \right)^2 + \frac{g_y^2}{2N} \left(\sum_c \bar{\psi}_c i\gamma_5 \psi_c \right)^2 \right) , \tag{2.1}$$

where ψ_c is the two component Dirac spinor for each of the flavors $c = 1, \ldots, N$. The matrices γ^μ satisfy the usual Clifford algebra $\{\gamma^\mu, \gamma^\nu\} = 2\eta^{\mu\nu}$ (we use $\eta = \mathrm{diag}(1, -1)$) and are used to define $\bar{\psi}_c = \psi_c^\dagger \gamma^0$, $\partial\!\!\!/ = \gamma^\mu \partial_\mu$, and $\gamma_5 = \gamma^0\gamma^1$. In the remainder of this section we review all the symmetries of this action, discuss the phase diagram and re-express the action in terms of bosonic fields.

2.1 Review of the continuum symmetries

In the general case $g_x^2 \neq g_y^2 \neq 0$, the relevant internal symmetries are:[1]

$$\begin{aligned}
&\mathrm{SU}(N) \text{ flavor rotation:} && \psi_c \to U_{cc'} \psi_{c'} \\
&\mathrm{U}(1) \text{ charge rotation:} && \psi_c \to e^{i\theta} \psi_c \\
&\mathbb{Z}_2^{\mathcal{D}} \text{ discrete chiral transformation:} && \psi_c \to \gamma_5 \psi_c \\
&\mathbb{Z}_2^{\mathcal{C}} \text{ charge conjugation:} && \psi_c \to \gamma_C \psi_c^* ,
\end{aligned} \tag{2.2}$$

where the unitary matrix γ_C is defined such that $\gamma_C^\dagger \gamma^0 \gamma_C = -(\gamma^0)^\mathsf{T}$ and $\gamma_C^\dagger \gamma_5 \gamma_C = (\gamma_5)^\mathsf{T}$. Besides these internal symmetries, the action naturally has spacetime symmetries, namely the full Poincaré group, which includes Lorentz transformations, spacetime translations, spatial reflection and time reversal. From these, we only highlight the reflection symmetry, which acts as

$$\mathbb{Z}_2^{\mathcal{R}} \text{ spatial reflection:} \qquad \psi \to \gamma_R \psi \,, \quad x \to -x \,, \tag{2.3}$$

where γ_R satisfies $\gamma_R^\dagger \gamma^0 \gamma_R = \gamma^0$ and $\gamma_R^\dagger \gamma_5 \gamma_R = -\gamma_5$. A typical choice is $\gamma_R = \gamma^0$.

[1] The various symmetries also interact. Charge conjugation flips the rotation angle of charge U(1) (and combines with it into an $O(2)$ group) as well as of chiral (axial) rotation. The discrete chiral transformation also anticommutes with the spatial reflection (toghether they generate the Pauli group).

JHEP06(2022)019

Let us now make a particular basis choice, such that the gamma matrices are given by the Pauli matrices $\gamma_5 = \sigma^x$ and $\gamma^0 = \sigma^y$. In this basis we find that $\gamma_C = \mathbb{1}$ and $\gamma_R = \sigma_y$. The bilinears $\bar{\psi}\psi$ and $\bar{\psi}i\gamma_5\psi$ transform respectively as scalar and pseudoscalar quantities with respect to both reflection and charge conjugation, whereas both or of course pseudoscalars with respect to the discrete chiral tranformation.

For $g_y^2 = 0$, the charge conjugation action $\mathcal{C}$ can be extended to a $\mathbb{Z}_2^{\otimes N}$ symmetry by applying it to each flavor separately. Furthermore, this $\mathbb{Z}_2^{\otimes N}$ symmetry can be combined with the charge U(1) and flavor SU(N) symmetries into a larger O($2N$) symmetry, which can be made manifest by rewriting the complex Dirac fermions ψ_c in terms of two real Majorana fermions: $\psi_c = (\chi_{2c-1} + i\chi_{2c})/\sqrt{2}$, where $\chi_c^\dagger = \chi_c$ and $\{\chi_c, \chi_{c'}\} = 2\delta_{c,c'}$. Similarly, an enhanced O($2N$) symmetry is also present when $g_x^2 = 0$. This O($2N$) group now contains the $\mathcal{DC}$ symmetry action (generating a $\mathbb{Z}_2^{\otimes N}$ symmetry group when $g_x^2 = 0$), and again the U(1) and SU(N) symmetry groups. The O($2N$) symmetry at $g_x^2 = 0$ becomes explicit after rewriting the complex Dirac fermions $\psi'_c = \exp(i\pi\sigma^x/4)\psi_c$ in terms of two real Majorana fermions: $\psi'_c = (\chi'_{2c-1} + i\chi'_{2c})/\sqrt{2}$.

Finally, when the two interaction coefficients g_x^2 and g_y^2 are equal, the generalized Gross-Neveu model is known as the 'chiral Gross-Neveu model', which can be interpreted as a (1+1)-dimensional version of the 'Nambu-Jona-Lasinio' model [16, 17]. Here the chiral symmetry becomes continuous, i.e.

$$\mathrm{U}_A(1) : \psi_c \to e^{i\theta_A\gamma_5}\psi_c \tag{2.4}$$

becomes a symmetry of the action.

2.2 Phase diagram and bosonization

The phase diagram of the generalized Gross-Neveu (GN) model is well-understood[2], and we review it here. First, for $g_y^2 = 0$, the action reduces to that of the conventional GN model. In this case, the interaction leads to dynamical mass generation for the Dirac fermions, spontaneously breaking the discrete chiral symmetry, which is characterized by the fact that the vacuum obtains a chiral condensate: $\langle\bar{\psi}\psi\rangle \neq 0$. For $g_x^2 = 0$, the situation is analogous to that of the conventional GN model, as we can transform the g_x^2 and g_y^2 interaction terms into each other with a chiral symmetry rotation, where now the chiral condensate is characterized as $\langle\bar{\psi}i\gamma_5\psi\rangle \neq 0$. As long as $g_x^2 \neq g_y^2$, the IR physics does not change if we move away from the lines with either $g_x^2 = 0$ or $g_y^2 = 0$. In particular, for $g_x^2 > g_y^2$, the dynamical mass generation is associated with a chiral condensate $\langle\bar{\psi}\psi\rangle \neq 0$, whereas $\langle\bar{\psi}i\gamma_5\psi\rangle$ remains zero (and vice versa for $g_x^2 < g_y^2$).

Along the $g_x^2 = g_y^2$ chiral line, the IR physics drastically changes due to the presence of the continuous chiral symmetry, which is a proper symmetry at the quantum level, as no gauge fields are included. The Coleman-Hohenberg-Mermin-Wagner (CHMW) theorem [25–27] excludes spontaneous breaking of this continuous chiral symmetry, which automatically implies that both $\langle\bar{\psi}\psi\rangle = 0$ and $\langle\bar{\psi}i\gamma_5\psi\rangle = 0$. However, despite the fact that there is

[2]The conventional ($g_x^2 = 0$ or $g_y^2 = 0$) and chiral ($g_x^2 = g_y^2$) GN models are even integrable, such that the entire spectrum can be computed exactly — see e.g. refs. [18–24].

JHEP06(2022)019

no chiral condensate along the line $g_x^2 = g_y^2$, the Dirac fermions nevertheless acquire a dynamically generated mass.

To better understand the mechanism responsible for dynamical mass generation along (and close to) the line $g_x^2 = g_y^2$, it is insightful to consider the bosonized version of eq. (2.1)[3]. Here, we only consider the $N = 2$ case, both for simplicity of the presentation and because this is also the model that we study numerically (for details of the bosonization procedure for general N, we refer to [32]). Bosonization allows us to map the fermion action to a theory of two compact bosons ϕ_1 and ϕ_2 with compactification radius 2π. Under this mapping, the kinetic term becomes

$$\bar{\psi}_1 i\partial\!\!\!/ \psi_1 + \bar{\psi}_2 i\partial\!\!\!/ \psi_2 \to \frac{1}{8\pi}\left[(\partial_\mu\phi_1)^2 + (\partial_\mu\phi_2)^2\right], \tag{2.5}$$

and the chiral transformation $\psi_c \to e^{i\theta_A\gamma_5}\psi_c$ corresponds to a shift of the scalar fields: $\phi_c \to \phi_c + \theta_A$. The mappings for fermion bilinears are:

$$\begin{cases} \bar{\psi}_1\psi_1 + \bar{\psi}_2\psi_2 & \to -\frac{1}{\alpha}(\cos\phi_1 + \cos\phi_2) \\ \bar{\psi}_1 i\gamma_5\psi_1 + \bar{\psi}_2 i\gamma_5\psi_2 & \to \frac{1}{\alpha}(\sin\phi_1 + \sin\phi_2)\,, \end{cases} \tag{2.6}$$

where $\frac{1}{\alpha}$ is a UV-cutoff. Using these relations, we arrive at the following bosonized action:

$$\begin{aligned} S &= \int \mathrm{d}^2x \frac{1}{8\pi}\left[(\partial_\mu\phi_1)^2 + (\partial_\mu\phi_2)^2\right] + \frac{g_x^2}{4\alpha^2}(\cos\phi_1 + \cos\phi_2)^2 + \frac{g_y^2}{4\alpha^2}(\sin\phi_1 + \sin\phi_2)^2 \\ &= \int \mathrm{d}^2x \frac{1}{8\pi}\left[(\partial_\mu\phi_1)^2 + (\partial_\mu\phi_2)^2\right] + \frac{g_x^2 + g_y^2}{4\alpha^2}\cos(\phi_1 - \phi_2) \\ &\quad + \frac{g_x^2 - g_y^2}{4\alpha^2}\cos(\phi_1 + \phi_2)\left(1 + \cos(\phi_1 - \phi_2)\right)\,. \end{aligned} \tag{2.7}$$

If we now write the boson fields as $\phi_1 = \theta + \varphi$ and $\phi_2 = \theta - \varphi$, then the bosonized action takes on a particularly simple form:

$$\begin{aligned} S = \int \mathrm{d}^2x &\frac{1}{2\pi K}(\partial_\mu\theta)^2 + \frac{1}{2\pi K}(\partial_\mu\varphi)^2 + \frac{g_x^2 + g_y^2}{4\alpha^2}\cos(2\varphi) \\ &+ \frac{g_x^2 - g_y^2}{4\alpha^2}\cos(2\theta)(1 + \cos(2\varphi))\,, \end{aligned} \tag{2.8}$$

where $K = 2$. Along the line with continuous chiral symmetry, i.e. when $g_x^2 = g_y^2$, this action describes one interacting boson φ, which transforms trivially under the chiral U(1) symmetry, and one free boson θ, which transforms as $\theta \to \theta + \theta_A$. The scaling dimension of $\cos(2\varphi)$ is equal to K, so this term is marginal at the classical level (recall that $K = 2$). However, $\cos(2\varphi)$ becomes relevant at the quantum level because the coefficient of the $(\partial_\mu\varphi)^2$ term renormalizes to a value $(2\pi K_{\mathrm{ren}})^{-1}$ with K_{ren} smaller than two (this can be seen from the Kosterlitz RG equations [33]). As a result, the $\cos(2\varphi)$ term causes the φ field to condense.

[3]Note that we are using Abelian bosonization in this work. One can also use non-Abelian bosonization [28–30], which shows that the chiral GN model is equivalent to a $\mathrm{SU}(N)_1$ Wess-Zumino-Witten CFT with a $J\bar{J}$ deformation [31].

JHEP06(2022)019

In the chiral GN model the compact boson θ is gapless because (1) the chiral U(1) symmetry forbids terms of the form $\cos(n\theta)$, and (2) θ can not be disordered by proliferating vortices (i.e. instantons which change the winding of θ). The reason for the latter is that the charge current in the presence of a spatially varying θ configuration, relative to the charge current of the vacuum, is given by the Goldstone-Wilczek formula [34]:

$$J_\mu = \frac{2}{2\pi}\epsilon_{\mu\nu}\partial_\nu\theta\,. \tag{2.9}$$

From this relation we see that the electric charge corresponds to the winding of θ along the spatial direction: $Q = \int \mathrm{d}x\, \partial_x\theta/\pi$. As a consequence, vortices in θ are forbidden by the charge conservation, i.e. by the U(1) charge symmetry. This is a manifestation of the 't Hooft anomaly, which rules out a trivial IR fixed point if both the charge and chiral U(1) symmetries are to be preserved. We thus arrive at the conclusion that the IR fixed point of the chiral GN model is a single compact boson. This conformal field theory has a central charge $c = 1$, instead of $c = 2$ as for two free Dirac fermions ($g_x^2 = g_y^2 = 0$). This is a manifestation of the fact that the fermions have acquired a mass.

When moving away from the line with equal couplings the continuous chiral symmetry breaks down to the discrete chiral symmetry $\mathbb{Z}_2^{\mathcal{D}}$. From eq. (2.8), we see that the effective action describing the IR physics close to the chiral line is

$$S = \int \mathrm{d}^2x \frac{1}{2\pi K}(\partial_\mu\theta)^2 + \delta\cos 2\theta\,, \tag{2.10}$$

where we have introduced $\delta = (g_x^2 - g_y^2)/4\alpha^2$ and we have dropped an irrelevant term. The $\cos(2\theta)$ term in eq. (2.10) is relevant for the same reason that the $\cos(2\varphi)$ discussed above is relevant (the classical value $K = 2$ gets renormalized to smaller values if $\delta \neq 0$). In section 4 we will show that we can recover the IR physics described by (2.10) by simulating the GGN on the lattice, even though we cannot preserve the chiral symmetry explicitly. As we will see below, one consequence of the loss of continuous chiral symmetry is that the relation $\delta = (g_x^2 - g_y^2)/4\alpha^2$ no longer holds for the parameters of our lattice model, which we introduce in the next section. Furthermore, on the lattice there are additional irrelevant perturbations, such that K is not guaranteed to be equal to 2. However, in section 4 we will show that K approaches 2 in the continuum limit.

2.3 Lattice model

Let us now introduce the specific lattice discretization of the GGN that we will study. We use a particular realization of the standard staggered fermion discretization [7, 35], where the two components of the Dirac fermions are defined to live on neighbouring lattice sites. The free/kinetic part of the Hamiltonian is obtained by using a symmetric finite difference approximation for the spatial derivative, and by using the same basis choice ($\gamma_5 = \sigma^x$ and $\gamma^0 = \sigma^y$) as in the previous section. In this way, we arrive at the following kinetic or hopping term on the lattice:

$$H_K = a^{-1}\sum_n K_{n,n+1} \tag{2.11}$$

$$= -ia^{-1}\sum_c \left(\varphi_{c,n}^\dagger\varphi_{c,n+1} - \varphi_{c,n+1}^\dagger\varphi_{c,n}\right)\,, \tag{2.12}$$

JHEP06(2022)019

where n (c) labels the lattice sites (flavors), a is the lattice constant, and $\varphi^\dagger_{c,n}$ and $\varphi_{c,n}$ are fermionic creation and annihilation operators satisfying $\{\varphi^\dagger_{c,n}, \varphi^\dagger_{c',n'}\} = \{\varphi_{c,n}, \varphi_{c',n'}\} = 0$ and $\{\varphi_{c,n}, \varphi^\dagger_{c',n'}\} = \delta_{c,c'}\delta_{n,n'}$. The kinetic term admits two different mass terms, which, with our basis choice, are given by

$$m\bar{\psi}\psi \to m\psi^\dagger\sigma^y\psi \to ma(-1)^n\left(\frac{K_{n-1,n} - K_{n,n+1}}{2}\right) \tag{2.13}$$

$$m\bar{\psi}i\gamma_5\psi \to m\psi^\dagger\sigma^z\psi \to ma(-1)^n\left(O_n - O_{n+1}\right)\,, \tag{2.14}$$

with $O_n = \sum_c \varphi^\dagger_{c,n}\varphi_{c,n}$. Note that both mass terms are odd under a translation by one lattice site, as expected from the fact that a single-site translation should behave as the discrete chiral transformation in the low-energy limit. The first mass term $m\psi^\dagger\sigma^y\psi$ translates on the lattice to a bond order parameter, which promotes dimerization on even or odd lattice bonds, whereas the second mass term $m\psi^\dagger\sigma^z\psi$ results in a polarization of the lattice fermions on either the even or odd lattice sites, i.e. it creates an imbalance between the average occupation of the even and odd lattice sites.

For the discretized interaction terms, we simply take the squares of both possible mass terms/order parameters. The final lattice Hamiltonian then takes on the following form:

$$H = a^{-1}\sum_n\left(K_{n,n+1} - \frac{g_x^2}{4N}\left(\frac{K_{n,n+1} - K_{n+1,n+2}}{2}\right)^2 - \frac{g_y^2}{4N}\left(O_n - O_{n+1}\right)^2\right)\,. \tag{2.15}$$

This Hamiltonian manifestly preserves the internal U(1), SU(N), $\mathbb{Z}_2^{\mathcal{C}}$ and $\mathbb{Z}_2^{\mathcal{D}}$ symmetries of the continuum model, as well as the spatial translation and reflection symmetries. As mentioned above, the discrete chiral symmetry of the QFT does not act as an exact internal symmetry, but can be related to one-site spatial translations $\mathcal{T}$ in the low-energy limit. Regarding the reflection symmetry, it should be noted that the lattice exhibits two possible reflection transformations, namely across bonds and across sites. From the form of γ_R in the reflection in the continuum, it can be noted that it interchanges the two components of the Dirac spinor. As we are using the staggered formulation, this should amount to interchanging even and odd sites on the lattice, which corresponds to a bond-centered reflection. A bond-centered reflection $n \to 1 - n$ in itself maps $K_{n,n+1}$ to $-K_{-n,-n+1}$, so we also need to add a local action, such that the ϕ_n operators on neighbouring sites acquire an opposite sign. A local charge rotation $\exp(in\pi\sum_c \phi^\dagger_{c,n}\phi_c)$ (which acts as the identity every second site) accomplishes this goal. Below, we denote with $\mathcal{R}_B$ this bond centered reflection, including the additional on-site action. A site-centered reflection (including the same on-site action) can be interpreted as $\mathcal{T}\mathcal{R}_B$, or thus as the combination of a discrete chiral transformation and a reflection.

For our MPS simulations, we further transform the lattice fermion Hamiltonian in eq. (2.15) into a lattice spin Hamiltonian via a Jordan-Wigner transformation, where each fermion operator is represented in terms of Pauli matrices as

$$\varphi_{c,n} = \left(\prod_{n'<n}\prod_{c'}\sigma^z_{c',n'}\right)\left(\prod_{c'<c}\sigma^z_{c',n}\right)\sigma^-_{c,n}\,, \tag{2.16}$$

JHEP06(2022)019

where $\sigma^- = (\sigma^x - i\sigma^y)/2$, and we have introduced a linear ordering for the different flavors. In a previous work [35], we have numerically studied the two-flavor version of the lattice Hamiltonian in eq. (2.15) with $g_y^2 = 0$ using MPS. We were able to take the continuum limit of our numerical results and recover some of the QFT results to very high accuracy, thus confirming the validity of both our lattice Hamiltonian and our MPS methods.

Before concluding our discussion of the lattice Hamiltonian, let us point out a subtlety about the O($2N$) symmetries which are present in the continuum action when either $g_y^2 = 0$ or $g_x^2 = 0$. If $g_y^2 = 0$, then the full O($2N$) symmetry of the continuum model is present in the lattice Hamiltonian, and acts in a local way. This is possible because the O($2N$) symmetry group contains the $\mathcal{C}$ symmetry action, which acts locally in the lattice model, and generates a $\mathbb{Z}_2^{\otimes N}$ symmetry by acting on each flavor separately if $g_y^2 = 0$. Indeed, this was the motivation for our basis choice of the gamma matrices, where $\gamma_C = \mathbb{1}$. As explained in the previous section, the continuum model at $g_x^2 = 0$ also possesses an O($2N$) symmetry, where now the $\mathbb{Z}_2^{\otimes N}$ subgroup is generated by acting with the $\mathcal{DC}$ on each flavor separately. The $\mathcal{DC}$ symmetry on the lattice, however, does not act locally as it contains a discrete chiral symmetry action $\mathcal{D}$, which we discussed above. As a result, there is no lattice analogue of acting with $\mathcal{DC}$ on a single fermion flavor. This implies that the duality for interchanging $g_x \leftrightarrow g_y$, which exist in the continuum and is generated by applying a $\pi/2$ chiral rotation, does not exist in the lattice model. Despite this shortcoming of the discretization, we argue below that our numerical results for $N = 2$ with both g_x^2 and g_y^2 non-zero agree well with the results expected from the continuum model.

3 Large-N solution

In this section we analyse the GGN model in the large-N limit, where mean-field theory becomes exact. In order to keep this paper self-contained, we first review the large-N solution of the continuum model. We compare the solutions of the continuum and lattice theories, and discuss the implications of the broken continuous chiral symmetry on the lattice.

3.1 Continuum model

The Hamiltonian of the generalized Gross-Neveu model in the continuum is:

$$H = \int \mathrm{d}x \left(\bar{\psi} i\gamma^x \partial_x \psi - \frac{g_x^2}{2N} (\bar{\psi}\psi)^2 - \frac{g_y^2}{2N} (\bar{\psi} i\gamma_5 \psi)^2 \right) , \tag{3.1}$$

where, as before, ψ is a $2N$-component Dirac spinor. In taking the $N \to \infty$ limit we can exploit the monogamy of entanglement to write the ground state as a product state over the different flavors: $|\Psi\rangle = |\phi\rangle^{\otimes N}$ (see e.g. ref. [36]). The energy per flavor of such states is given by:

$$\begin{aligned} \frac{E}{N} = \int \mathrm{d}x \left\langle \bar{\psi}_s i\gamma^x \partial_x \psi_s - \frac{g_x^2}{2N} (\bar{\psi}_s \psi_s)^2 - \frac{g_y^2}{2N} (\bar{\psi}_s i\gamma_5 \psi_s)^2 \right\rangle \\ - \frac{g_x^2}{2} \frac{N-1}{N} \left\langle \bar{\psi}_s \psi_s \right\rangle^2 - \frac{g_y^2}{2} \frac{N-1}{N} \left\langle \bar{\psi}_s i\gamma_5 \psi_s \right\rangle^2 , \end{aligned} \tag{3.2}$$

JHEP06(2022)019

where ψ_s is a 2-component single-flavor Dirac spinor. For sufficiently large N the terms proportional to the expectation values of the fluctuations, i.e. $\langle(\bar{\psi}_s\psi_s)^2\rangle$ and $\langle(\bar{\psi}_s i\gamma_5\psi_s)^2\rangle$, can be neglected. Varying the energy with respect to the single-flavor wave function while using a Lagrange multiplier to ensure normalisation, gives the following eigenvalue problem:

$$\int \mathrm{d}x \left(\bar{\psi}_s i\gamma^x \partial_x \psi_s - g_x^2 \sigma\, \bar{\psi}_s\psi_s - g_y^2 \pi\, \bar{\psi}_s i\gamma_5 \psi_s\right) |\phi\rangle = H_{\mathrm{MF}}\, |\phi\rangle = E_{\mathrm{MF}}\, |\phi\rangle \ , \tag{3.3}$$

where σ and π respectively are the (translationally invariant) expectation values $\langle\bar{\psi}_s\psi_s\rangle$ and $\langle\bar{\psi}_s i\gamma_5\psi_s\rangle$, such that these equations have to be solved self-consistently. For now we can easily diagonalize the effective mean-field Hamiltonian in momentum space and we find the following single-particle dispersion relation:

$$\varepsilon_{\mathrm{MF}}(k) = \pm\sqrt{k^2 + g_x^4\sigma^2 + g_y^4\pi^2}\,. \tag{3.4}$$

The groundstate $|\Omega\rangle$ of H_{MF} simply corresponds to the filled Dirac sea of the states with negative energy. We define the effective potential as the energy density of $|\Omega\rangle$:

$$V_{\mathrm{eff}}(\sigma,\pi) = \frac{g_x^2}{2}\sigma^2 + \frac{g_y^2}{2}\pi^2 - \int \frac{\mathrm{d}k}{2\pi}\sqrt{k^2 + g_x^4\sigma^2 + g_y^4\pi^2}\,. \tag{3.5}$$

Let us now introduce polar coordinates for the order parameters:

$$\begin{cases} \sigma = \rho\cos\theta \\ \pi = \rho\sin\theta\,, \end{cases} \tag{3.6}$$

where we have used, not coincidentally, the same notation as in the bosonization formula (2.6). Indeed, under chiral transformations the θ field from eq. (3.6) transforms identically to the θ field introduced in eq. (2.8). Using the ρ and θ variables, the effective potential can be written as

$$V_{\mathrm{eff}}(\rho,\theta) = \frac{g^2}{2}\rho^2 + \frac{\Delta g}{2}\rho^2\cos 2\theta - \int \frac{\mathrm{d}k}{2\pi}\sqrt{k^2 + (g^4+\Delta g^2)\rho^2 + 2g^2\Delta g\rho^2\cos 2\theta}\,, \tag{3.7}$$

where $g^2 = (g_x^2+g_y^2)/2$ and $\Delta g = (g_x^2 - g_y^2)/2$. Minimizing this effective potential (after introducing a cutoff Λ) is equivalent to solving the mean-field self-consistency equations. If $\Delta g \neq 0$, and assuming $\rho^2 \neq 0$, one finds that the minima of V_{eff} are located at either $\theta = 0, \pi$ or $\theta = \pm\pi/2$ because V_{eff} depends only on θ via $\cos 2\theta$. Using this fact, we find from minimizing the effective potential with respect to ρ^2 that

$$\rho^2 = \begin{cases} \frac{4\Lambda^2}{g_x^2} e^{-2\pi/g_x^2} & \text{if } g_x^2 \geq g_y^2 \\ \frac{4\Lambda^2}{g_y^2} e^{-2\pi/g_y^2} & \text{if } g_x^2 \leq g_y^2\,, \end{cases} \tag{3.8}$$

such that σ and π are never simultaneously equal to zero, except when $g_x^2 = g_y^2 = 0$. We are therefore led to the conclusion that the Dirac fermions acquire a mass for all non-zero values of the couplings.

A non-zero value for ρ also implies that the chiral symmetry is spontaneously broken. For the chiral GN model, however, this is an artefact of the large-N limit, as the CHMW

JHEP06(2022)019

theorem implies that in $1+1$ spacetime dimensions fluctuations around mean-field theory will restore the continuous chiral symmetry at any finite N [37]. However, although the chiral symmetry is restored beyond mean-field theory, the Dirac fermions nevertheless remain everywhere gapped. The physical picture is that, at finite N, the field $\rho^2 = \sigma^2 + \pi^2$ retains a non-zero expectation value, thus providing a mass scale for the fermions, while at the same time, the long-range order for the θ field in mean-field theory is replaced with quasi-long range or algebraic order at finite N. The effective IR action describing these fluctuations is exactly the compact boson introduced previously in eq. (2.10).

3.2 Lattice model

Let us next perform the mean-field analysis of our proposed lattice version of GGN model. Once again we exploit the monogamy of entanglement and calculate the energy of the groundstate with respect to the states $|\Psi\rangle = |\phi\rangle^{\otimes N}$:

$$\frac{\langle H\rangle}{N} = \sum_n \langle k_{n,n+1}\rangle - \frac{g_x^2}{2}\langle \sigma_{n,n+1,n+2}\rangle^2 - \frac{g_y^2}{2}\langle \pi_{n,n+1}\rangle^2 \,, \tag{3.9}$$

where we have already neglected terms proportional to expectation values of fluctuations and introduced the following shorthand notations:

$$k_{n,n+1} = -i(\varphi^\dagger_{c,n}\varphi_{c,n+1} - \varphi^\dagger_{c,n+1}\varphi_{c,n}) \tag{3.10}$$

$$\sigma_{n,n+1,n+2} = \frac{1}{2}(k_{n,n+1} - k_{n+1,n+2}) \tag{3.11}$$

$$\pi_{n,n+1} = \varphi^\dagger_{c,n}\varphi_{c,n} - \varphi^\dagger_{c,n+1}\varphi_{c,n+1}\,. \tag{3.12}$$

Variation with respect to the single-flavor wave function while using a Lagrange multiplier to ensure normalisation, gives the following eigenvalue problem

$$\sum_n \left(k_{n,n+1} - g_x^2\langle\sigma_{n,n+1,n+2}\rangle\,\sigma_{n,n+1,n+2} - g_y^2\langle\pi_{n,n+1}\rangle\,\pi_{n,n+1}\right)|\phi\rangle = E_{\rm MF}\,|\phi\rangle \,, \tag{3.13}$$

similar to what we found in the continuum model. We are interested in states with a two-site unit cell. Consequently, we diagonalize (3.13) under the conditions that $\langle\sigma_{n,n+1,n+2}\rangle = (-1)^n\sigma$ and $\langle\pi_{n,n+1}\rangle = (-1)^n\pi$. The resulting single-particle dispersion relation is very similar to that obtained for the continuum model in eq. (3.4):

$$\varepsilon_{\rm MF}(k) = \pm\sqrt{4\sin^2(k/2) + g_x^4\sigma^2\cos^2(k/2) + g_y^4\pi^2}\,, \tag{3.14}$$

and leads to the following effective potential for σ and π:

$$V^L_{\rm eff}(\sigma,\pi) = \frac{\langle H\rangle}{N_s N} = \frac{g_x^2}{2}\sigma^2 + \frac{g_y^2}{2}\pi^2 - \int_{-\pi}^{\pi}\frac{{\rm d}k}{2\pi}\sqrt{4\sin^2(k/2) + g_x^4\sigma^2\cos^2(k/2) + g_y^4\pi^2}\,, \tag{3.15}$$

where N_s is the number of lattice sites. In contrast to the continuum effective potential in eq. (3.5), the lattice effective potential is never invariant under continuous chiral rotations, i.e. rotations in the (σ,π) plane. As we will now argue, this has some non-trivial implications.

JHEP06(2022)019

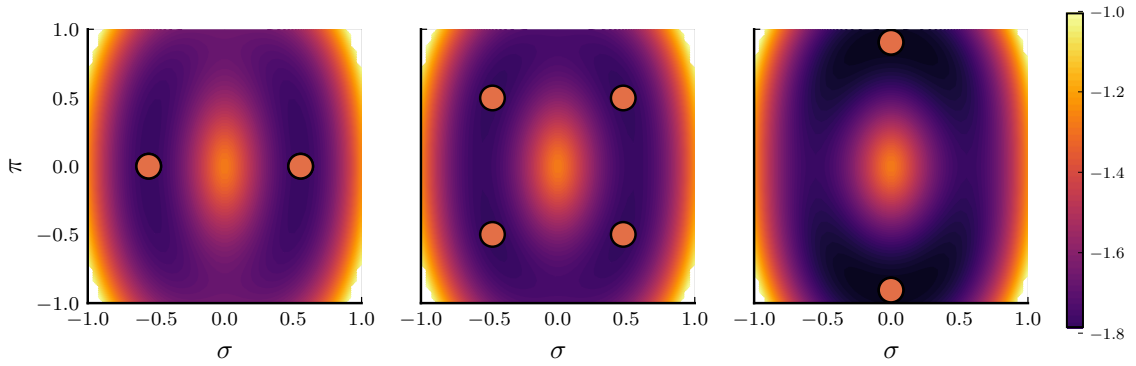

Figure 1. *(The colorscale and y-axis is the same for all three figures).* The effective potential $V_{\text{eff}}(\sigma, \pi)$ of the lattice model as a function of σ and π for three different combinations of the coupling constants. All figures have $g_x^2 = 6.0$ but g_y^2 is taken from 2.6 to 2.8 and finally to 3.2. These couplings are chosen so that the leftmost figure sits in the bond density wave phase, where the effective potential has two minima with nonzero σ. The second figure represents the coexistence region where both order parameters are nonzero. Note that in this coexistence region the effective potential is close to spherically symmetric even this far away from the continuum limit. Finally, we show the effective potential for a value of g_y^2 where the minima are found for nonzero π and the groundstate has a sublattice-polarized fermion occupation.

Most notably, we will find that the absence of continuous chiral symmetry leads to a different mean-field phase diagram on the lattice as in the continuum.

For $g_x^2 \gg g_y^2$, V_{eff}^L is shown in the left panel of figure 1, where we find two mimima along the $\pi = 0$ axis. Increasing g_y^2 eventually brings us into a coexistence region where both σ and π are non-zero, corresponding to four distinct minima in the effective potential as shown in the central panel of figure 1. Further increasing g_y^2 gradually moves the four minima towards the $\sigma = 0$ axis and eventually causes them to merge in pairs on said axis. The resulting mean-field phase diagram is shown in figure 2. In figure 3, we plot both σ and π along a cut of constant $g_x^2 = 6$. This plot clearly shows the coexistence region where both σ and π are non-zero. Fig. 3 also reveals that both σ and π change continuously as a function of g_y^2, which implies that the coexistence region is bounded by two mean-field Ising transitions.

In the second panel of figure 3 we plot the width of the coexistence region along g_y^2 as a function of g_x^2. Interestingly, we find that this width becomes extremely narrow for small couplings. In particular, the width decays exponentially according to $\Delta g_y^2 \propto g_x^2 e^{-2\pi/g_x^2}$. This suggests that fluctuations beyond mean-field theory can have a non-trivial effect on the phase diagram. Generically, the only effect of fluctuations on a continuous mean-field transition consists of slightly shifting the location of the transition and changing the critical exponents. Here, however, because we have two mean-field transitions that are exponentially close to each other in parameter space, it is conceivable that quantum fluctuations can cause them to merge into a single transition. One reason to expect this is that quantum fluctuations generically tend to restore the symmetry and thus increase the extent of the

JHEP06(2022)019

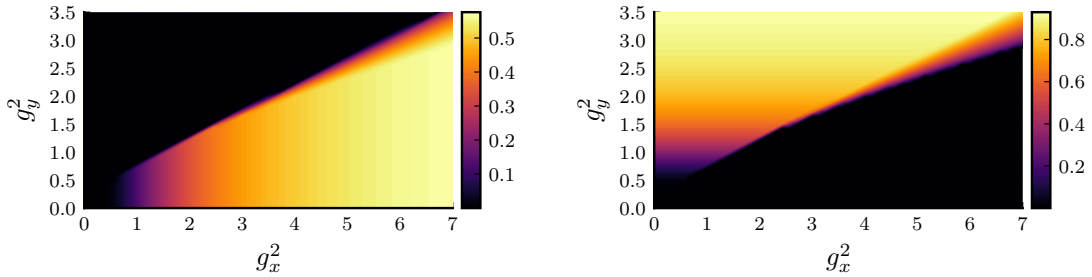

Figure 2. The value of the order parameters σ (left) and π (right) that minimize the large-N effective potential $V_{\text{eff}}^{L}(\sigma, \pi)$ as a function of the two couplings g_x^2 and g_y^2.

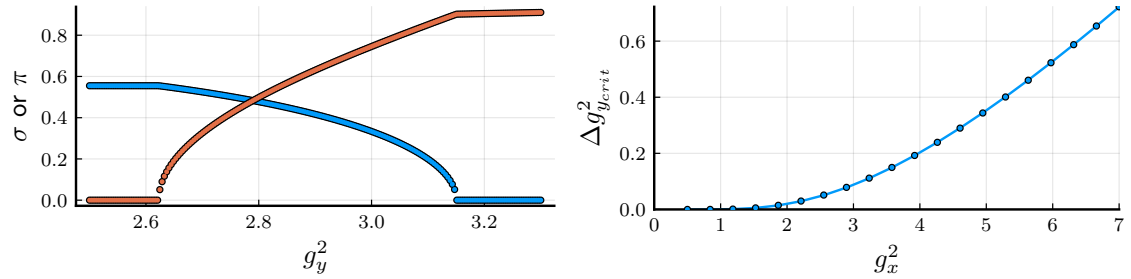

Figure 3. The left panel depicts the behavior of the order parameters σ and π throughout the phase transitions for fixed $g_x^2 = 6$. Here we can clearly see that there is a coexistence phase where both order parameters are nonzero. The right panel plots the width of this coexistence region as a function of g_x^2. The fitted curve is of the form $\Delta g_y^2 \propto g_x^2 \exp(-2\pi/g_x^2)$.

symmetric (i.e. disordered) phase in favor of the symmetry broken phase. Applied to our setting, this implies that the two phase boundaries of the coexistence region, which are already exponentially close in mean-field theory, will be pushed even closer together by the quantum fluctuations. In the following section, we will simulate the $N = 2$ GGN model with MPS and show that the coexistence region indeed disappears in favor of a direct continuous transition.

To summarize, we have found that, although a large-N or mean-field analysis can be used to correctly capture the physics of dynamical mass generation in the GN model (both in the continuum and on the lattice), near the line with continuous chiral symmetry one is nevertheless forced to go beyond mean-field theory. In the continuum, quantum fluctuations are necessary to restore the broken continuous chiral symmetry, whereas on the lattice these same fluctuations are required to merge the two mean-field Ising transitions into a single $c = 1$ CFT. It is interesting that even though the quantum fluctuations play a different physical role in the continuum and on the lattice, they ultimately give rise to the same physics.

4 Matrix product state simulations at $N = 2$

This section presents the results of our numerical simulations of the $N = 2$ GGN model with tensor networks. We use matrix product states (MPS) [38] as a variational class of states for

JHEP06(2022)019

approximating the ground state of the lattice Hamiltonian in eq. (2.15) at different values for (g_x^2, g_y^2). More specifically, we work with infinite MPS with a two-site unit cell and use the VUMPS algorithm [39] to find a variationally optimal ground-state approximation directly in the thermodynamic limit. We have explicitly encoded the $\mathrm{SU}(2) \otimes \mathrm{U}(1)$ symmetry into the MPS tensors, allowing us to reach much higher accuracy.[4] The only approximation in our simulations comes from the finite MPS bond dimension D, which controls the amount of quantum fluctuations that are taken into account. The bond dimension D corresponds to a truncation of the Schmidt spectrum at a certain treshold ϵ along any cut in the MPS. In our simulations, we set this truncation threshold ϵ to a fixed value (which indirectly determines D), extract an effective length scale associated to this truncation [42, 43], and use this scale to extrapolate our results to the infinite-D limit. We estimate the error on the extrapolation as the change in its value when the highest bond dimension ground state is discarded from the extrapolation procedure. For more details concerning the numerical procedures, we refer to our previous paper, where we applied the same MPS techniques to the conventional GN model [35].

To get a first rough idea of the location of the phase transition for $N = 2$ we have scanned the parameter space using MPS with truncation error of the order $\epsilon \approx 10^{-4}$. The corresponding bond dimensions range from $D \sim 10$ for points far from criticality to $D \sim 120$ for points close to criticality. The resulting approximate phase diagram is shown in figure 4. We clearly find two large different regions characterized by either $\sigma = \langle \bar{\psi}\psi \rangle \neq 0$ and $\pi = \langle \bar{\psi} i\gamma_5 \psi \rangle = 0$ or $\sigma = 0$ and $\pi \neq 0$. For these low values of the MPS bond dimension, we also find a small coexistence region, where both expectation values are nonzero, in line with the lattice mean-field results from the previous section.

Let us now focus on a particular cut $g_y^2 = 0.77 - 1.94(g_x^2 - 1.96)$, indicated by the full white line in figure 4, through the phase transition and check whether the two mean-field Ising transitions and the coexistence region in between survive, or whether these transitions actually merge into a single continuous transition. In the left/right panel of figure 5 we respectively show the two order parameters/inverse correlation length $(1/\xi)$ as g_x^2 is tuned along the cut. To each of these quantities, we fit a power law and extract a value for the critical point, resulting in values $g_x^2 = 1.929$ (for σ), 1.930 (for π) and 1.929 (for $1/\xi$) that agree reasonably well, thus indicating a direct transition.

To further confirm the scenario of a direct transition, we now try to verify that, close to the critical line, we recover a compact boson theory in the infrared so that the transition has central charge $c = 1$. For compact bosons, the scaling dimensions of operators $e^{in\theta}$ are well known (see e.g. ref. [44]), and are given by $\Delta_n = \frac{n^2 K}{4}$. The scaling dimensions of the operators relevant to our discussion, i.e. the operator driving the phase transition ($\cos 2\theta$) and the order parameters ($\cos\theta$ and $\sin\theta$), are respectively $\Delta_{\mathrm{pert}} = K$ and $\Delta_{\mathrm{order}} = K/4$. From this we find that the critical exponents for the correlation length ν and order parameter β are

$$\nu = \frac{1}{2 - K}\,, \qquad \beta = \frac{K}{8 - 4K}\,. \tag{4.1}$$

[4] Our implementation of the MPS algorithms can be found in the Julia package "MPSKit.jl" [40], whereas the (non-abelian) symmetric tensor operations are performed using the "TensorKit.jl" [41] package.

JHEP06(2022)019

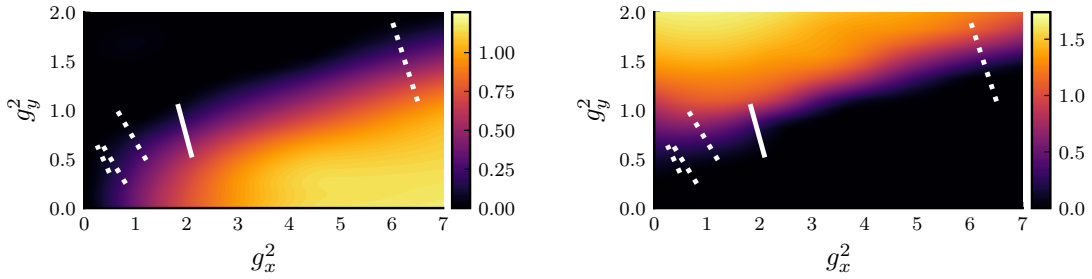

Figure 4. The phase diagram as computed with infinite MPS with truncation error $\epsilon \approx 10^{-4}$. We show the expectation value of the σ (left) and π (right) order parameters as a function of g_x^2 and g_y^2. The full white line indicates the cut that we will analyse in detail below, the dotted lines depict lines we used to study the scaling of K towards the continuum limit.

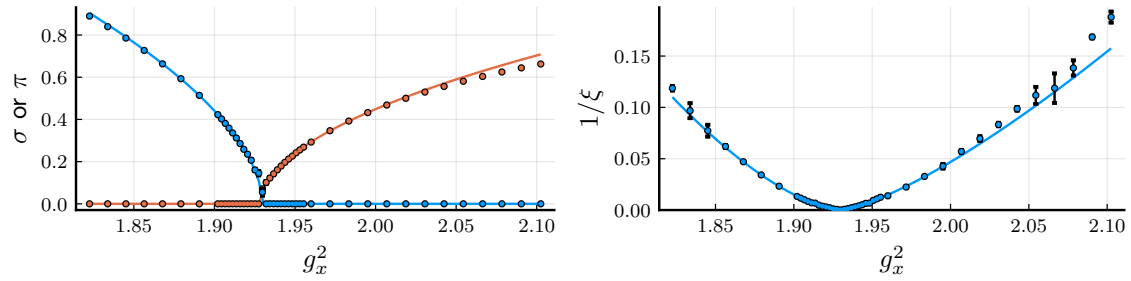

Figure 5. (Left) The extrapolated order parameters σ and π (plotted in orange and blue respectively) as g_x^2 and g_y^2 are tuned to take us trough the transition along $g_y^2 = 0.77 - 1.94(g_x^2 - 1.96)$. (Right) The extrapolated inverse correlation length for the same couplings. The highest bond dimensions used for these simulations are of the order 1100. The continuous lines represent four independent power-law fits to the numerical data (for σ, π, and for both sides of ξ^{-1} separately).

Using these relations, we obtain four different estimates for K at the point $(g_x^2, g_y^2) \approx (1.93, 0.83)$, corresponding to the critical exponents ν for both order parameters and two critical exponents for the correlation length, i.e. one for either side of the phase transition. The four values for K we obtain in this way are respectively $K = 1.351$, 1.381, 1.351 and 1.267, and agree reasonably well with each other.

Finally, we note that extracting K via the scaling of the order parameter or correlation length is numerically very costly due to the fact that we need many data points close to the transition to accurately fit the critical exponents. Alternatively, we can also obtain K directly from the two-point function of the operators $e^{i\theta} = \frac{\sigma + i\pi}{\sqrt{\sigma^2+\pi^2}}$ at the critical line, which at large distances should fall off as

$$\langle e^{i\theta(x)} e^{-i\theta(x')} \rangle \sim \frac{1}{|x - x'|^{K/2}} \,. \tag{4.2}$$

In the left panel of figure 6 the two-point function of the data point closest to the extrapolated critical coupling $(g_x^2, g_y^2) \approx (1.93, 0.83)$ is shown. The different colors correspond to decreasing values of the MPS truncation threshold. We have fitted a power law to the data with the highest bond dimension, and find a value $K \approx 1.257$, again consistent with the previous methods.

JHEP06(2022)019

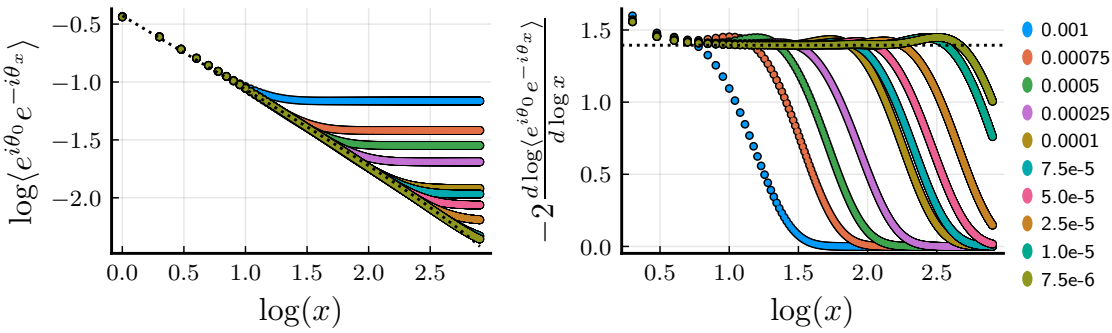

Figure 6. (Left) The two-point correlator of the $e^{i\theta}$ field at transition for the data point closest to the transition i.e. $(g_x^2, g_y^2) \approx (1.93, 0.83)$. The exponent for the fitted decay is $K \approx 1.257$ consistent with all previous estimates. (Right) The logarithmic derivative of the two point function, using a finite difference estimator of the data in the left panel. For the larger bond dimensions we see a plateau spanning over roughly 80 sites; the value of this plateau coincides with K. In both figures the different colors correspond to decreasing values of the MPS truncation threshold, which are shown on the right.

In order to make the algebraic decay more clear from the MPS data, in the right panel of figure 6 we show the logarithmic derivative of the two-point function, i.e.

$$\eta(x) := -2\frac{\mathrm{d}\left(\log|\langle e^{i\theta(0)}e^{-i\theta(x)}\rangle|\right)}{\mathrm{d}\log x}\,, \tag{4.3}$$

where again the different colored points correspond to increasing bond dimensions. For the smallest bond dimensions $\eta(x)$ is monotonically decreasing, corresponding to faster than algebraic decay. However, for the larger bond dimensions we can clearly identify a range where $\eta(x)$ is constant, corresponding to a range of algebraic decay; the value for K can now simply be read off as the value of $\eta(x)$ at the plateau. We estimate the error for K by considering the standard deviation σ_K away from the plateau value η_p, i.e. $\sigma_K^2 = \langle(\eta(x) - \eta_p)^2\rangle$, calculated using the data points near the centre of the plateau. Using the plateau in $\eta(x)$ obtained at the largest bond dimensions, we find $K = 1.3944 \pm 0.0006$. Note that the value for K extracted from $\eta(x)$ ($K = 1.394$) is slightly different from the value we previously obtained via the direct fit in the leftmost plot of figure 6 ($K = 1.257$). The value obtained from $\eta(x)$ is less prone to fitting errors, and it also agrees better with the previous estimates for K based on the scaling behaviour of the order parameters and the correlation length.

Finally, to establish a critical continuum limit we need to study the running of K as we move towards $g_x^2 = g_y^2 = 0$ along the critical line. To do this, we studied four additional cuts $g_y^2 = 1.47 - 1.65(g_x^2 - 6.25)$, $g_y^2 = 0.81 - (g_x^2 - 0.81)$, $g_y^2 = 0.49 - (g_x^2 - 0.49)$ and $g_y^2 = 0.42 - (g_x^2 - 0.42)$, indicated by the dotted white lines in figure 4. For these cuts, we first estimate the position of the critical point from low bond dimension MPS calculations of the order parameters, and then estimate K by identifying the plateaus at the transition point. These plateaus, and the respective estimates for K, are shown in figure 7 and

JHEP06(2022)019

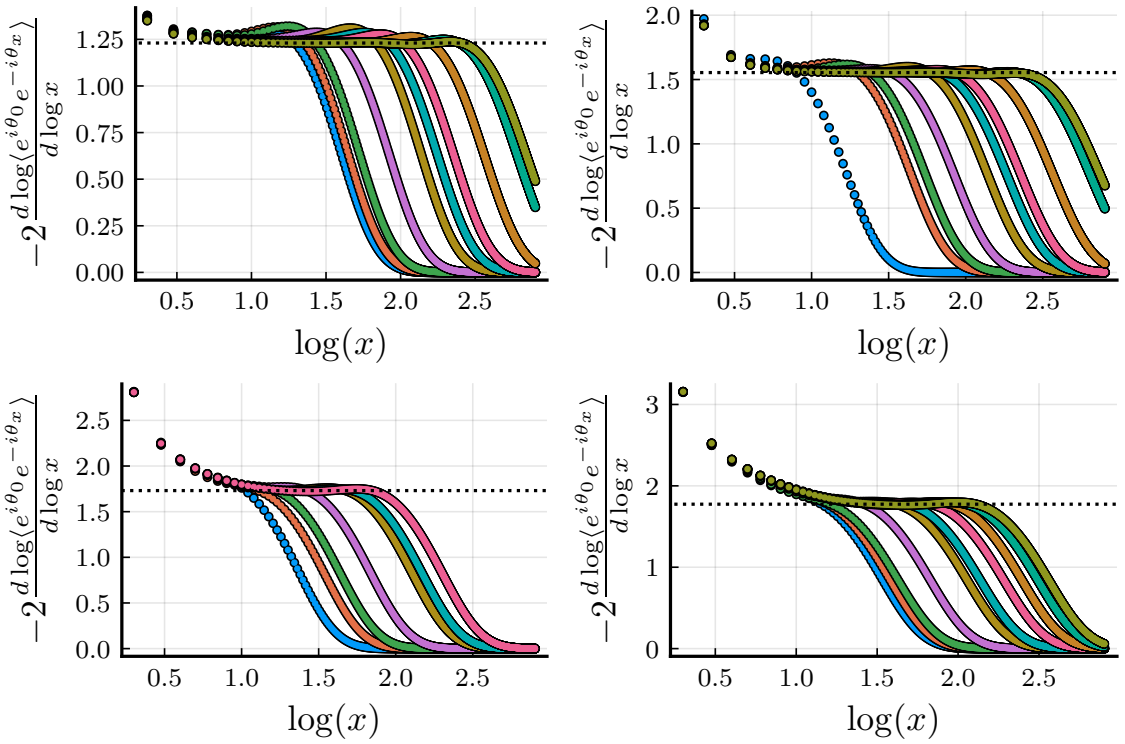

Figure 7. The logarithmic derivative of the two-point function for various points $(g_x^2, g_y^2) \approx (6.22, 1.52)$ top-left, $(1.05, 0.57)$ top-right, $(0.56, 0.42)$ bottom-left and $(0.47, 0.37)$ bottom-right, close to the phase transition. The dotted lines indicate the value of the plateau and the corresponding extrapolated value of K. The bond dimensions used in these simulations range up to 2500 for the $g_x^2 \approx 0.47$ point. *The color coding is the same as in figure 6.*

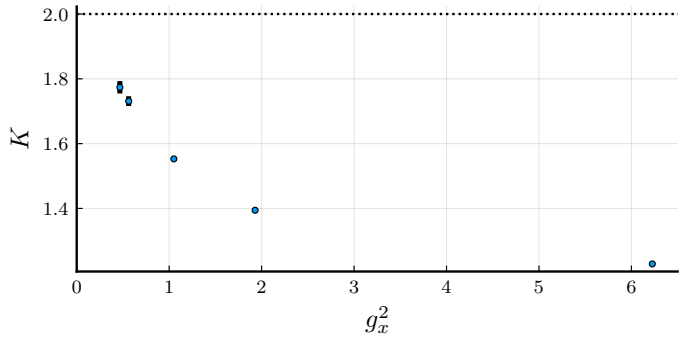

Figure 8. The running Luttinger parameter K as a function of the coupling g_x^2. We also show the error measure σ_K as defined in the text. The dotted line indicates the expected continuum behaviour and for sufficiently small couplings we see a clear trend towards this line.

figure 8 respectively. For sufficiently small values of (g_x^2, g_y^2) we find a clear trend towards $K = 2$, indicating that the continuum limit of our lattice model along the critical line is consistent with the bosonized QFT description of the chiral Gross-Neveu model discussed in section 2.2.

JHEP06(2022)019

5 The chiral GN model as a Landau-forbidden phase transition

In the previous section, we have shown that we can recover the behavior of the continuum GGN model at $N = 2$ on the lattice, despite the absence of an exact microscopic continuous chiral symmetry. In this section, we will interpret this result from a condensed matter point of view, and discuss the connection to Landau-forbidden phase transitions.

We will again focus on the region of parameter space close to where we recover the chiral GN model. The IR physics is then described by the compact boson action in eq. (2.10). The discrete symmetries of the GGN model that act non-trivially on the compact boson θ, as discussed in section 2.1, are:

$$\mathbb{Z}_2^{\mathcal{D}} : \theta \to \theta + \pi \tag{5.1}$$

$$\mathbb{Z}_2^{\mathcal{C}} : \theta \to -\theta \tag{5.2}$$

$$\mathbb{Z}_2^{\mathcal{R}} : \theta \to -\theta. \tag{5.3}$$

The value of K in eq. (2.10) is such that the $\cos 2\theta$ operator is relevant, which means that the IR fixed point is indeed a compact boson only when $\delta = 0$. For $\delta > 0$, the cosine term will pin θ to either $\pi/2$ or $-\pi/2$, such that $\mathbb{Z}_2^{\mathcal{D}}$, $\mathbb{Z}_2^{\mathcal{C}}$ and $\mathbb{Z}_2^{\mathcal{R}}$ are all spontaneously broken. However, for $\delta > 0$ the ground states are still symmetric under the products $\mathcal{DR}$ and $\mathcal{DC}$ (which act non-trivially on θ). For $\delta < 0$, the cosine term will pin θ to either 0 or π, in which case $\mathbb{Z}_2^{\mathcal{D}}$ is spontaneously broken, but $\mathbb{Z}_2^{\mathcal{C}}$ and $\mathbb{Z}_2^{\mathcal{R}}$ are preserved.

On the lattice, the reflection operator $\mathcal{R}$ corresponds to a *bond-centered* reflection $\mathcal{R}_B$ (which also includes an on-site action), as discussed in section 2.3. The $\mathcal{DR}$ symmetry, on the other hand, is realized on the lattice as a *site-centered* reflection $\mathcal{R}_S$, i.e. the reflection center now coincides with a lattice site. These two different reflection operators are related by $\mathcal{R}_S = \mathcal{T}\mathcal{R}_B$, where $\mathcal{T}$ is the translation operator, which is consistent with the fact that the latter implements the discrete chiral symmetry on the lattice. The bond-centered reflection symmetry $\mathcal{R}_B$ is broken when $\delta > 0$ ($\pi = \langle\bar{\psi} i\gamma_5 \psi\rangle \neq 0$), and is preserved when $\delta < 0$ ($\sigma = \langle\bar{\psi}\psi\rangle \neq 0$). For the site-centered inversion symmetry, the converse is true, i.e. $\mathcal{R}_S$ is preserved when $\delta > 0$, and broken when $\delta < 0$. That the two different gapped phases indeed respect either the bond- or site-centered reflection symmetry can also be understood intuitively from the fixed-point, i.e. zero correlation length, representatives of these two phases. This is shown schematically in figure 9.

The above discussion brings us to the interesting conclusion that the chiral GN model can be interpreted as a continuous phase transition between two gapped phases which break different global symmetries. According to the standard Landau theory of phase transitions, such a continuous transition should be a fine-tuned or multi-critical point, which can only be realized by tuning two independent relevant parameters to zero. Here, we find that this is not the case, and we can go between the two symmetry-broken phases via a single continuous transition, by tuning a single parameter. A natural question is thus what is special about our model that makes a direct transition generic and not fine-tuned. As we will now argue, it is the 't Hooft anomaly which places the GGN model outside the standard Landau theory.

JHEP06(2022)019

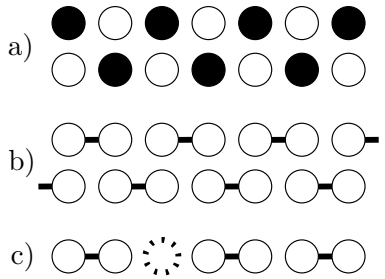

Figure 9. A cartoon picture of zero correlation length representatives of the two symmetry broken phases. a) represents the two charge density waves that occur for large g_y^2 ($\pi \neq 0$). Full/empty dots represent filled/empty sites. b) represents the two different ground states with bond order for large g_x^2 ($\sigma \neq 0$). The connected dots represent the dimerized states $(|10\rangle + |01\rangle)/\sqrt{2}$ in the fermion occupation basis. c) represents a kink in the σ condensate. Imposing inversion symmetry around the central site automatically breaks all possible inversion symmetries around bonds, which ensures that any such defect nucleates a non-zero value of the π order parameter.

On the lattice, the 't Hooft anomaly between the $\mathbb{Z}_2^{\mathcal{D}}$ and the U(1) charge symmetry is known as the 'Lieb-Schultz-Mattis' (LSM) theorem [13–15]. It states that at half-filling, the lattice Hamiltonian can only be gapped if either the charge U(1) or the translation symmetry is broken. Note that in our case, with $N = 2$ flavors of fermions per site, half filling actually implies that we have one unit of charge per lattice site. We thus also need to invoke the SU(2) flavor symmetry to argue that the average charge is 1/2 per flavor per site. The LSM theorem then states that a gapped ground state implies that either charge, flavor or translation symmetry are broken. In $1+1$ dimensions, we know from the CHMW theorem that the continuous charge and flavor symmetries cannot be broken spontaneously, so every gapped phase must necessarily break translation symmetry. Let us now assume that we are in a gapped phase where $\mathcal{R}_S$ is broken. A general mechanism to restore the $\mathcal{R}_S$ symmetry is to condense the kink or domain wall excitations. However, because of the relation $\mathcal{R}_S = \mathcal{T}\mathcal{R}_B$, and from the fact that $\mathcal{T}$ must be broken, we conclude that restoring the $\mathcal{R}_S$ symmetry must necessarily imply that we break the $\mathcal{R}_B$ symmetry (assuming that we transition to a gapped phase). This means that condensing the kink excitations must simultaneously *restore* the $\mathcal{R}_S$ symmetry, and *break* the $\mathcal{R}_B$ symmetry. We thus conclude that the 't Hooft anomaly must endow the kink excitations with a special property that their condensation triggers the spontaneous breaking of $\mathcal{R}_B$. In figure 10, we plot the large-N mean-field solution for the ground state of the lattice model with twisted boundary conditions, such that the ground state contains a single kink in the σ order parameter. Near the center of the kink, we see that the π order parameter becomes non-zero, such that condensing these kinks will induce a uniform non-zero value for the π order parameter, signaling a spontaneous breaking of $\mathcal{R}_B$.

Finally, let us comment on the role of the $\mathbb{Z}_2^{\mathcal{C}}$ symmetry. It turns out that there is a further 't Hooft anomaly, i.e. a LSM obstruction on the lattice, between the charge and flavor symmetries, the $\mathcal{C}$ symmetry, and the $\mathcal{R}_S$ symmetry. As we show in the appendix, a ground state of a local and gapped Hamiltonian with an average charge of 1/2 per flavor and

JHEP06(2022)019

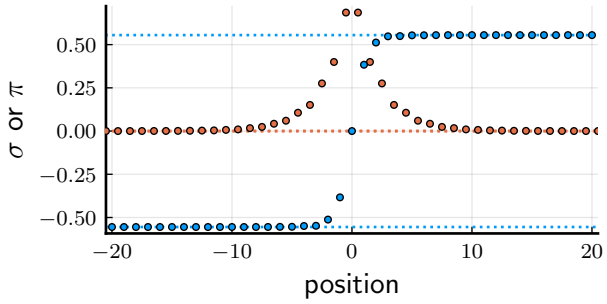

Figure 10. A site-dependent solution of the large-N self-consistency equations with antiperiodic boundary conditions for σ (blue), the orange points indicate the π order parameter. The couplings are $g_x^2 = 6.0$ and $g_y^2 = 2.3$ ie. in bond ordered phase but close to the transition. Note that the expectation value of π becomes nonzero near the domain wall in σ.

per site cannot be invariant under site-centered reflection symmetry. Because the charge and flavor symmetries cannot be broken due to the CHMW theorem, it thus follows that the $\mathbb{Z}_2^{\mathcal{C}}$ symmetry must be broken in the gapped phase which preserves $\mathcal{R}_S$, i.e. when $\delta > 0$ such that $\pi = \langle \bar{\psi} i \gamma_5 \psi \rangle \neq 0$. We thus again arrive at the conclusion that kink condensation in the $\mathcal{C}$-broken (and also $\mathcal{R}_B$-broken) phase, which restores the charge conjugation symmetry, must necessarily induce $\mathcal{R}_S$ breaking if we are to transition to a gapped phase.

The above discussion of course does not imply that in the presence of the 't Hooft anomalies, there is necessarily a direct continuous transition between a gapped phase with broken $\mathcal{R}_S$ symmetry and a gapped phase with broken $\mathcal{R}_B$ symmetry. It is always possible to have 1) an intermediate region of coexistence where both symmetries are broken, 2) an intermediate gapless region where both symmetries are restored, or 3) a first order transition between the two phases. The 't Hooft anomalies only provide us with a mechanism to explain why a direct continuous transition, if it occurs, is not fine-tuned. This is similar to how the Lieb-Schultz-Mattis theorem is used to motivate the 'deconfined quantum critical points' [45, 46], which are a special type of Landau-forbidden continuous phase transitions in $2+1$-dimensional lattice spin models [47].

6 Conclusion

In this work we have studied the GGN model on the lattice. In discretizing the GGN model, particular attention was paid to maintaining the maximal amount of global symmetries of the continuum theory. The lattice model used here only fails to preserve the $\mathrm{O}(2N)$ symmetry along the line with $g_x^2 = 0$, and the continuous chiral symmetry, which is present when $g_x^2 = g_y^2$. The latter symmetry has a 't Hooft anomaly, and plays a crucial role in determining the phase diagram of the continuum model. In large-N or mean-field theory, we found that the broken continuous chiral symmetry results in a coexistence region where both $\langle \bar{\psi} \psi \rangle$ and $\langle \bar{\psi} i \gamma_5 \psi \rangle$ are non-zero. Interestingly, the width of this coexistence region decreases exponentially with the couplings. To go beyond mean-field theory, we have simulated the $N = 2$ lattice GGN model with MPS. We found that the effect of quantum fluctuations beyond mean-field theory is to remove the coexistence region completely, and replace it with

JHEP06(2022)019

a single continuous transition between the phase with $\langle\bar{\psi}\psi\rangle \neq 0$ and $\langle\bar{\psi}i\gamma_5\psi\rangle = 0$, and the phase with $\langle\bar{\psi}\psi\rangle = 0$ and $\langle\bar{\psi}i\gamma_5\psi\rangle \neq 0$. The critical line is described by a single compact boson CFT, which is the IR fixed point of the chiral GN model. Although on the lattice the critical line is no longer a straight line under 45° in the $g_x^2 - g_y^2$ plane (as is the line with continuous chiral symmetry in the continuum model), we found from our MPS simulations that the scaling behaviour of the chiral condensates $\langle\bar{\psi}\psi\rangle$ and $\langle\bar{\psi}i\gamma_5\psi\rangle$ away from the critical line is the same as that predicted by the continuum theory. We have also interpreted the lattice phase diagram from a condensed matter perspective, and explained how the chiral GN model can be recognized as a 'Landau-forbidden' phase transition (similar to the deconfined quantum critical point in $2+1$ dimensions) which is not fine-tuned because of the presence of *two* different 't Hooft anomalies, or Lieb-Schultz-Mattis theorems on the lattice.

This type of continuous transition has been discussed before in the condensed matter literature. Indeed, on the lattice the chiral condensates $\langle\bar{\psi}\psi\rangle$ and $\langle\bar{\psi}i\gamma_5\psi\rangle$ are the order parameters for respectively a bond order density wave or a 'Valence Bond State' (VBS) and a 'Charge Density Wave' (CDW). The VBS breaks the site-centered reflection symmetry, but preserves the bond-centered reflection and charge-conjugation symmetries. For the CDW, the situation is reversed, i.e. it preserves the site-centered reflection symmetry, but breaks the bond-centered reflection and charge-conjugation symmetries. Haldane has found a similar transition in a study of the phase diagram of the antiferromagnetic XXZ chain with next-nearest-neighbour interactions [48] (in the spin language, the CDW corresponds to antiferromagnetic or Néel order). This model is closely related to the $N = 1$ GGN model, and it was recently discussed in more detail and generalized in ref. [49]. In ref. [50], the authors studied the phase diagram of the one-dimensional half-filled Hubbard model with an additional nearest-neighbour repulsive interaction using quantum Monte Carlo, and again evidence for a direct continuous transition between a VBS and CDW was found. Because the authors of [50] considered spinful fermions, their Hubbard model is closely related to the $N = 2$ GGN model, although the two interaction terms used in ref. [50] are different from the ones we obtained here by directly discretizing the continuum GGN model. Another place where a direct continuous transition between VBS and CDW phases has been found (again using quantum Monte Carlo) is the Su-Schrieffer-Heeger model [51]. This is a model of fermions hopping on a chain coupled to phonons, and its connections to the GN model were discussed early on in ref. [52]. The work presented here makes the connection between the continuous VBS-CDW transition and the GGN model more explicit, as we start by directly discretizing the continuum action of the GGN model. In contrast to the above mentioned previous studies of the VBS-CDW transition, we have also emphasized the importance of two different Lieb-Schultz-Mattis theorems for obtaining a direct continuous transition. Recently, the authors of ref. [53] have constructed a spin Hamiltonian which was shown [54] to exhibit a direct continuous transition between a VBS phase and an Ising ferromagnet phase. The different Lieb-Schultz-Mattis theorems present in this spin model and their importance for the Landau-forbidden phase transition were also discussed in great detail [53].

In the future, it will be interesting to generalize our numerical results to the GGN model with an odd number of Majorana fermions, in which case the kinks bind an odd number of

JHEP06(2022)019

Majorana zero modes [55] and transform as isospinors under the SO($\tilde{N}$) symmetry group, where $\tilde{N}$ counts the number of Majorana fermions [56]. To simulate these kinks with MPS, one can make use of the results of ref. [57], where it was explained how Majorana zero modes are realized in tensor network states. Another interesting direction is of course to generalize our results to 2+1 dimensional systems, where discretizing a continuum theory with 't Hooft anomalies might provide a route to construct lattice models with a deconfined quantum critical point. Such a construction is highly desirable, as there is currently no conclusive proof for the existence of a direct phase transition between two different symmetry-broken phases in 2+1 dimensions, despite an impressive numerical effort [58–70].

Acknowledgments

We acknowledge valuable discussions with Erez Zohar, Mike Zaletel, and Bram Vanhecke. This work has received funding from the European Research Council (ERC) under the European Unions Horizon 2020 research and innovation programme (grant agreements No 715861 (ERQUAF)), and from Research Foundation Flanders (FWO) via grant GOE1520N and postdoctoral fellowships of LV and NB.

A Lieb-Schultz-Mattis obstructions from charge and flavor symmetries, charge conjugation and site-reflection symmetry

In this appendix we show that there exists a Lieb-Schultz-Mattis (LSM) obstruction (i.e. a 't Hooft anomaly on the lattice) in the presence of charge, flavor, $\mathcal{C}$ and $\mathcal{R}_S$ symmetry. In particular, we will show that there cannot exist a quantum state which simultaneously satisfies the following two properties: 1) it is the ground state of a local and gapped Hamiltonian describing a quantum many-body system on a one-dimensional lattice, and 2) it respects all the symmetries mentioned above. To show this, we will rely on the fact that the ground state of every local Hamiltonian with an energy gap can be approximated by an injective[5] finite-bond dimension MPS to arbitrary precision [71, 72]. So, it remains to prove that there cannot exist an injective MPS which respects the charge and flavor symmetries, the charge conjugation symmetry and the site-centered reflection symmetry. Our proof will make heavy use of the 'fundamental theorem of MPS' [73], which allows us to express the global symmetry properties of MPS's in terms of local conditions on the constituent tensors.

Recall that the gapped phases of interest in this work break translation over a single lattice site (which is the lattice version of the discrete chiral symmetry, so it must be broken in the gapped phases). Because our system has a two-site unit cell, we need two different rank-three tensors $[A_1]^i_{\alpha\beta}$ and $[A_2]^i_{\alpha\beta}$ to construct the MPS (we call i the physical index of the MPS tensor, and α and β the virtual indices). Concretely, the MPS's we are interested

[5] The injectivity property is a technical condition on MPS tensors which we only mention for completeness in this work — we will not define it in detail. It suffices to mention that the injectivity condition is physically equivalent to the requirement that the MPS is not a macroscopic superposition or a so-called 'cat state'.

JHEP06(2022)019

in take the form

$$|\psi\rangle = \lim_{L\to\infty} \sum_{\{i_j\}} \langle v|A_1^{i_1} A_2^{i_2} A_1^{i_3} A_2^{i_4} \cdots A_1^{i_{2L-1}} A_2^{i_{2L}}|v\rangle |i_1, i_2, i_3, i_4, \cdots, i_{2L-1}, i_{2L}\rangle \,, \tag{A.1}$$

where the states $|i_j\rangle$ are a basis for the local Hilbert space on site j. For injective MPS, the effect of the choice of boundary vector $|v\rangle$ decays exponentially away from the edge, such that in the limit $L \to \infty$, the state is independent of $|v\rangle$.

We now use the fact that we can combine the total charge U(1) and flavor SU(2) symmetry in order to apply separate U(1) transformations on the two flavors (i.e. the total charge combined with the diagonal elements from SU(2)). We henceforth refer to this as the charge and flavor U(1) symmetries. The fundamental theorem now implies that an injective MPS of the form in eq. (A.1) can only be invariant under the charge and flavor U(1) symmetry if the following relations hold [73, 74]:

$$\sum_j \left[U_c(\theta)\right]_{ij} A_1^j = e^{iq_1\theta} V(\theta) A_1^i \tilde{V}(\theta)^\dagger \tag{A.2}$$

$$\sum_j \left[U_c(\theta)\right]_{ij} A_2^j = e^{iq_2\theta} \tilde{V}(\theta) A_2^i V(\theta)^\dagger \,, \tag{A.3}$$

where $U_c(\theta)$ is the local unitary symmetry action corresponding to a U(1) rotation over an angle θ on flavor c, and $V(\theta)$ and $\tilde{V}(\theta)$ are invertible matrices acting on the virtual indices, which without loss of generality can be taken to be unitary matrices [73]. It is straightforward to see that eqs. (A.2) and (A.3) are sufficient for the MPS in eq. (A.1) to be invariant under the U(1) symmetries. The fact that these local conditions are also necessary is not obvious, but has been proven rigorously in the MPS literature [73, 74].

Similarly, the fundamental theorem also implies that the MPS in eq. (A.1) is invariant under the charge conjugation and site-centered reflection symmetries iff the following relations are true [73, 74]:

$$\sum_j \left[M_C\right]_{ij} A_1^j = (-1)^{n_1} C A_1^i \tilde{C}^\dagger \tag{A.4}$$

$$\sum_j \left[M_C\right]_{ij} A_2^j = (-1)^{n_2} \tilde{C} A_2^i C^\dagger \tag{A.5}$$

$$\sum_j \left[M_R^1\right]_{ij} \left[A_1^j\right]^T = (-1)^{m_1} R A_1^i \tilde{R}^{-1} \tag{A.6}$$

$$\sum_j \left[M_R^2\right]_{ij} \left[A_2^j\right]^T = (-1)^{m_2} \tilde{R} A_2^i R^{-1} \,, \tag{A.7}$$

where $n_i, m_i \in \{0, 1\}$, and M_C and M_R^i are the local unitary matrices respectively implementing the charge conjugation symmetry and site-centered reflection symmetry on the physical indices; for our specific model the on-site action depends on the site (even or odd). Furthermore, the site-centered reflection also transposes the MPS matrices as a result of the reordering of the lattice sites. The matrices C, $\tilde{C}$, R and $\tilde{R}$ are invertible, and C and $\tilde{C}$ can without loss of generality be taken to be unitary.

JHEP06(2022)019

To start our proof, we first note that the U(1) symmetries and the charge conjugation satisfy the following commutation relation:

$$M_C U_c(\theta) = e^{i\theta} U_c(-\theta) M_C \tag{A.8}$$

Using this relation, we can evaluate $\sum_j \left[M_C U(\theta)\right]_{ij} A_1^j$ and $\sum_j \left[M_C U(\theta)\right]_{ij} A_2^j$ in two different ways. The first way gives us

$$\sum_j \left[M_C U(\theta)\right]_{ij} A_1^j = (-1)^{n_1} e^{iq_1\theta} \left(V(\theta)C\right) A_1^i \left(\tilde{V}(\theta)\tilde{C}\right)^\dagger \tag{A.9}$$

$$\sum_j \left[M_C U(\theta)\right]_{ij} A_2^j = (-1)^{n_2} e^{iq_2\theta} \left(\tilde{V}(\theta)\tilde{C}\right) A_2^i \left(V(\theta)C\right)^\dagger \tag{A.10}$$

The second way of evaluating this expression leads to

$$\sum_j \left[M_C U(\theta)\right]_{ij} A_1^j = (-1)^{n_1} e^{i(1-q_1)\theta} \left(CV(-\theta)\right) A_1^i \left(\tilde{C}\tilde{V}(-\theta)\right)^\dagger \tag{A.11}$$

$$\sum_j \left[M_C U(\theta)\right]_{ij} A_2^j = (-1)^{n_2} e^{i(1-q_2)\theta} \left(\tilde{C}\tilde{V}(-\theta)\right) A_2^i \left(CV(-\theta)\right)^\dagger \tag{A.12}$$

For injective MPS, equating (A.9) and (A.10) with (A.11) and (A.12), tells us that the following conditions must hold:

$$V(\theta)C = e^{iq\theta} CV(-\theta) \tag{A.13}$$

$$\tilde{V}(\theta)\tilde{C} = e^{i\tilde{q}\theta} \tilde{C}\tilde{V}(-\theta) \tag{A.14}$$

$$q_1 = \frac{1 - q + \tilde{q}}{2} \tag{A.15}$$

$$q_2 = \frac{1 + q - \tilde{q}}{2} \tag{A.16}$$

At this point, we find it convenient to fix the phase of the matrices $V(\theta)$ and $\tilde{V}(\theta)$ by redefining them as $e^{-iq\theta/2}V(\theta) \to V(\theta)$ and $e^{-i\tilde{q}\theta/2}\tilde{V}(\theta) \to \tilde{V}(\theta)$ (note that this also implies $q_1 + q/2 - \tilde{q}/2 \to q_1$ and $q_2 - q/2 + \tilde{q}/2 \to q_2$), such that the above equations become

$$V(\theta)C = CV(-\theta) \tag{A.17}$$

$$\tilde{V}(\theta)\tilde{C} = \tilde{C}\tilde{V}(-\theta) \tag{A.18}$$

$$q_1 = q_2 = \frac{1}{2} \tag{A.19}$$

From these relations, we conclude that one of two situations is realized. Either $V(\theta)$ contains integer charges 0 and $\{Q, -Q\}$ ($Q \in \mathbb{N}^+$) and $\tilde{V}(\theta)$ contains half odd-integer charge pairs $\{q/2, -q/2\}$ ($q \in 2\mathbb{N}+1$), or $V(\theta)$ contains half odd-integer charge pairs and $\tilde{V}(\theta)$ contains integer charges.

For the final step in our proof we use that the reflection and U(1) symmetries commute:

$$M_R U_c(\theta) = U_c(\theta) M_R\,, \tag{A.20}$$

JHEP06(2022)019

and evaluate $\sum_j \left[U_c(\theta)M_R\right]_{ij}\left[A_1^j\right]^T$ in two different ways, similarly as before. Equating the two different outcomes now produces the following relations:

$$RV(\theta) = e^{iQ_R\theta}\tilde{V}^*(\theta)R \tag{A.21}$$

$$\tilde{R}\tilde{V}(\theta) = e^{iQ_R\theta}V^*(\theta)\tilde{R} \tag{A.22}$$

These equations imply that the charges of $V(\theta)$ are equal, up to a permutation, to the charges of $\tilde{V}(\theta)$ shifted by Q_R. If such a Q_R exists, then from our considerations above it follows that it should be a half odd-integer. However, it is not hard to see that the integer charges 0 and $\{Q, -Q\}$ cannot be obtained by shifting the half odd-integer charges $\{q/2, -q/2\}$ by some overall half odd-integer (provided that there are a finite number of charges, i.e. provided that the MPS bond dimension is finite). So we have arrived at an inconsistency, from which we conclude that there cannot exist an MPS which is invariant under all the symmetries.

References

[1] M. Creutz, *Quarks, gluons and lattices*, vol. 8, Cambridge University Press, Cambridge, U.K. (1983).

[2] I. Montvay and G. Münster, *Quantum fields on a lattice*, Cambridge University Press, Cambridge, U.K. (1997).

[3] H.J. Rothe, *Lattice gauge theories: an introduction*, World Scientific, Singapore (2012).

[4] M.C. Bañuls et al., *Simulating lattice gauge theories within quantum technologies*, *Eur. Phys. J. D* **74** (2020) 165 [arXiv:1911.00003] [INSPIRE].

[5] Y. Meurice, R. Sakai and J. Unmuth-Yockey, *Tensor field theory with applications to quantum computing*, arXiv:2010.06539 [INSPIRE].

[6] H.B. Nielsen and M. Ninomiya, *A no-go theorem for regularizing chiral fermions*, *Phys. Lett. B* **105** (1981) 219 [INSPIRE].

[7] J.B. Kogut and L. Susskind, *Hamiltonian Formulation of Wilson's Lattice Gauge Theories*, *Phys. Rev. D* **11** (1975) 395 [INSPIRE].

[8] G. 't Hooft, *Naturalness, chiral symmetry, and spontaneous chiral symmetry breaking*, *NATO Sci. Ser. B* **59** (1980) 135 [INSPIRE].

[9] X.-G. Wen, *Classifying gauge anomalies through symmetry-protected trivial orders and classifying gravitational anomalies through topological orders*, *Phys. Rev. D* **88** (2013) 045013 [arXiv:1303.1803] [INSPIRE].

[10] S.L. Adler, *Axial-vector vertex in spinor electrodynamics*, *Phys. Rev.* **177** (1969) 2426 [INSPIRE].

[11] J.S. Bell and R. Jackiw, *A PCAC puzzle: $\pi^0 \to \gamma\gamma$ in the σ model*, *Nuovo Cim. A* **60** (1969) 47 [INSPIRE].

JHEP06(2022)019

[12] D.J. Gross and A. Neveu, *Dynamical symmetry breaking in asymptotically free field theories*, *Phys. Rev. D* **10** (1974) 3235 [INSPIRE].

[13] E.H. Lieb, T. Schultz and D. Mattis, *Two soluble models of an antiferromagnetic chain*, *Annals Phys.* **16** (1961) 407 [INSPIRE].

[14] M.B. Hastings, *Lieb-Schultz-Mattis in higher dimensions*, *Phys. Rev. B* **69** (2004) 104431 [cond-mat/0305505] [INSPIRE].

[15] M. Oshikawa, *Commensurability, excitation gap, and topology in quantum many-particle systems on a periodic lattice*, *Phys. Rev. Lett.* **84** (2000) 1535.

[16] Y. Nambu and G. Jona-Lasinio, *Dynamical model of elementary particles based on an analogy with superconductivity. I*, *Phys. Rev.* **122** (1961) 345 [INSPIRE].

[17] Y. Nambu and G. Jona-Lasinio, *Dynamical model of elementary particles based on an analogy with superconductivity. II*, *Phys. Rev.* **124** (1961) 246 [INSPIRE].

[18] B. Berg and P. Weisz, *Exact S Matrix of the Chiral Invariant* SU(N) *Thirring Model*, *Nucl. Phys. B* **146** (1978) 205 [INSPIRE].

[19] M. Karowski and P. Weisz, *Exact Form-Factors in (1+1)-Dimensional Field Theoretic Models with Soliton Behavior*, *Nucl. Phys. B* **139** (1978) 455 [INSPIRE].

[20] A.B. Zamolodchikov and A.B. Zamolodchikov, *Factorized s Matrices in Two-Dimensions as the Exact Solutions of Certain Relativistic Quantum Field Models*, *Annals Phys.* **120** (1979) 253 [INSPIRE].

[21] N. Andrei and J.H. Lowenstein, *Diagonalization of the Chiral Invariant Gross-Neveu Hamiltonian*, *Phys. Rev. Lett.* **43** (1979) 1698 [INSPIRE].

[22] A.A. Belavin, *Exact solution of the two-dimensional model with asymptotic freedom*, *Phys. Lett. B* **87** (1979) 117 [INSPIRE].

[23] P.B. Wiegmann, *Exact solution for the* SU(N) *main chiral field in two dimensions*, *JETP Lett.* **39** (1984) 214 [INSPIRE].

[24] P. Forgács, S. Naik and F. Niedermayer, *The exact mass gap of the chiral Gross-Neveu model*, *Phys. Lett. B* **283** (1992) 282 [INSPIRE].

[25] S.R. Coleman, *There are no Goldstone bosons in two-dimensions*, *Commun. Math. Phys.* **31** (1973) 259 [INSPIRE].

[26] P.C. Hohenberg, *Existence of Long-Range Order in One and Two Dimensions*, *Phys. Rev.* **158** (1967) 383 [INSPIRE].

[27] N.D. Mermin and H. Wagner, *Absence of ferromagnetism or antiferromagnetism in one-dimensional or two-dimensional isotropic Heisenberg models*, *Phys. Rev. Lett.* **17** (1966) 1133 [INSPIRE].

[28] E. Witten, *Nonabelian Bosonization in Two-Dimensions*, *Commun. Math. Phys.* **92** (1984) 455 [INSPIRE].

[29] I. Affleck, *On the Critical Behavior of Two-dimensional Systems With Continuous Symmetries*, *Phys. Rev. Lett.* **55** (1985) 1355 [INSPIRE].

[30] I. Affleck, *Exact critical exponents for quantum spin chains, non-linear σ-models at $\theta = \pi$ and the quantum hall effect*, *Nucl. Phys. B* **265** (1986) 409 [INSPIRE].

JHEP06(2022)019

[31] V.G. Knizhnik and A.B. Zamolodchikov, *Current Algebra and Wess-Zumino Model in Two-Dimensions*, *Nucl. Phys. B* **247** (1984) 83 [INSPIRE].

[32] Y.K. Ha, *Symmetries in Bosonization*, *J. Phys. Conf. Ser.* **474** (2013) 012034 [arXiv:1402.5061] [INSPIRE].

[33] J.M. Kosterlitz, *The critical properties of the two-dimensional xy model*, *J. Phys. C* **7** (1974) 1046 [INSPIRE].

[34] J. Goldstone and F. Wilczek, *Fractional Quantum Numbers on Solitons*, *Phys. Rev. Lett.* **47** (1981) 986 [INSPIRE].

[35] G. Roose, N. Bultinck, L. Vanderstraeten, F. Verstraete, K. Van Acoleyen and J. Haegeman, *Lattice regularisation and entanglement structure of the Gross-Neveu model*, *JHEP* **21** (2020) 207 [arXiv:2010.03441] [INSPIRE].

[36] C.M. Caves, C.A. Fuchs and R. Schack, *Unknown quantum states: The quantum de finetti representation*, *J. Math. Phys.* **43** (2002) 4537.

[37] E. Witten, *Chiral Symmetry, the 1/n Expansion, and the SU(N) Thirring Model*, *Nucl. Phys. B* **145** (1978) 110 [INSPIRE].

[38] U. Schollwöck, *The density-matrix renormalization group in the age of matrix product states*, *Annals Phys.* **326** (2011) 96.

[39] V. Zauner-Stauber, L. Vanderstraeten, M.T. Fishman, F. Verstraete and J. Haegeman, *Variational optimization algorithms for uniform matrix product states*, *Phys. Rev. B* **97** (2018) 045145 [arXiv:1701.07035] [INSPIRE].

[40] M. Van Damme, G. Roose, M. Hauru and J. Haegeman, *MPSKit.jl*, https://github.com/maartenvd/MPSKit.jl.

[41] J. Haegeman, *TensorKit.jl*, https://github.com/Jutho/TensorKit.jl.

[42] M.M. Rams, P. Czarnik and L. Cincio, *Precise extrapolation of the correlation function asymptotics in uniform tensor network states with application to the bose-hubbard and xxz models*, *Phys. Rev. X* **8** (2018) 041033.

[43] B. Vanhecke, J. Haegeman, K. Van Acoleyen, L. Vanderstraeten and F. Verstraete, *Scaling Hypothesis for Matrix Product States*, *Phys. Rev. Lett.* **123** (2019) 250604 [arXiv:1907.08603] [INSPIRE].

[44] T. Giamarchi, *Quantum physics in one dimension*, Clarendon Press, Oxford, U.K. (2004).

[45] M. Levin and T. Senthil, *Deconfined quantum criticality and néel order via dimer disorder*, *Phys. Rev. B* **70** (2004) 220403.

[46] C. Wang, A. Nahum, M.A. Metlitski, C. Xu and T. Senthil, *Deconfined quantum critical points: symmetries and dualities*, *Phys. Rev. X* **7** (2017) 031051 [arXiv:1703.02426] [INSPIRE].

[47] T. Senthil, A. Vishwanath, L. Balents, S. Sachdev and M.P.A. Fisher, *Deconfined Quantum Critical Points*, *Science* **303** (2004) 1490 [cond-mat/0311326] [INSPIRE].

[48] F.D.M. Haldane, *Spontaneous dimerization in the $s = \frac{1}{2}$ heisenberg antiferromagnetic chain with competing interactions*, *Phys. Rev. B* **25** (1982) 4925.

[49] C. Mudry, A. Furusaki, T. Morimoto and T. Hikihara, *Quantum phase transitions beyond Landau-Ginzburg theory in one-dimensional space revisited*, *Phys. Rev. B* **99** (2019) 205153 [arXiv:1903.05646] [INSPIRE].

JHEP06(2022)019

[50] A.W. Sandvik, L. Balents and D.K. Campbell, *Ground state phases of the half-filled one-dimensional extended hubbard model*, *Phys. Rev. Lett.* **92** (2004) 236401.

[51] M. Weber, F. Parisen Toldin and M. Hohenadler, *Competing orders and unconventional criticality in the su-schrieffer-heeger model*, *Phys. Rev. Res.* **2** (2020) 023013.

[52] E. Fradkin and J.E. Hirsch, *Phase diagram of one-dimensional electron-phonon systems. i. the su-schrieffer-heeger model*, *Phys. Rev. B* **27** (1983) 1680.

[53] S. Jiang and O.I. Motrunich, *Ising ferromagnet to valence bond solid transition in a one-dimensional spin chain: Analogies to deconfined quantum critical points*, *Phys. Rev. B* **99** (2019) 075103 [arXiv:1808.07981] [INSPIRE].

[54] B. Roberts, S. Jiang and O.I. Motrunich, *Deconfined quantum critical point in one dimension*, *Phys. Rev. B* **99** (2019) 165143 [arXiv:1904.00010] [INSPIRE].

[55] P. Fendley and H. Saleur, *BPS kinks in the Gross-Neveu model*, *Phys. Rev. D* **65** (2002) 025001 [hep-th/0105148] [INSPIRE].

[56] E. Witten, *Some properties of the* $(\psi\psi)^2$ *model in two dimensions*, *Nucl. Phys. B* **142** (1978) 285 [INSPIRE].

[57] N. Bultinck, D.J. Williamson, J. Haegeman and F. Verstraete, *Fermionic matrix product states and one-dimensional topological phases*, *Phys. Rev. B* **95** (2017) 075108 [arXiv:1610.07849] [INSPIRE].

[58] A.B. Kuklov, M. Matsumoto, N.V. Prokof'ev, B.V. Svistunov and M. Troyer, *Deconfined Criticality: Generic First-Order Transition in the* SU(2) *Symmetry Case*, *Phys. Rev. Lett.* **101** (2008) 050405 [INSPIRE].

[59] F.-J. Jiang, M. Nyfeler, S. Chandrasekharan and U.-J. Wiese, *From an antiferromagnet to a valence bond solid: evidence for a first-order phase transition*, *J. Stat. Mech.* **2008** (2008) P02009.

[60] K. Chen, Y. Huang, Y. Deng, A.B. Kuklov, N.V. Prokof'ev and B.V. Svistunov, *Deconfined criticality flow in the Heisenberg model with ring-exchange interactions*, *Phys. Rev. Lett.* **110** (2013) 185701 [arXiv:1301.3136] [INSPIRE].

[61] A.W. Sandvik, *Evidence for deconfined quantum criticality in a two-dimensional Heisenberg model with four-spin interactions*, *Phys. Rev. Lett.* **98** (2007) 227202 [cond-mat/0611343] [INSPIRE].

[62] J. Lou, A.W. Sandvik and N. Kawashima, *Antiferromagnetic to valence-bond-solid transitions in two-dimensional* SU(n) *heisenberg models with multispin interactions*, *Phys. Rev. B* **80** (2009) 180414.

[63] A.W. Sandvik, *Continuous quantum phase transition between an antiferromagnet and a valence-bond-solid in two dimensions: evidence for logarithmic corrections to scaling*, *Phys. Rev. Lett.* **104** (2010) 177201 [arXiv:1001.4296] [INSPIRE].

[64] H. Shao, W. Guo and A.W. Sandvik, *Quantum criticality with two length scales*, *Science* **352** (2016) 213.

[65] P. Serna and A. Nahum, *Emergence and spontaneous breaking of approximate* $O(4)$ *symmetry at a weakly first-order deconfined phase transition*, *Phys. Rev. B* **99** (2019) 195110 [arXiv:1805.03759] [INSPIRE].

JHEP06(2022)019

[66] G.J. Sreejith, S. Powell and A. Nahum, *Emergent* SO(5) *symmetry at the columnar ordering transition in the classical cubic dimer model*, *Phys. Rev. Lett.* **122** (2019) 080601 [arXiv:1803.11218] [INSPIRE].

[67] S. Pujari, K. Damle and F. Alet, *Néel-state to valence-bond-solid transition on the honeycomb lattice: Evidence for deconfined criticality*, *Phys. Rev. Lett.* **111** (2013) 087203.

[68] R.G. Melko and R.K. Kaul, *Scaling in the fan of an unconventional quantum critical point*, *Phys. Rev. Lett.* **100** (2008) 017203.

[69] N. Ma, Y.-Z. You and Z.Y. Meng, *Role of Noether's Theorem at the Deconfined Quantum Critical Point*, *Phys. Rev. Lett.* **122** (2019) 175701 [arXiv:1811.08823] [INSPIRE].

[70] J. D'Emidio, A.A. Eberharter and A.M. Läuchli, *Diagnosing weakly first-order phase transitions by coupling to order parameters*, arXiv:2106.15462 [INSPIRE].

[71] F. Verstraete and J.I. Cirac, *Matrix product states represent ground states faithfully*, *Phys. Rev. B* **73** (2006) 094423.

[72] M.B. Hastings, *An area law for one-dimensional quantum systems*, *J. Stat. Mech.* **2007** (2007) P08024.

[73] J.I. Cirac, D. Perez-Garcia, N. Schuch and F. Verstraete, *Matrix product states and projected entangled pair states: Concepts, symmetries, theorems*, *Rev. Mod. Phys.* **93** (2021) 045003 [arXiv:2011.12127] [INSPIRE].

[74] D. Perez-Garcia, F. Verstraete, M.M. Wolf and J.I. Cirac, *Matrix product state representations*, quant-ph/0608197.

JHEP06(2022)019

7

CONCLUDING REMARKS AND OUTLOOK

> The important thing is to never stop questioning
>
> Albert Einstein

In this thesis we studied quantum field theories on the lattice via the Hamiltonian formalism. The advantage of the lattice regulator is the minimal length scale a that naturally removes all UV divergences from the field theory. Furthermore, the resulting lattice theories have well defined Hilbert spaces, so that they are a natural candidate for numerical simulations that are crucial to gain a nonperturbative understanding of strongly interacting field theories such as QCD. In this work, these numerical simulations were performed within the framework of tensor networks which are a class of variational ansätze that, due the area law of entanglement, provide a natural description of the ground state and first few excited states of these lattice models. Note that a Lagrangian formulation of lattice regularized field theories is also possible and has been extensively studied using Monte Carlo simulations, and more recently by applying tensor-based implementations of the renormalization group. The advantage of the tensor-based approaches, either for the Hamiltonian or the path integral, is that they do not suffer from the sign problem that arises in Monte Carlo sampling of fermionic path integrals at finite density. Furthermore, the Hamiltonian formulation of quantum field theory, and quantum mechanics in general, also allows to study dynamical processes such as the scattering and decay of particles, for which the (Euclidean) path integral is not really suitable.

Furthermore, the MPS ansatz, and tensor network states in general, can be thought of as states built from the action of a finite depth unitary circuit on a product state. In the, hopefully relatively near, future quantum computers will be able to manipulate and optimize such finite depth quantum circuits. They would thus be able to simulate Hamiltonian quantum lattice systems (and Hamiltonian lattice field theory in particular). With this in mind, it is very timely to study Hamiltonian lattice field theory and identify the correct discretization procedures. However, in the first part of this thesis found that certain properties of quantum field theories, in particular chiral symmetry, cannot be captured through (Hamiltonian) lattice field theory. Consequently, it might seem as if these concepts can never be simulated on a (quantum) computer which, in turn, seems to imply that something is missing from this description. Also the infinite-dimensional local Hilbert space associated with bosonic fields poses issues for tensor network simulations and (future) quantum simulations. In the second part we nevertheless managed to perform numerical matrix product state simulations of the compact boson as the low energy description of a modified Ising chain, and the chiral Gross-Neveu model as a non fine-tuned direct transition between an antiferromagnetic and a dimer phase. The upshot of this is that chiral symmetries, and perhaps other anomalous symmetries, are not really symmetries of the underlying regularized field theory, but rather an artefact of our perturbative treatment of field theory. For the chiral Gross Neveu model in particular, we found that the anomalous chiral symmetry emerged from the fact that kinks in one order parameter carried charge of the other, as well as from the non-trivial interplay between different reflection and translation symmetries. Indeed, we found that the direct transition required to get a continuum limit with continuous chiral symmetry was not only present, but is also the expected behaviour of these lattice models.

Another interesting observation is that certain predictions of Einstein's famous general relativity are also inherently incompatible with the lattice regulator. For example, the Nielsen-Ninomiya theorem excludes regions of spacetime with a single left or right mover that are predicted to exist in the interior of a black hole. Consequently, a lattice regularization of a black hole and the related Hawking radiation may shed some light onto the physics behind horizons.

Another generalization of the work presented in this thesis would be to construct a lattice model with a nonlocal $Z_2 \otimes Z_2$ symmetry. Similarly to the modified Ising model, such models cannot have symmetric gapped phases and would therefore most likely display a non-trivial phase diagram with an infrared description that is again closely related to compact bosons.

Finally, we note that this thesis only dealt with quantum physics in one spatial dimension, whereas the world around us most certainly has three (macroscopic) spatial dimensions. In principle, one can quite easily generalize the MPS ansatz to two or even three spatial dimensions, but the resulting tensor networks do not have a gauge-fixed representation, so that it is more difficult to optimize such states. Nevertheless, this is still possible and in future work it would be very interesting to construct lattice regularizations of field theories in higher dimensions. For example, the 2+1 dimensional version of the Gross Neveu model has recently been shown to emerge as the low energy description of certain twisted bilayer graphene materials.